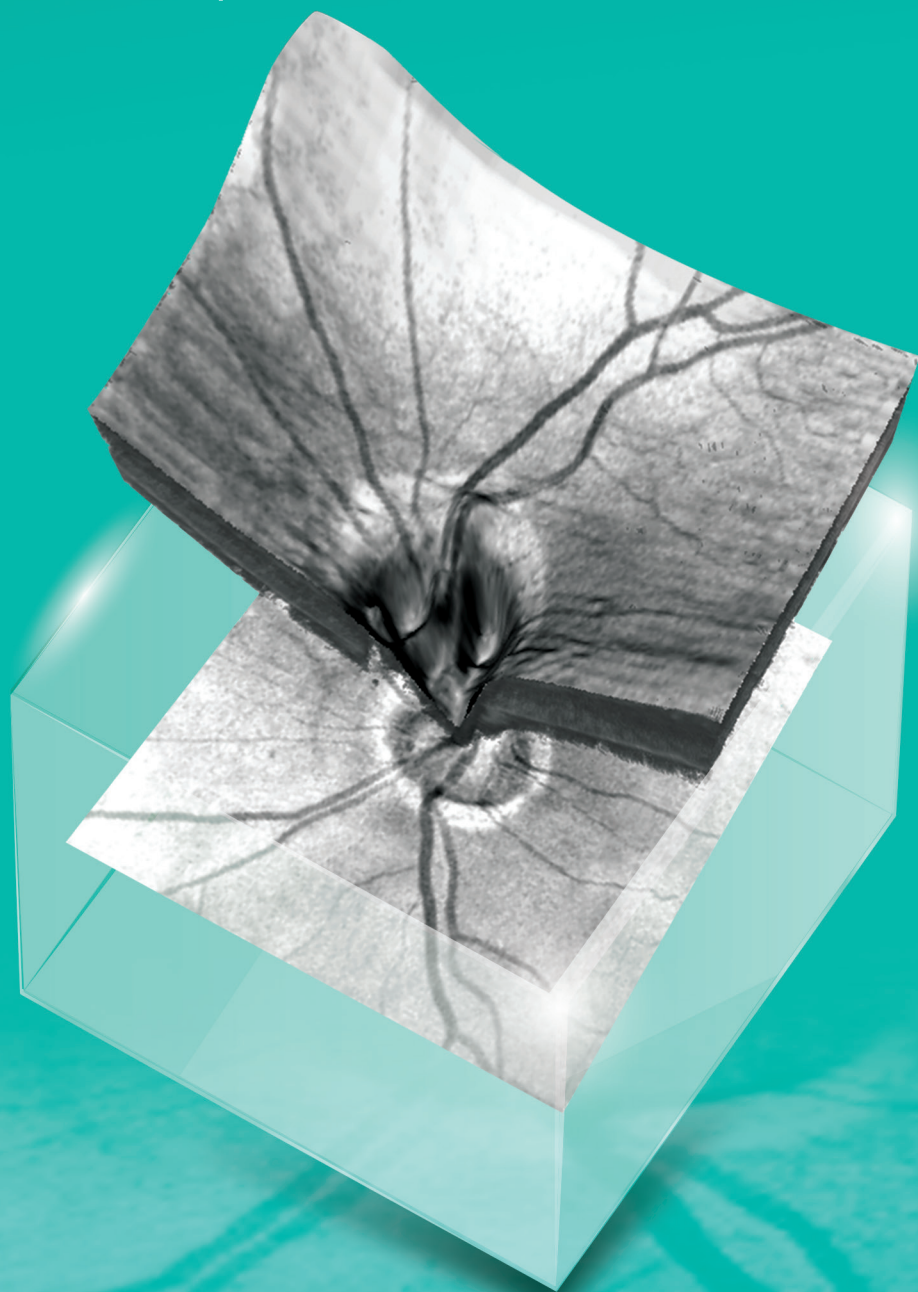


& OCT & GLAUCOMA

Professor Jean-Paul Renard

Professor Antoine Labbé

Professor Christophe Baudouin



Cirrus HD-OCT 3D SD-OCT analysis of the optic disc in a patient with early glaucoma

& OCT & GLAUCOMA

Pr Jean-Paul **Renard** - Pr Antoine **Labbé** - Pr Christophe **Baudouin**

**Centre Ophtalmologique
Breteuil - Paris**

Hôpital d'Instruction
des Armées Bégin
- Saint-Mandé

**Ophtalmopôle
Groupe Hospitalier
Paris-Centre (HUPC -
Hôpitaux Universitaires
Paris Centre) Paris 5
Université Sorbonne
Paris Descartes.**

**Centre Hospitalier
National
d'Ophtalmologie
des Quinze-Vingts**

Institut de la Vision,
Université Pierre et
Marie Curie

**Hôpital Ambroise
Paré, AP-HP,
Université de
Versailles
St-Quentin-
en-Yvelines**

**Centre Hospitalier National
d'Ophtalmologie des
Quinze-Vingts**

Institut de la Vision, Université
Pierre et Marie Curie
**Hôpital Ambroise Paré,
AP-HP,
Université de Versailles
St-Quentin-en-Yvelines**

with the collaboration of:

Jean-Marie Giraud, Jean-Rémi Fénolland, Bénédicte Dupas, Adil El Maftouih



Nadja Abbas, Marie-Julie Bovis, Emmanuelle Brasnu, Yann Destaebel, Pascale Hamard, Stéphanie Hayek, Sofiene Kallel, Laetitia Luponis, Lyes Meziani, Candice Rados, Laetitia Raissac, Rémi Rosenberg, Damien Sendon

Published by Théa and Carl Zeiss Meditec France SAS



Foreword

Considerable progress has been made in imaging techniques for the management of glaucomatous optic neuropathy over recent years, with improvement of both imaging and image analysis methods.

With a follow-up of 10 years, Optical Coherence Tomography or SD-OCT (Spectral-Domain OCT) now provides objective, reliable and reproducible quantification of lesions of the various tissues affected by glaucoma. Continuing improvement of new image acquisition algorithms and new image analysis software result in ever-increasing diagnostic precision in the analysis of the posterior segment and the anterior segment.

This book, based on the experience and close collaboration of two teams, is designed to provide an overview, without attempting to be comprehensive, of current practices concerning the use, indications, careful interpretation of the results, limitations and traps of OCT in glaucoma. We have selected a number of characteristic images. The reader will easily recognize the various clinical forms, while bearing in mind that detailed and complete analysis of all the elements of the results are essential and that SD-OCT imaging data must always be carefully correlated with clinical findings and visual field testing in the diagnostic and therapeutic approach.

We hope that this book will provide updated complementary practical training to ensure optimal management of our patients.

Prof Jean-Paul Renard

Prof Antoine Labb  

Prof Christophe Baudouin

Contents

PART I

Posterior segment OCT in glaucoma

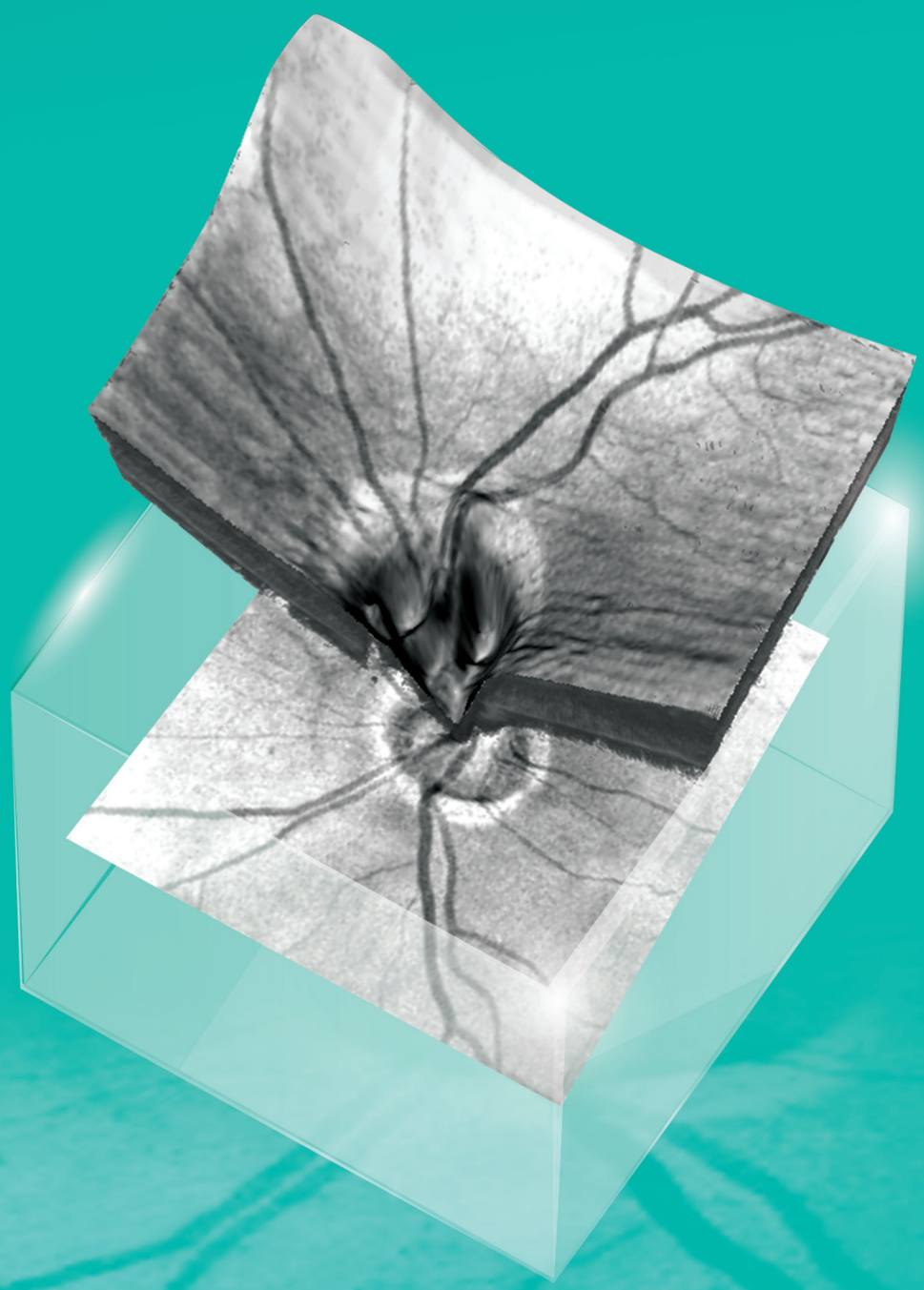
| | |
|--|------------|
| 1. Principle and objectives | 11 |
| 2. Various steps of a good OCT imaging acquisition..... | 17 |
| 2.1. Before acquisition | 19 |
| 2.2. During acquisition | 20 |
| 2.3. After acquisition | 22 |
| 3. SD-OCT imaging of the retinal nerve fibre layer | 25 |
| 3.1. Interpretation | 26 |
| 3.2. Limitations | 40 |
| 3.3. In clinical practice | 42 |
| 4. SD-OCT imaging of the optic nerve head | 45 |
| 4.1. Interpretation | 46 |
| 4.2. A new index | 48 |
| 4.3. In clinical practice | 52 |
| 5. Macular ganglion cell complex analysis | 55 |
| 5.1. Various types of SD-OCT analysis | 58 |
| 5.2. Interpretation | 66 |
| 5.3. Complementary indices | 68 |
| 5.4. Mapping of macular defects better defined | 70 |
| 5.5. In clinical practice | 72 |
| 6. SD-OCT interpretation guidelines | 75 |
| 7. Clinical features of glaucomatous optic neuropathy on SD-OCT | 83 |
| 7.1. Glaucoma suspect | 84 |
| 7.2. Early glaucoma | 88 |
| 7.3. Myopia and tilted disc | 95 |
| 7.4. Moderate glaucoma | 96 |
| 7.5. Unilateral glaucoma | 98 |
| 7.6. Advanced glaucoma | 100 |
| 8. Special cases in SD-OCT | 103 |
| 8.1. Isolated OCT defect | 104 |
| 8.2. Tilted disc syndrome | 106 |
| 8.3. Optic disc drusen | 112 |
| 8.4. High myopia | 115 |

| | |
|---|------------|
| 9. Traps in SD-OCT | 119 |
| 9.1. During acquisition | 121 |
| 9.1.1. Patient-related factors | 121 |
| 9.1.2. Operator-related factors | 125 |
| 9.1.3. Machine-related factors | 128 |
| 9.2. After acquisition | 130 |
| 9.2.1. Abnormalities of the vitreoretinal interface, thickened posterior hyaloid, ERM | 130 |
| 9.2.2. Vitreoretinal traction | 131 |
| 9.2.3. POAG and maculopathy | 132 |
| 9.2.4. POAG and AMD | 133 |
| 9.2.5. Fovea plana | 134 |
| 10. SD-OCT markers of progression | 137 |
| 10.1. Markers of RNFL progression | 140 |
| 10.2. Markers of GCC progression | 146 |
| 10.3. New progression analyses | 160 |
| 11. Current place of OCT angiography in glaucoma | 167 |

PART II

Anterior segment OCT in glaucoma

| | |
|--|------------|
| 1. Detection of closed iridocorneal angles and quantitative parameters | 197 |
| 2. Analysis of the mechanisms of angle closure | 209 |
| 2.1. Pupillary block | 211 |
| 2.2. Plateau iris mechanism | 214 |
| 2.3. Lens mechanisms | 218 |
| 2.4. Malignant glaucoma | 221 |
| 2.5. Choroidal effusion | 222 |
| 2.6. Other forms of secondary iridocorneal angle closure | 224 |
| 3. Analysis of the mechanisms of certain forms of secondary glaucoma | 229 |
| 4. Follow-up of surgery and laser surgery | 235 |
| 4.1. Follow-up of surgery and laser surgery | 236 |
| 4.2. Follow-up of filtering surgery | 240 |
| 5. New imaging developments: direct visualization of vessels of the trabecular meshwork and Schlemm's canal | 265 |



Posterior segment OCT in glaucoma

Introduction

Identification of structural changes of the retinal nerve fibre layer (RNFL), optic nerve head (ONH) and macular ganglion cell complex (GCC) is an essential component of the diagnosis and management of glaucoma.

Optical coherence tomography (OCT), which has been used in ophthalmology for more than 25 years, allows *in vivo* examination of all layers of the retina.

New SD-OCT (Spectral-Domain OCT) systems now provide continually improving objective quantification of lesions of these structures.

The use of recently available new image acquisition and new image analysis algorithms on larger tissue volumes now allows a higher level of diagnostic precision of the parameters obtained, as well as more reliable interpretation of the features of certain clinical forms at the various stages of glaucomatous optic neuropathy.

Lastly, the development of OCT angiography, providing «*en face*» visualization of the capillary architecture and clear distinction of the deep and superficial capillary plexuses, provides perspectives with various interesting extensions. The contribution of OCT angiography, in terms of its objective to evaluate the dynamic aspects of the tissues in addition to tissue morphology, needs to be more clearly defined.

1. Principle and objectives

Principle and objectives

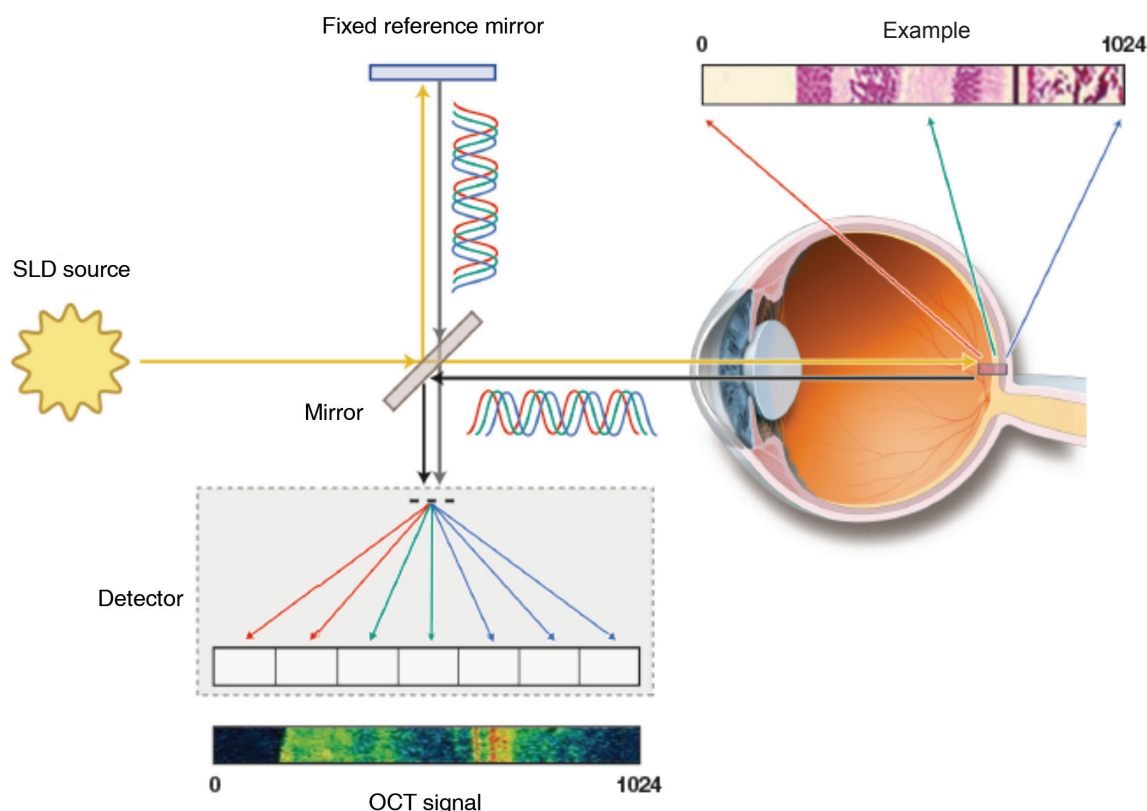
The reconstituted image obtained by optical coherence tomography depends on the absorption and reflection of light by the tissues. The very rapid light propagation (backscattered) over distances of several micrometres that separate posterior structures of the eye can be measured by means of interferences. The light reflected by retinal layers is therefore made to interfere with that of another beam derived from the same source that has travelled over a reference optical path. Interferences only occur over a certain distance: the coherence length, leading to the name of optical coherence tomography.

Spectral-Domain OCT (SD-OCT) is a form of low coherence interferometry, in which the light source is a superluminescent diode (SLD) between 840 and 880 nm and the detector is a spectrometer, which immediately resolves interference signals throughout the entire depth of each axial examination of the tissue without needing to vary the length of the reference path (mirror).

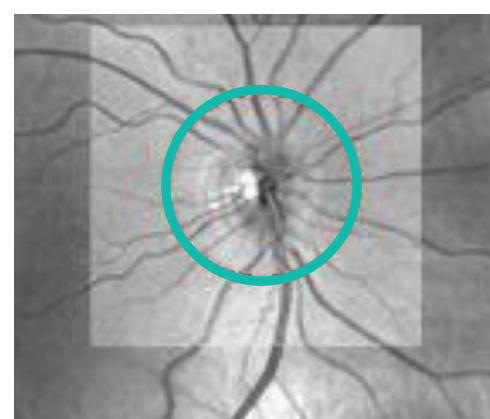
The spatial representation of the reflectivity values obtained allows the construction of two- or three-dimensional images that are closely correlated with histological images of the retina.

SD-OCT now scans tissues at a speed between 25,000 and 70,000 A-scans/s, allowing very rapid acquisition of volumetric data sets with an axial resolution of about 3-5 µm and a transverse resolution of 12-20 µm depending on the SD-OCT device.

OPTICAL DIAGRAM OF SPECTRAL-DOMAIN OCT



Study of the frequencies of refracted light (spectrometer)

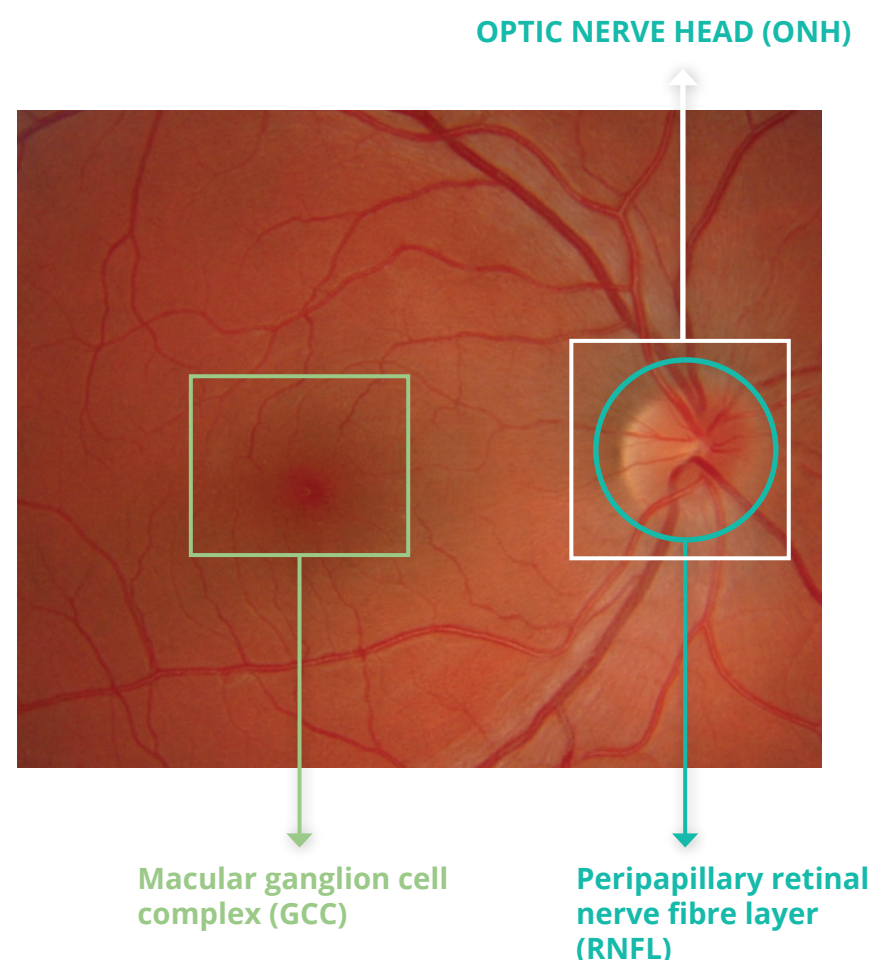


Principle and objectives

The 3 sites of the posterior pole examined by SD-OCT, comprising analysis of the peripapillary RNFL, analysis of the ONH and analysis of the macular ganglion cell complex, are acquired sequentially during the same acquisition protocol.

They must be considered to be indissociable because they constitute different and complementary sources of information that must be interpreted according to each clinical form of glaucoma, as will be described below.

ANALYSIS OF THREE SITES





2. Steps of a good OCT imaging acquisition

- 2.1. Before acquisition**
- 2.2. During acquisition**
- 2.3. At the end of acquisition**

The image acquisition protocols of new SD-OCT systems are now clearly defined. A number of prerequisites before, during and the end of acquisition must be kept in mind to ensure optimal examination quality.

Before acquisition

Inform the patient about the objective and modalities of the examination (noise, light).

Emphasize the importance of fixing the specific light target (green or blue colour that must be known by the operator) inside the lens.

Pupillary dilation is generally unnecessary (except in patients with small pupils or opaque media).

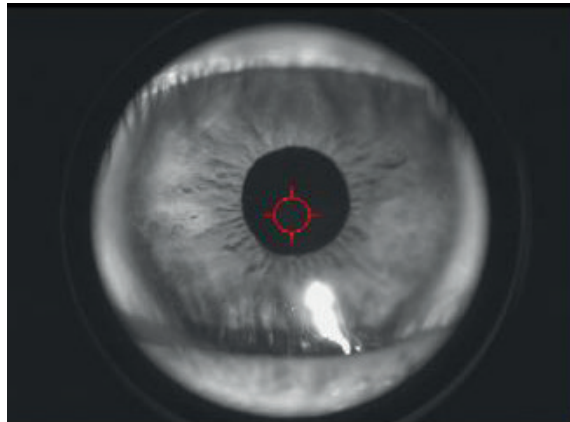
Ensure that the patient is comfortably installed:

- **Check the contact between the forehead and the headrest before and during acquisition to limit** anteroposterior movements (z axis) in view of the very short focal range of OCT. This task is facilitated by OCT systems that allow the examiner to be placed perpendicularly to the patient during acquisition.

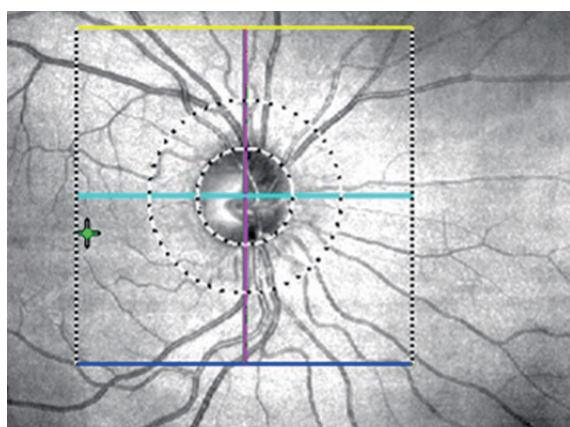
- **Record the patient's identity**, including the **patient's age** and **ethnic group**.



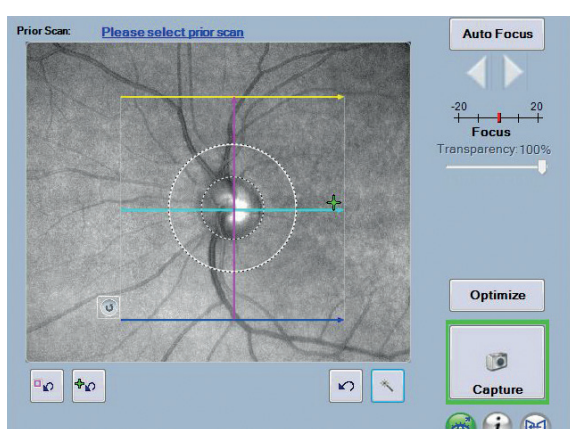
During acquisition



Ensure a good perpendicular alignment of the vertical and horizontal planes to optimize reflectance and the signal-to-noise ratio.

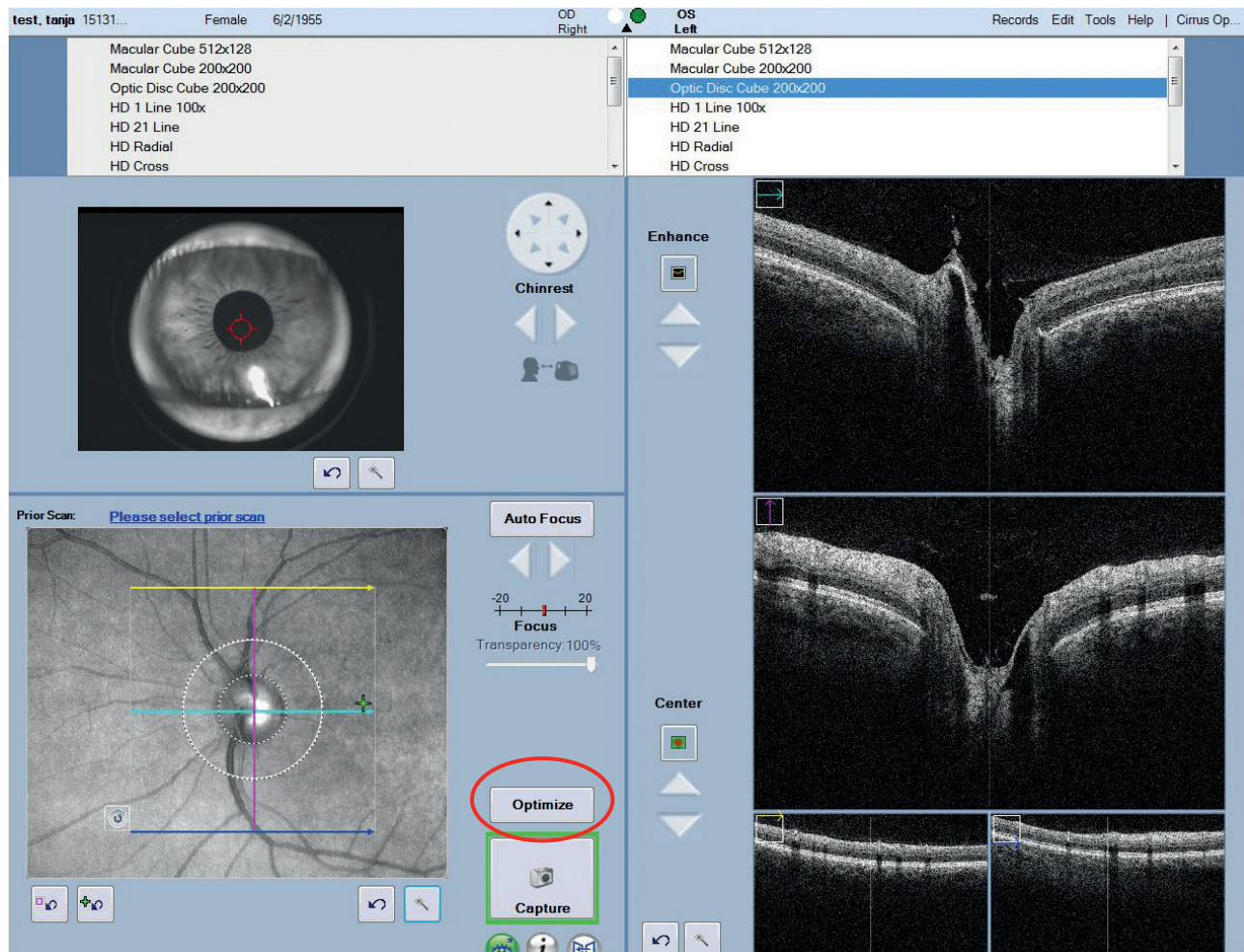


After determining the focal plane, use the « optimization » function to obtain a better signal.



Activate eye-tracker systems in order to limit movement artefacts and optimize scan reproducibility.

Use the image averaging function of the software to enhance the signal/noise ratio.



At the end of the acquisition

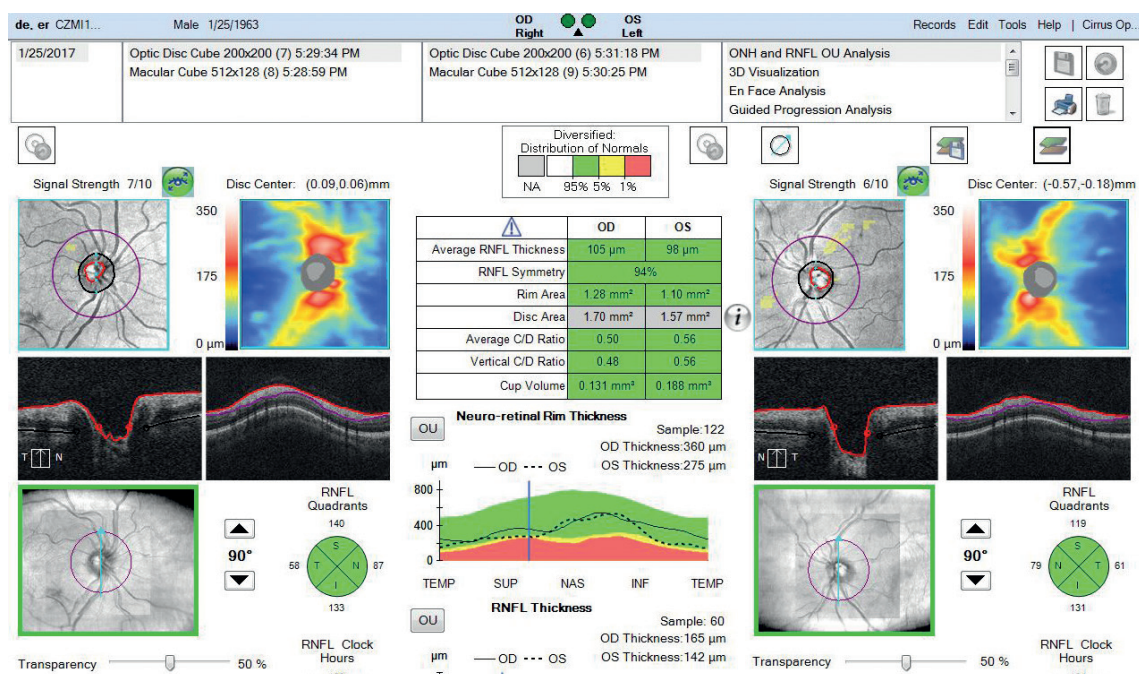
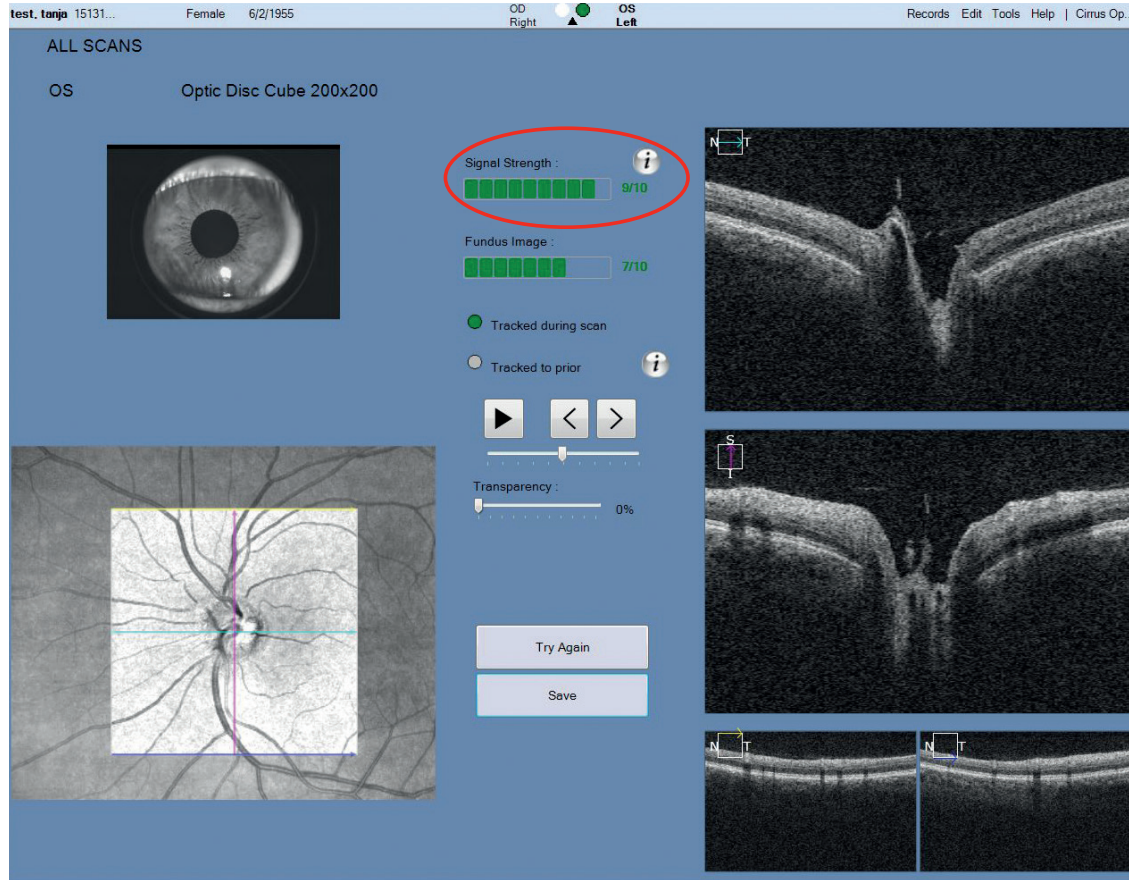
Check the signal strength specific to each SD-OCT system:

HD-OCT: SS ≥ 6, Triton > 35, XR Avanti > 30, Spectralis > 15, RS3000 and HS-100 > 7.0

A weak signal indicates an unreliable recording and should be rejected.

Eliminate any acquisitions with micromovement artefacts (poor alignment of retinal vessels on “en face” images), observed less frequently with the «eye tracker» system.

Check good segmentation of B-scans (arrows). It is essential to be able to recognize and understand segmentation of the various retinal layers. Segmentation is performed automatically by the OCT software and all measurements of the various retinal layers reported by the examination depend on the good quality of segmentation. Poor segmentation of retinal layers by the software, despite a good signal strength, may be observed. In which case the acquisition should be repeated.





3. SD-OCT imaging of the Retinal Nerve Fibre Layer

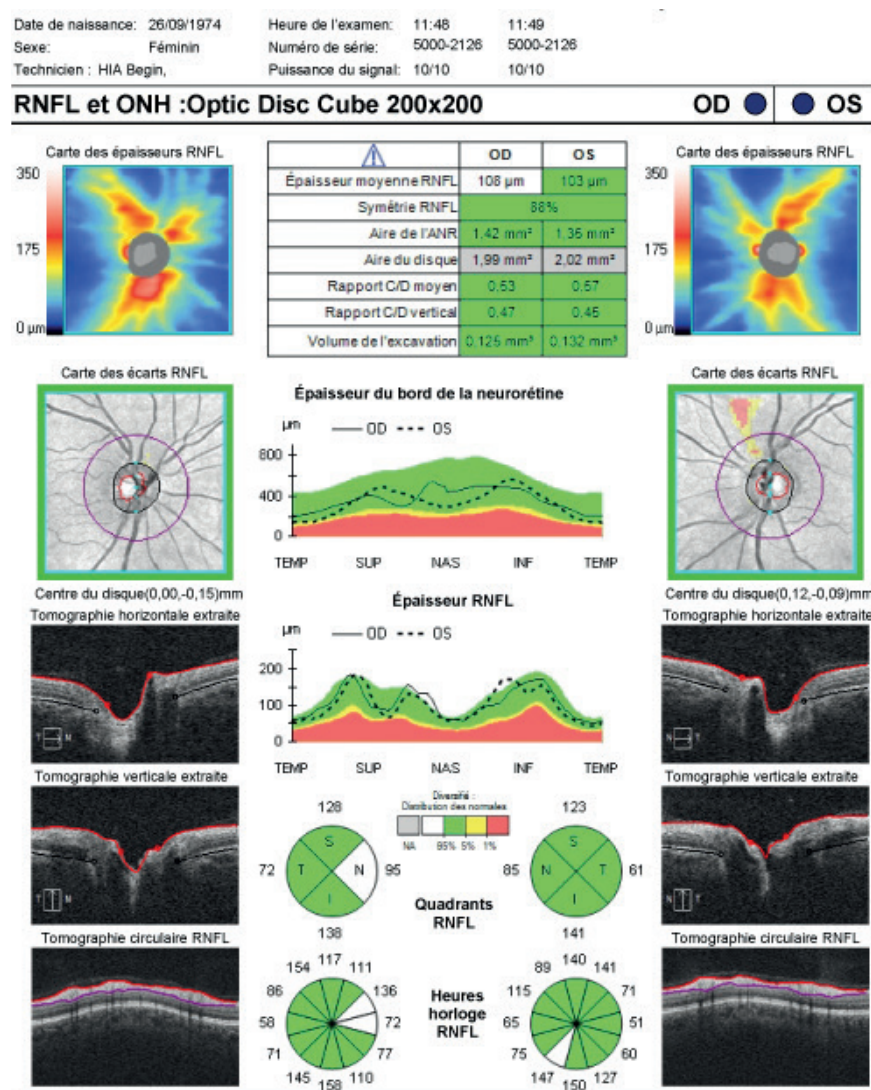
- 3.1. Interpretation**
- 3.2. Limitations**
- 3.3. In clinical practice**

Interpretation of SD-OCT images

Volumetric acquisition of the RNFL is indissociable from acquisition of ONH parameters.

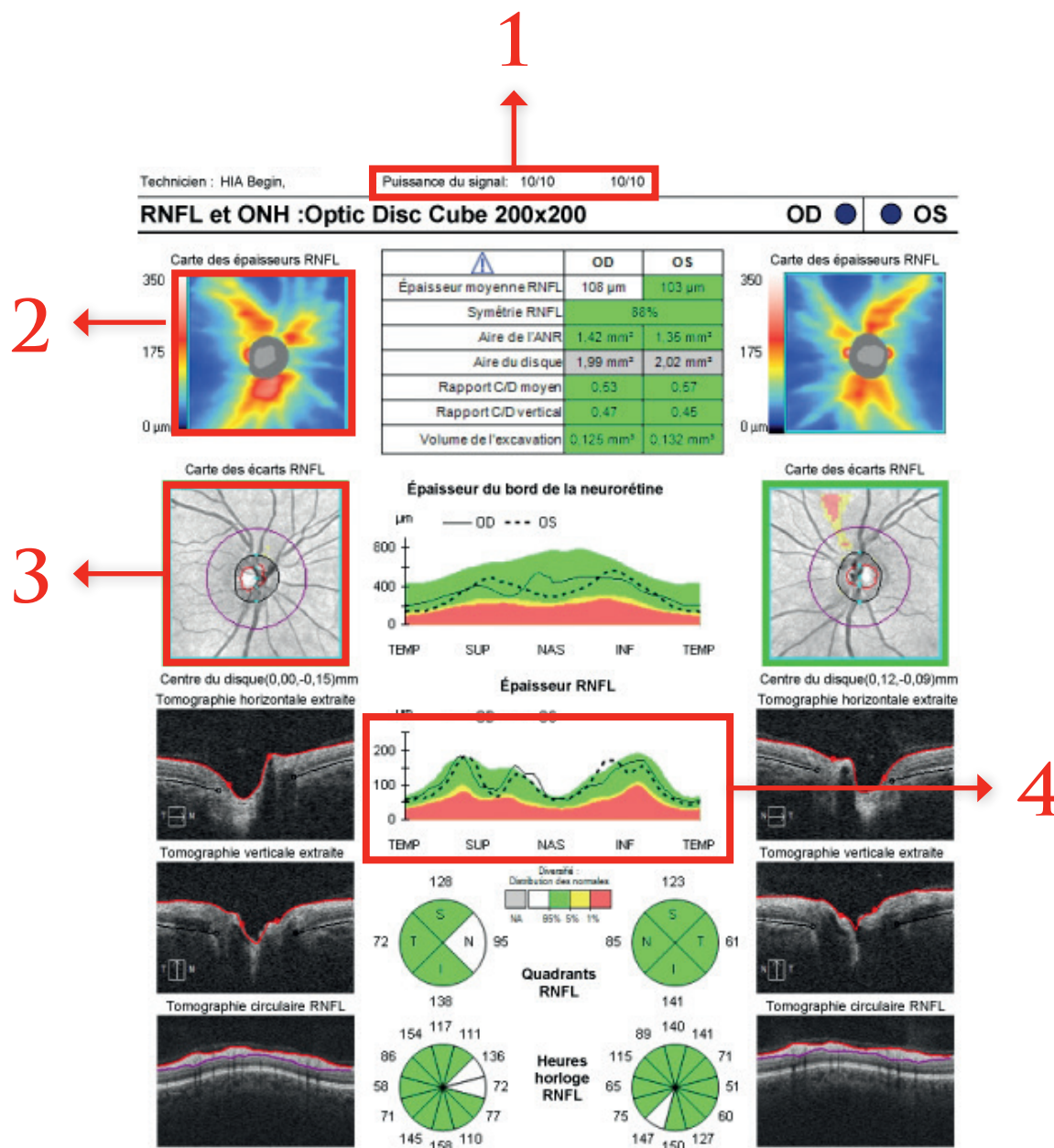
OCT images must be examined from top to bottom and from left to right within 8 steps.

In the upper part of the statement, check the patient's identity and date of birth, which allows statistical analyses and comparison of the results to those of age-matched subjects recorded in the system's normative database.



Interpretation of SD-OCT images

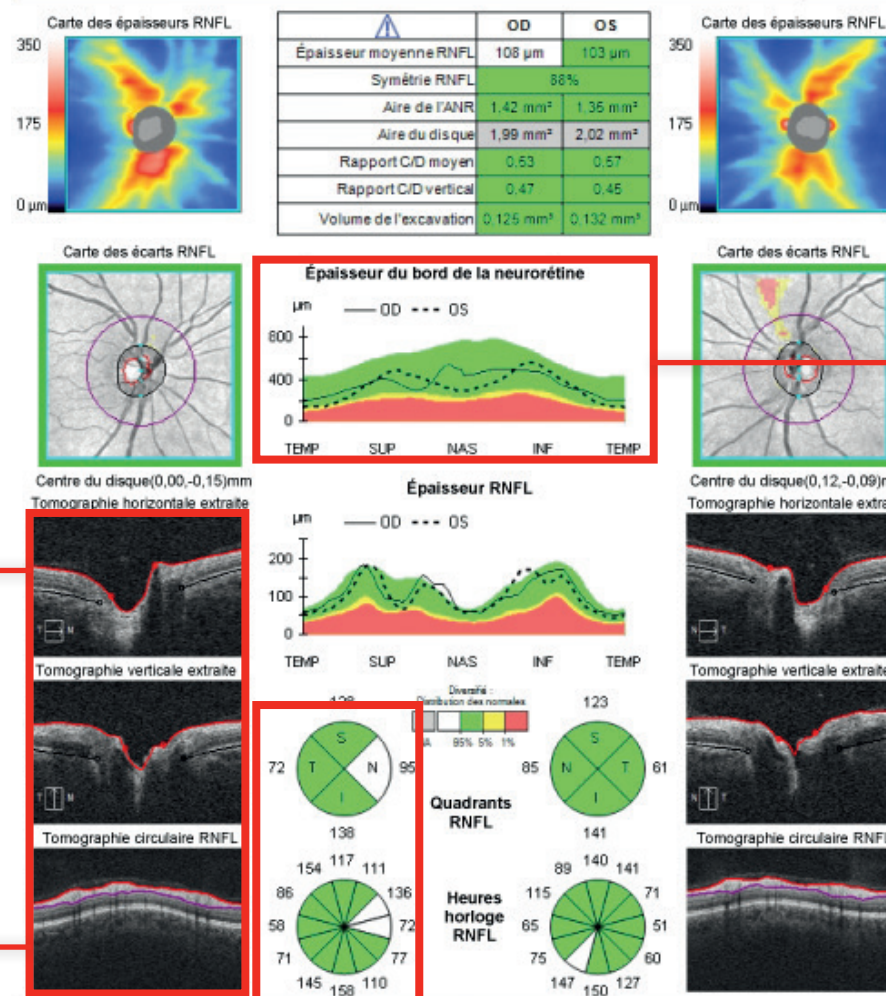
- 1 As we have seen, it is very important to check **the signal strength (SS)**. SD-OCT Cirrus: SS ≥ 6, Triton > 35, XR Avanti > 30, Spectralis > 15, RS3000 and HS-100 > 7.0.
- 2 The RNFL **thickness map over the entire surface of the acquisition cube on a normal OCT image** has an hourglass or butterfly wing appearance (yellow and red), in which it is important to **detect asymmetry between superior and inferior sectors as well as early signs of a peripheral defect** (blue notch in yellow-red sectors).
- 3 The **RNFL thickness deviation map**, compared to normal values for an age-matched subject, demonstrates points situated outside the confidence interval defined from the normative database (yellow and red). **The major value of the deviation map is to detect abnormalities situated outside the classical peripapillary RNFL B-scan, of 3.46 mm in diameter, used as the reference zone for evaluation of RNFL thickness.**
- 4 Representation of **RNFL thickness**, measured on each A-scan of the peripapillary measurement circle, as a developed image or "**TSNIT graph**" with a colour-coded distribution of normal values according to the subject's age compared to the normative database of the SD-OCT system used. **This graph must be examined to detect a localized notch (defect)** or more extensive flattening (frequent in tilted disc syndrome).



Interpretation of SD-OCT images

- 5 **The TSNIT graph of the neuroretinal rim** (NRR) evaluates the NRR thickness map measured from the extremities of Bruch's membrane with the colour-coded distribution of normative values according to the subject's age. **Analysis of the TSNIT graph looks for a more or less extensive notch (defect).**
- 6 **An enlarged horizontal B-scan and vertical** B-scan can be used to check the correct localization, by the OCT software, of the extremities of Bruch's membrane (black), which define the limits of the ONH, and projections on to the surface of the **internal limiting** membrane (red) to determine the edge of the NRR.
- 7 Particular attention must be paid to mean RNFL **thickness values, RNFL thickness in the superior and inferior quadrants, as well as the thickness of least two contiguous meridians**, with a colour-coded representation compared to the OCT system's normative database.
- 8 **The representation of the circular B-scan extracted from the optic disc cube, as well as the internal and external limits of the RNFL**, constitute an important reliability criterion to confirm good centering of the acquisition window and the quality of segmentation of retinal layers by the software when an abnormality is detected on OCT images. It searches for an error of segmentation or a localized signal loss despite good signal strength (SS).

Technicien : HIA Begin, Puissance du signal: 10/10 10/10
RNFL et ONH :Optic Disc Cube 200x200 OD OS



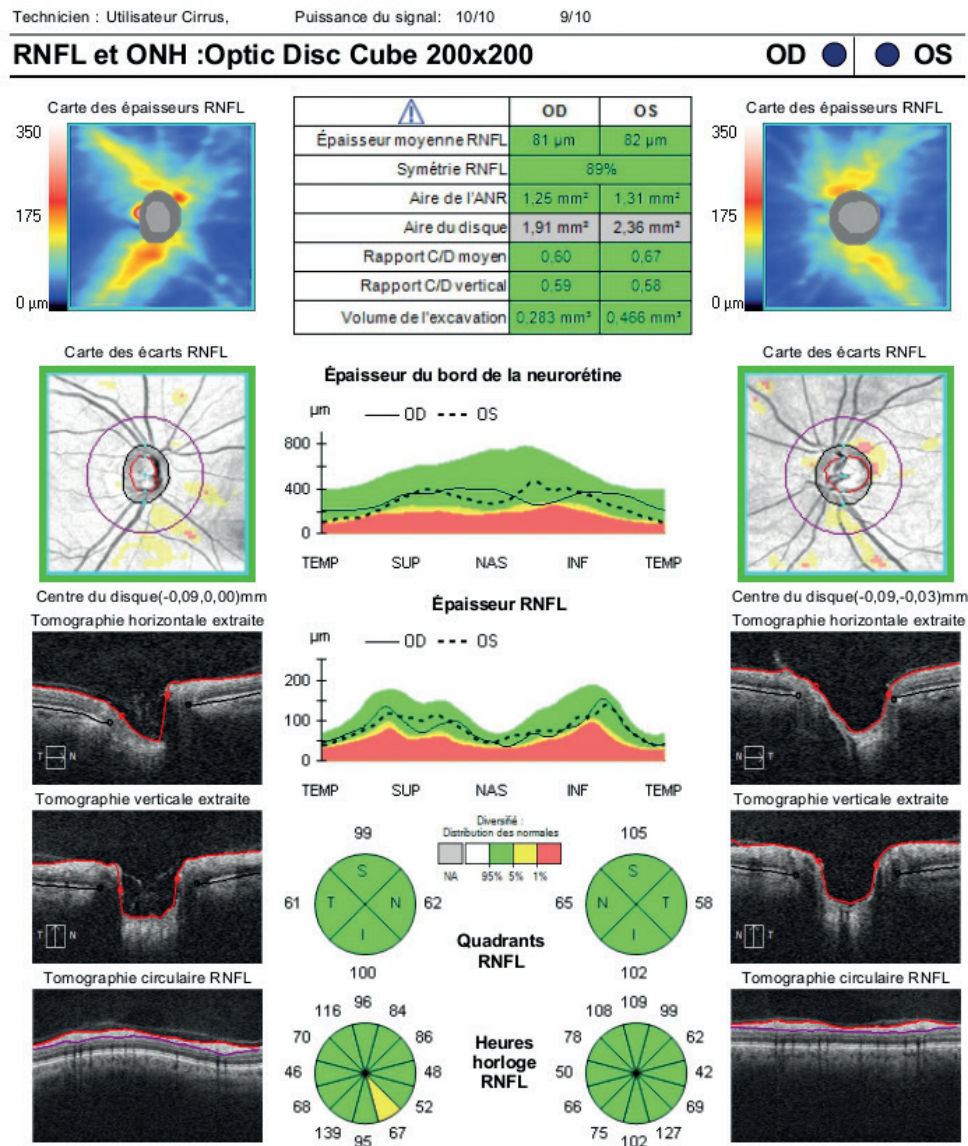
6

8

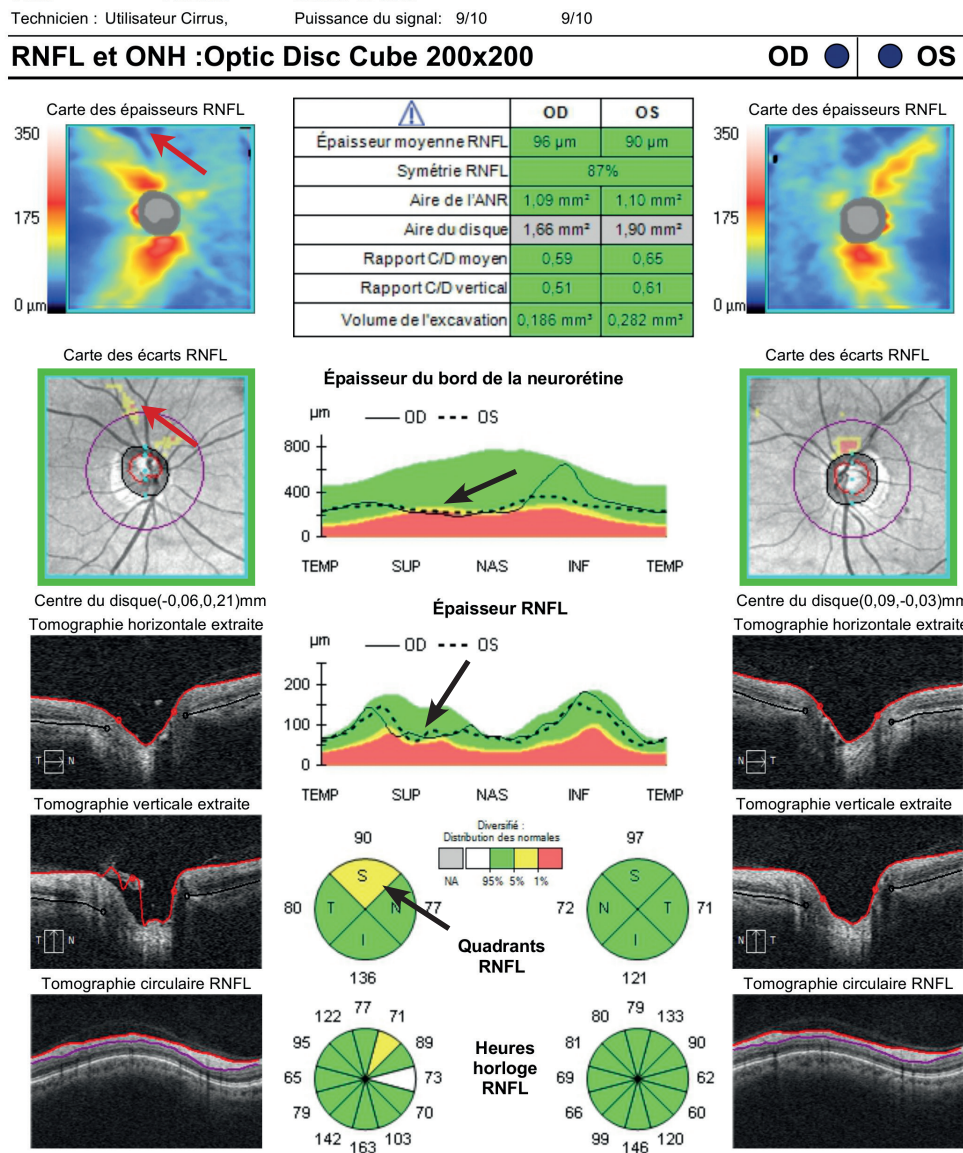
5

7

Interpretation of SD-OCT images



SD-OCT image with no detectable RNFL defect



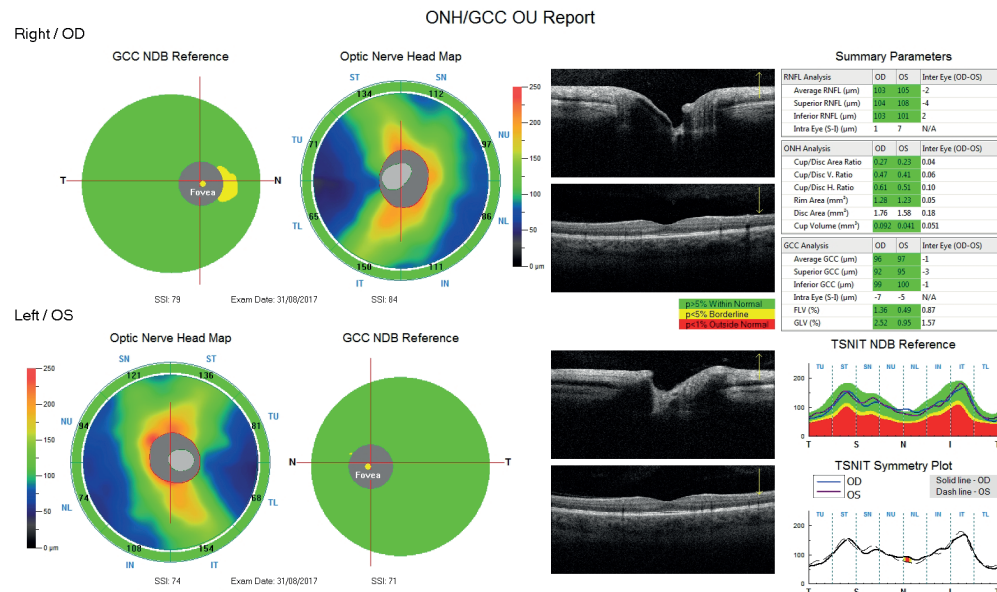
Suspicion of an early defect in the superior quadrant of the right eye on the thickness map, deviation map, TSNIT graph of the RNFL and NRR and on the RNFL thickness in the superior quadrant. This image should be compared with clinical ophthalmoscopy and visual fields, as this slight superior thinning could also be explained by the slightly tilted optic disc in this case.

Interpretation of SD-OCT images

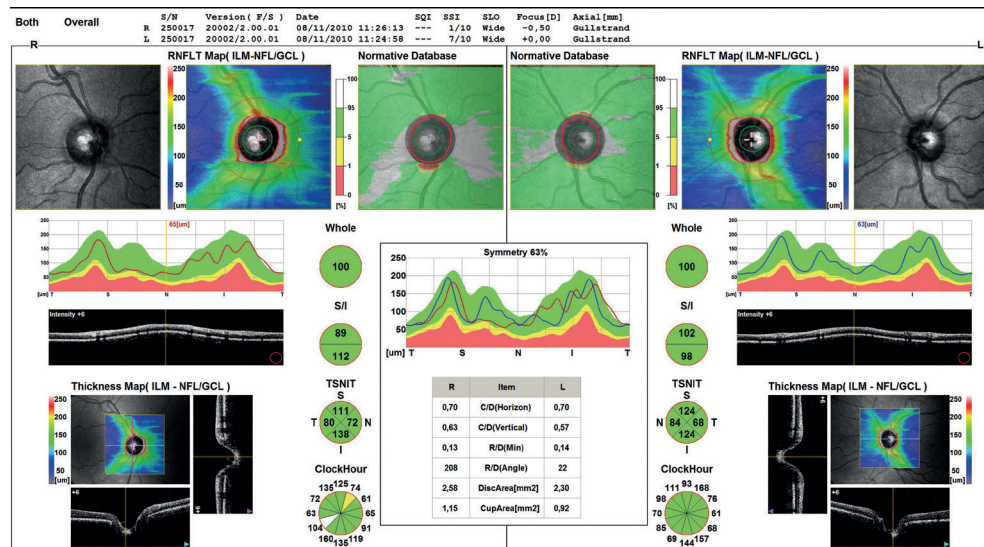
The RNFL displays provided by the various SD-OCT systems comprise similar maps and graphs.

RNFL thickness maps on volumetric acquisitions must be examined very carefully to detect defects beyond the classical 3.4 mm diameter zone of analysis.

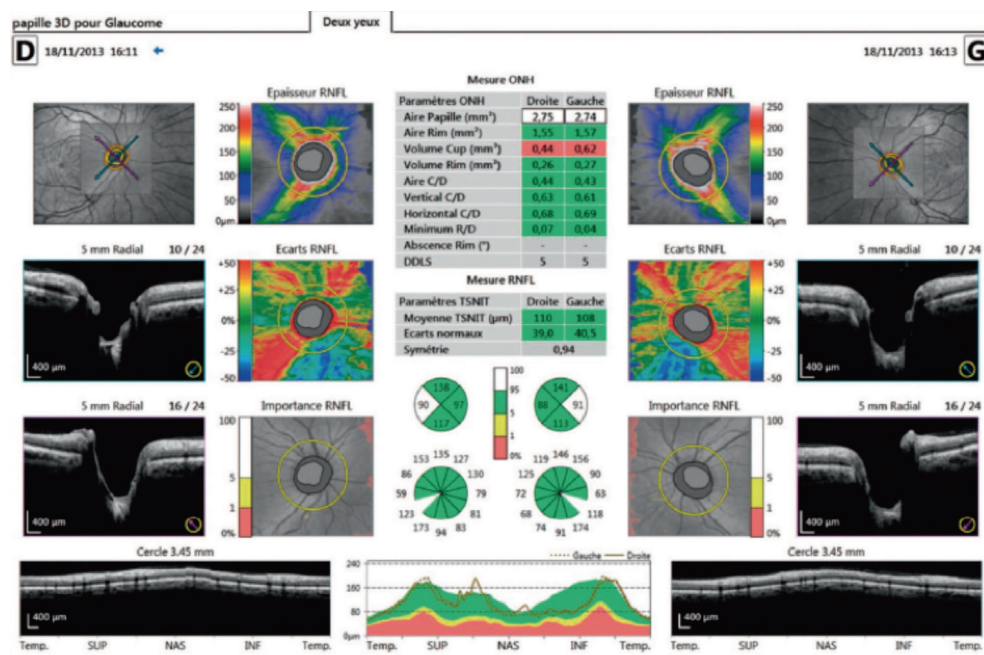
XR AVANTI SD-OCT NORMAL EXAM



NIDEK RS 3000 NORMAL EXAM



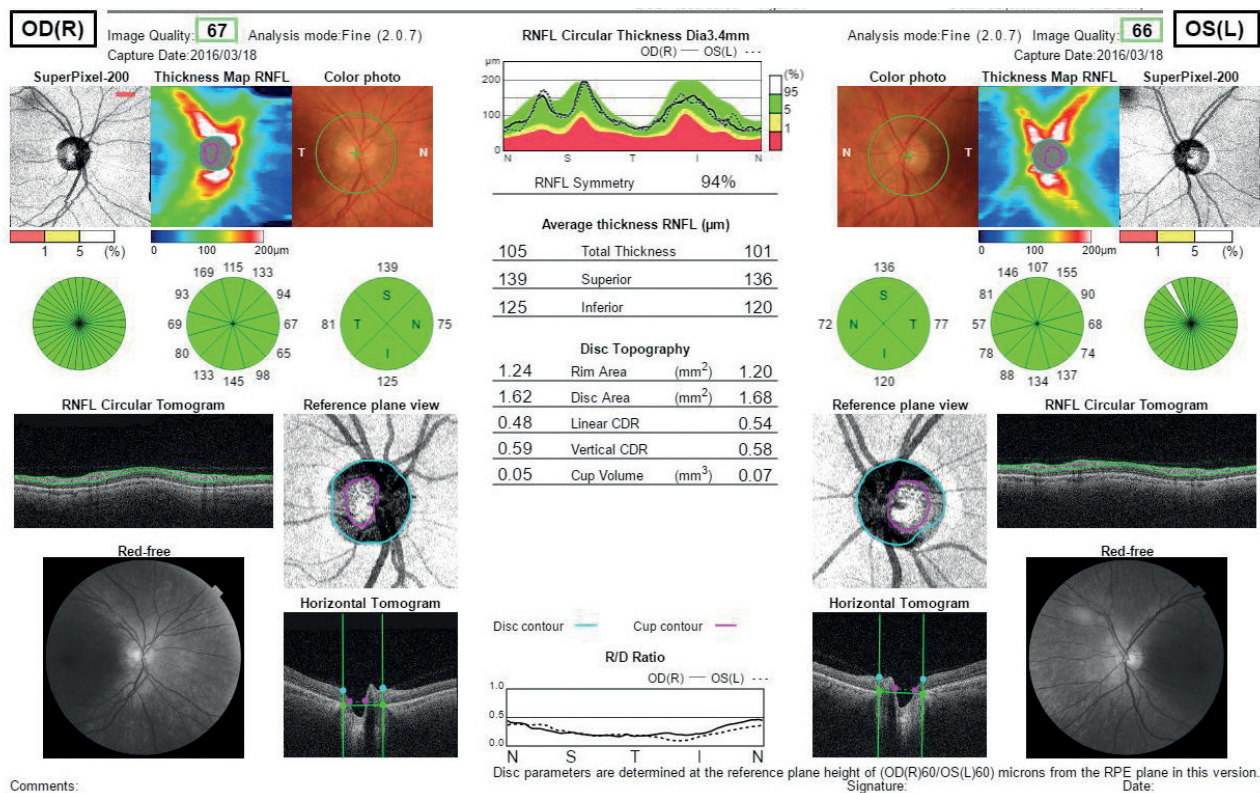
CANON SD-OCT HS 100 NORMAL EXAM



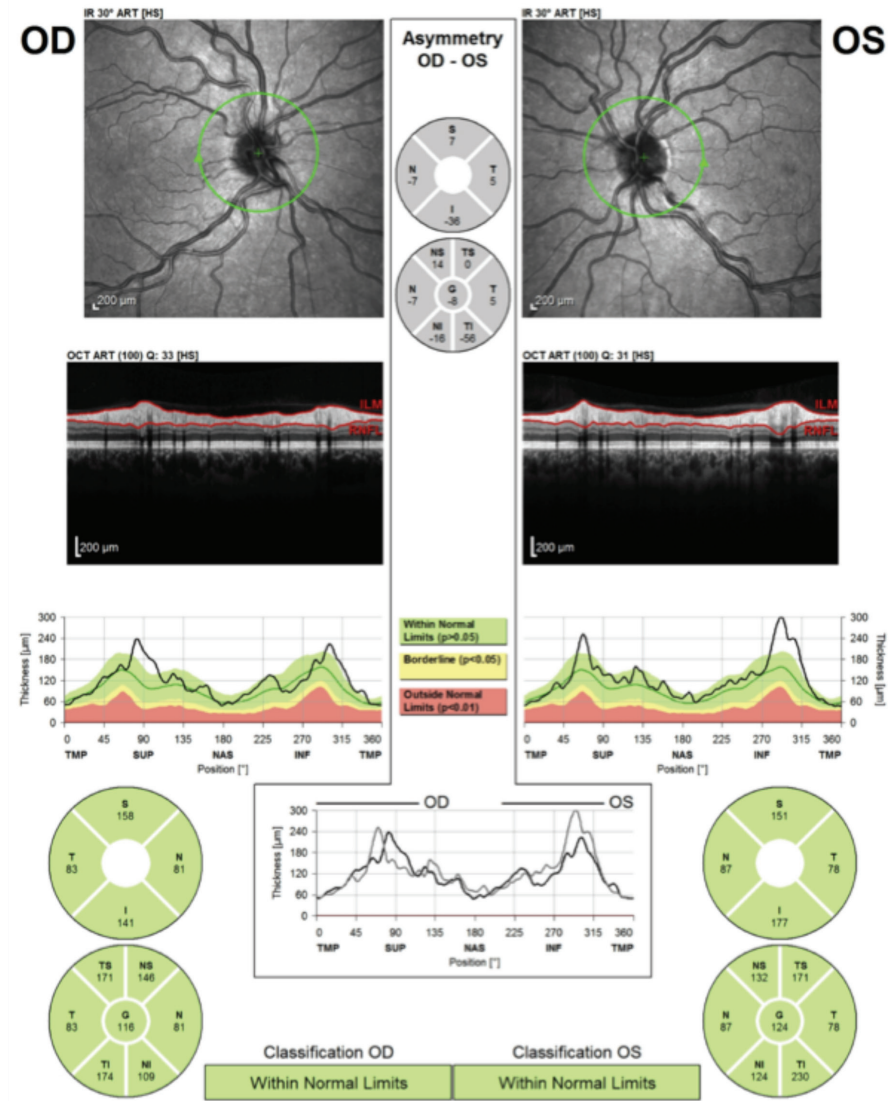
Interpretation of SD-OCT images

The RNFL displays provided by the various SD-OCT systems comprise similar maps and graphs.

TRITON - TOPCON SD-OCT NORMAL EXAM



HEIDELBERG SPECTRALIS SD-OCT NORMAL EXAM



Interpretation of SD-OCT images

MEAN RNFL THICKNESS

Caucasians: 98 µm (11)

Hispanics: 103 µm (12)

Asians ≈ 105 µm (9)

Loss 2 µm per decade

CONSIDER

Size of the optic disc (OD)

Measurement of the RNFL thickness 3.4 mm from the centre of the OD will be thinner in the case of a small diameter OD, as the measurement will be performed in a zone in which the RNFL is more spread out, and thicker in the case of a large diameter OD, as it will be closer to the edge of the OD, where the RNFL is thicker.

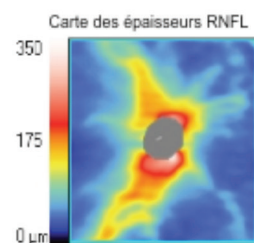
Long axes (LA)

A 1 mm increase of axial length is accompanied by a 2.2 µm reduction of RNFL thickness.

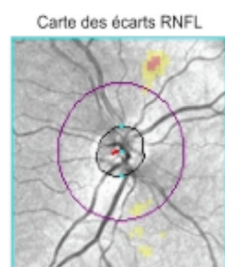
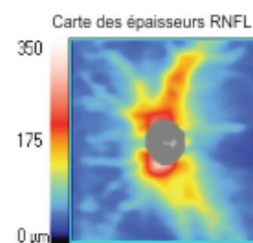
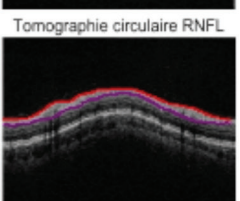
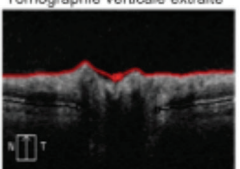
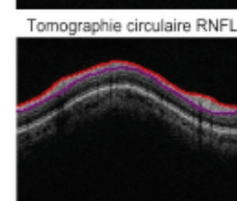
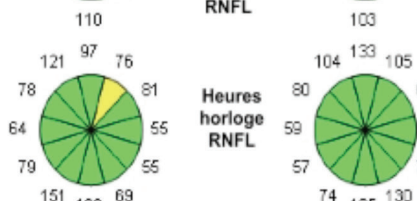
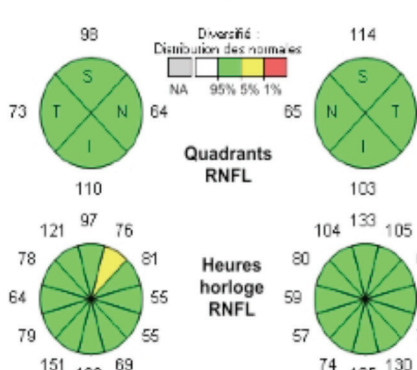
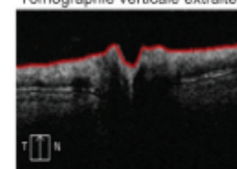
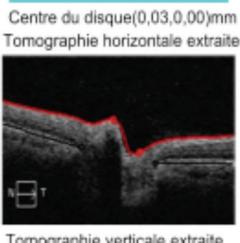
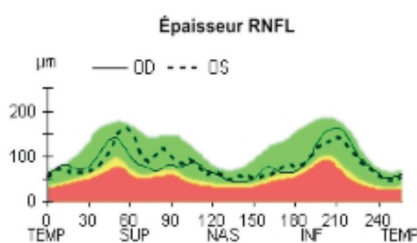
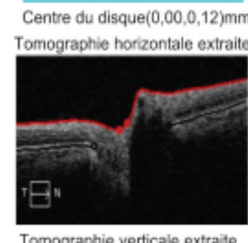
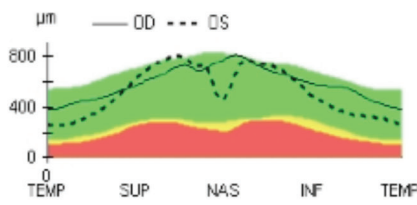
Médecin:

Puissance du signal: 9/10

10/10

RNFL et ONH :Optic Disc Cube 200x200**OD** ● **OS** ●

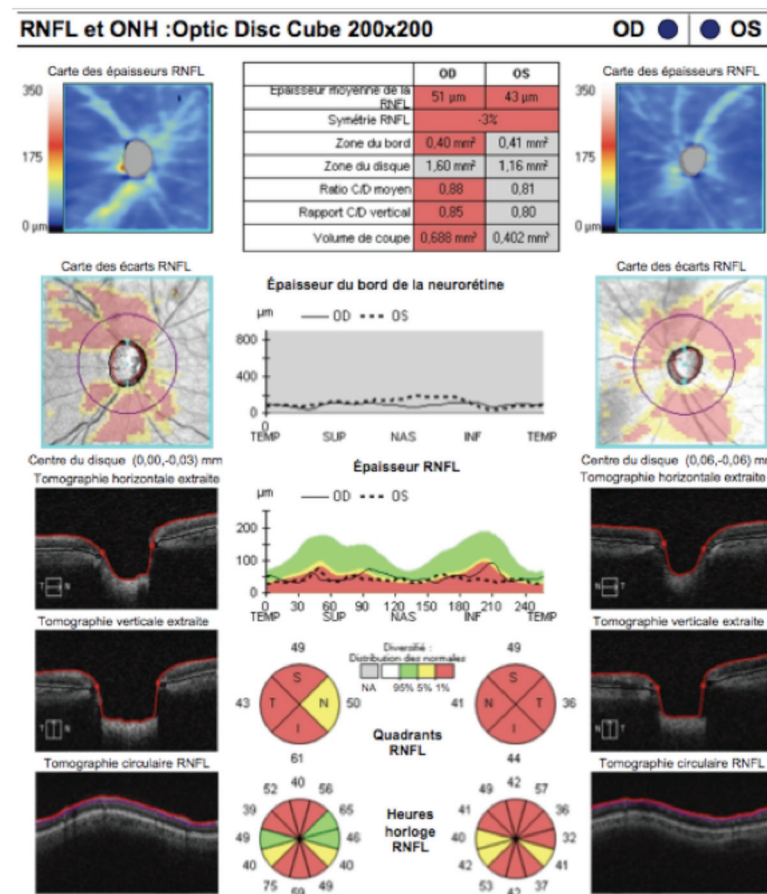
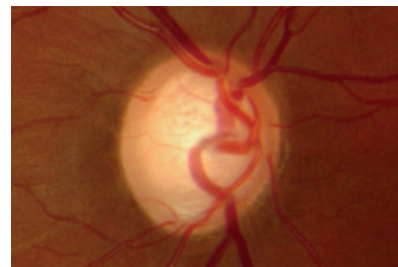
| | OD | OS |
|------------------------------|-----------------------|-----------------------|
| Epaisseur moyenne de la RNFL | 85 μm | 87 μm |
| Symétrie RNFL | 81% | |
| Aire de l'ANR | 1,31 mm ² | 1,29 mm ² |
| Aire du disque | 1,33 mm ² | 1,37 mm ² |
| Rapport C/D moyen | 0,12 | 0,23 |
| Rapport C/D vertical | 0,10 | 0,18 |
| Volume de l'excavation | 0,005 mm ³ | 0,011 mm ³ |

**Épaisseur du bord de la neurorétine**

Limitations

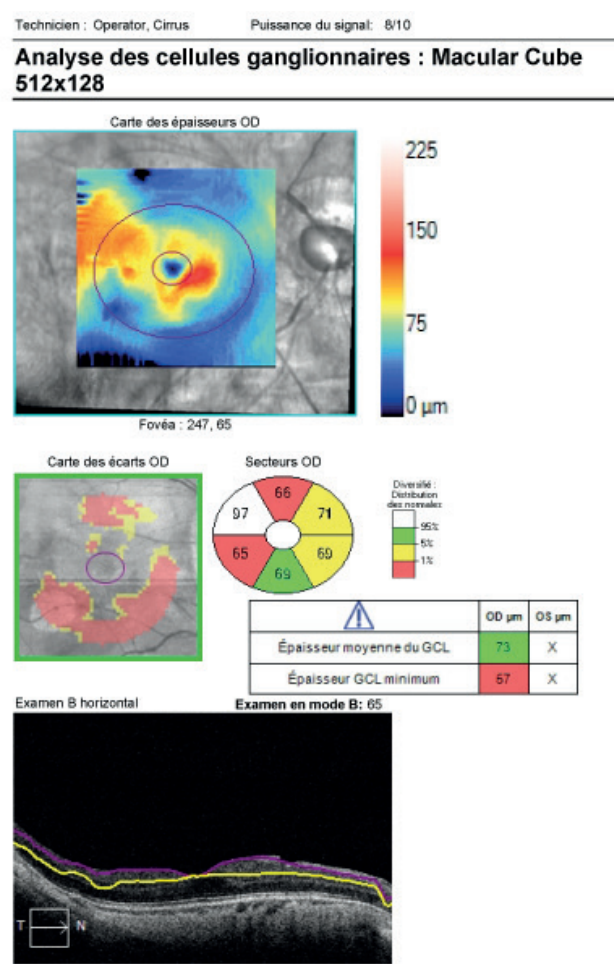
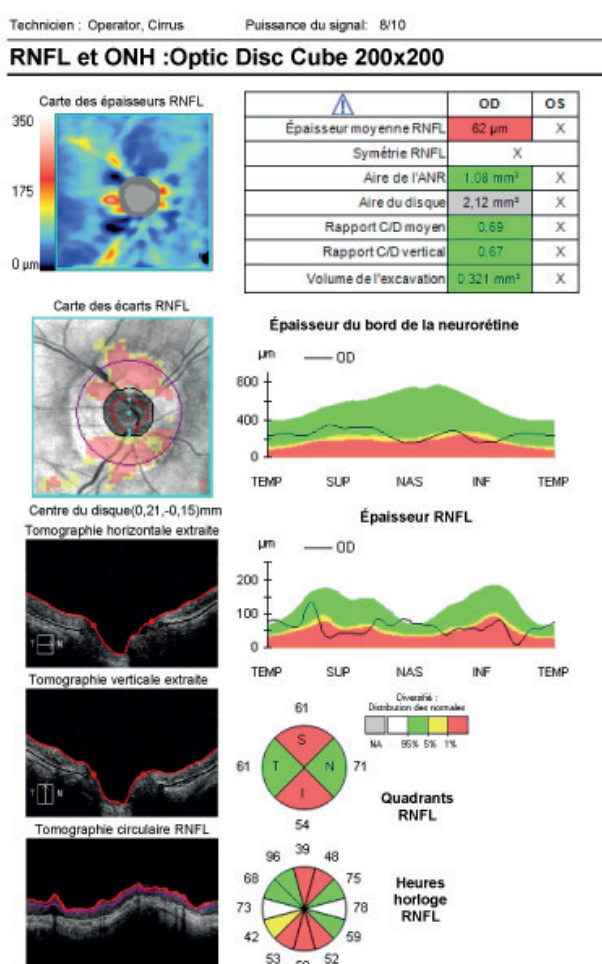
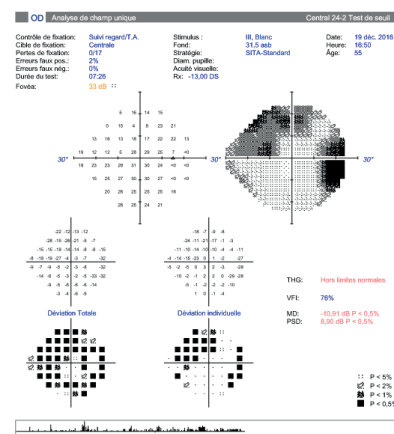
Severe glaucoma

RNFL thickness is never equal to zero microns, because of the persistence of residual glial tissue (\approx 30 to 40 μm): follow-up of the progression of peripapillary RNFL by SD-OCT is no longer possible in the presence of advanced glaucoma.



In patients with high myopia, in this case -15 D, analysis of the peripapillary RNFL is often altered by the presence of a large staphyloma and/or pathological myopia. GCC analysis is preferable in these cases in the absence of myopic macular degeneration.

The RS 3000 is the only SD-OCT system that has developed a normative database for high myopia with axial lengths ranging from 26 to 31 mm.



IN CLINICAL PRACTICE

Limitations

To know the quality of acquisition (SS)

Artefacts (Blurred ocular media, floating bodies, nystagmus, etc.)

Peripapillary atrophy, myopia, etc.

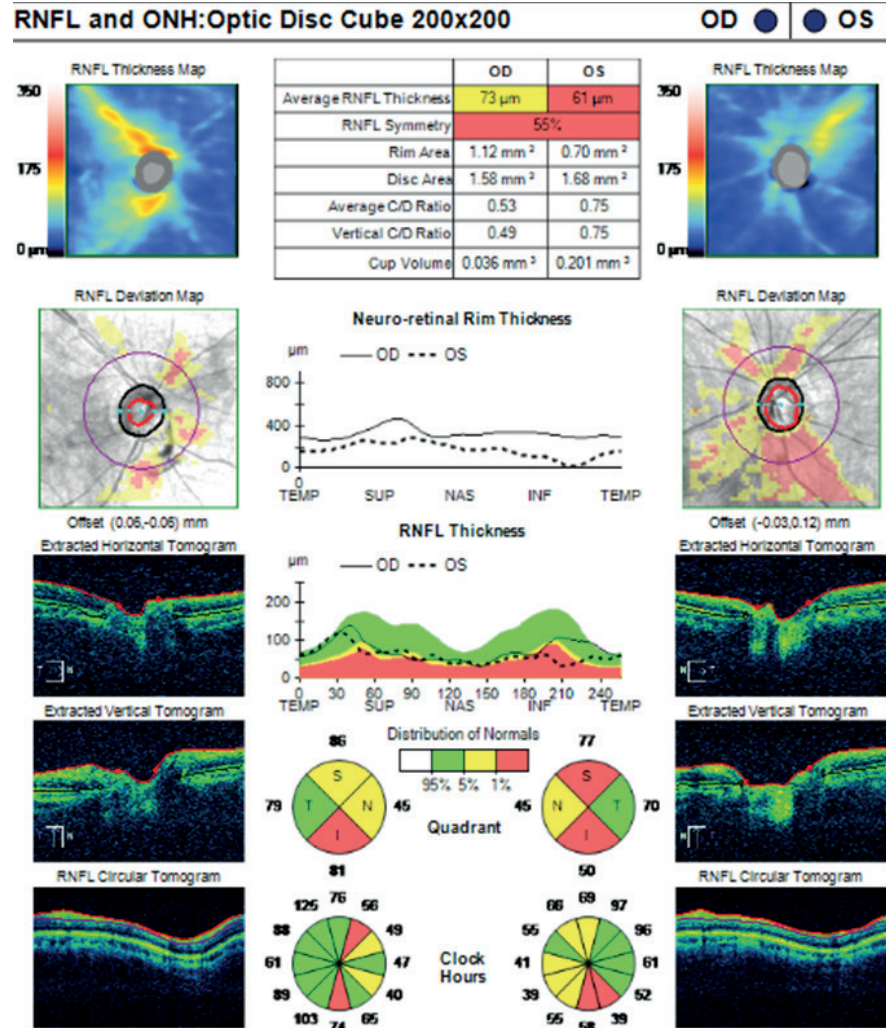
Floor effect of advanced glaucoma

Caution

Colour-coded interpretation

Size of the optic disc: small, large OD

Compare with clinical examination and complementary investigations: visual fields, etc.





4. SD-OCT imaging of the Optic Nerve Head

4.1. Interpretation of the results

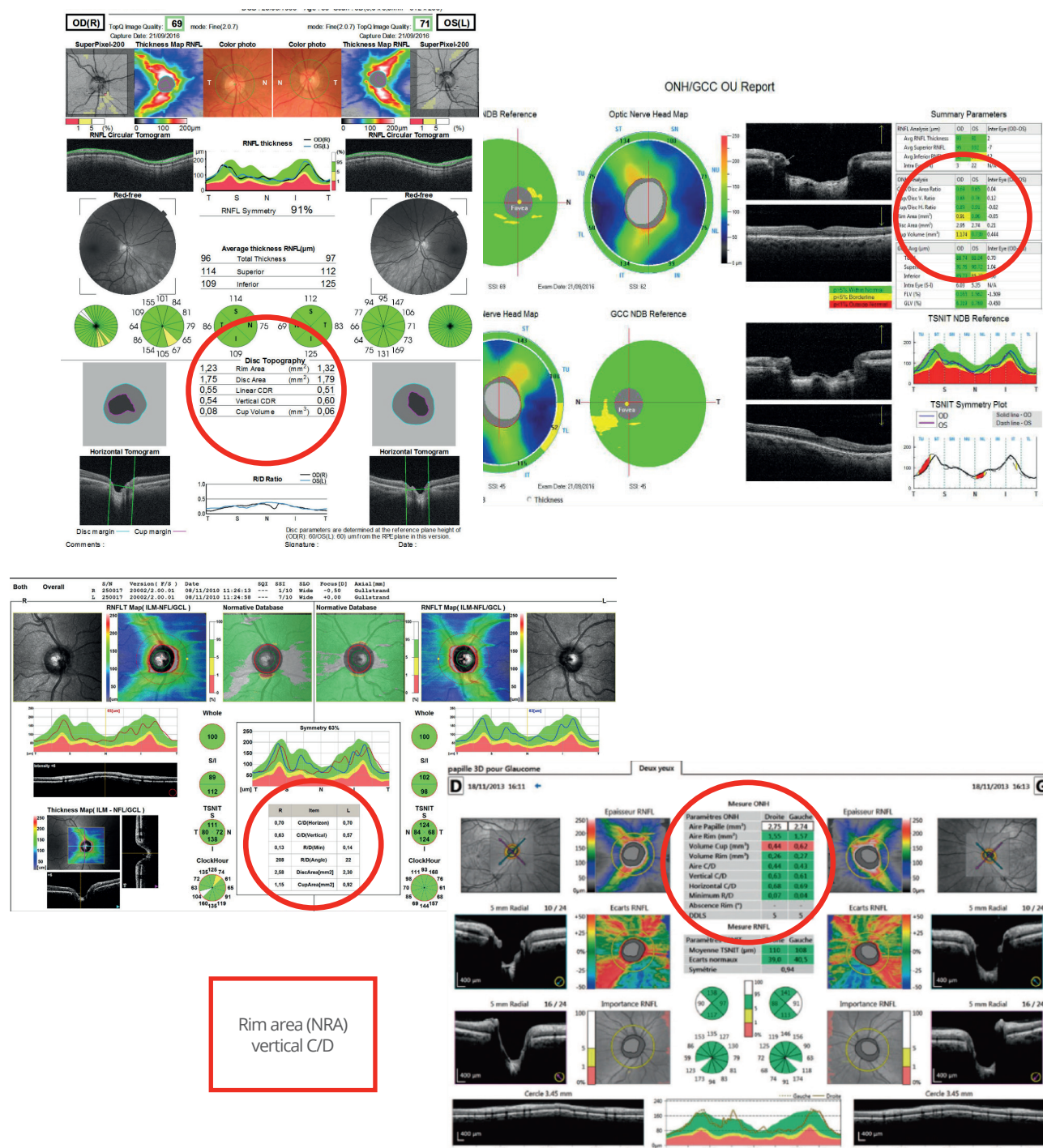
4.2. A new index

4.3. In clinical practice

Interpretation

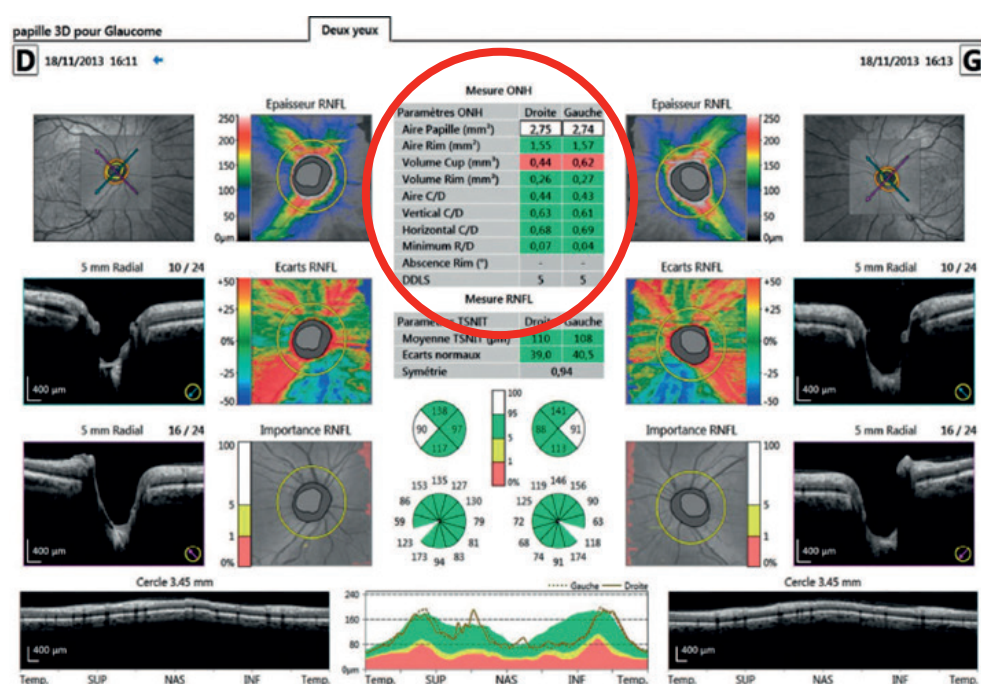
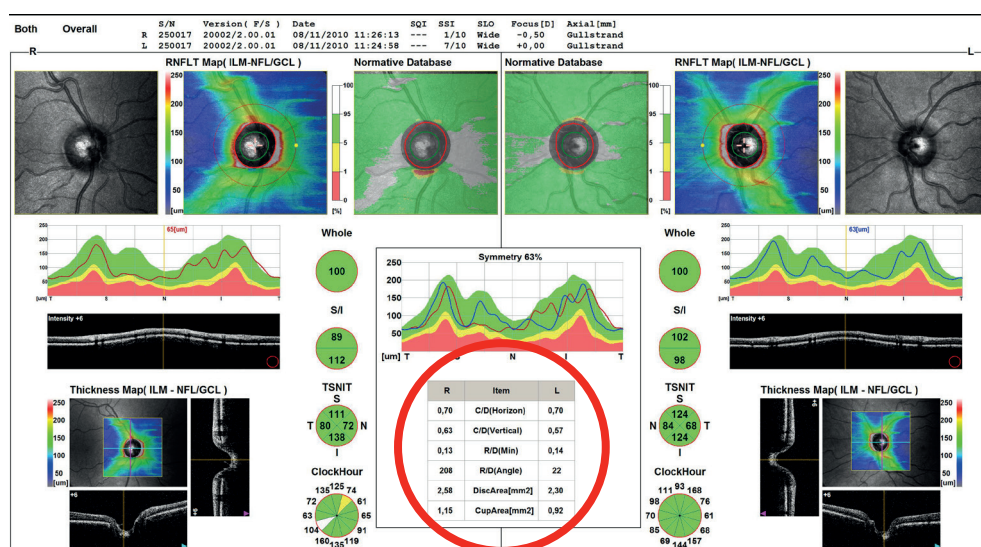
In SD-OCT, volumetric acquisition of the ONH is associated with that of the RNFL. At the early stages of glaucoma, it is difficult to identify an optimal OCT parameter, due to the multiple interindividual anatomical variants of the ONH and the type of initial optic disc lesion.

Analysis of OCT parameters must take into account the clinical appearance of the optic disc and is more useful for follow-up once the diagnosis of glaucoma has been established.



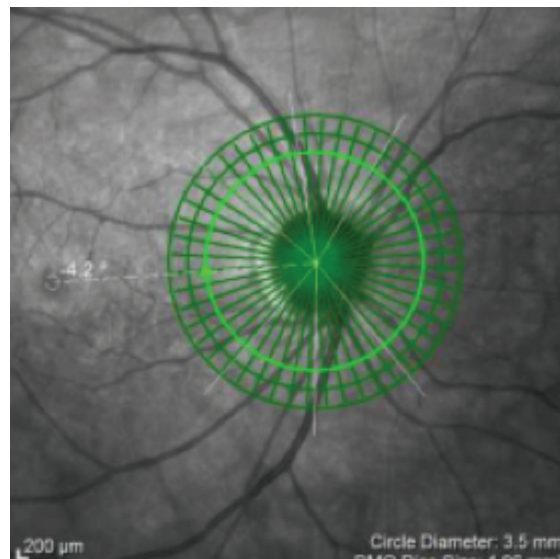
The SD-OCT parameters currently considered to be the most discriminant in ONH are:

- area of the NRR,
- and the vertical C/D ratio.

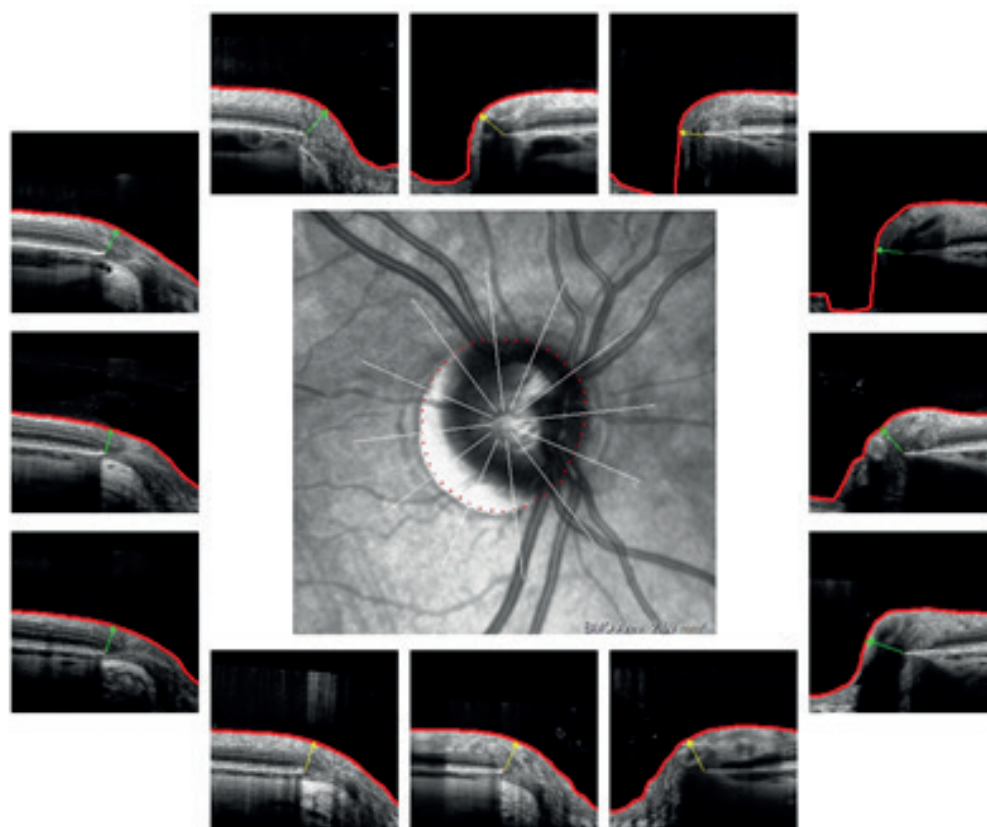


A new index

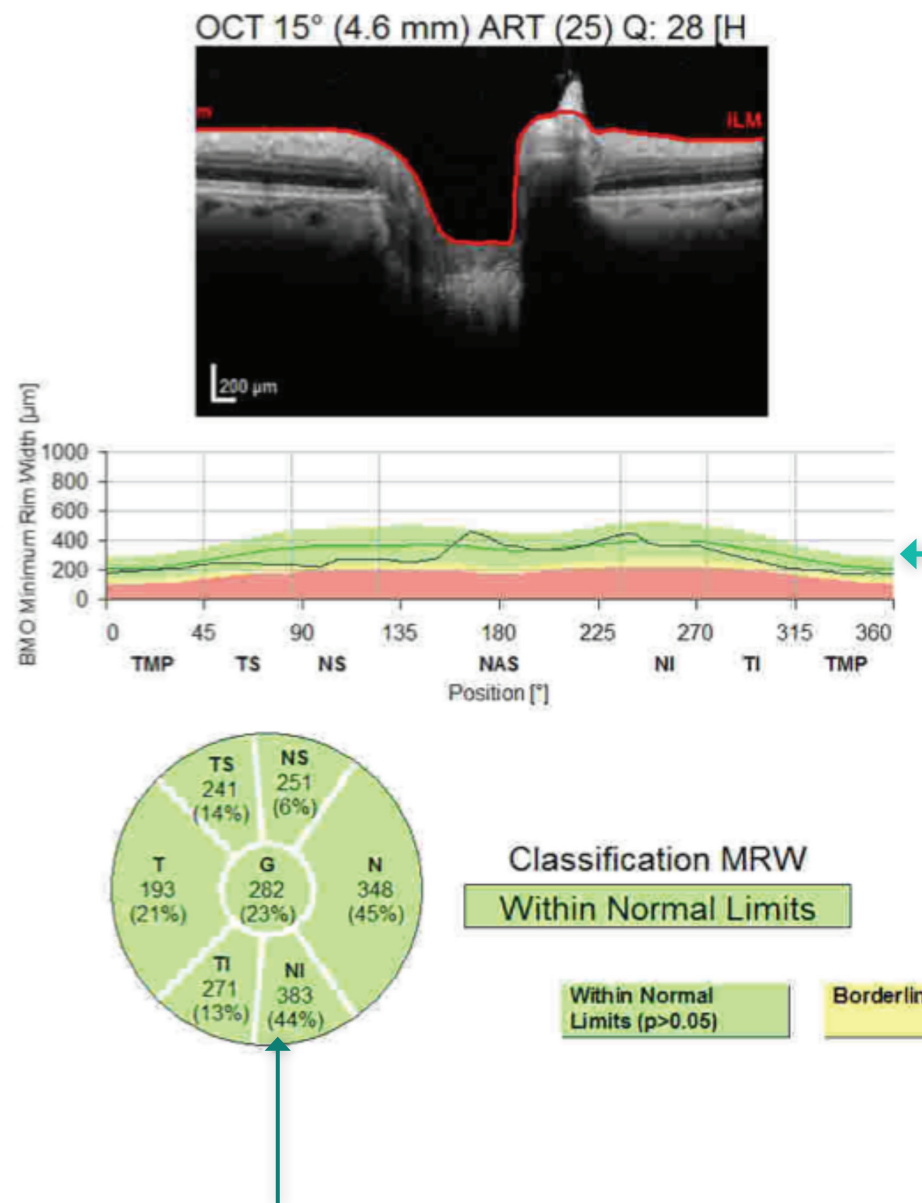
A new ONH index is available on the Spectralis SD-OCT: BMO-MRW, corresponding to minimum rim width at the level of the Bruch's membrane opening (BMO).



24 radial scans centered on the ONH localize the extremities of the BM at 48 points, which are used to determine the minimum rim width, at each point, defining the BMO-MRW index.

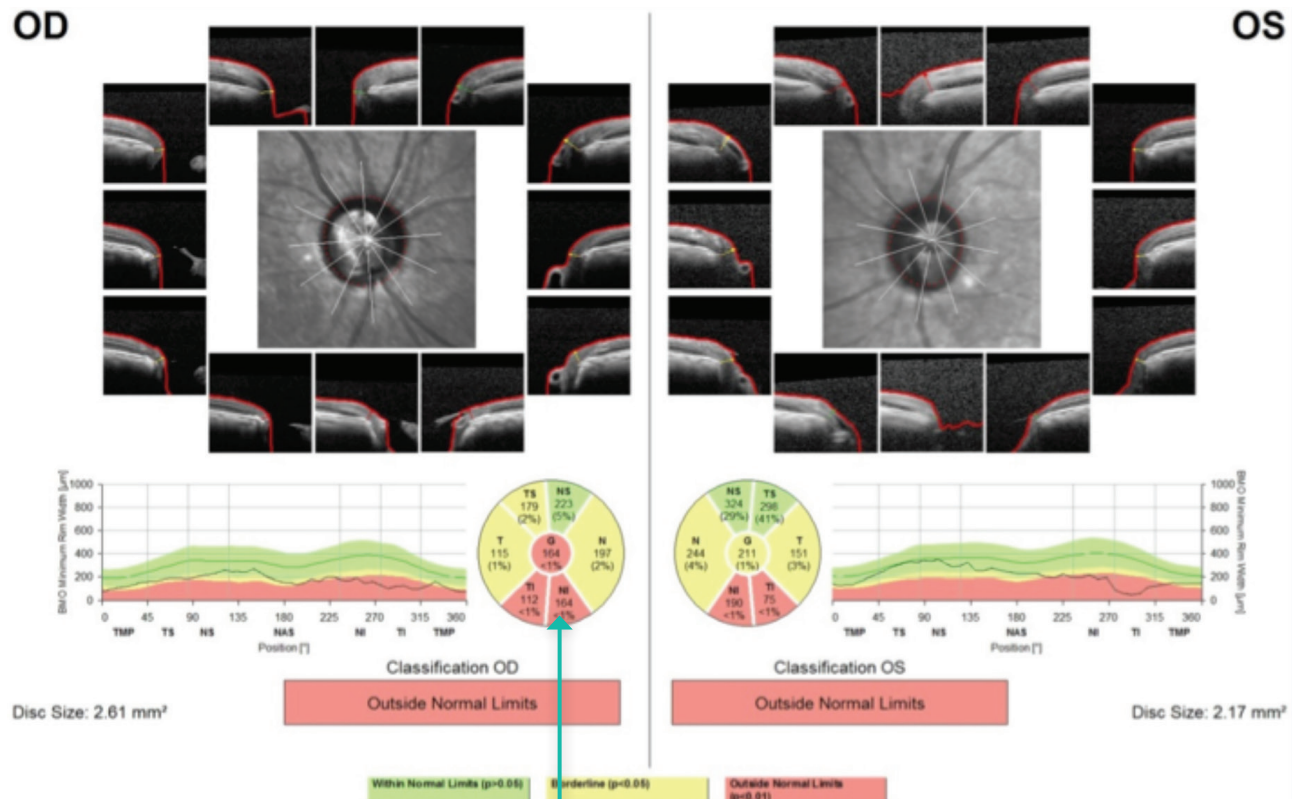


Developed representation of minimum rim width (MRW) at the extremities of BM on the ONH with analysis based on a normative database of age-matched subjects.

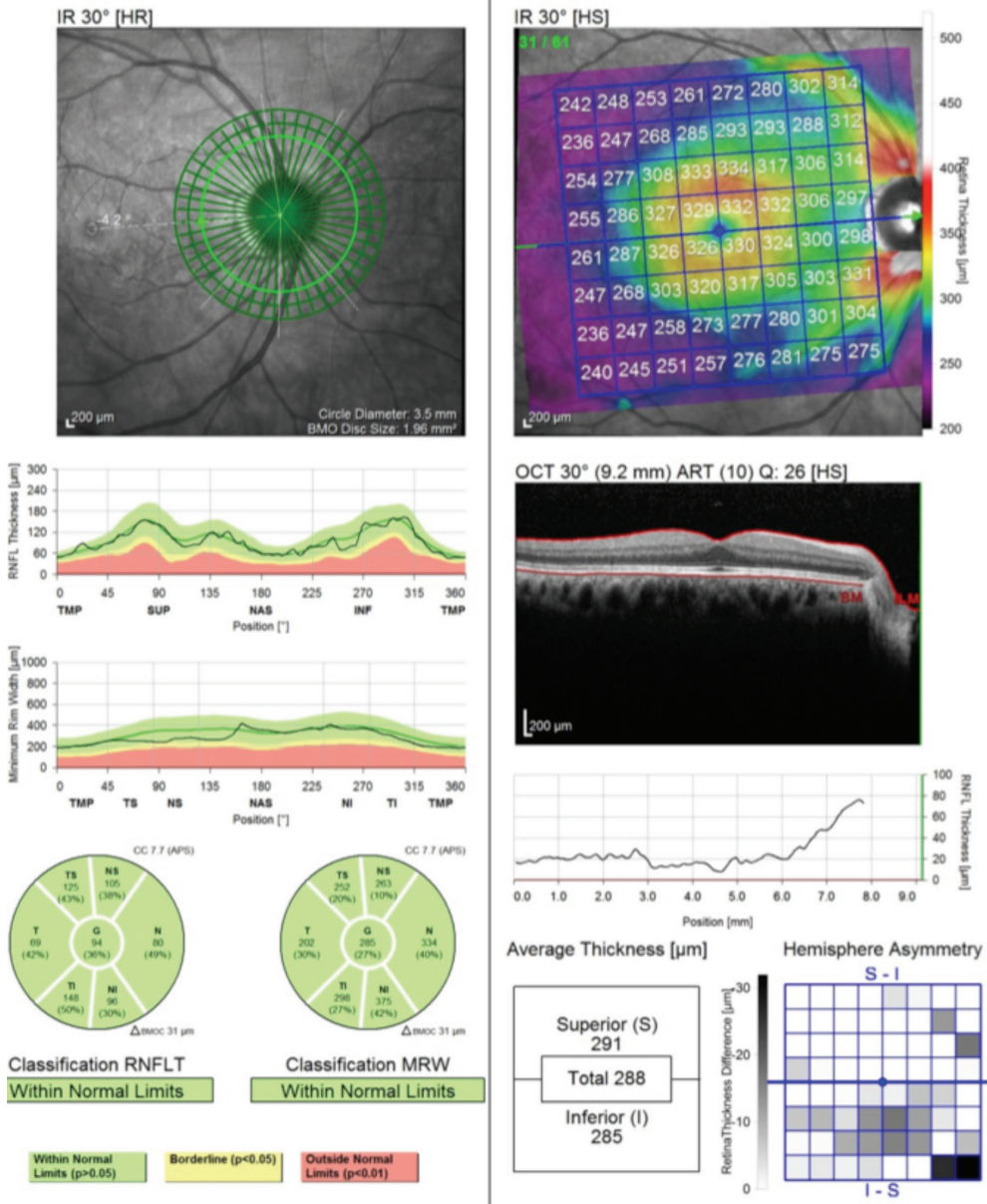


Evaluation of the mean index (G) and in 6 sectors of the ONH and comparative analysis of the results with the normative database.

A new index



High diagnostic sensitivity of the value of the mean global (G) and inferior temporal BMO-MRW at the early stages of glaucoma based on comparative analysis of the result with those of the normative database.



Spectralis SD-OCT analysis of RNFL and MRW of the ONH.

SD-OCT analysis of the ONH

IN CLINICAL PRACTICE

Limitations

Tilted disc syndrome, drusen...

Optic disc anomalies

High myopia

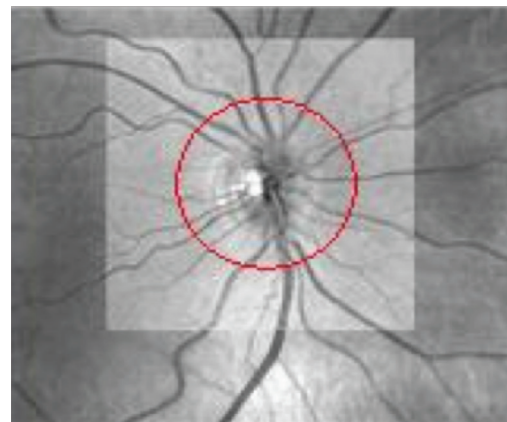
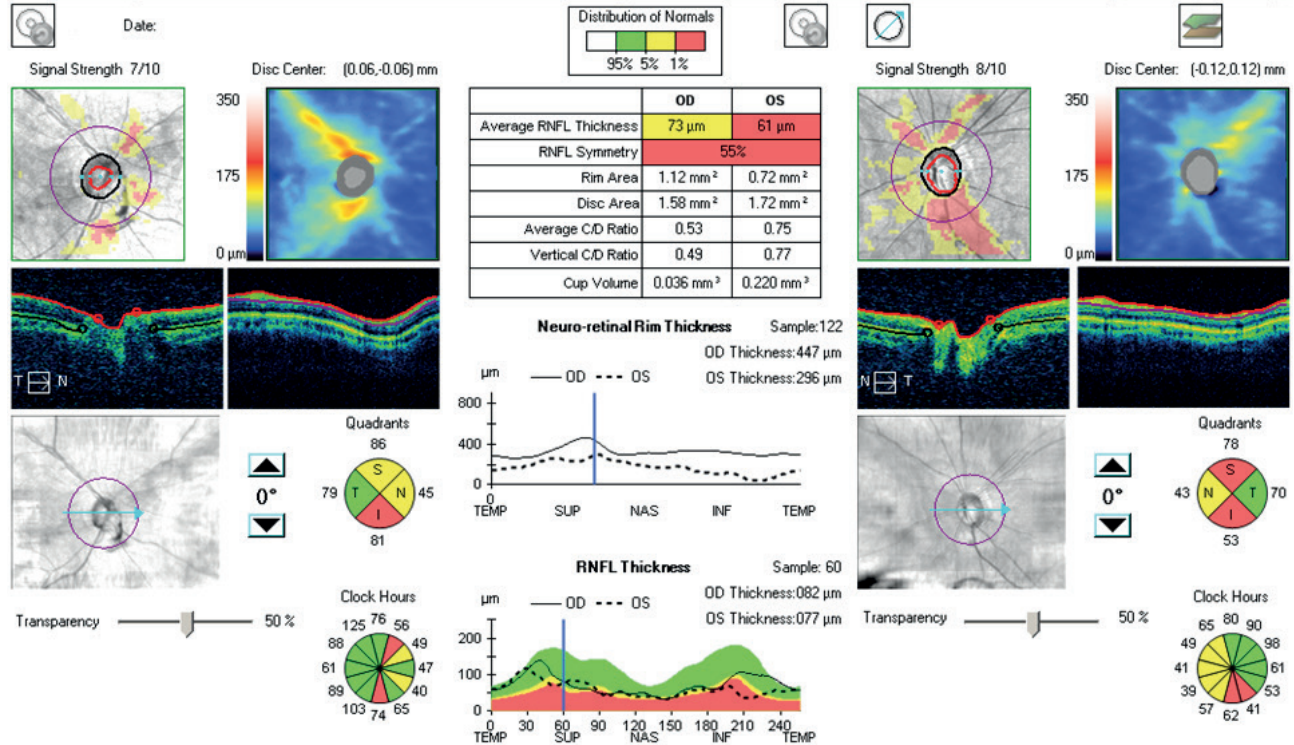
Caution

Asymmetrical left eye/right eye lesions = Warning sign,

Small, large OD

Reliable parameters: RIM area, vertical C/D ratio

Less relevant than RNFL and GCC analysis for early diagnosis





5. Macular ganglion cell complex analysis

- 5.1. Various types of SD-OCT analysis**
- 5.2. Interpretation of the results**
- 5.3. Complementary indices**
- 5.4. Mapping of macular defects**
- 5.5. In clinical practice**

Macular ganglion cell complex analysis

The prevalence of early macular glaucomatous lesions, similar to that of extramacular lesions, justifies analysis of the macular ganglion cell complex (GCC), which represents the highest concentration of ganglion cells on about the central 8 degrees of the foveola, with a relatively constant and simple macular structure, with less anatomical variability (macular slope) than the other structures analysed by OCT (RNFL and ONH).

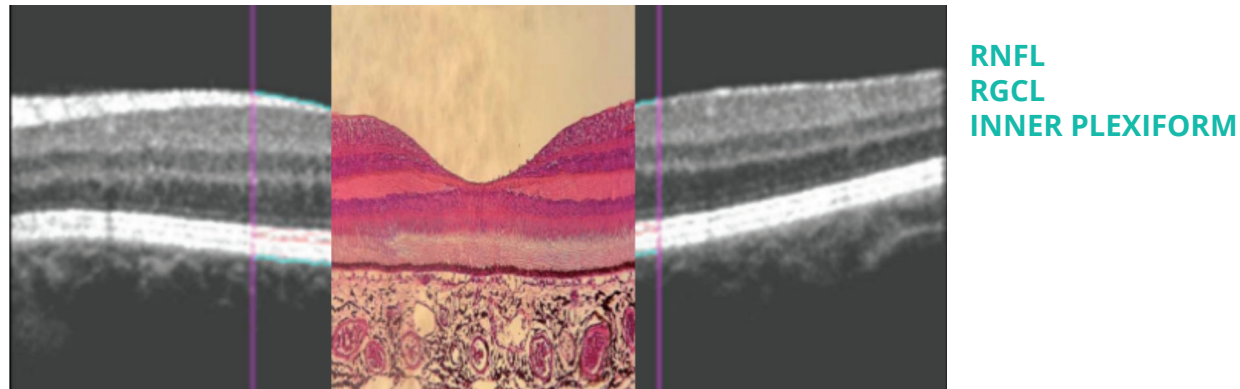
The GCC complex comprises the 3 innermost layers of the retina:

- RNFL,
- Retinal ganglion cell (RGC) layer,
- inner plexiform layer (IPL).

The GCC has the advantage of relatively invariable imaging of the central retina, avoiding the confounding effect of optic disc variability.

All SD-OCT devices comprise a GCC analysis programme, but the acquisition programmes, the various image analysis algorithms and the data acquired are specific to each type of SD-OCT.

Each SD-OCT comprises an analysis programme of either all layers of the GCC, or only 2 layers, or of each layer of the GCC.



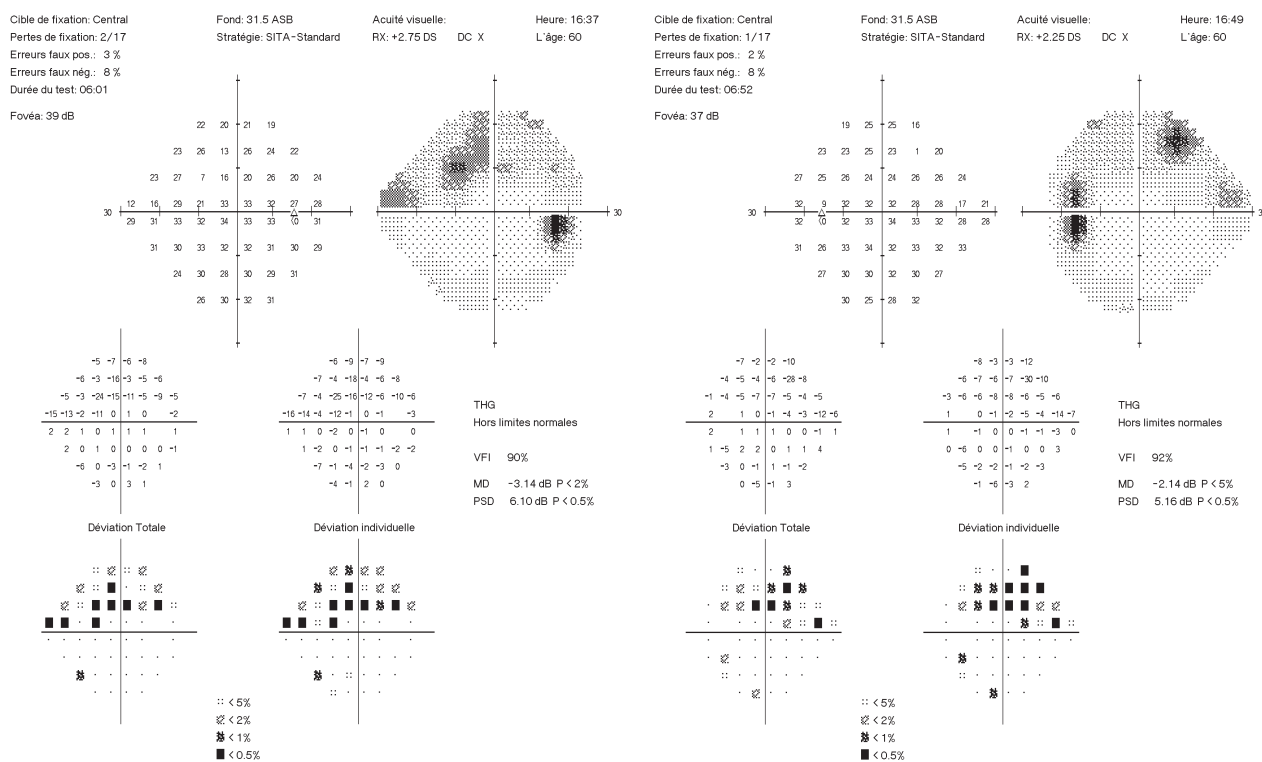
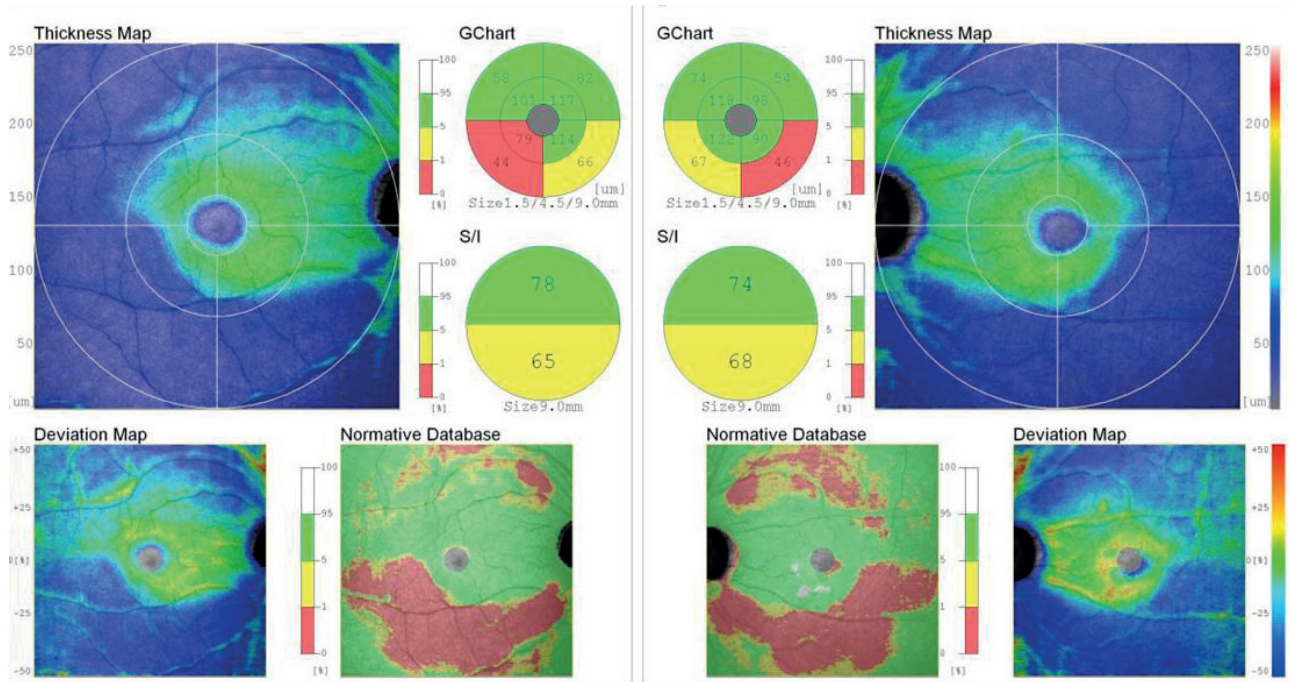
Various types of analysis according to the SD-OCT device

Nidek RS 3000 SD-OCT

Global analysis of the 3 layers of the GCC: RNFL, RGC, Inner plexiform

The Nidek RS 3000 SD-OCT analyses the 3 layers of the GCC, on a large 9 x 9 mm acquisition cube. The case illustrated here presents an inferior macular lesion, predominantly involving the inferior temporal sector, which is well correlated with the functional impairment in the superior Bjerrum areas of the visual field, in a 70-year-old man followed and treated for POAG by dual therapy.

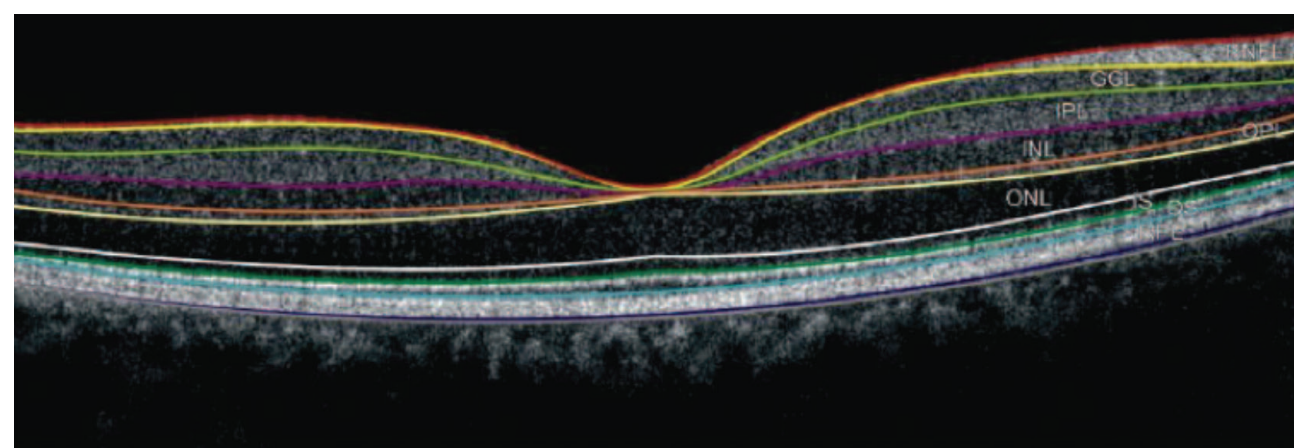
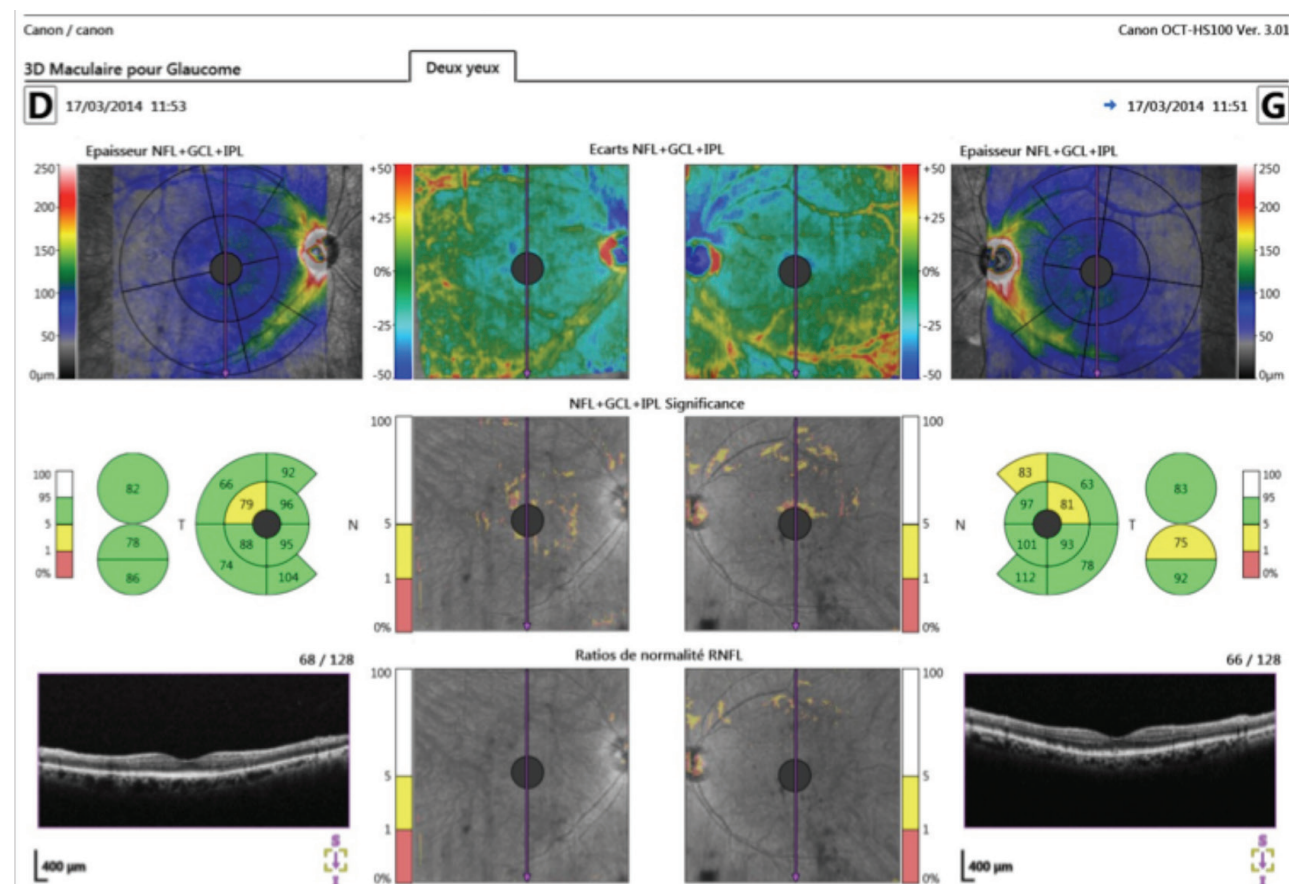
EARLY POAG



Various types of analysis according to the SD-OCT device

Canon HS-100 SD-OCT

Global analysis of the 3 layers of the GCC: RNFL, RGC, Inner plexiform

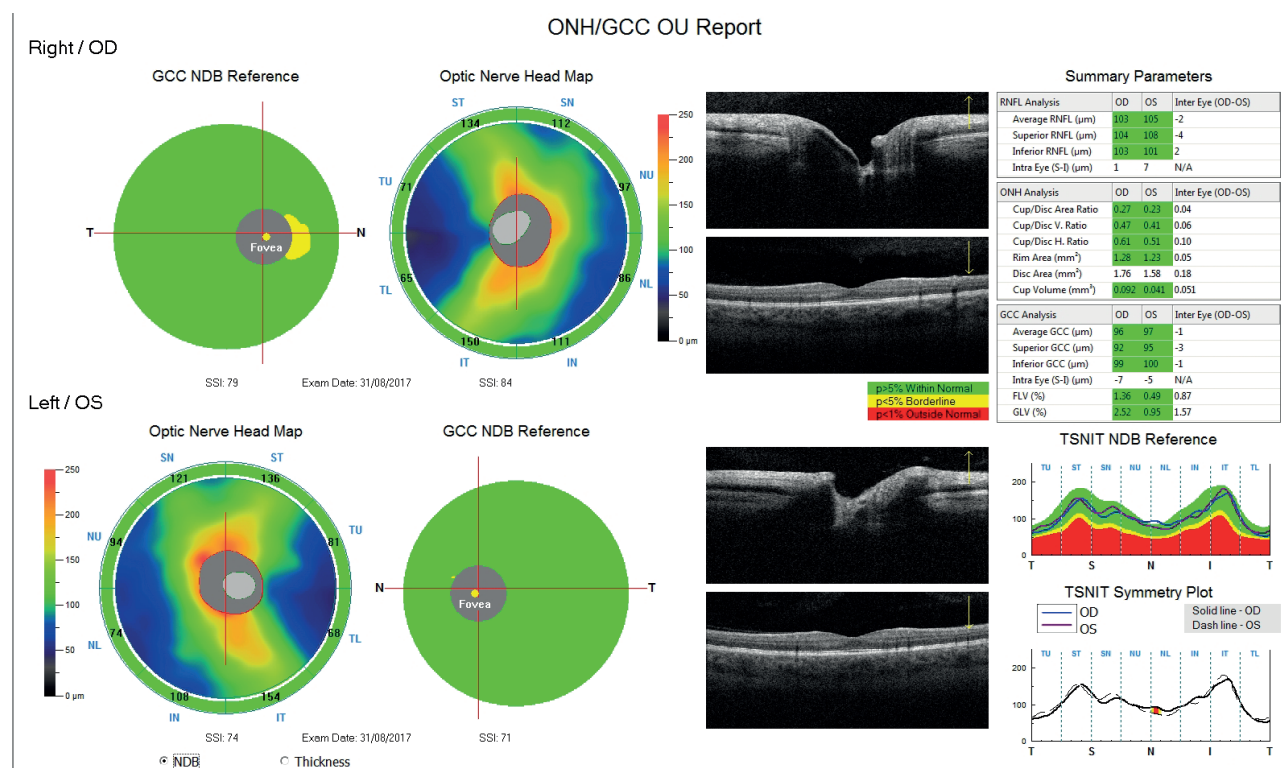


XR AVANTI SD-OCT

Analysis of the 3 layers of the GCC: RNFL, RGC, Inner plexiform

+ Complementary indices:

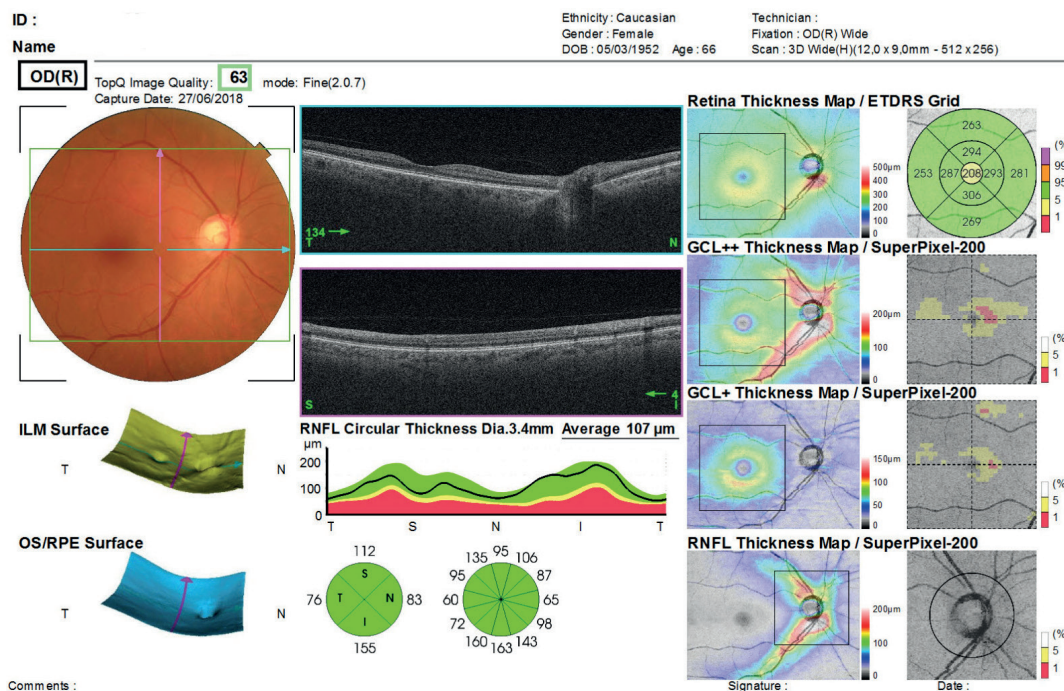
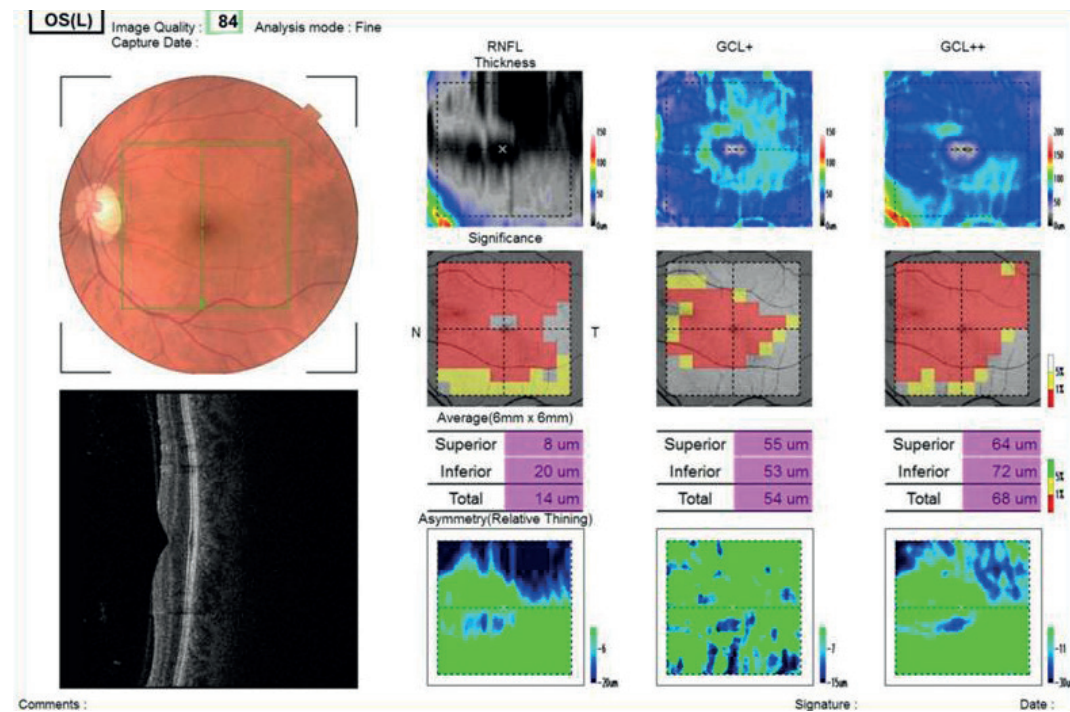
- **FLV (Focal Loss Volume)** = percentage volume of significant focal loss on all of the GCC map analysed.
- **GLV (Global Loss Volume)** = percentage of the mean volume of ganglion cells lost on all of the GCC map analysed.



Various types of analysis according to the SD-OCT device

Topcon Triton SD-OCT

Analysis of each layer of the GCC: RNFL, RGC, Inner plexiform

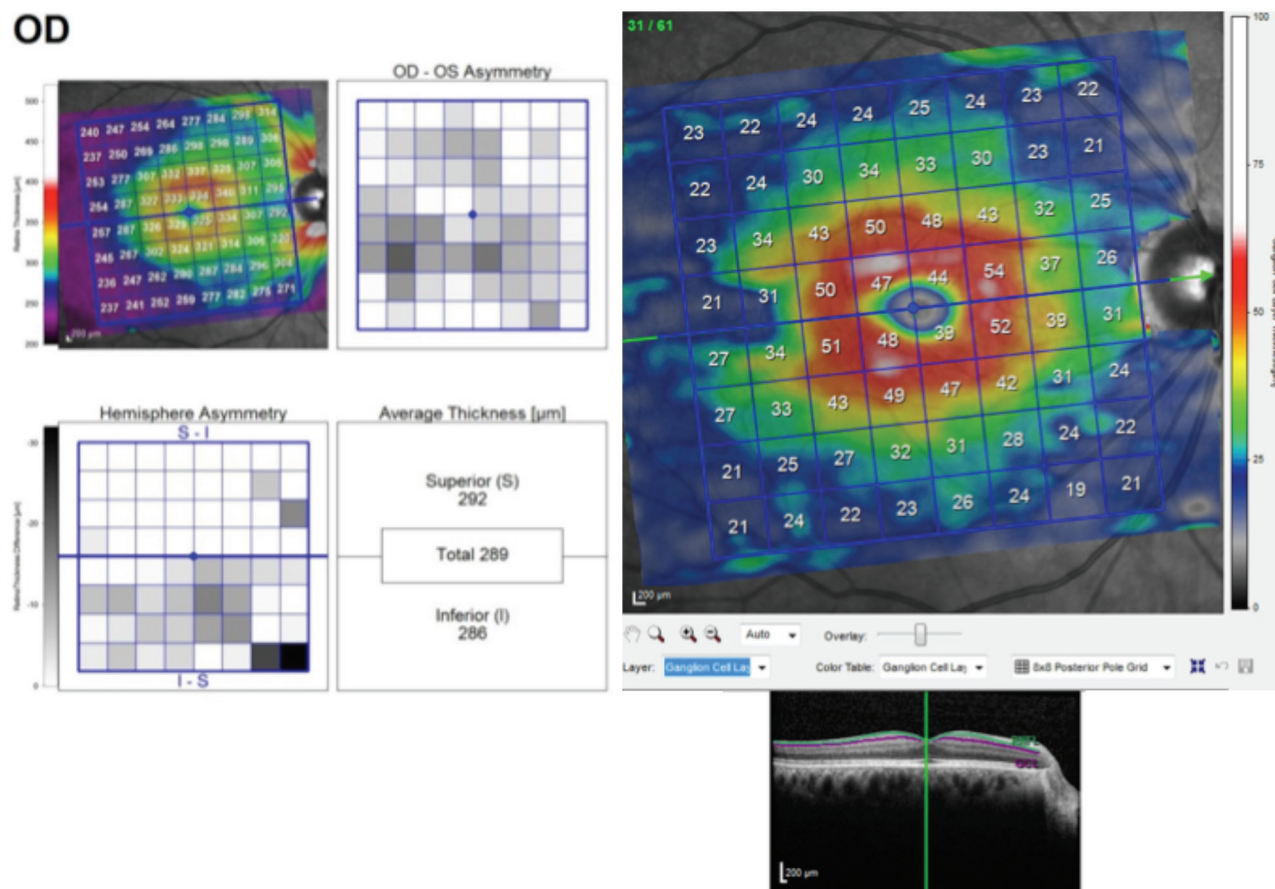


Acquisition of a 12 x 9 mm cube, global analysis of GCC and RNFL

Heidelberg Spectralis SD-OCT

Separate analysis of each layer of the GCC: RNFL, RGC, Inner plexiform, according to the fovea-centre axis of the optic disc

Evaluation of glaucoma progression indicated by the numerical difference of the ganglion cell complex thickness compared to the patient's first reference examination, but without time trend analysis that would specify a slope of progression.



Various types of analysis according to the SD-OCT device

Zeiss Cirrus HD-OCT SD-OCT

Analysis of the GCL complex or ganglion cell + inner plexiform layer (GCIPL) due to the interindividual variability of the topographic arrangement of the RNFL in the posterior pole.

Measurement of the mean thickness of the GCL complex and the minimum thickness of the GCL complex.

The **minimum GCL** index corresponds to the radius of the radial measurement of the GCL complex from the fovea, with the smallest mean value on all of the 360 radii of measurement of the elliptical zone recorded. **This marker is well correlated with an early lesion of the GCL complex with demonstrated diagnostic sensitivity in the early stages of glaucoma.**

EXCELLENT REPRODUCIBILITY

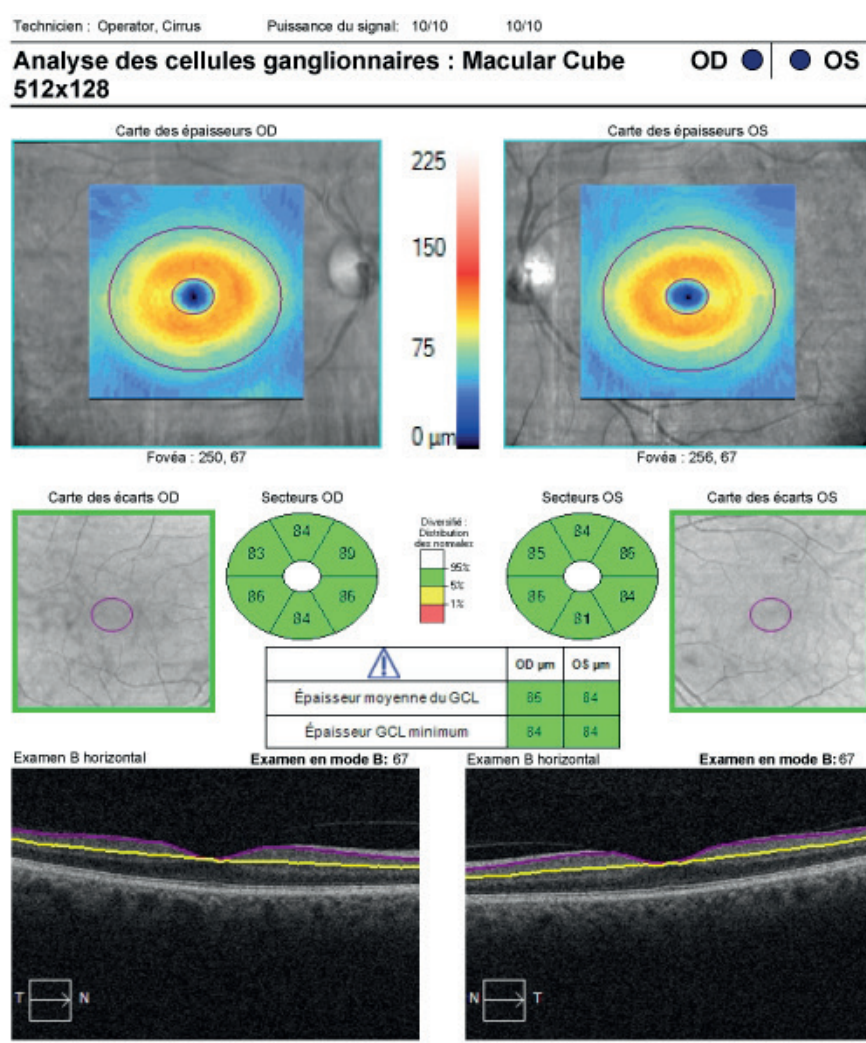
| | Intra-observer reproducibility | Inter-observer reproducibility |
|----------------------------|--|--|
| Controls | ICC: 99.7 %-99.8 % CV: 0.7 %-0.8 % TRTV: 1 µm-1.1 µm | ICC: 99.1 % CV: 2.2% TRTV: 1.1 µm |
| Ocular hypertension | ICC 99.6 %-99.9 % CV 0.7 %-0.8 % 1.1 µm-0.6 µm | ICC: 99.7% CV: 1.1 % TRTV: 0.84 µm |
| POAG | ICC: 99.5 %-99.8 % CV: 0.7 %-0.8 % TRTV: 1.2 µm-0.9 µm | ICC: 99.2% CV: 2.1 % TRTV: 1.1 µm |

ICC: intraclass correlation coefficient

CV: coefficient of variation

TRTV: test-retest variability

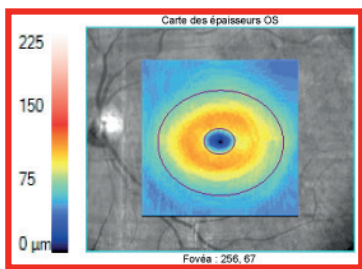
Francoz M et al. Reproducibility of macular GCIPL thickness measurement with Cirrus HD-OCT in normal, hypertensive and glaucomatous eyes. Br J Ophthalmol. 2014;98:322-8.



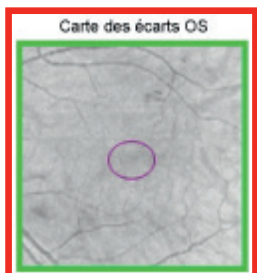
Interpretation

Puissance du signal: 10/10 10/10

The **signal score or signal strength** must be checked to ensure compliance with the minimum signal quality values specific to each device.



Thickness map. Assessment and analysis of the regular or irregular distribution in the various sectors can highlight zones with early or advanced defects and directly visualize large lesions that often involve only one hemifield and spare the median raphe. Early lesions are generally more marked in the temporal sector, especially in the inferior temporal sector.



Deviation map in the zone of analysis displayed below. Yellow and red pixels correspond to abnormal thinning for age at $p<0.05$ or $p<0.01$. An early lesion of the inferior temporal sector, frequently the first sector affected by thinning in early glaucoma, must be systematically investigated.

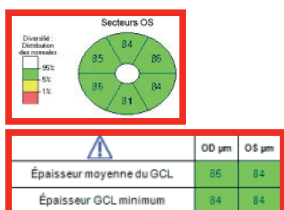
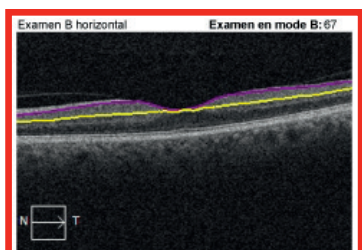
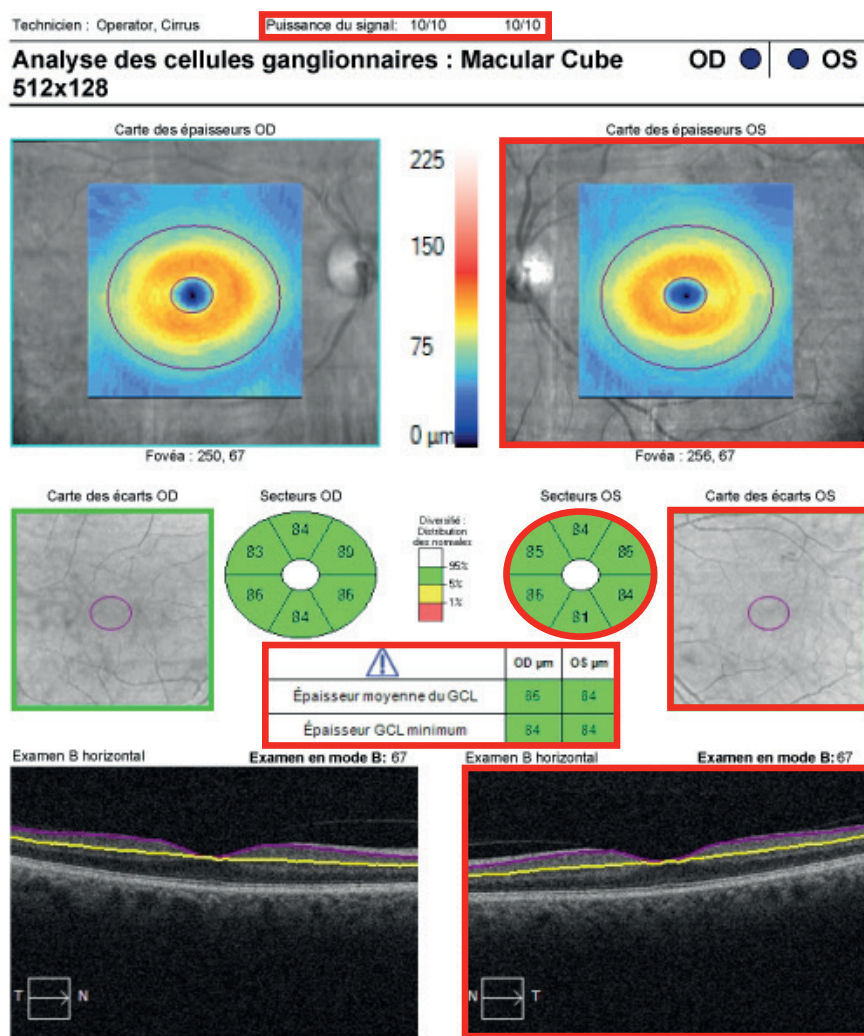


Table of the various parameters: mean thickness; superior and inferior sectoral macular thickness according to the OCT device's; supplementary values for certain SD-OCT systems (minimum GCL with Cirrus HD-OCT, GLV and FLV with XR Avanti).

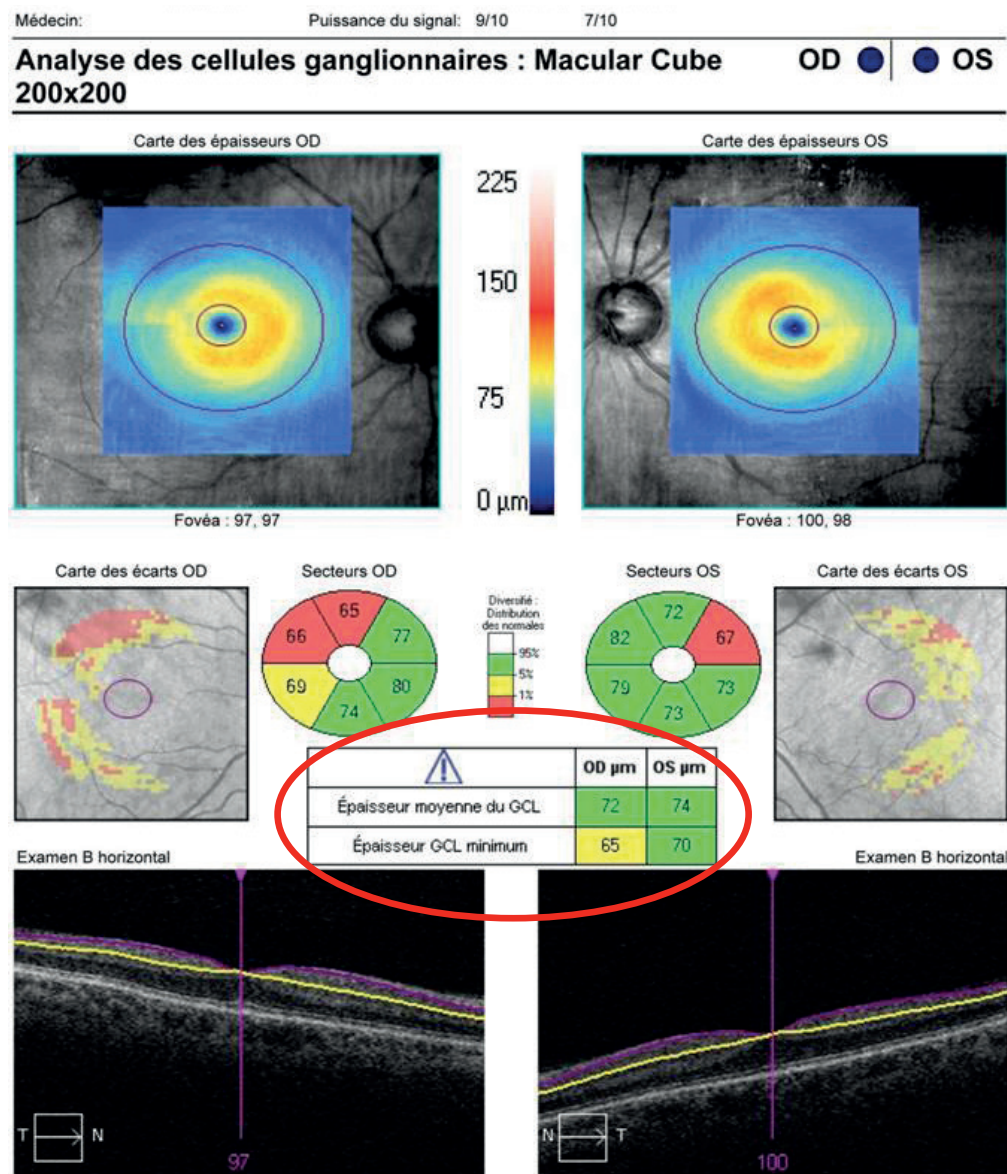


Horizontal B-scan: confirms the good quality of segmentation of ganglion cell and inner plexiform layers by the software and ensures the normal appearance of the macular profile.

Colour-coded analysis of the results must comply with the same rules as analysis of the peripapillary RNFL.

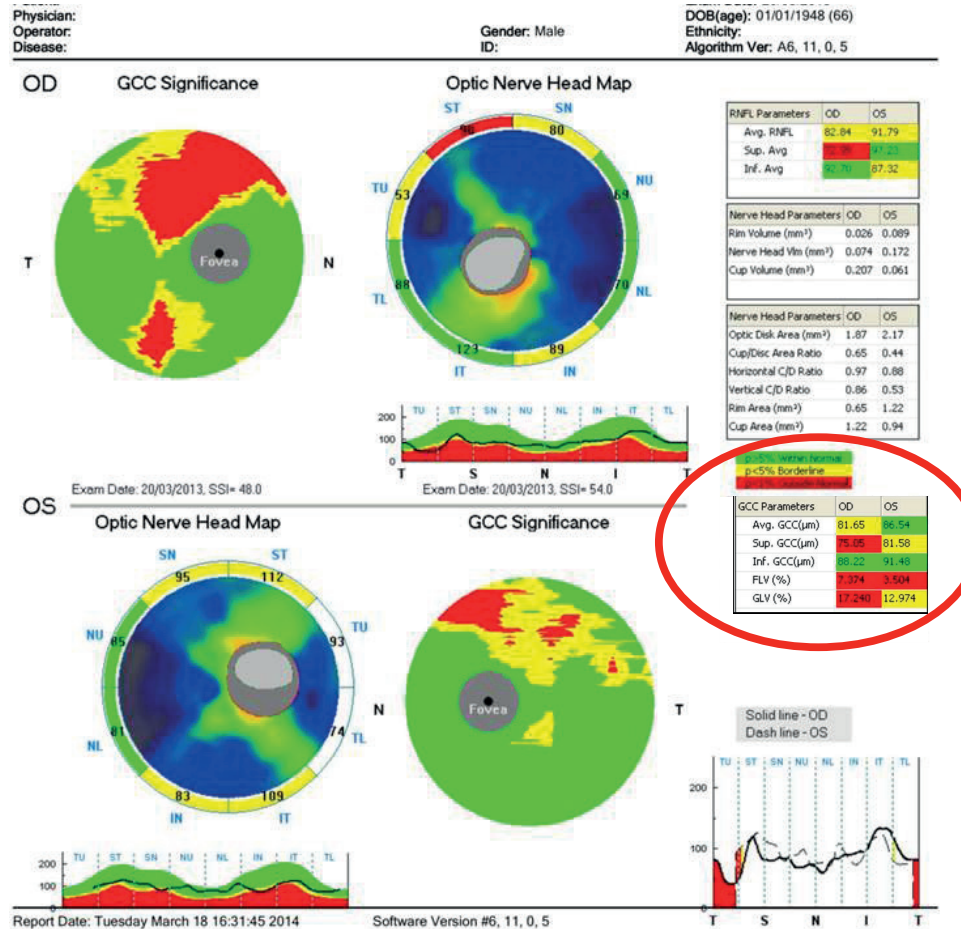


Complementary indices



| ⚠ | OD μm | OS μm |
|--------------------------|-------|-------|
| Épaisseur moyenne du GCL | 72 | 74 |
| Épaisseur GCL minimum | 65 | 70 |

Zeiss Cirrus HD-OCT
Minimum GCL or GCIPL



| GCC Parameters | OD | OS |
|----------------|--------|--------|
| Avg. GCC(μm) | 81.65 | 86.54 |
| Sup. GCC(μm) | 75.05 | 81.58 |
| Inf. GCC(μm) | 88.22 | 91.48 |
| FLV (%) | 7.374 | 3.504 |
| GLV (%) | 17.240 | 12.974 |

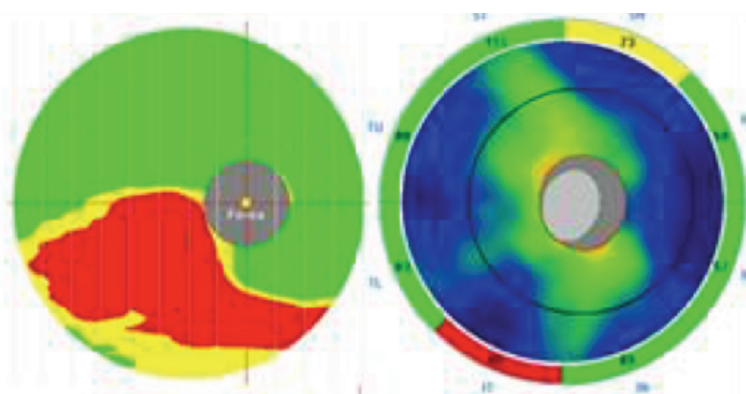
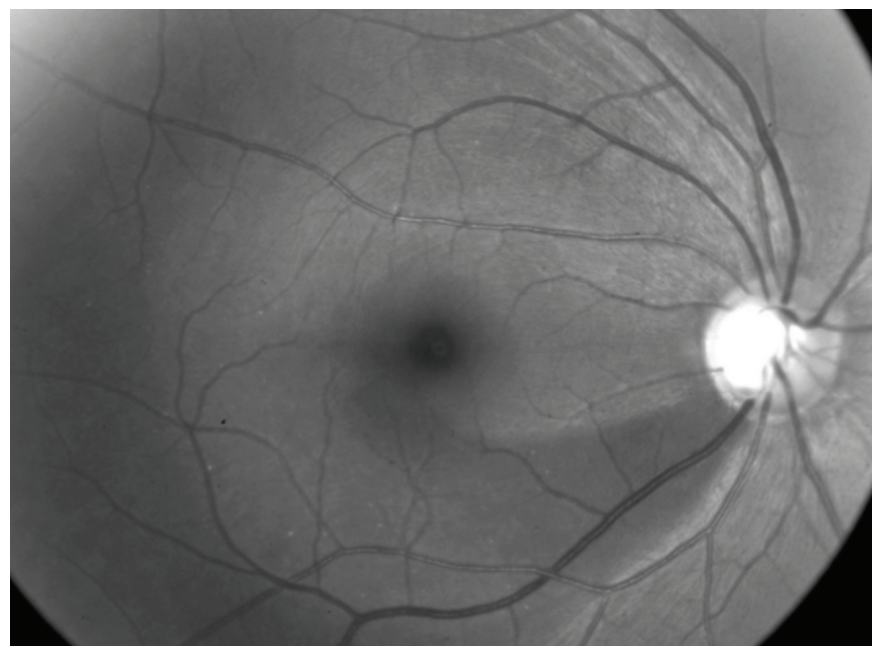
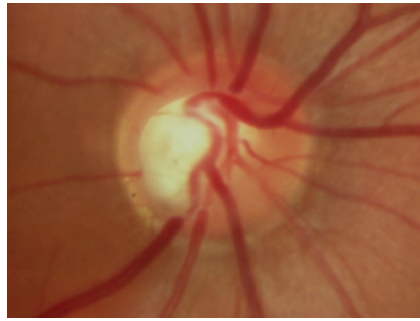
XR Avanti Optovue
FLV (Focal Loss Volume)
GLV (Global Loss Volume)

The diagnostic sensitivity of these complementary indices has been clearly demonstrated in early structural lesions associated with early forms of glaucoma.

Macular defect mapping

Macular defect mapping has been more clearly defined and comprises five essential points:

- high sensitivity for the temporal macular region,
- more frequent involvement of the inferior temporal sector and inferior macular sector,
- arcuate appearance of macular defects continuous with peripapillary RNFL (pRNFL) defects,
- projection of inferior macular defects onto the 7 and 8 o'clock meridians of the ONH's OD, and onto the 4 and 5 o'clock of the ONH's OG, described as the macular vulnerability zones,
- lastly, the high diagnostic sensitivity of complementary indices (minimum GCL, FLV, GLV).



Analysis of the macular GCC

IN CLINICAL PRACTICE

Limitations

To know the quality of SSI acquisition
Artefacts (opaque media, etc.)
Macular disease (drusen, etc.)
Always in combination with macular examination
Check good segmentation

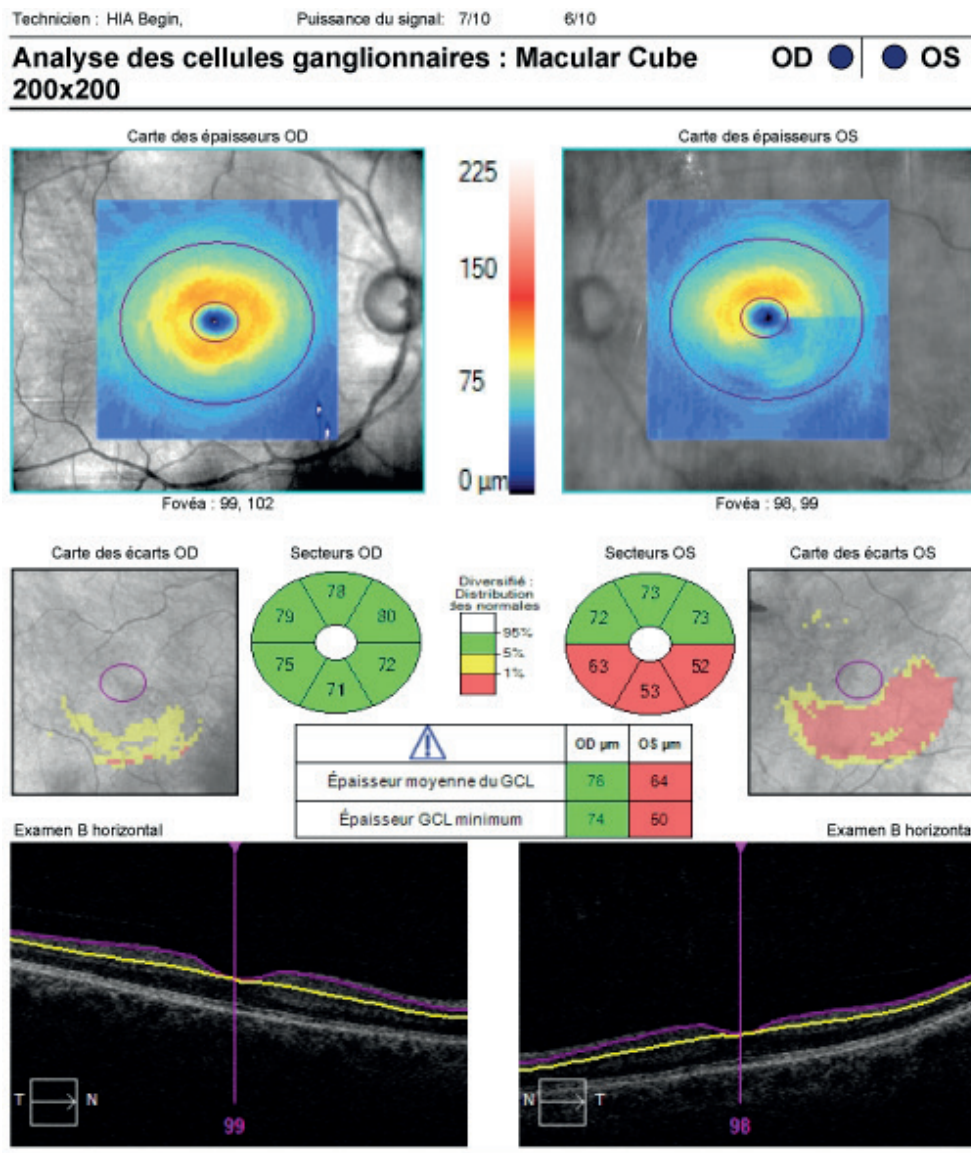
Caution

Interpretation of local indices
In the presence of isolated deterioration:

- Compare with RNFL analysis
- Compare with clinical findings (AMD, etc.)

Advantages

Better reproducibility





6. SD-OCT interpretation recommendations

Interpretation recommendations

Interest of the pRNFL, BMO-MRW, GCIPL, FLV, GLV and GCC parameters for the detection of glaucoma has been clearly established.

The following factors must always be taken into account:

Patient-related factors

Refraction

RNFL and GCC thickness values are generally lower in myopic subjects and higher in hypermetropic subjects.

Axial length

Any increase in the axial length of the eyeball is accompanied by an overall reduction of RNFL thickness by 2.2 µm per millimetre.

Size and variations of the optic disc

A small diameter disc induces a reduction of the measured RNFL thickness because of the circle of measurement, which is always 3.4 mm from the centre of the OD and therefore situated in a sector in which the RNFL is more spread out. Measurements on a large diameter optic disc are performed closer to the edge of the disc, in a sector in which the RNFL is thicker. GCC analysis has the advantage of allowing independent evaluation of these anatomical variants.



In the presence of any disc anomalies, tilted disc syndrome and peripapillary atrophy, GCC analysis also allows independent evaluation of these anatomical variants.

Color code

SD-OCT-related factors

SS quality index

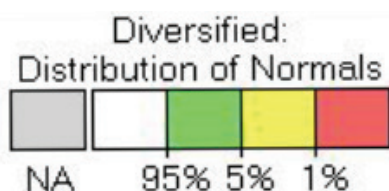
Colour coding must be interpreted cautiously

Although all of the OCT devices currently available present globally comparable good sensitivity and specificity, these values never reach 100%.

The results are compared to data of the SD-OCT normative database according to age and ethnic group.

- The white colour indicates that the thickness values are higher than the limits of the confidence interval (5% of subjects present higher thickness values). These results generally correspond to normal subjects or subjects with other diseases (papilloedema, vitreopapillary adhesion and traction, etc.) responsible for thickening of the RNFL.
- The green colour indicates a 95% probability of a normal value, and should be considered to be normal.
- The yellow colour indicates a probability of a normal measurement of less than 5% probability of a normal result (suspicious value).
- The red colour $p < 0.01$ corresponds to a probability of a normal measurement of less than 1%, and must be considered to be statistically abnormal.
- Colour-coded results must be interpreted cautiously, as they are expressed in relation to a normative database specific to each SD-OCT device often based on a limited number of subjects per decade, which does not cover all possible variations that can be observed in the population.

It is therefore essential to systematically compare OCT results with clinical data.



Interpretation recommendations

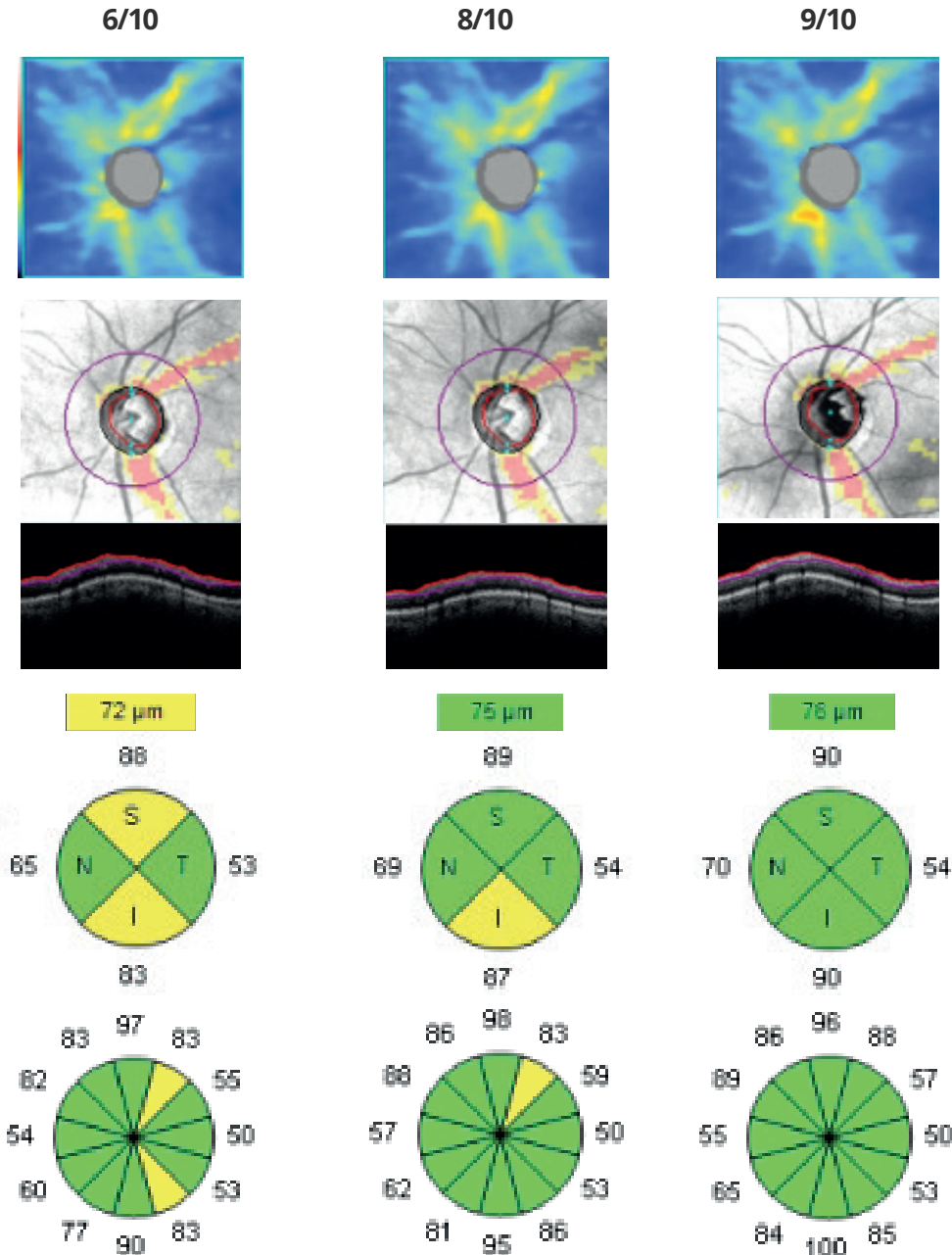
The frequency of false-positive results in SD-OCT, about 40% for RNFL and 55% for GCC in preperimetric and early glaucoma, requires:

- confirmation of all suspicious OCT result
- all SD-OCT examinations must present a maximum reliability index,
- the absence of clinical and/or treatment decisions in the presence of an isolated new OCT defect.

All isolated OCT defects or all new defects in the context of follow-up must always be confirmed and compared with changes in clinical and functional parameters (visual field).

Signal quality

Check the signal strength by the signal strength index (SSI): always ensure a maximal SSI reliability index; the minimum signal strength index asked by the SD-OCT is not sufficient.



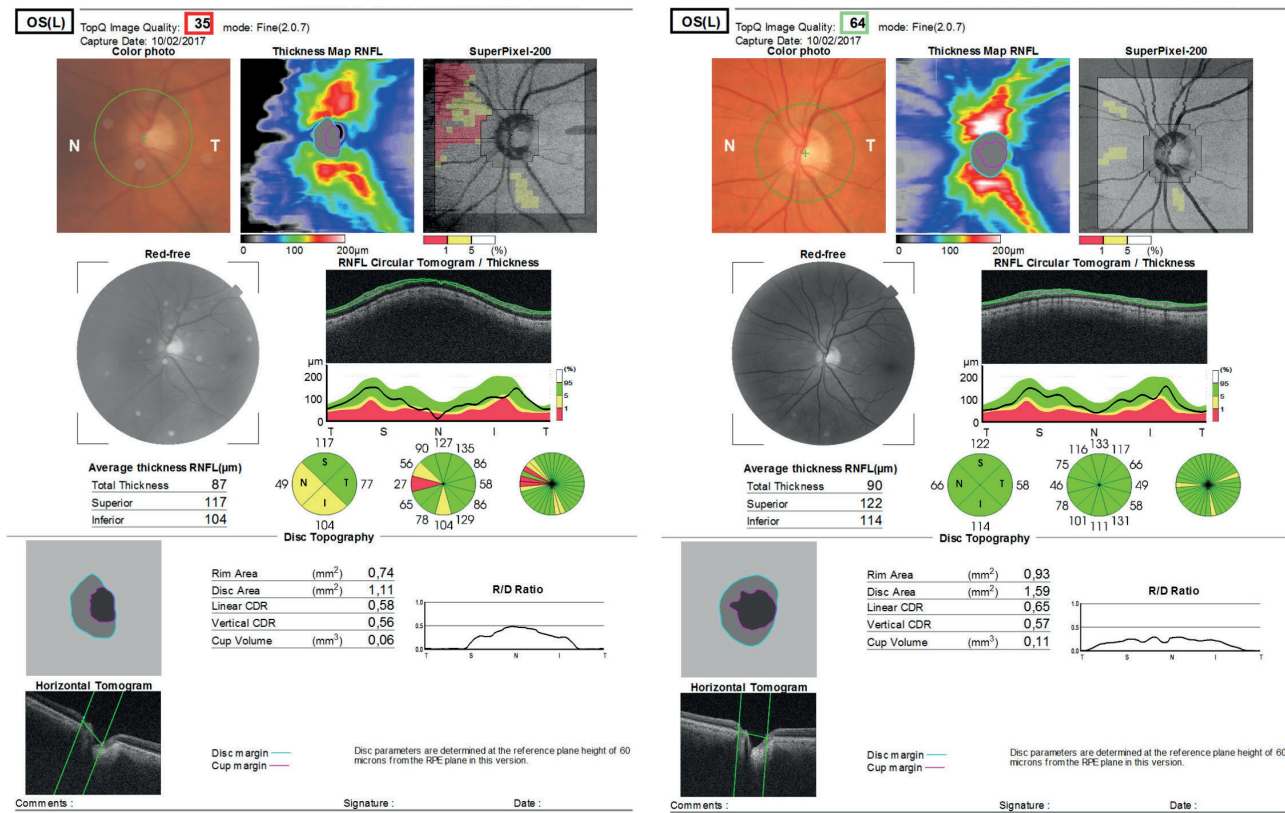
Results obtained in a case of early OAG with signal strength indices of 6.8 and 9/10 on Cirrus HD-OCT.

The higher reliability index indicates less advanced structural defects of the RNFL in this left eye.

Signal quality

Triton SD-OCT images acquired in a 69-year-old healthy subject with signal strength indices of 35 and 64.

The higher reliability index on the right, does not reveal any structural defect of the RNFL suspected on the examination with a signal strength index of 34, considered to be reliable by the Triton SD-OCT in this left eye. It is important to always obtain the maximum SSI reliability index.





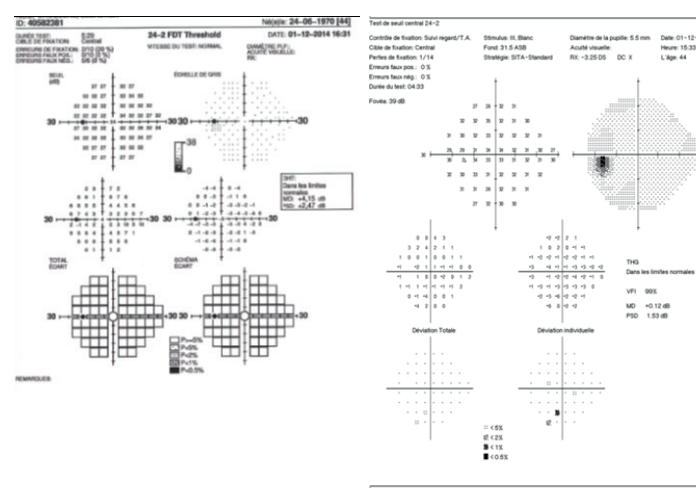
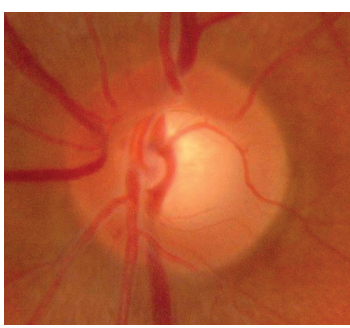
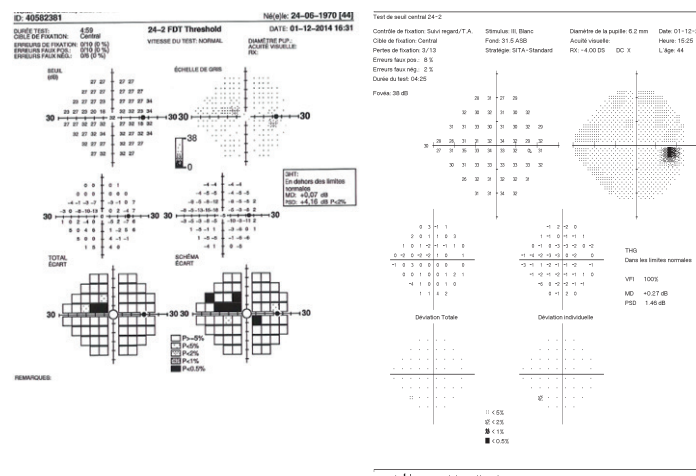
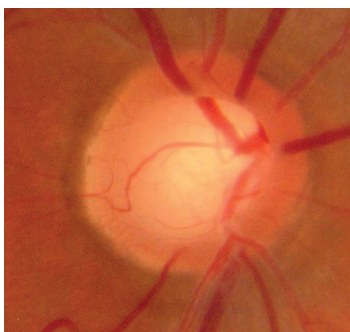
7. Clinical aspects of glaucoma on SD-OCT

- 7.1. Glaucoma suspect**
- 7.2. Early glaucoma**
- 7.3. Myopia and tilted disc syndrome**
- 7.4. Moderate glaucoma**
- 7.5. Unilateral glaucoma**
- 7.6. Advanced glaucoma**

Glaucoma suspect

Preperimetric glaucoma

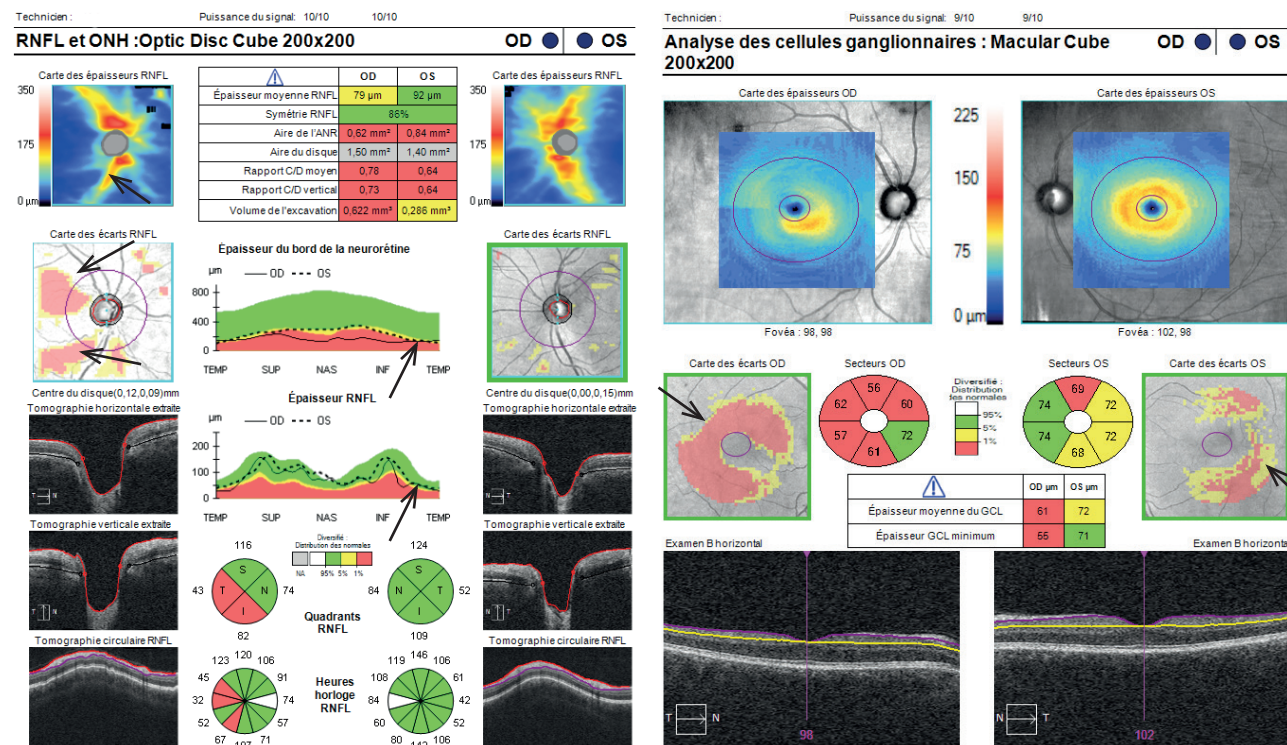
During a routine examination in a 44-year-old subject with an IOP of 14 mmHg and a central corneal thickness of 530 µm, discovery on ophthalmoscopic examination of a suspicious right optic disc with a lesion of the inferior temporal NRR. The absence of abnormality on the visual field examination by white-on-white 24-2 Standard Automated Perimetry (SAP) and the confirmed detection of a superior arcuate defect with the FDT Matrix examination indicated a diagnosis of preperimetric glaucoma. Note that Matrix perimetry or FDT-Matrix perimetry investigates other pathways of transmission of visual information, and allows much earlier detection of a functional visual field defect than white-on-white SAP.



SD-OCT thickness maps and deviation maps detect an extensive lesion of the right inferior temporal RNFL, with a suspected associated lesion of the superior temporal RNFL. The defect is also found on the TSNIT graph of the RNFL, with thinning of the NRR and decreased mean thickness of the right RNFL and the inferior and inferior temporal quadrants of the optic disc. SD-OCT exam does not reveal any defect of the RNFL in the left eye.

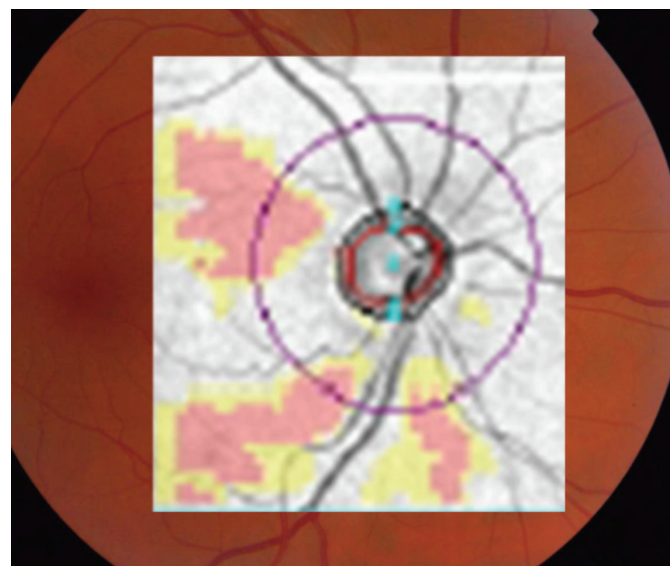
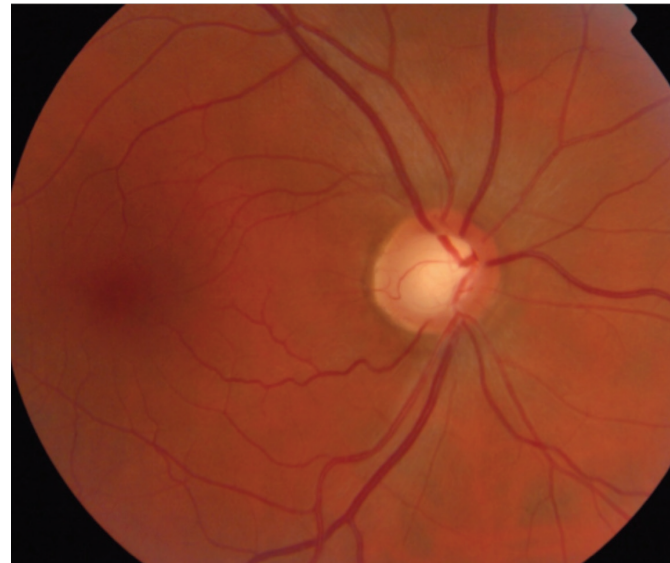
Although clinical examination of the macula did not reveal any abnormality, GCL analysis detect a corresponding right inferior temporal lesion and also demonstrated an extensive defect in the right superior macular sector and a lesion of the mean GCL in the left superior and inferior temporal.

This clinical case clearly illustrates the value of the complementary information provided by OCT analysis of the peripapillary RNFL and GCC, with demonstration of a more extensive lesion of the GCC in the right eye and an early lesion in the left eye, in which a lesion of the macular ganglion cell complex is therefore already visualized.



Glaucoma suspect

Posterior pole fundus photography clearly demonstrates the RNFL defect in the right eye with a good topographic correlation of the defect detected on SD-OCT in the patient described on the previous page.

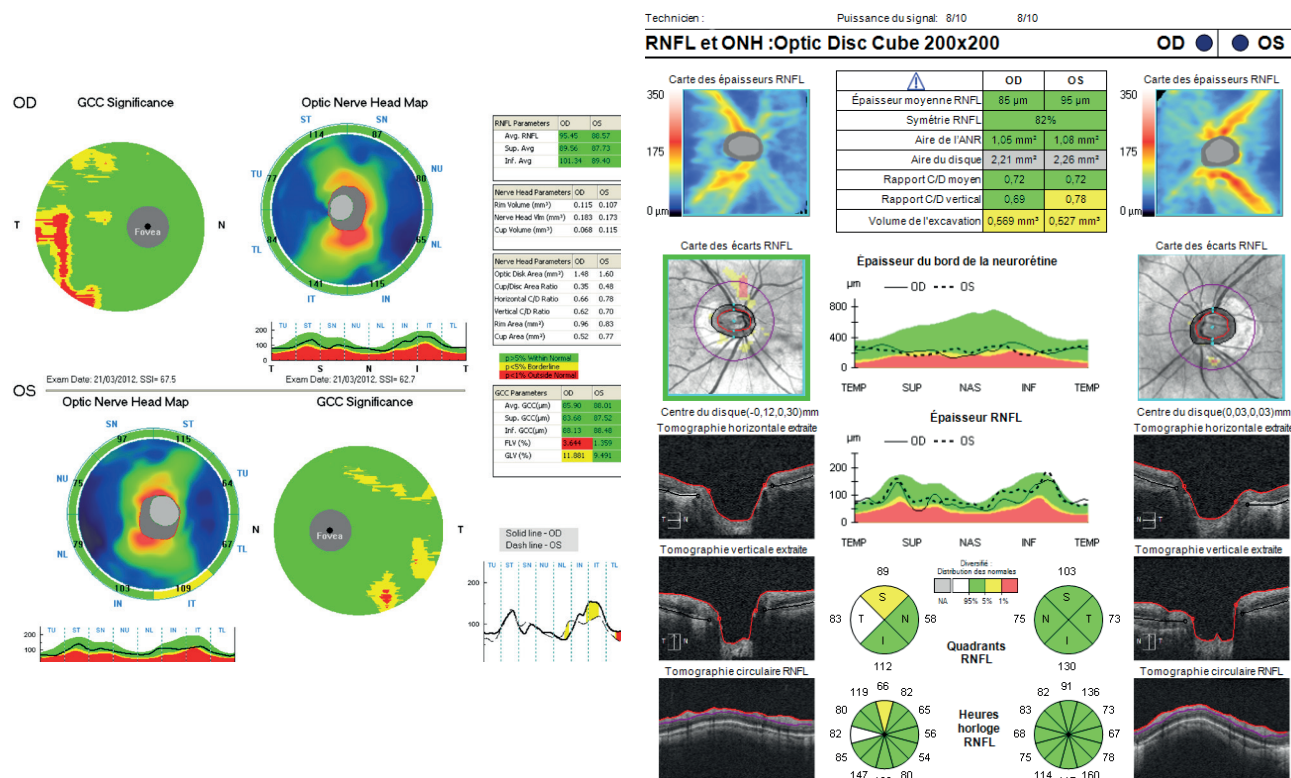


SD-OCT analysis of the RNFL provides a more sensitivity of the analysis in the superior and inferior temporal sectors. In the current state of knowledge, numerical values for global, sectorial and meridian mean RNFL thickness on the OCT display do not allow reliable diagnosis of structural lesions of preperimetric glaucoma or early glaucoma, partly because of interindividual variations of mean RNFL thickness, ranging between 89.8 and 113 μ m.

Evaluation of the macular ganglion cell complex highlights the value of certain parameters, particularly the FLV and GLV indices provided by XR Avanti SD-OCT and the GCIPL or GCL index provided by Cirrus HD-OCT, for the detection of preperimetric glaucoma and early glaucoma. Alterations of these parameters in case of glaucoma suspect and preperimetric glaucoma would be a marker of progressive 5-year alteration in almost 60% of cases.

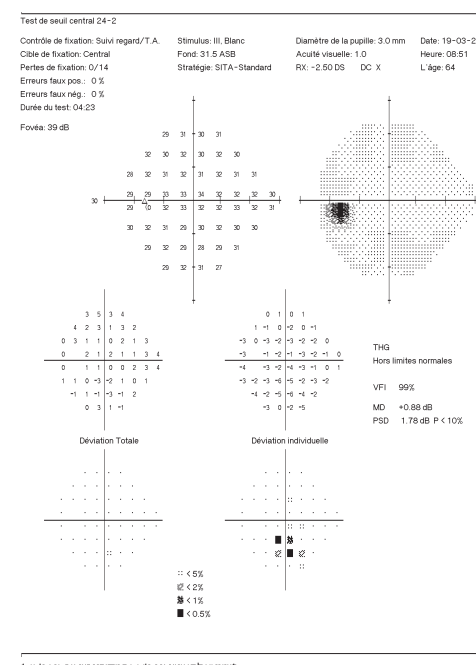
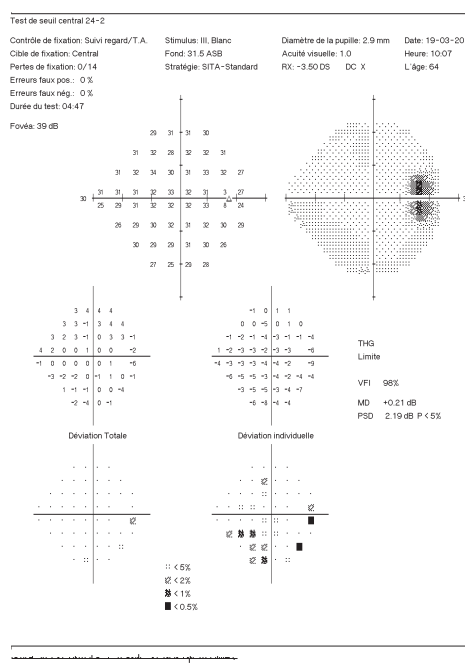
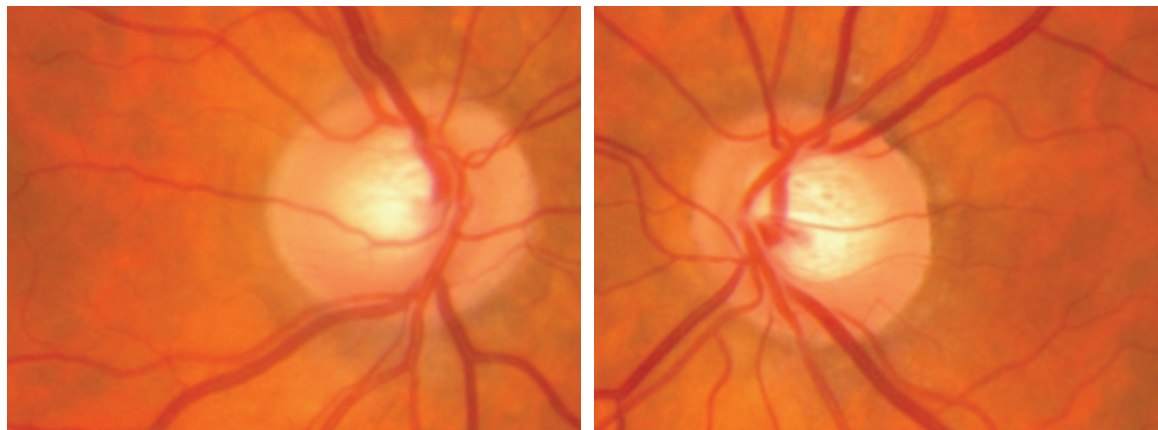
Interpretation of SD-OCT examinations requires a rigorous technique, with elimination of false-positive results, and careful comparison with all data of the clinical examination. Longitudinal evaluation and reproducibility of the results are also essential.

Finally, recent quantitative data of blood flow on OCT angiography of the optic nerve report significant reductions of ONH perfusion in patients with PPG compared to normal subjects.

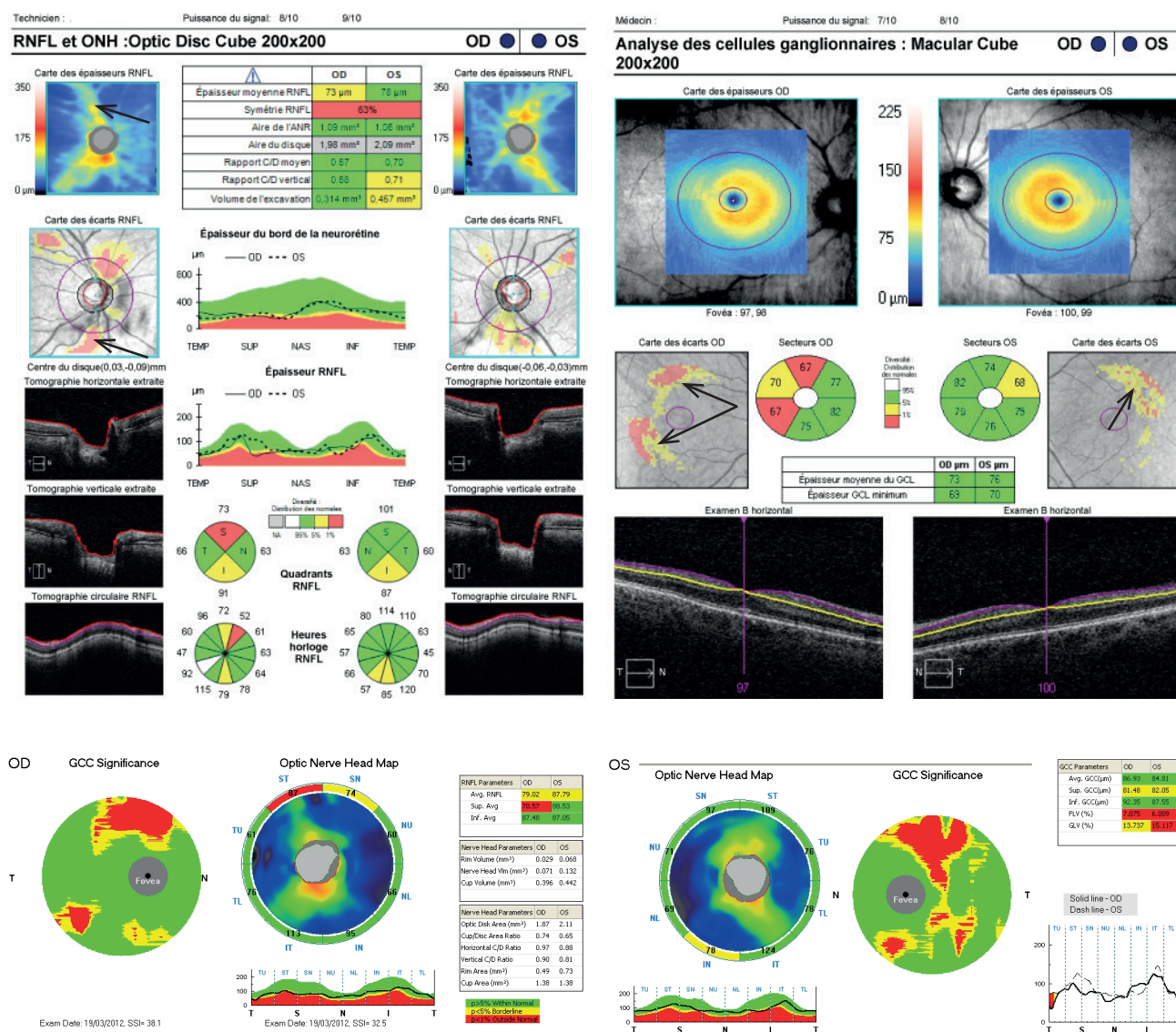


Early glaucoma

64-year-old man followed and treated for early POAG with IOP of 24 mmHg in the left and right eyes, consulting for a second opinion. ONH analysis in the right eye reveals a small notch of the neuroretinal rim on the 10 to 11 o'clock meridians with an inferior arcuate defect in the corresponding territory of the white-on-white SAP visual field; examination of the left eye reveals slight superior thinning of the NRR with a small early inferior visual field defect in the left eye.

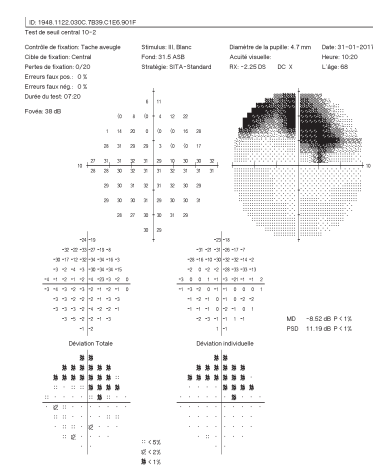
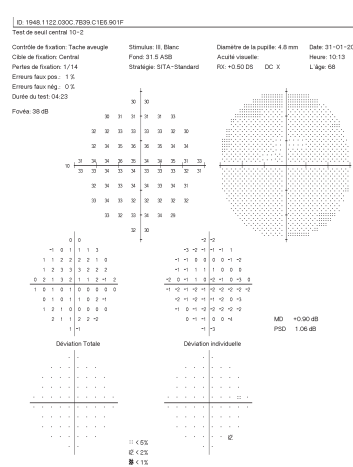
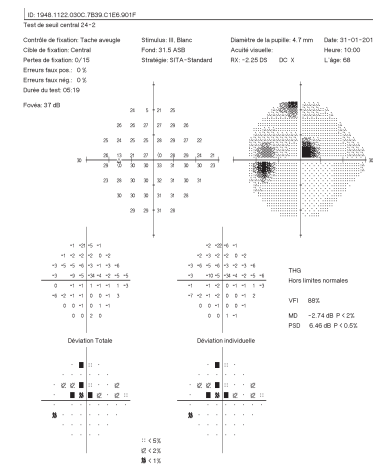
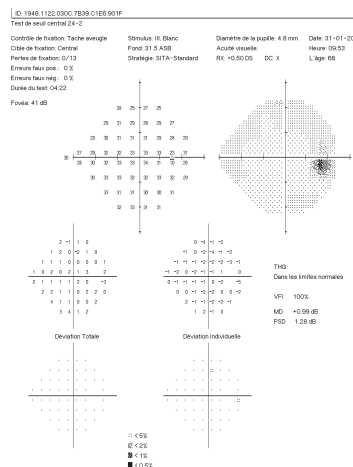
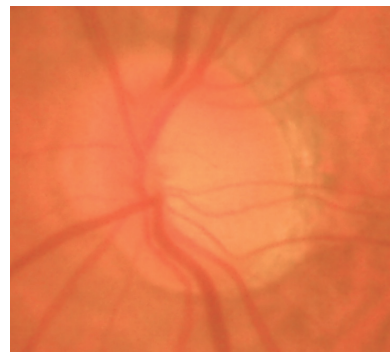
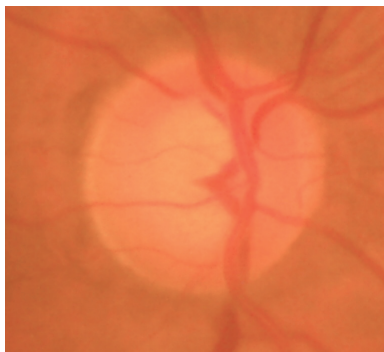


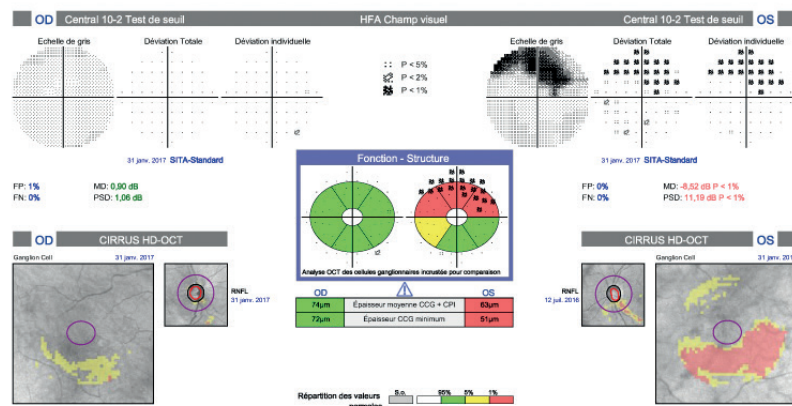
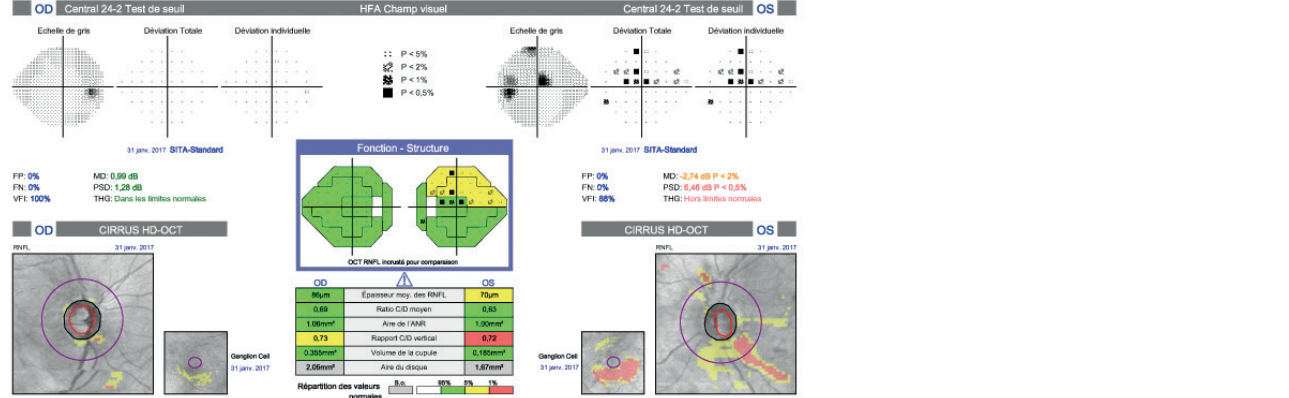
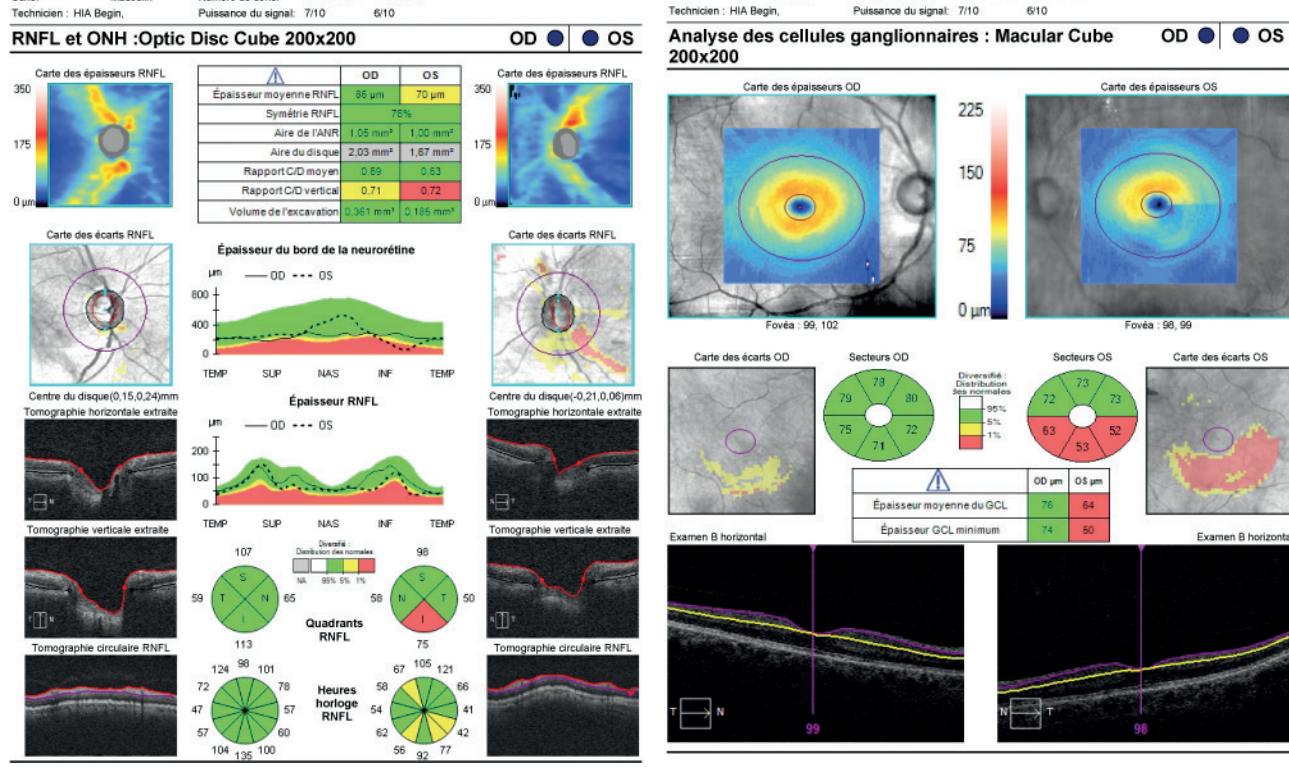
SD-OCT analysis of the RNFL reveals a lesion of the right superior temporal RNFL, with a suspected inferior lesion, associated with an early macular GCL lesion in the temporal sector, the zone initially affected in early clinical forms. Note the visualization of an early temporal macular defect in the left eye, with no apparent detectable lesion of the left PRNFL. The XR Avanti SD-OCT results are closely correlated with those obtained with the Cirrus HD-OCT.



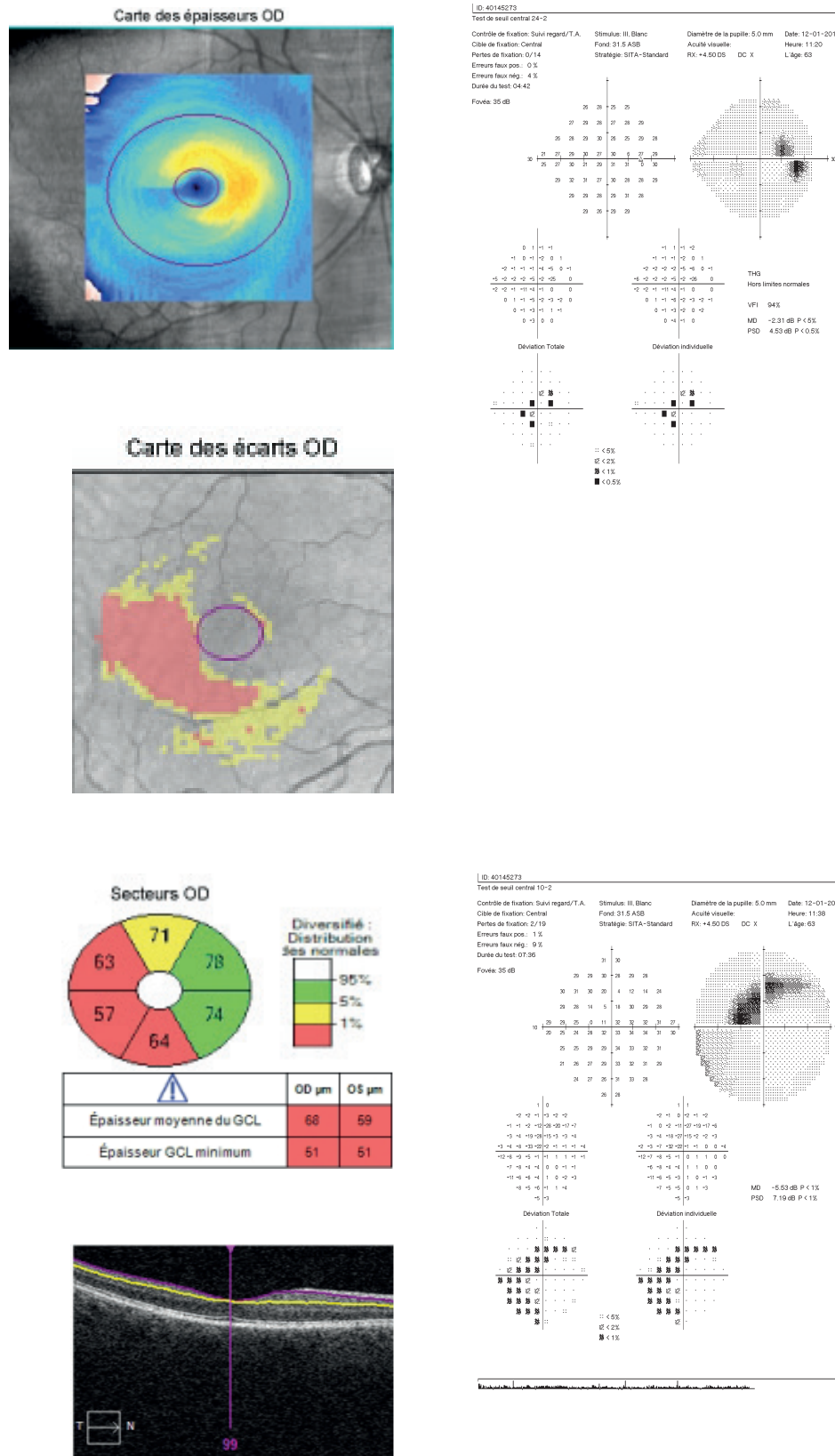
Early glaucoma - Paracentral scotoma

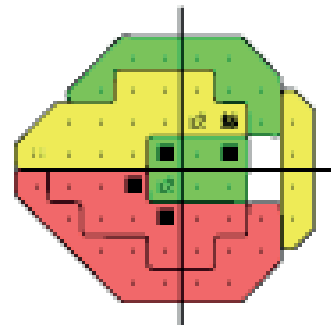
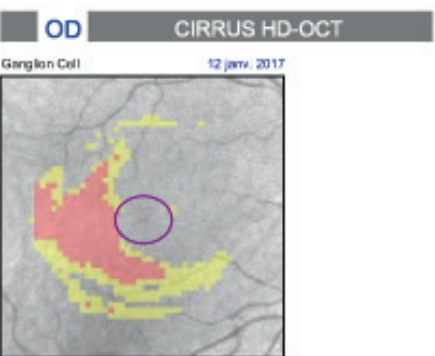
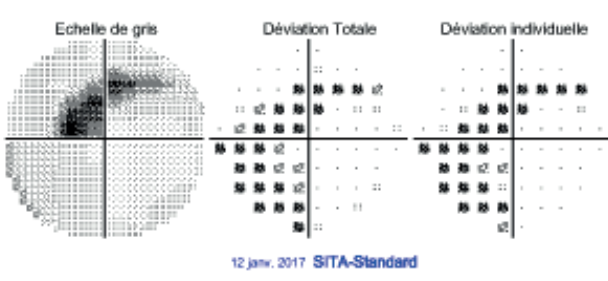
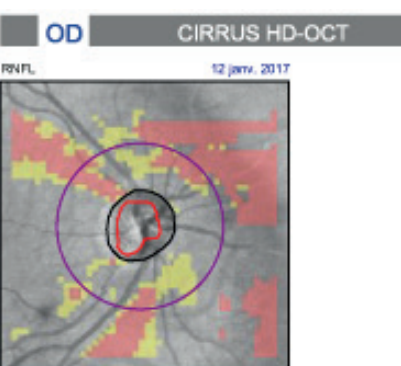
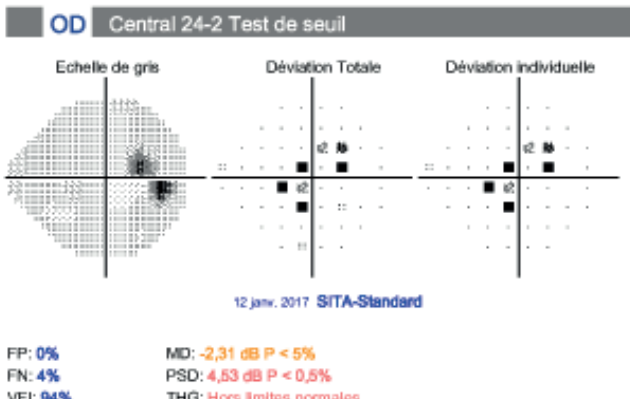
68-year-old man with early POAG with a paracentral scotoma detected by 24-2 SAP and more clearly defined on the 10-2 visual field with a close correlation of the RNFL and GCC defects, clearly demonstrated on the combined reports VF - Cirrus HD-OCT examinations.



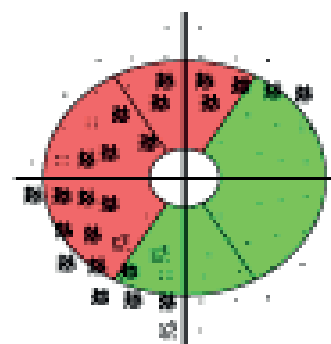


Early glaucoma - Paracentral scotoma





In the presence of a paracentral scotoma, 10° visual field examination more clearly demonstrates the severity of the functional repercussions and its strongest correlation with the severity of the GCL complex defect visualized on the OCT report. Projection of this lesion onto the 10-2 VF examination provides a more demonstrative comparative analysis.

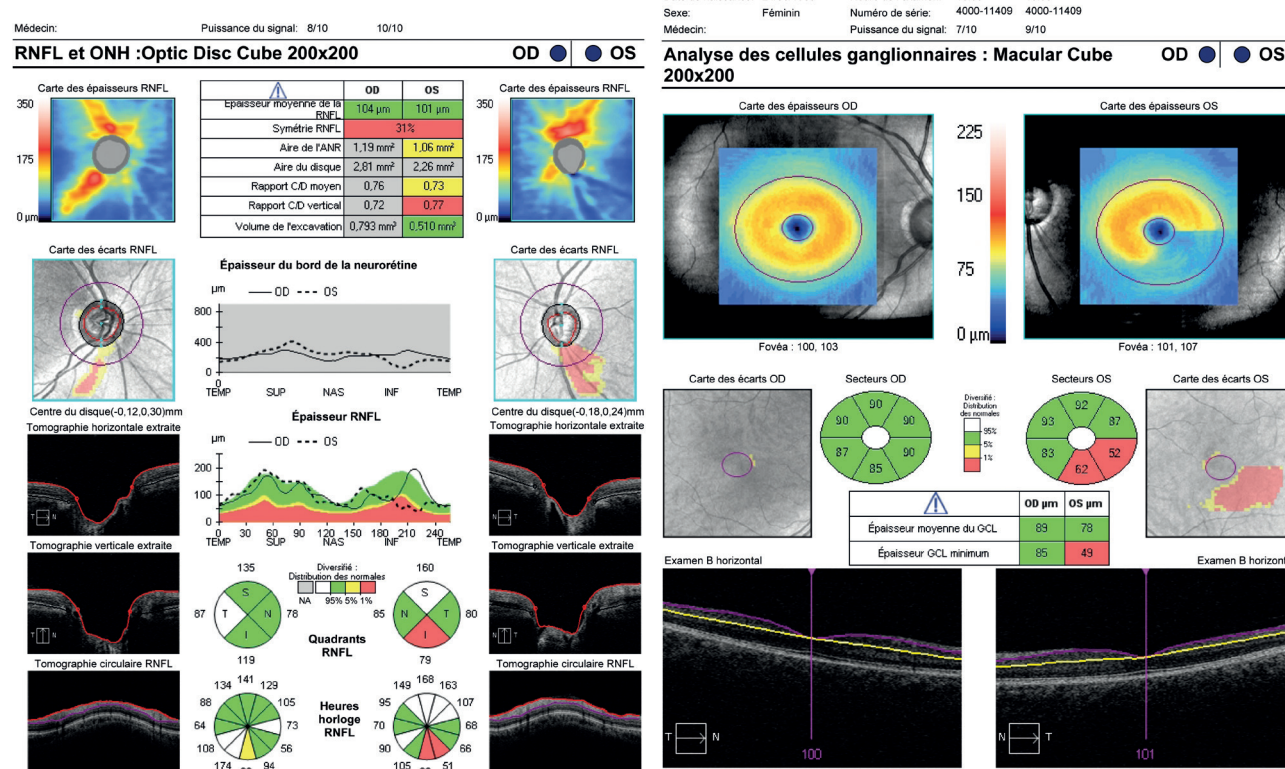
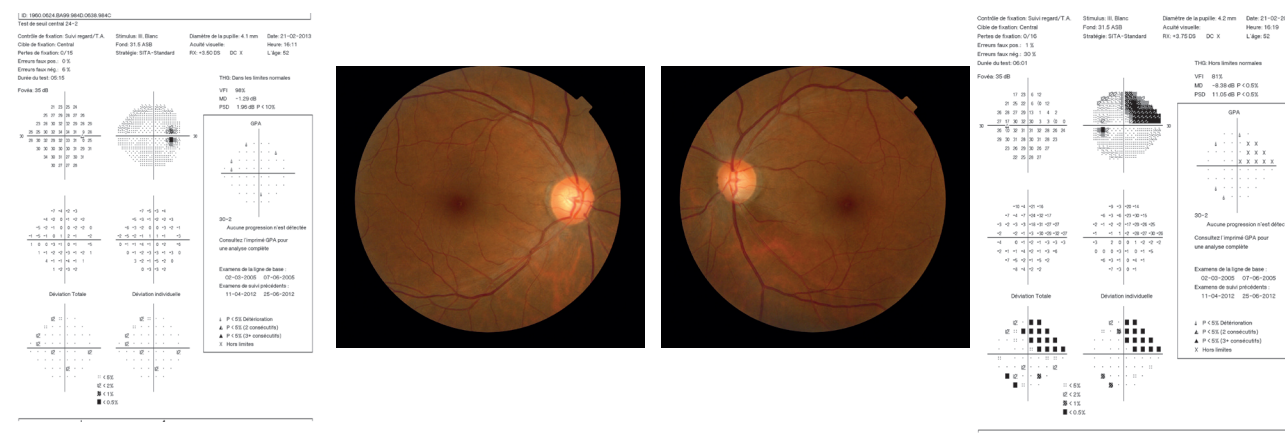


Early glaucoma

53-year-old woman followed for early POAG.

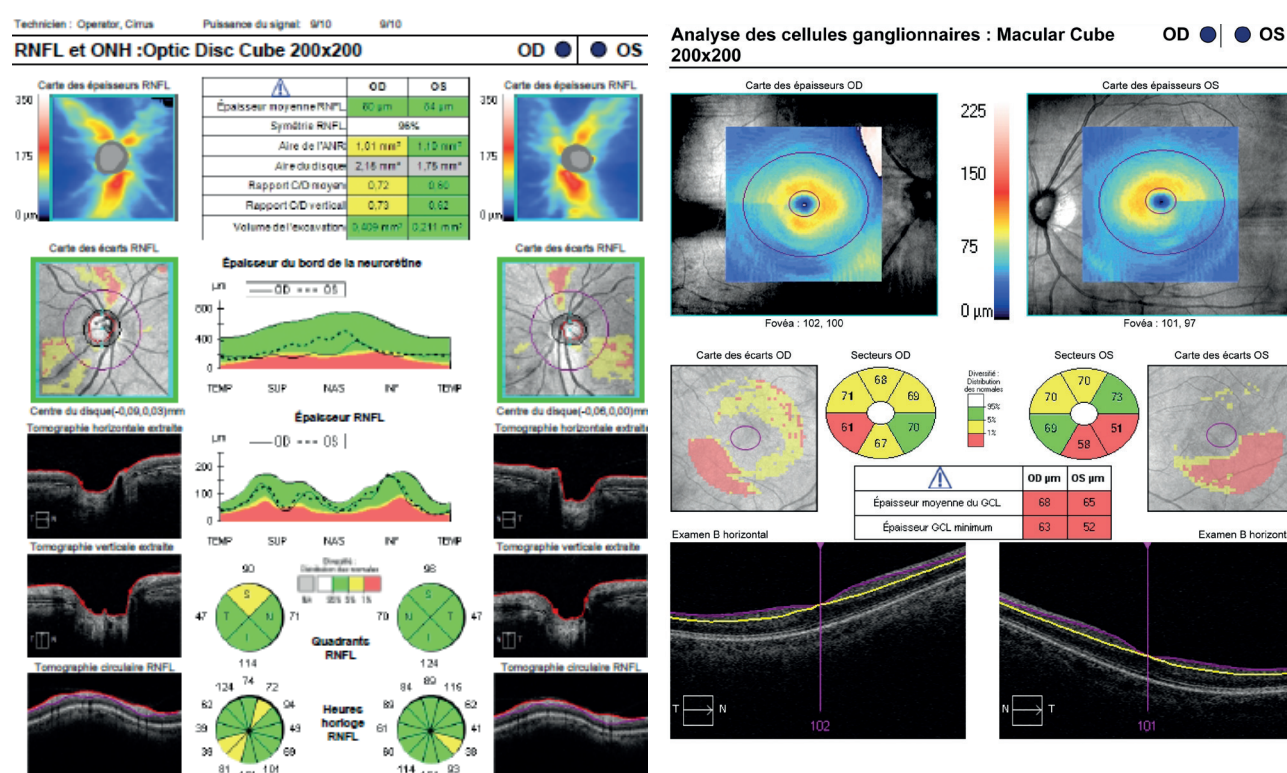
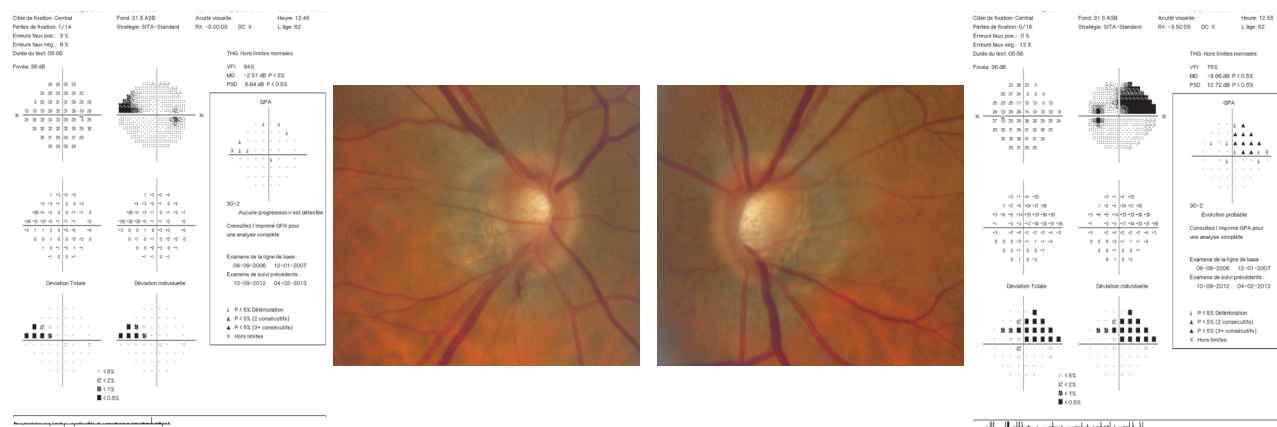
SD-OCT report reveals an early lesion of the inferior RNFL in the right eye, with no GCC lesion, not observed on the ONH analysis and not clearly identified on visual field examination.

The inferior arcuate defect of the RNFL of the left eye extends beyond the RNFL derived from the inferior macular zone, highlighting the complementary value of OCT analysis of the peripapillary RNFL and GCC, allowing more extensive evaluation of the various anatomical sectors involved.



-6D myopia and tilted disc syndrome

Clinical examination of the ONH is often difficult in the presence of tilted disc syndrome and in myopic patients. SD-OCT confirms the lesion of the inferior RNFL in the right eye in the sector of the 7 o'clock haemorrhage, and in the left eye, correlated with the superior VF defects. SD-OCT also visualizes bilateral superior RNFL and GCC lesions with no associated inferior VF defect and not identified lesion on clinical examination.

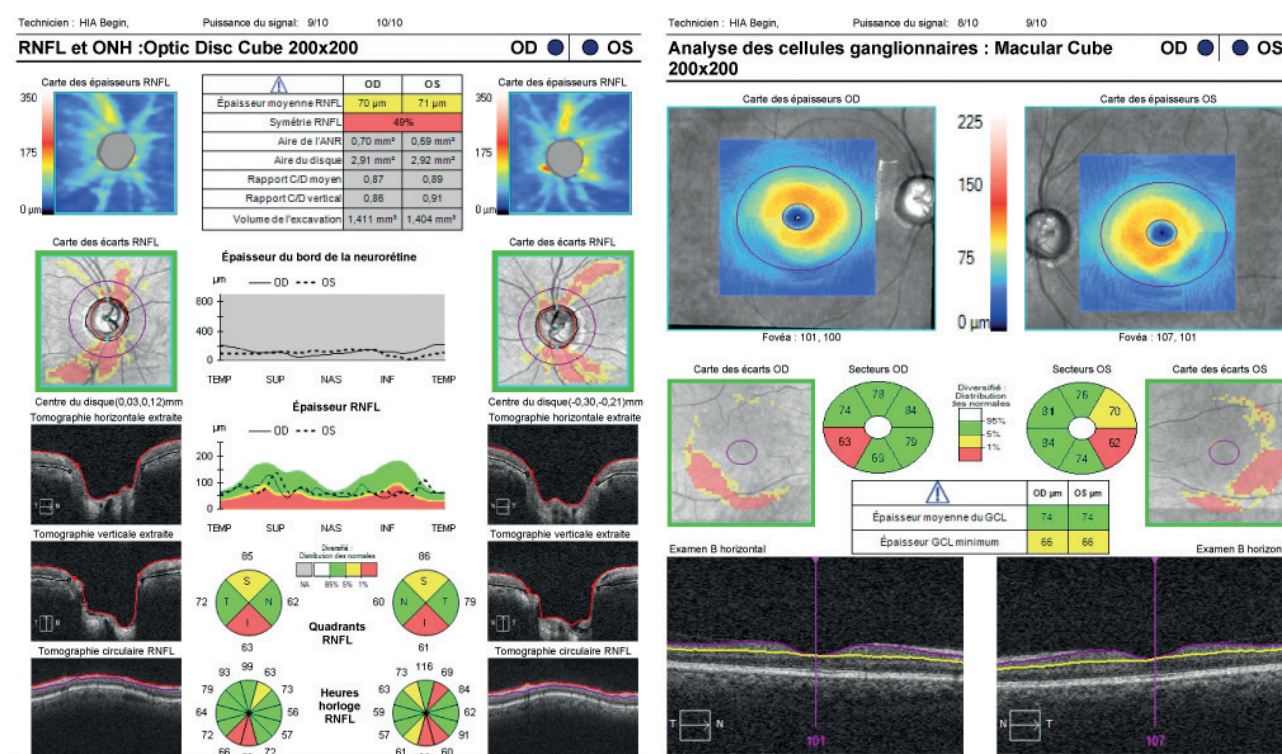
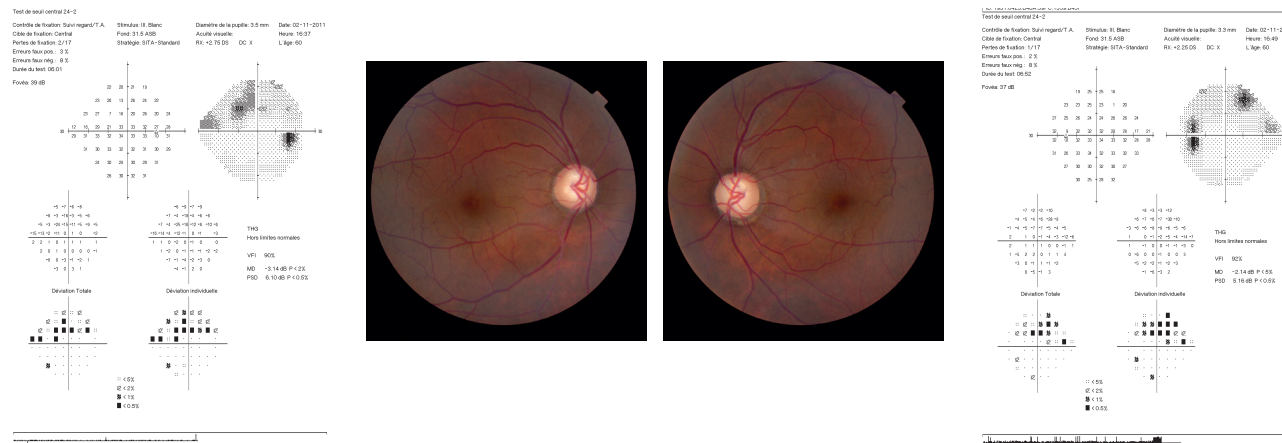


Moderate glaucoma

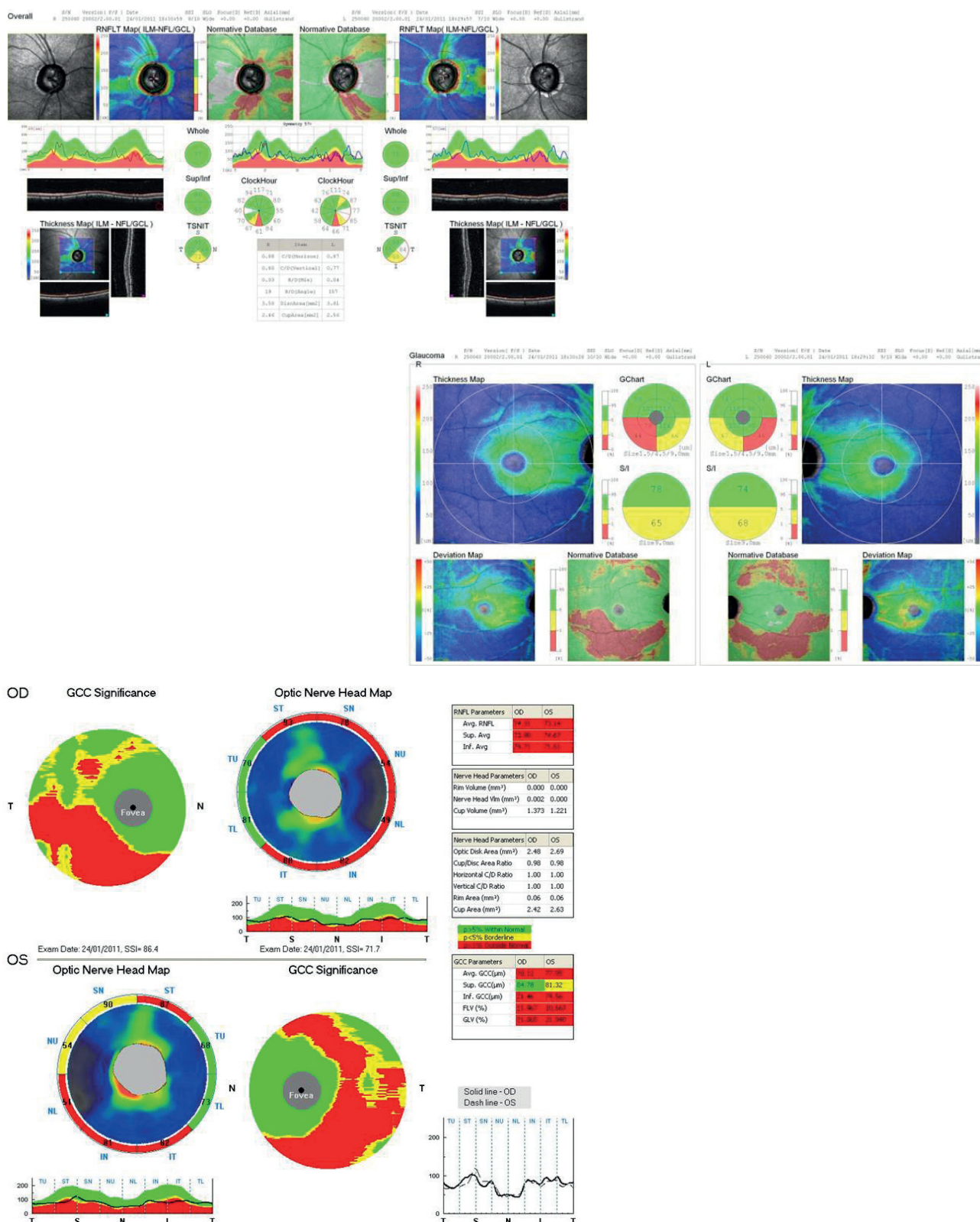
A 63-year-old man undergoing treatment for 15 years, with IOP of 11 and 12 mmHg and pachymetry of 540/535 µm.

The lesion of the superior RNFL demonstrated by OCT in both 2 eyes with no lesion of the inferior visual fields is accompanied by inferior temporal GCC defects in both eyes that are less severe than expected in view of the OCT RNFL analysis.

This result is confirmed on fundus photography, which shows an inferior arcuate defect extending, here too, well beyond the territory of the macular ganglion cell complex.

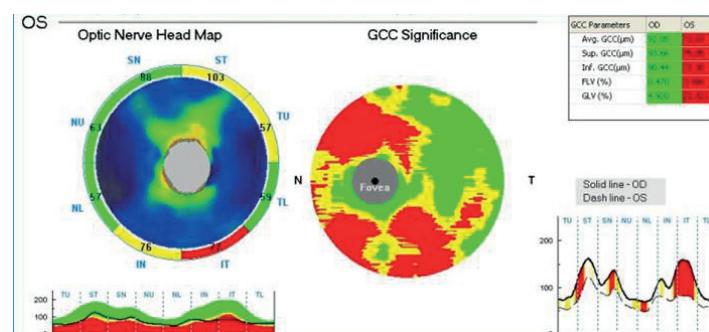
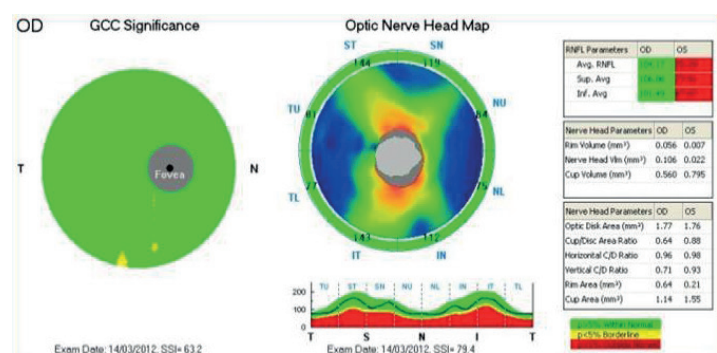
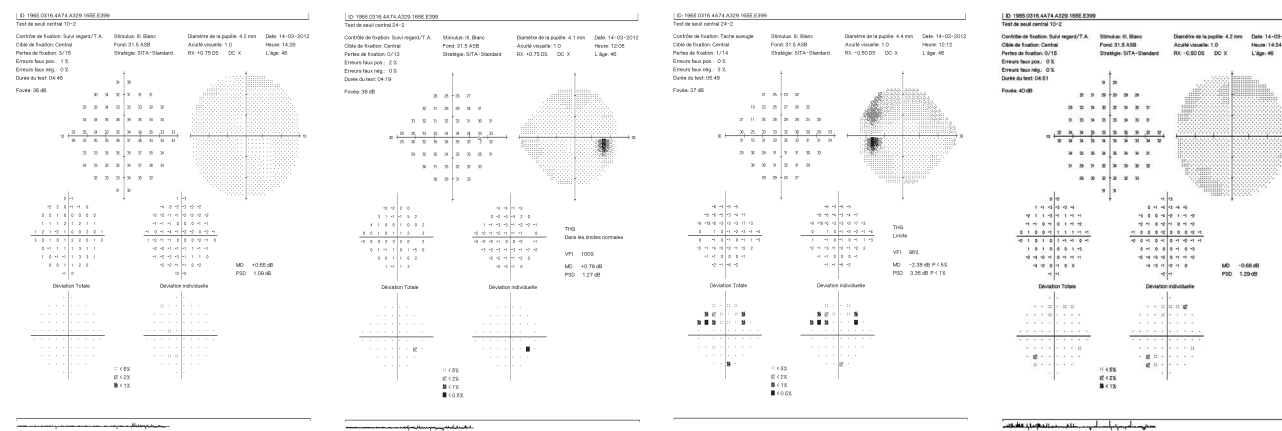


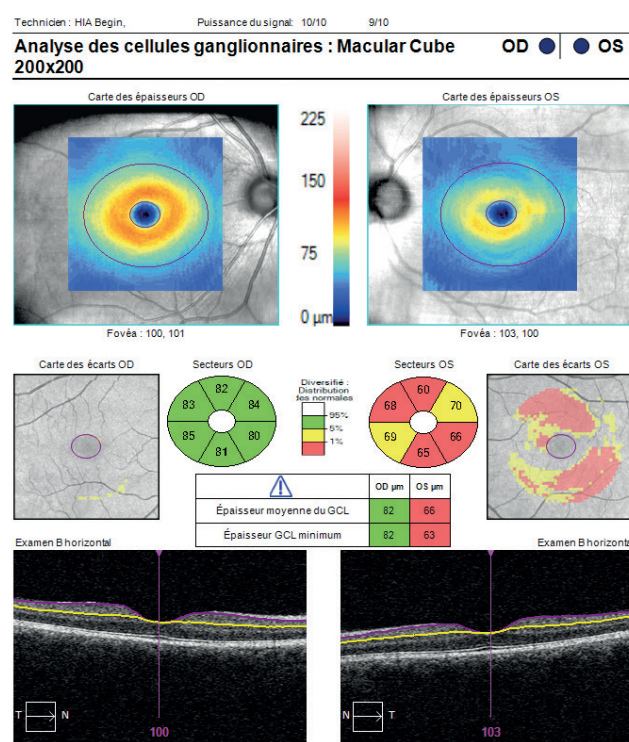
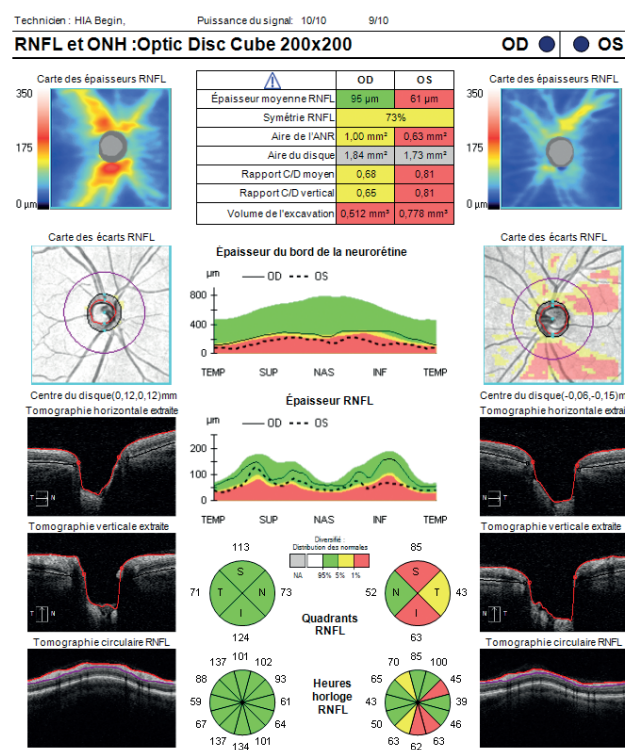
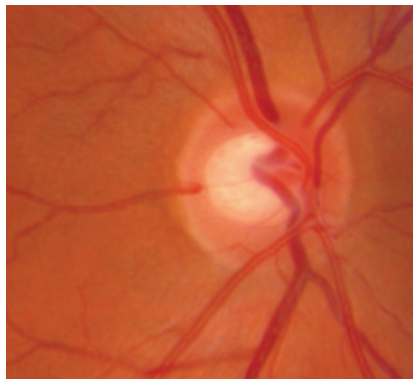
Nidek RS 3000 and XR Avanti SD-OCT demonstrate a good correlation of the topographic distribution of the RNFL and GCC lesions reported by Cirrus HD-OCT.



Unilateral glaucoma

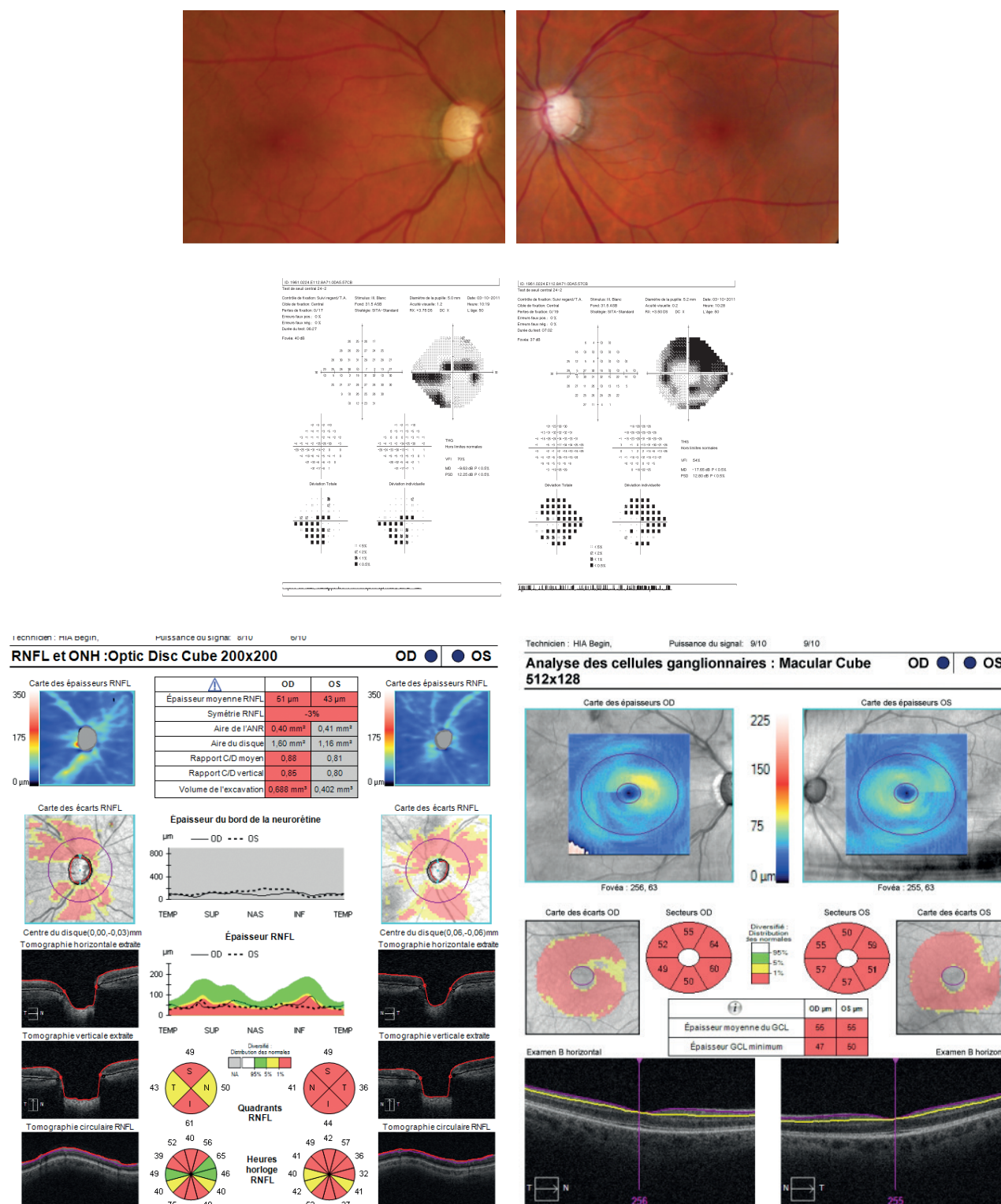
A 47-year-old man followed and treated for unilateral left glaucoma that first appeared 3 years ago, in the context of regular surveillance of big cup optic discs with marked excavations. The advanced GCC lesion of the left eye visualized on XR Avanti SD-OCT with marked alteration of the FLV and GLV indices, is well correlated with GCL complex analysis reported by Cirrus HD-OCT.



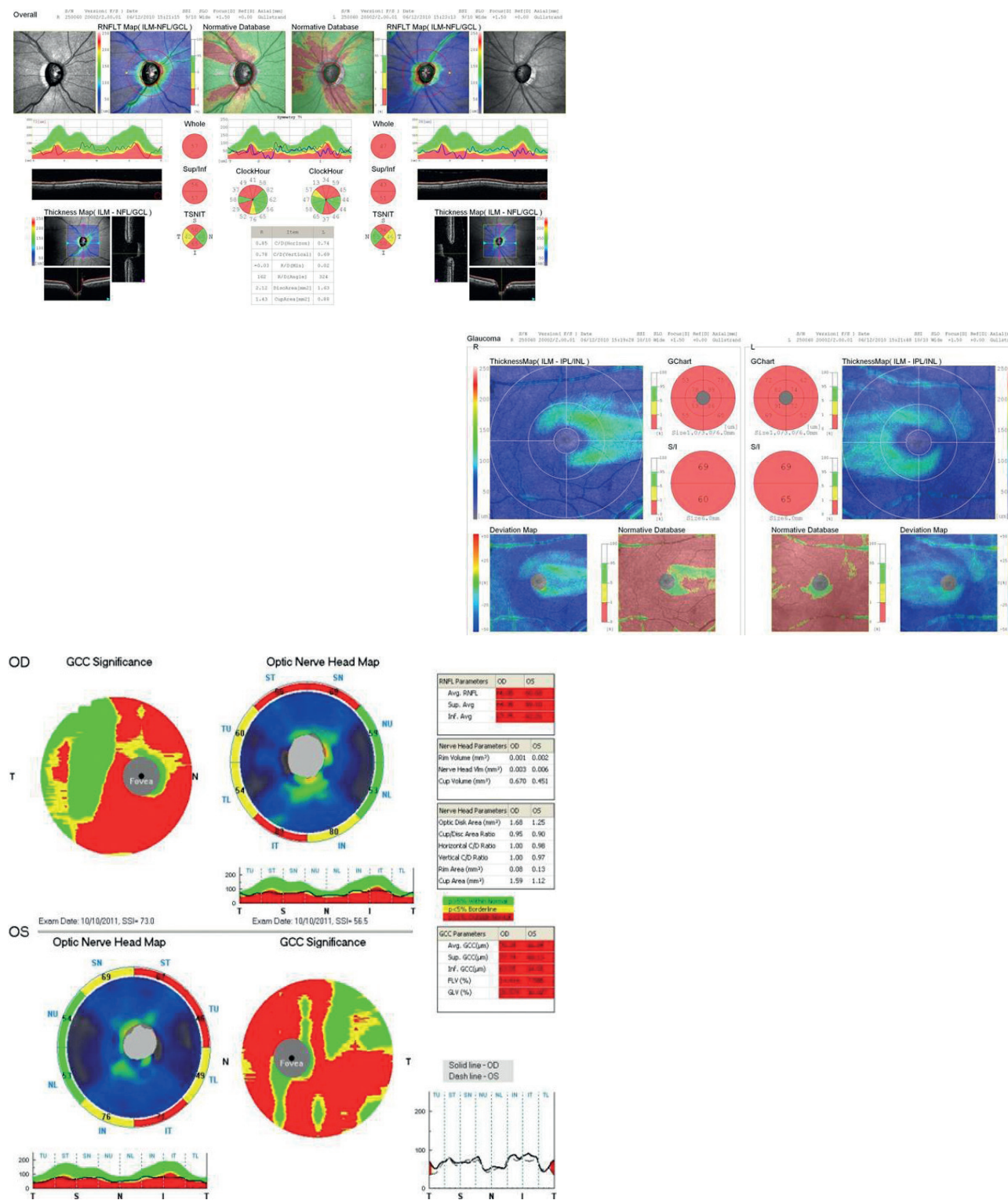


Advanced glaucoma

Analysis of peripapillary RNFL, as previously mentioned, presents certain limitations in more advanced glaucoma that reach a floor threshold. GCC analysis allows evaluation of structural lesions in these clinical forms and certain indices can be used to monitor glaucoma progression.



Nidek RS 3000 and XR Avanti SD-OCT demonstrate a good correlation of the topographic distribution of the RNFL and GCC defects identified by Cirrus HD-OCT.





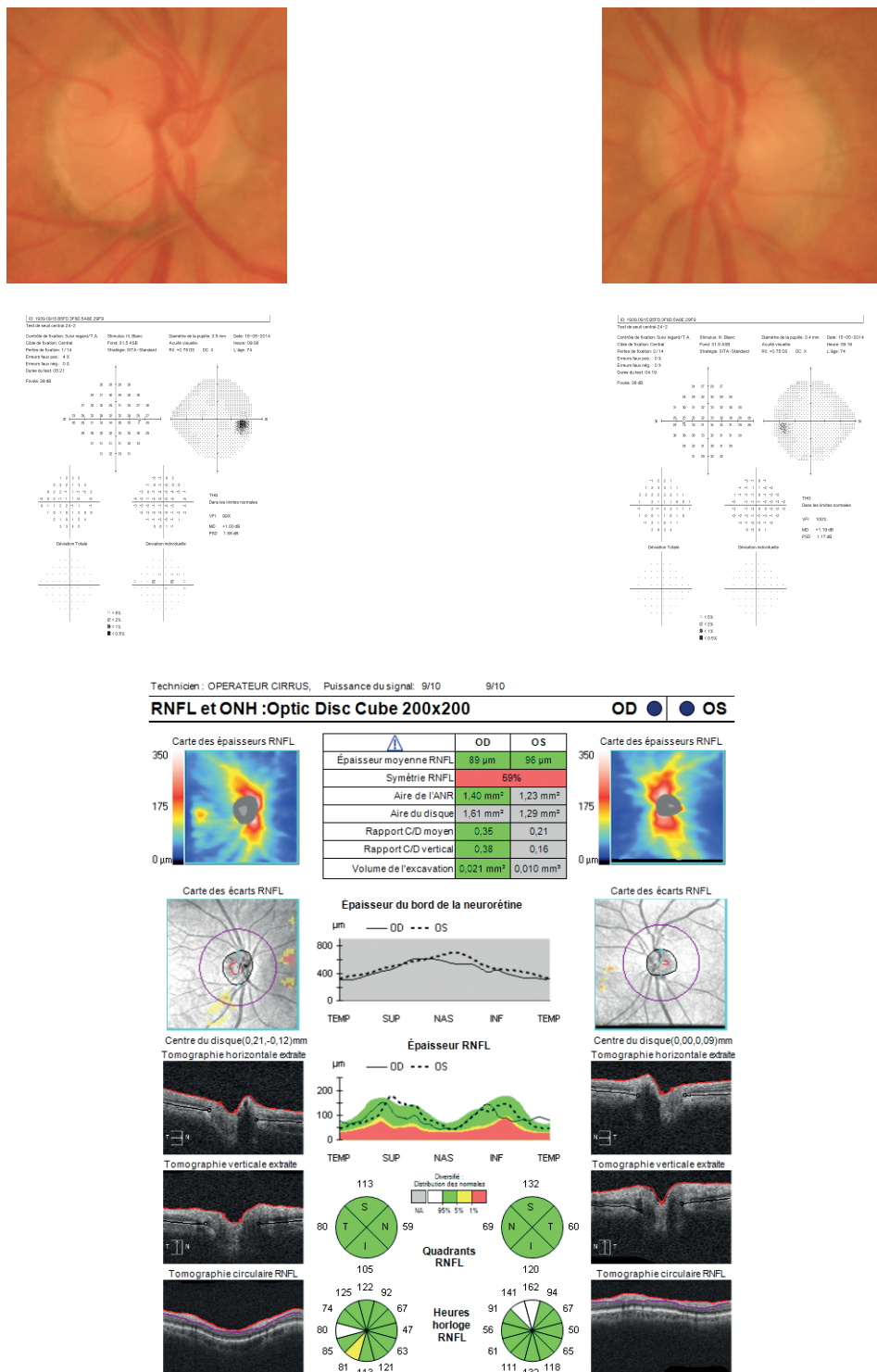
8. Some special cases in SD-OCT

- 8.1. Isolated OCT lesion**
- 8.2. Interest of central 10° visual field**
- 8.3. Tilted disc syndrome**
- 8.4. Optic disc drusen**
- 8.5. High myopia**

Isolated OCT defect

Discovery, in a 75-year-old woman, of OHT of 27 mmHg in both eyes with central corneal thickness (CCT) of 540 and 530 µm. White-on-white SAP did not reveal any systematized functional impairment.

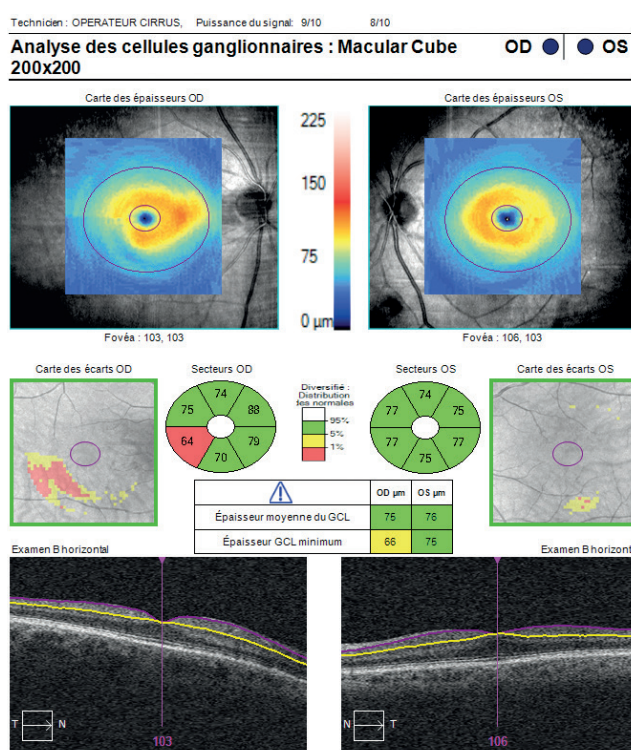
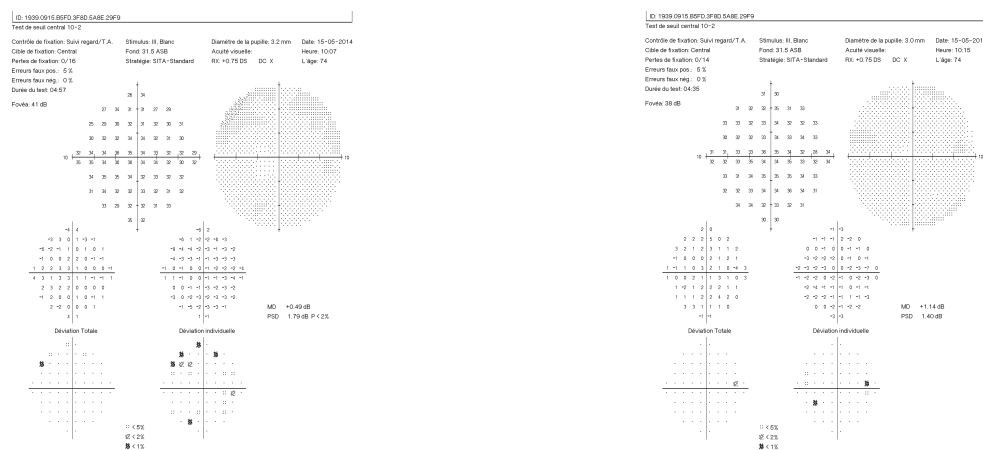
SD-OCT RNFL analysis suggests the presence of a right inferior temporal lesion on the thickness map and deviation map.



Macular ganglion cell complex analysis confirms an early GCC lesion in the inferior temporal sector of the right eye, highlighting the value of more precise screening for functional impairment. Analysis of the central 10° of the visual field reveals a central scotoma, the topography of which is correlated with that of the GCC lesion.

This clinical case illustrates the value of 10-2 central visual field examination in patients with glaucoma or glaucoma suspect in the presence of an isolated lesion on SD-OCT GCC analysis with normal 24-2 visual field examination.

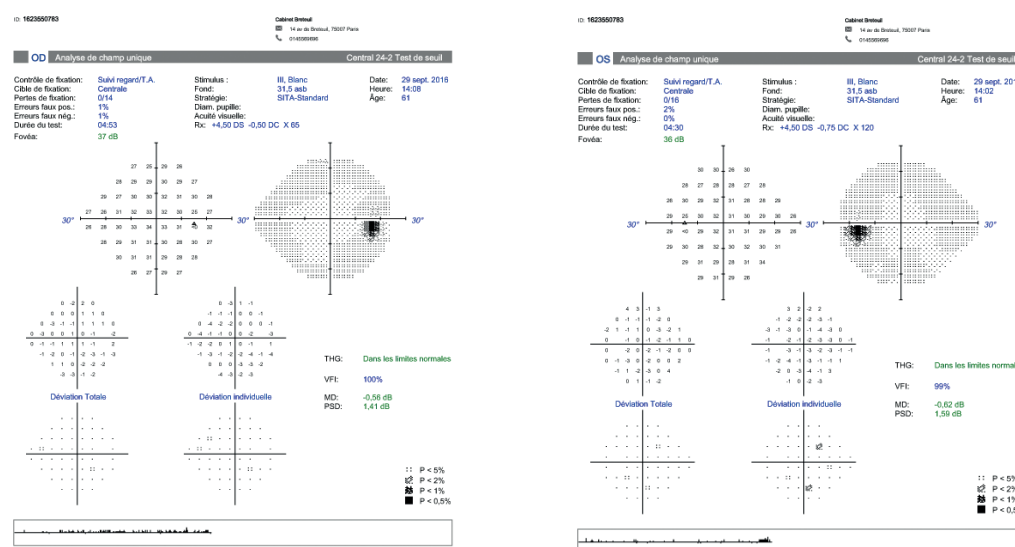
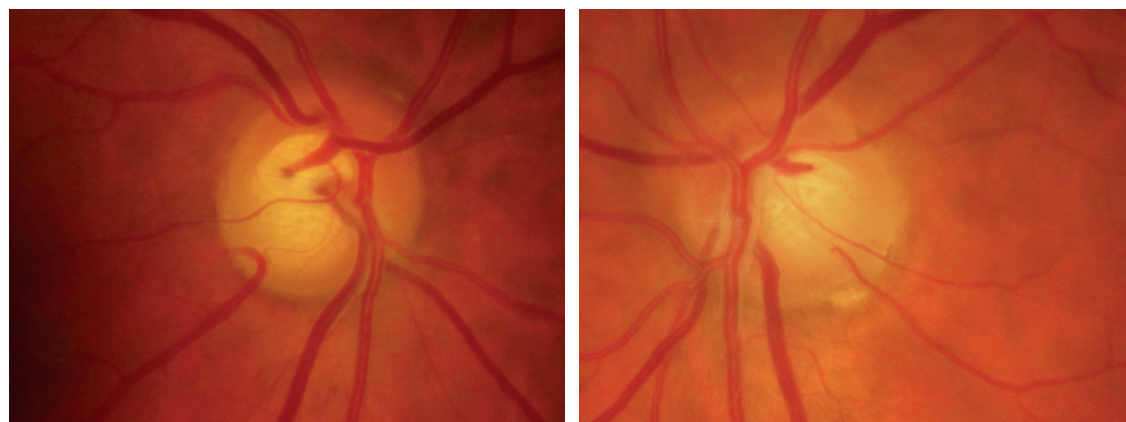
Several studies have reported the value of GCC analysis for the diagnosis of early glaucoma with initial central and paracentral visual field defects in 18 to 20% of these clinical forms, with particularly high sensitivity of the Cirrus HD-OCT GCIPL index.

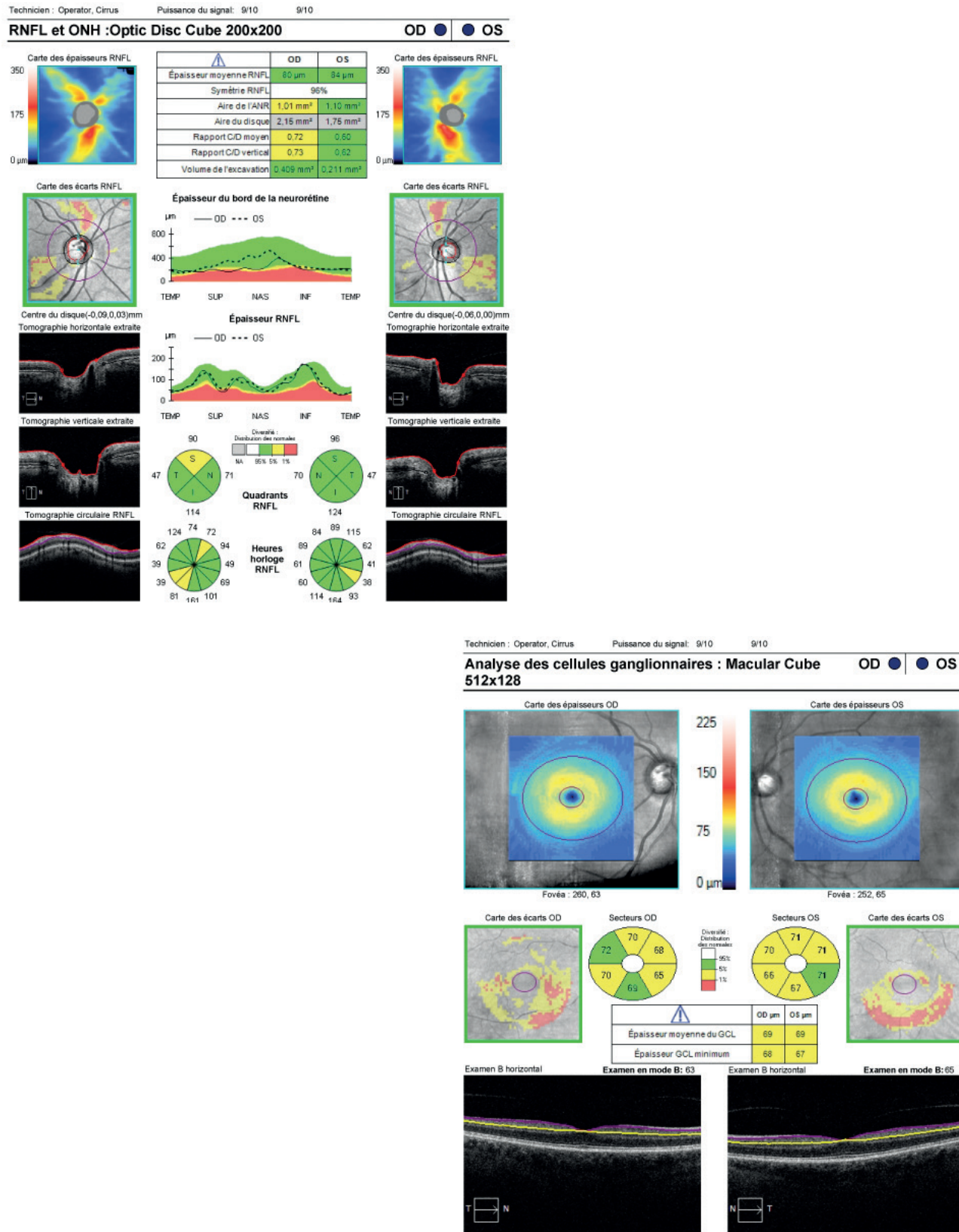


Tilted disc syndrome

A 62-year-old woman with hypermetropia of + 1.50D and tilted disc syndrome without OHT.

In patients with severe tilted disc syndrome, SD-OCT may be altered with the presence of a suspected RNFL defect related to modification of the topographic distribution of the posterior pole RNFL. These false-positive OCT results are due to statistical analysis of the OCT results based on comparison with the limited SD-OCT normative database, which does not include all possible interindividual variations of the RNFL and their anatomical distributions. This clinical case also illustrates the absolute necessity to compare all SD-OCT examinations with the findings of the clinical examination.

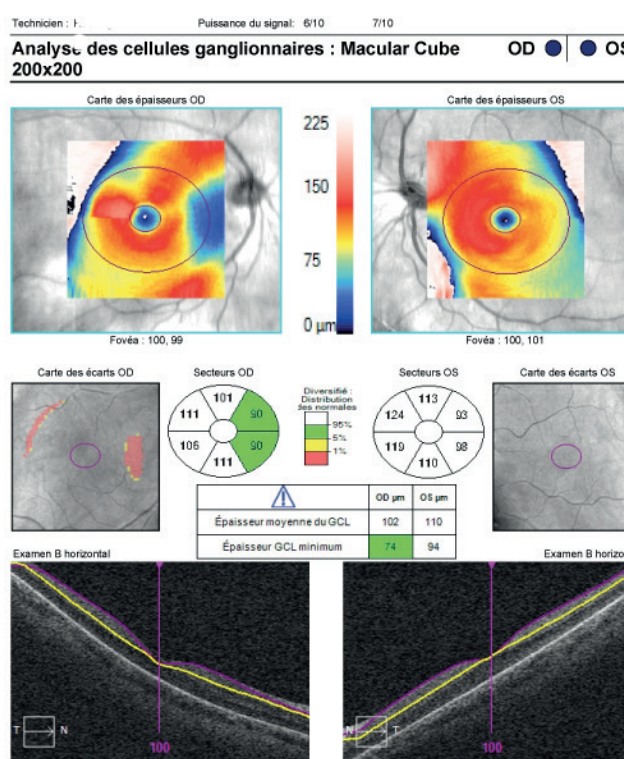
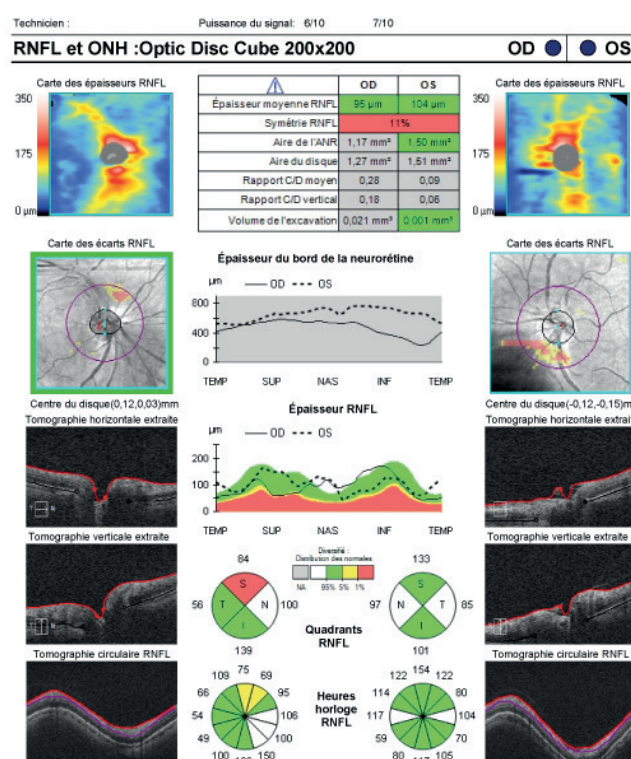
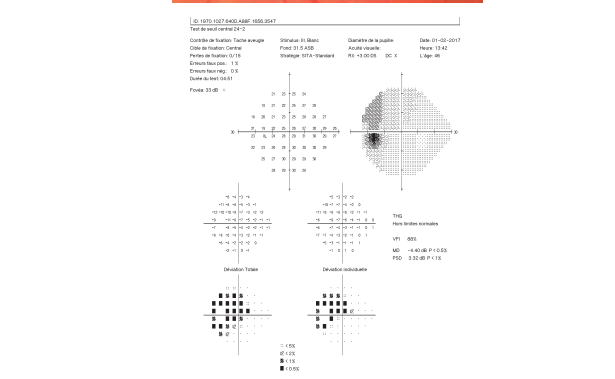
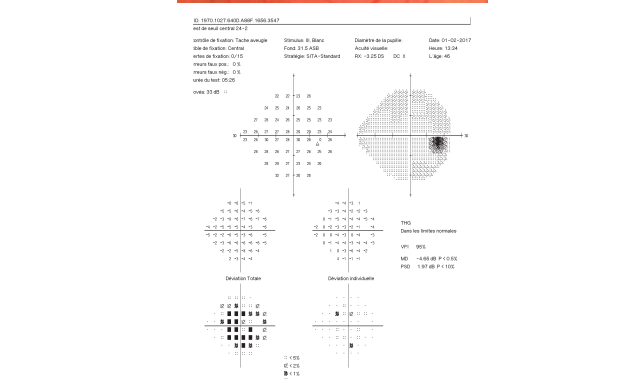
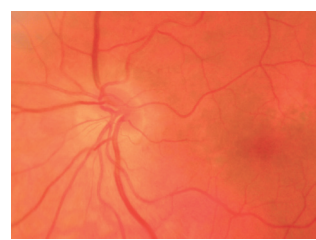
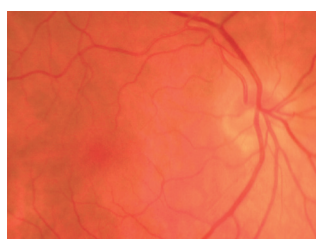




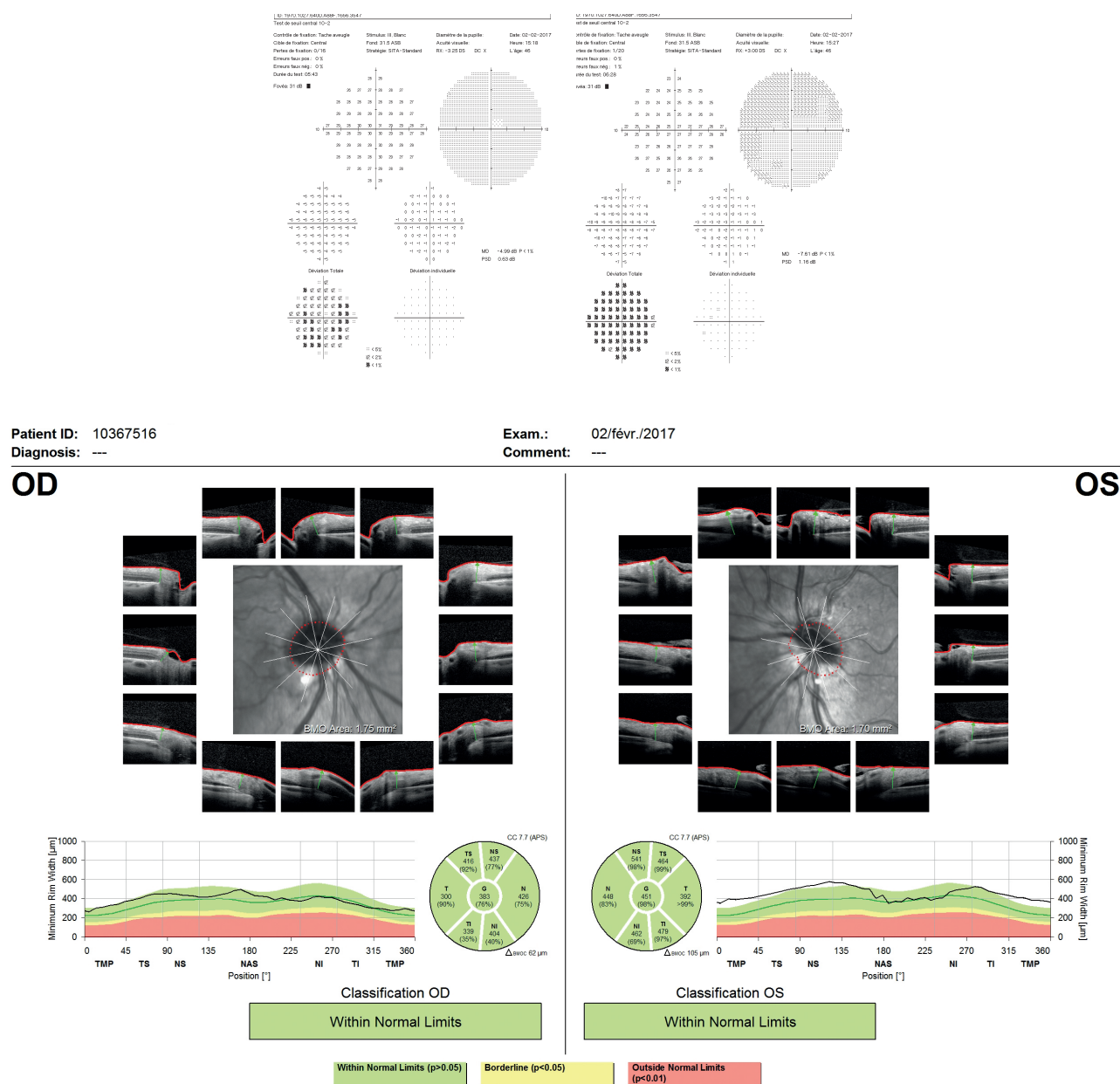
Tilted disc syndrome

A 47-year-old man, with no notable history, with IOP of 16 mmHg and pachymetry of 560 µm.

Horizontal tilted disc syndrome of the -8D myopic right eye with high astigmatism of 6D interferes with the OCT RNFL analysis, falsely suggesting a lesion of the superior RNFL. Although severe inferior nasal tilted disc syndrome of the -5D myopic left eye with astigmatism of 1D has a lesser impact on OCT RNFL analysis, it explains the superior temporal defect observed on 24-2 SAP visual field examination.



Analysis of the ONH BMO-MRW index in this clinical form of tilted disc syndrome confirms the absence of RNFL lesion at the extremities of Bruch's membrane (real limits of the scleral canal), which contains all of the RNFL axons.



Notes:

Date: 03/02/2017

Signature:

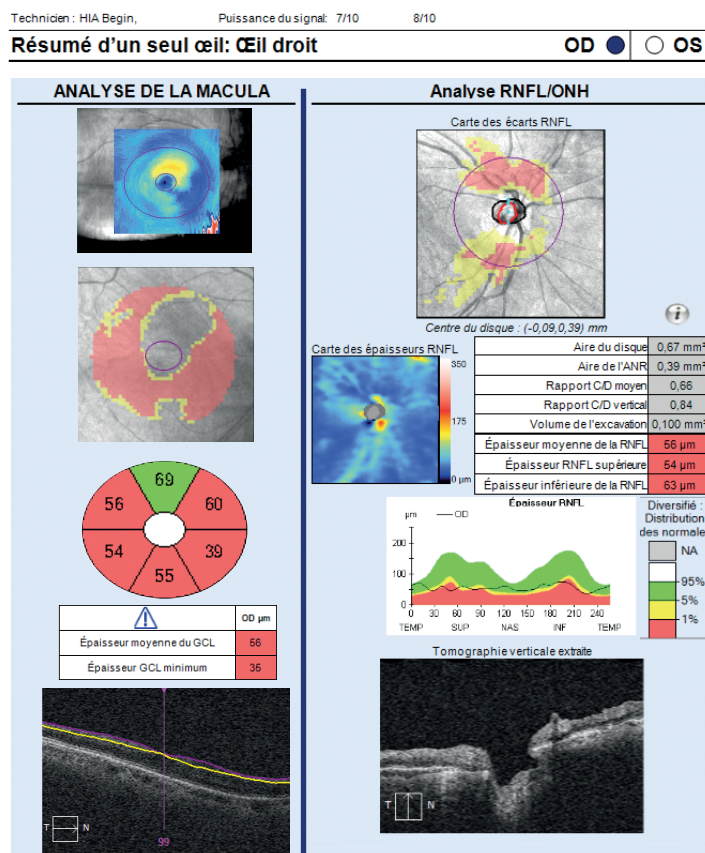
Software Version: 6.3.4

www.HeidelbergEngineering.com

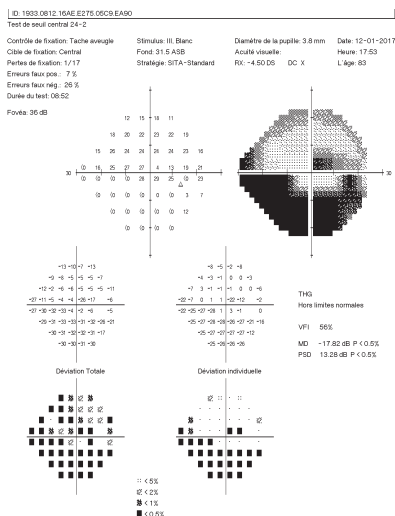
Minimum Rim Width Analysis Page 1

Tilted disc syndrome and glaucoma

The consequences of horizontal tilted disc syndrome on the topographic distribution of the RNFL and peripapillary atrophy give an appearance of superior and inferior RNFL defect on SD-OCT. In this clinical case, tilted disc syndrome associated with -8D myopia and open-angle glaucoma raised difficulties of interpretation of the SD-OCT RNFL analysis at the first examination. Comparison with visual field examination allows more reliable assessment of the inferior functional impairment related to glaucoma.



Comparison with visual field examination allows more reliable assessment of the inferior functional impairment related to glaucoma



24-2 visual field examination of the right eye reveals an inferior Bjerrum scotoma and an early arcuate superior scotoma.

Spectralis SD-OCT RNFL analysis is identical to that of Cirrus HD-OCT. The BMO-MRW index precises an optic nerve head lesion

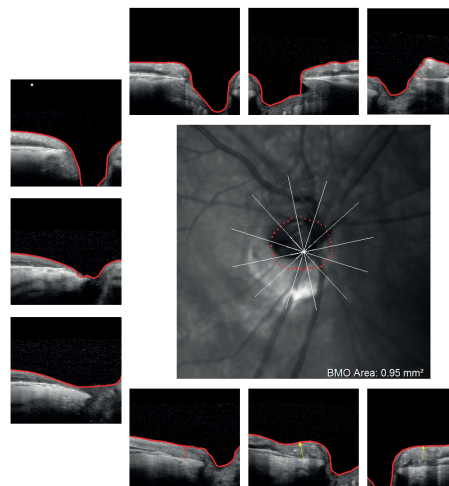
Minimum Rim Width & RNFL Analysis Single Exam Report SPECTRALIS® Tracking Laser Tomography

**HEIDELBERG
ENGINEERING**

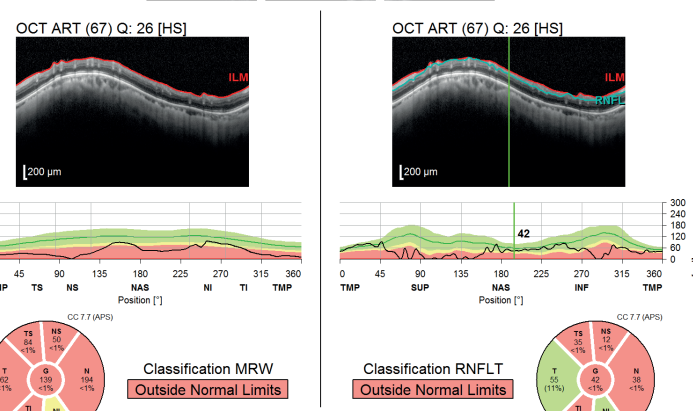
Patient: --- DOB: 12/août/1933
Patient ID: --- Exam.: 09/févr./2017
Diagnosis: --- Comment: ---

Sex: M OD

Minimum Rim Width



RNFL Thickness

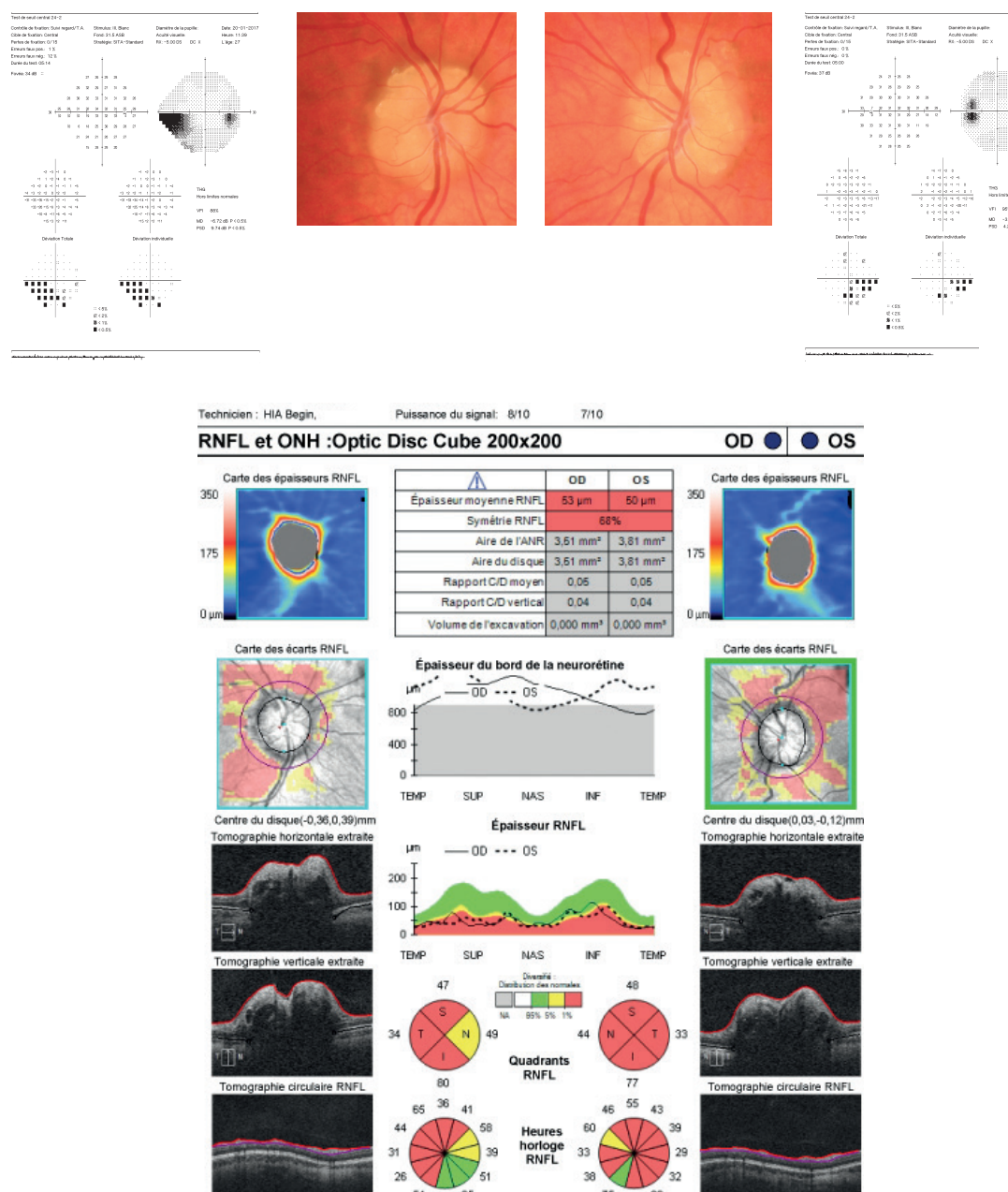


Optic disc drusen

A 28-year-old man, with no signs of OHT and pachymetry of 530 µm.

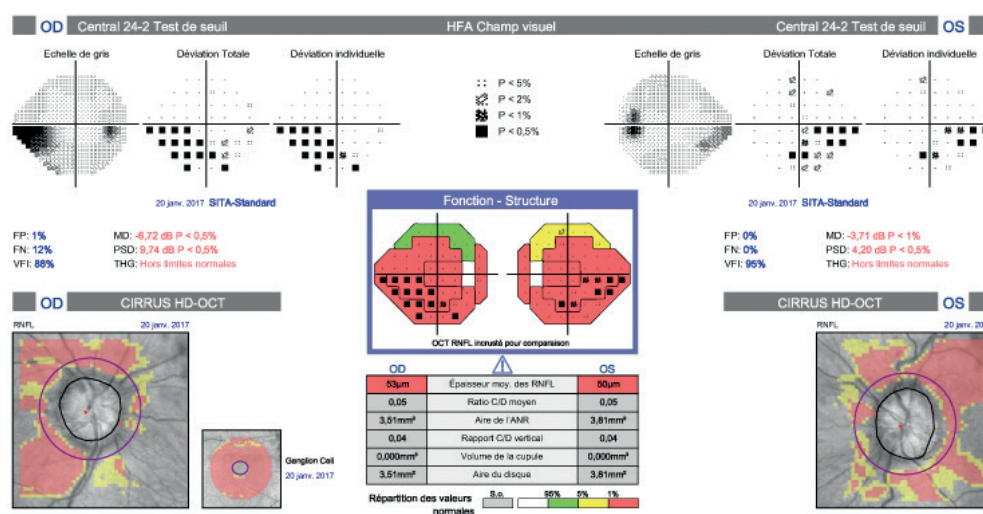
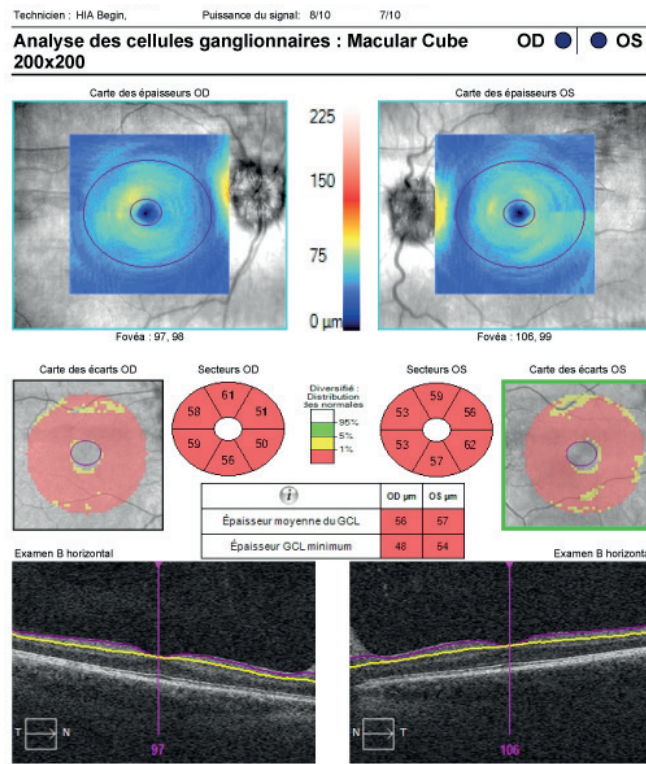
The presence of optic disc drusen markedly interferes with RNFL analysis, resulting in the appearance of a large defect over almost 360° on SD-OCT.

Drusen can be responsible for pseudoglucomatous visual field defects, resulting in difficulties of interpretation commanding regular clinical surveillance.

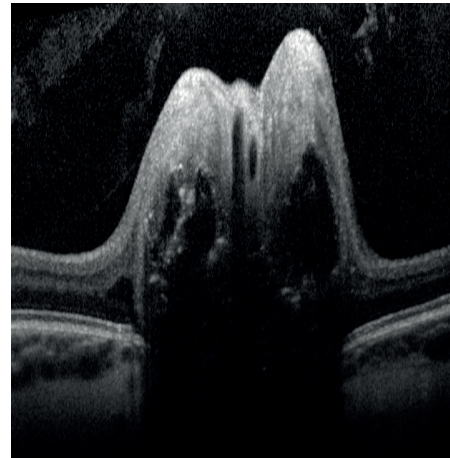
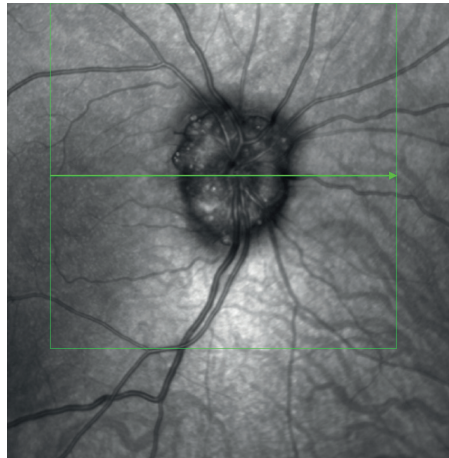


SD-OCT GCC analysis is also severely altered.

“Glaucoma Workplace” software provides a projection of RNFL structural defects onto the representation of functional visual field defects, allowing more precise discrimination of functional visual field defects from RNFL lesions related to drusen.

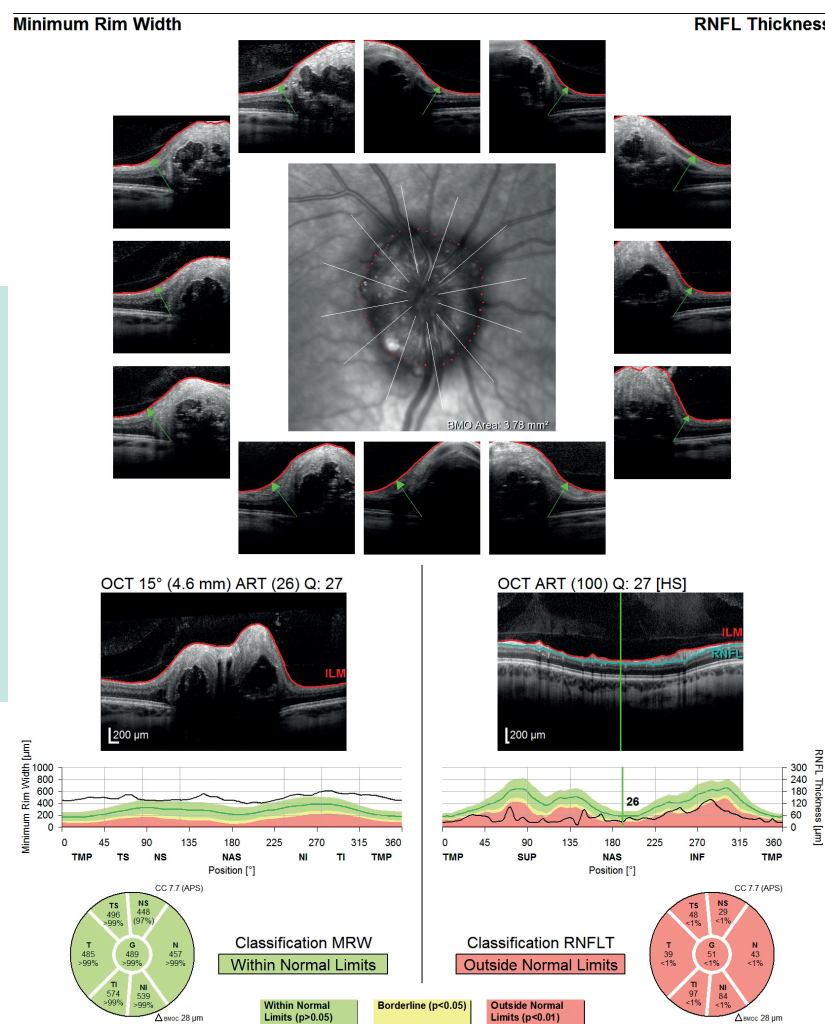


Optic disc drusen



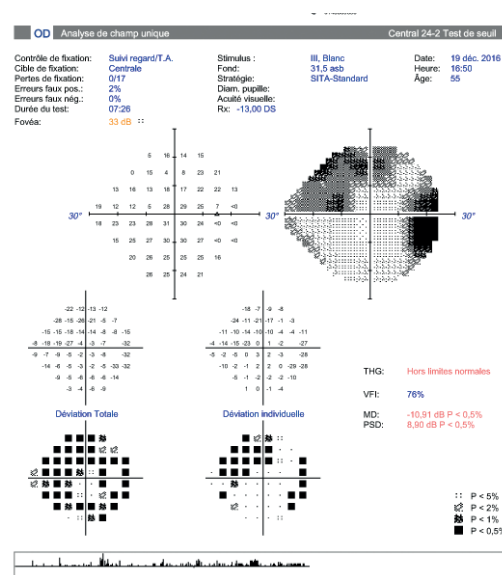
Examination of the optic disc demonstrates the extent of the drusen.

Spectralis SD-OCT reveals a severely altered RNFL with a normal BMO-MRW index on ONH analysis of Bruch's membrane.

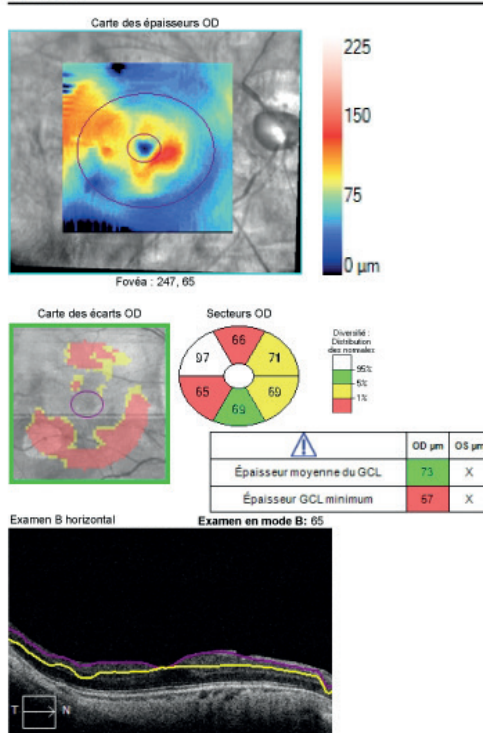


High myopia -15D

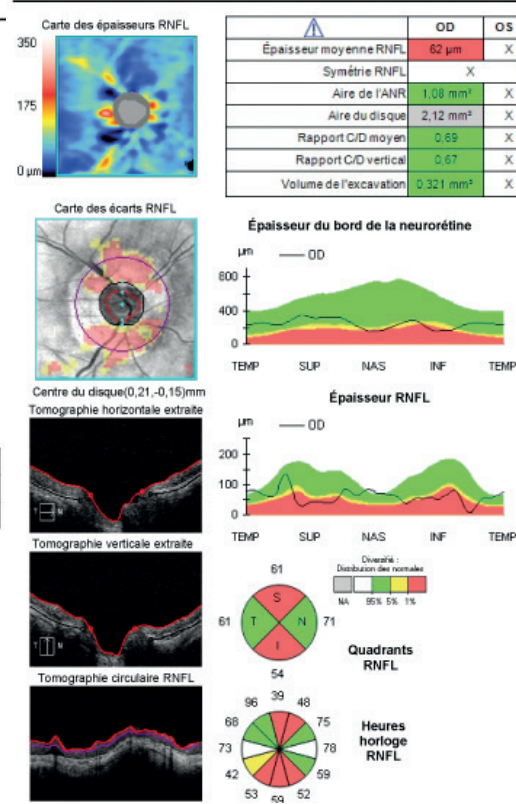
The case of this 55-year-old man, with -15D of myopia clearly illustrates the limitations of RNFL analysis in patients with high myopia associated with severe peripapillary atrophy. Analysis of the macular ganglion cell complex, which is more reliable and more reproducible, should be preferred in these clinical forms.



Technicien : Operator, Cirrus
Puissance du signal: 8/10
Analyse des cellules ganglionnaires : Macular Cube 512x128



Technicien : Operator, Cirrus
Puissance du signal: 8/10
RNFL et ONH :Optic Disc Cube 200x200



In summary, the macular measurements provided by SD-OCT are just as sensitive as RNFL measurements for the detection of glaucoma, and can sometimes be superior to RNFL measurements in certain very early clinical forms, especially in the frequent case of early initial paracentral lesions, in which only macular measurements are able to detect early lesions in about 20% of cases.

Measurement of the peripapillary RNFL remains the optimal OCT parameter for the diagnosis of more advanced perimetric glaucoma. Analysis of the GCC complex improves diagnostic precision and more reliable assessment of the extent of the lesions. At the present time, RNFL analysis remains superior to analysis of ONH parameters.

In the case of tilted disc syndrome, SD-OCT analysis of the peripapillary RNFL and ONH remains less reliable than analysis of the GCC complex. New methods of detection of the limits of Bruch's membrane on ONH acquisitions (BMO-MRW index) should allow more reliable analysis of these clinical forms.

The diagnosis of glaucoma in patients with high myopia remains difficult due to the numerous anatomical variants observed in these moderate or high myopic eyes, associated with a higher false-positive rate. Macular parameters ensure better diagnostic precision in high myopes, particularly with the use of complementary indices (GLV, FLV), but with at least 10% of poor quality acquisitions.



9. Traps in SD-OCT

9.1. During acquisition

- 9.1.1. Patient-related factors**
- 9.1.2. Operator-related factors**
- 9.1.3. Devices-related factors**

9.2. After acquisition

- 9.2.1. Abnormalities of the vitreoretinal interface,
thickened posterior hyaloid, ERM**
- 9.2.2. Vitreoretinal traction**
- 9.2.3. POAG and maculopathy**
- 9.2.4. POAG and AMD**
- 9.2.5. Fovea plana**

Many traps have been identified in SD-OCT performed for the assessment of glaucoma. These traps are responsible for false-positive results, reported in up to 26% of healthy subjects and in about 40% of cases of early glaucoma.

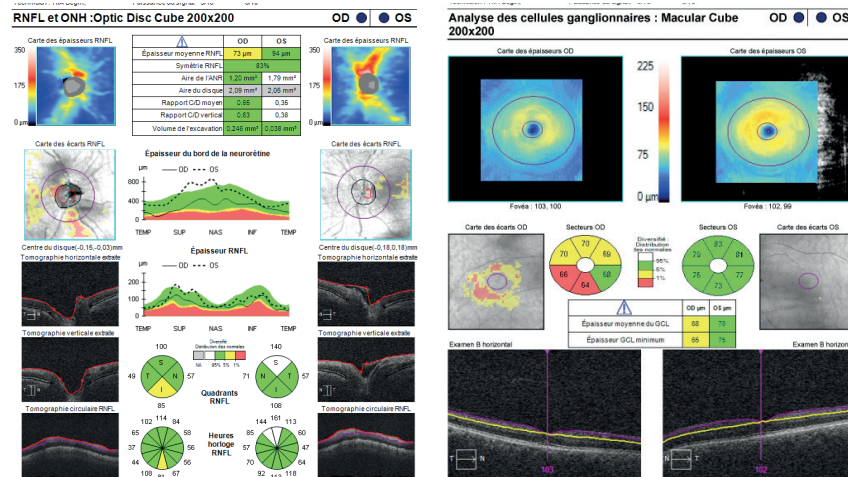
These SD-OCT traps comprise all of the acquisitions and analyses that do not accurately reflect the reality of the structural lesion, corresponding to either an abnormal image with no real structural lesion, or an apparently normal image despite the presence of a structural lesion.

These traps must be well known and recognized, not only during acquisition, during which they must be immediately corrected, but also following a good quality acquisition, on which false-positive results are identified by good quality interpretation of the SD-OCT images and a good understanding of the limitations of the examination.

Traps during acquisition can be patient-, operator- or device-related.

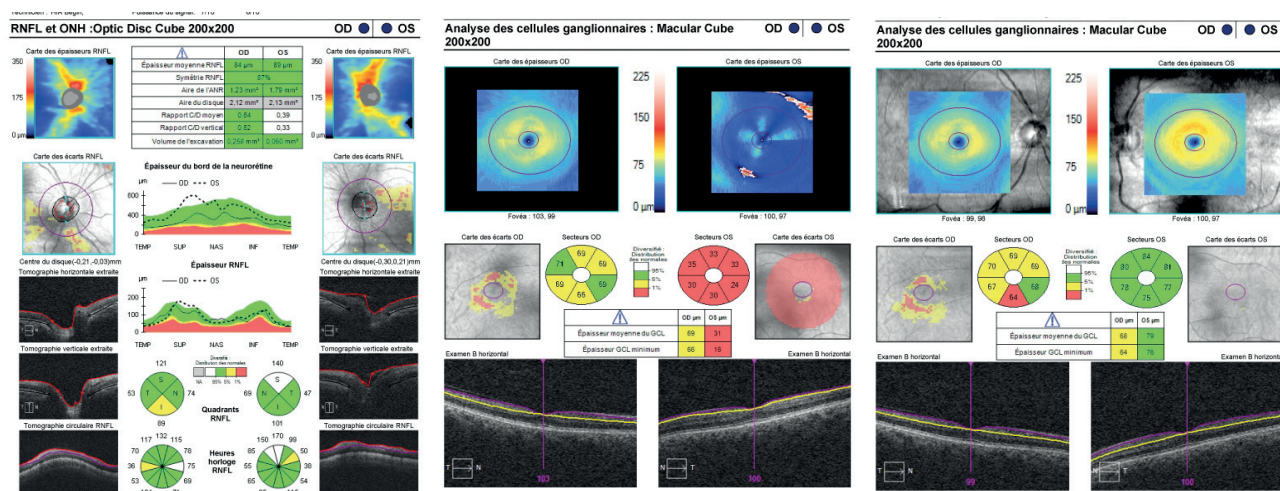
Traps after acquisition are related to analysis of SD-OCT reports and various anatomical factors.

During acquisition – Patient-related factors



Early glaucoma

Minor lesion of the inferior RNFL and inferior temporal GCC in the right eye



Follow-up at 1 year

Surprisingly severe GCC lesion of the left eye despite apparently normal segmentation of the B-scan.

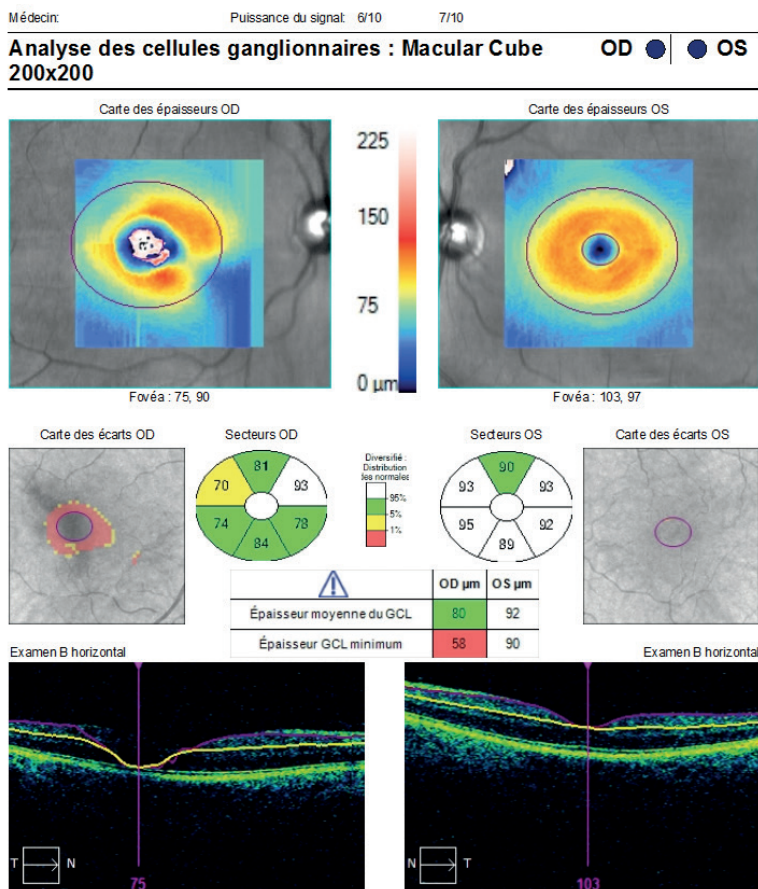
After dilatation

Disappearance of the false-positive lesion of the left eye. The SD-OCT image is more consistent with the initial analysis

Remember that an adequate pupillary dilatation is essential to obtain a reliable SD-OCT examination

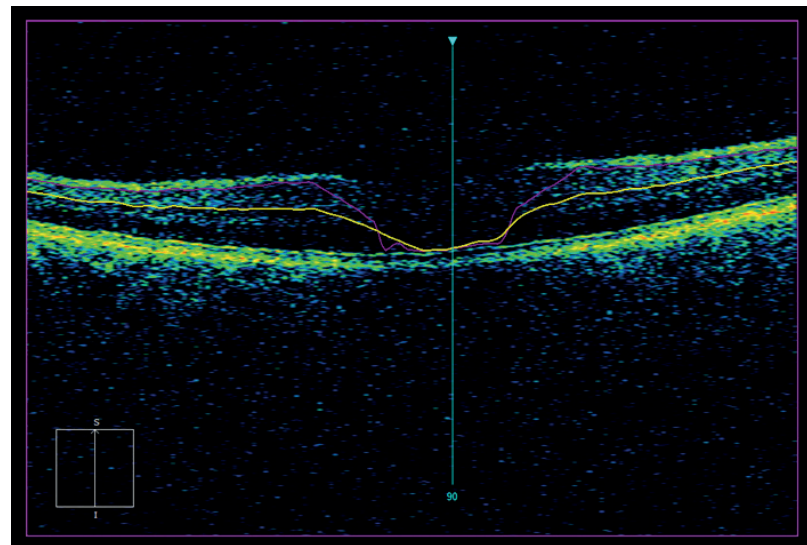
During acquisition – Patient-related factors

Lens opacity



A 73-year-old man, with visual acuity of 7/10, and a small central posterior subcapsular cataract responsible for diffuse signal attenuation, resulting in an error of segmentation of the retinal layers with decreased RNFL and GCC thickness on OCT.

When the lens opacity is more peripheral, better acquisition can be achieved by avoiding the opacity.



Floating body

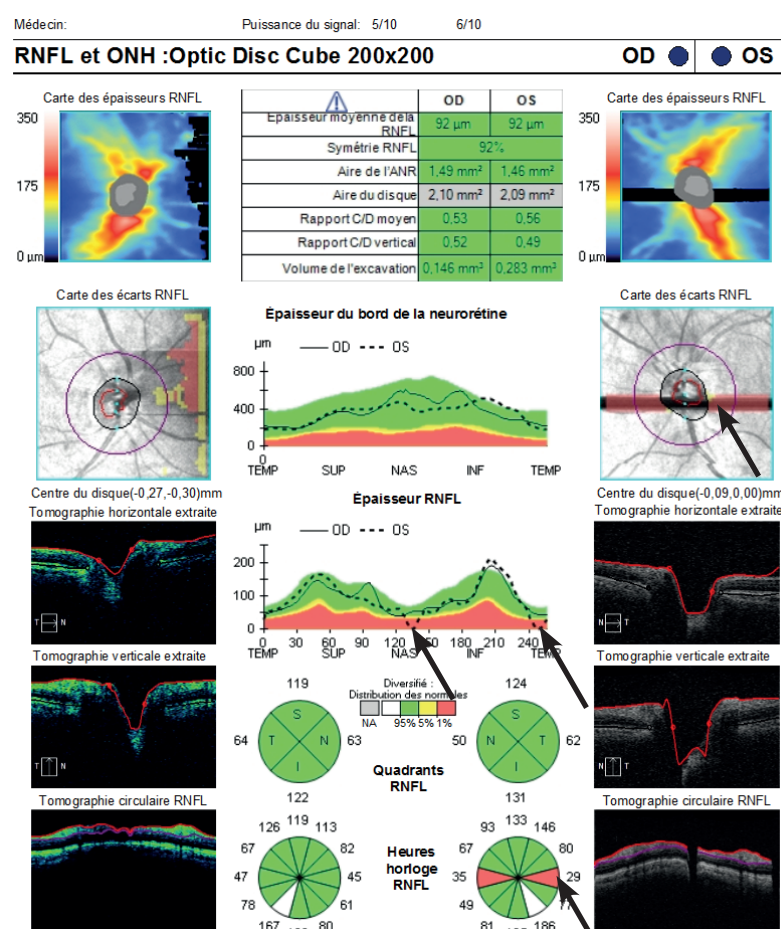
A 90-year-old man followed and treated for bilateral POAG with more advanced glaucoma in the left eye. OCT follow-up examination reveals the shadow of a vitreous floating body localized in the inferior temporal sector of the arcuate fibres of the right eye, suggesting the presence of a new RNFL defect with localized signal loss. Repeated acquisitions after several eye movements allowing displacement of the floating body and its projection provide more reliable reports.



During acquisition – Patient-related factors

Blinking

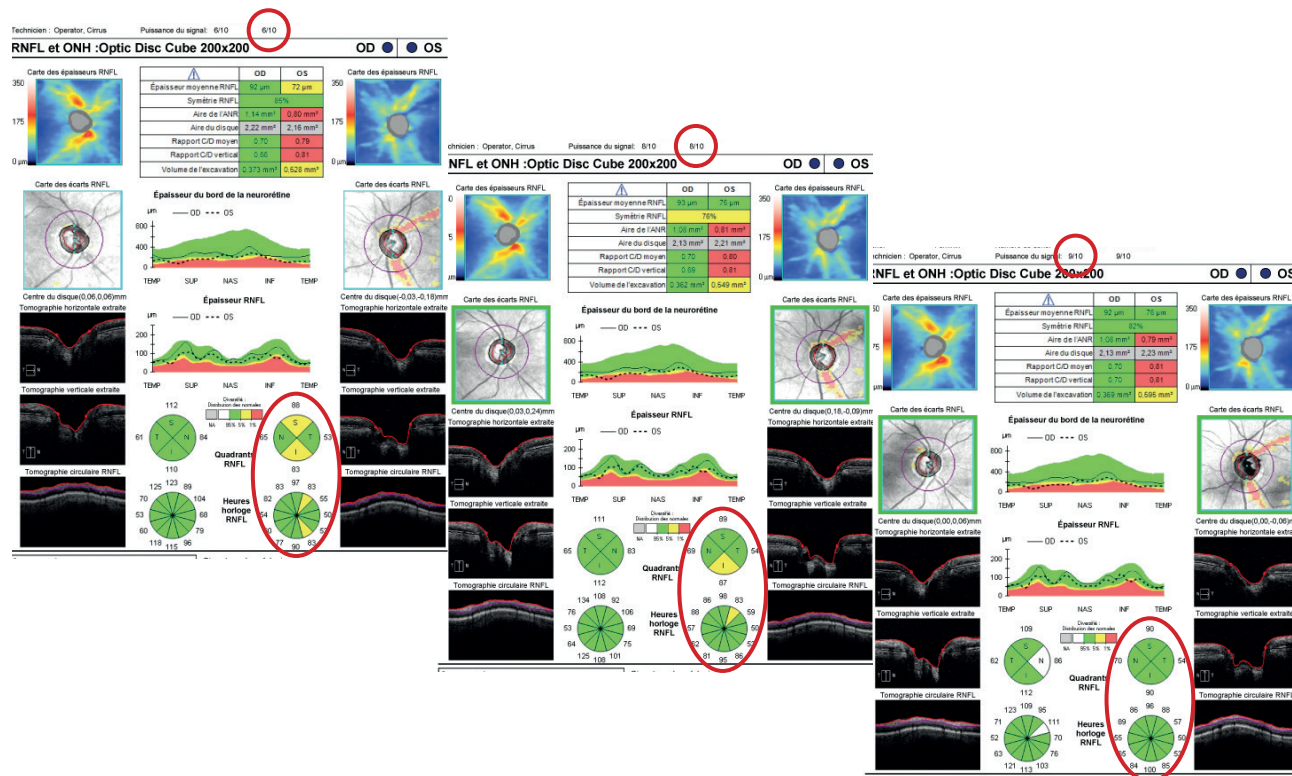
Blinking during acquisition is responsible for a horizontal band of signal loss, the width of which corresponds to the duration of blinking. It presents in the form of a band of abnormal points on the deviation map with decreased RNFL thickness in the same sector, requiring another acquisition.



During acquisition – Operator-related factors

Try to achieve the higher SSI index

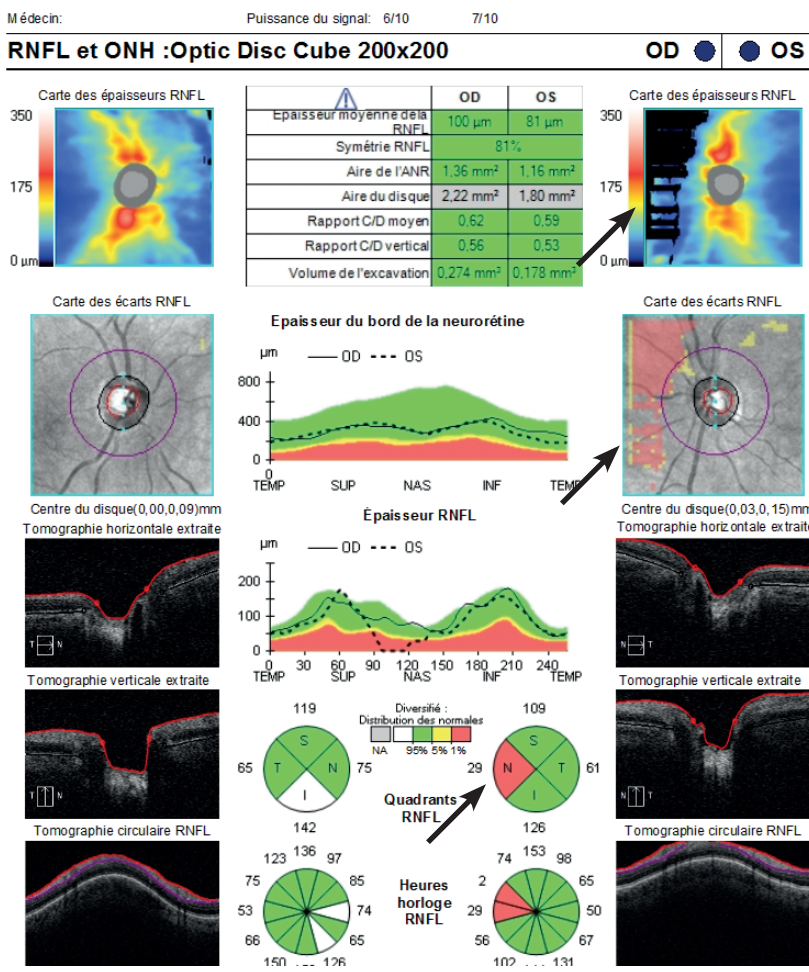
SD-OCT examination in a patient with early OAG with signal strength indices of 6.8 and 9/10 on Cirrus HD-OCT. The higher SSI reveals fewer RNFL structural defects, especially in the left eye.



The minimum of quality signal strength index provided by the SD-OCT may not be sufficient.

During acquisition – Operator-related factors

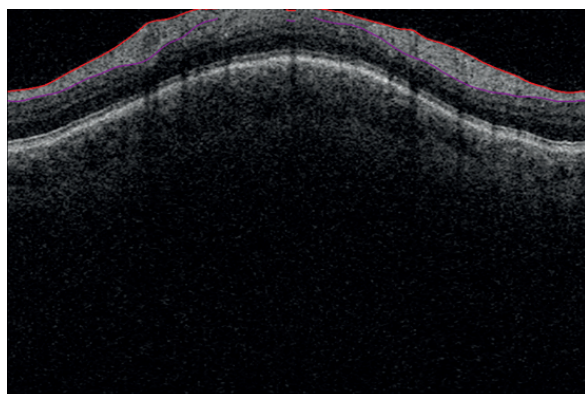
Z centering artifact



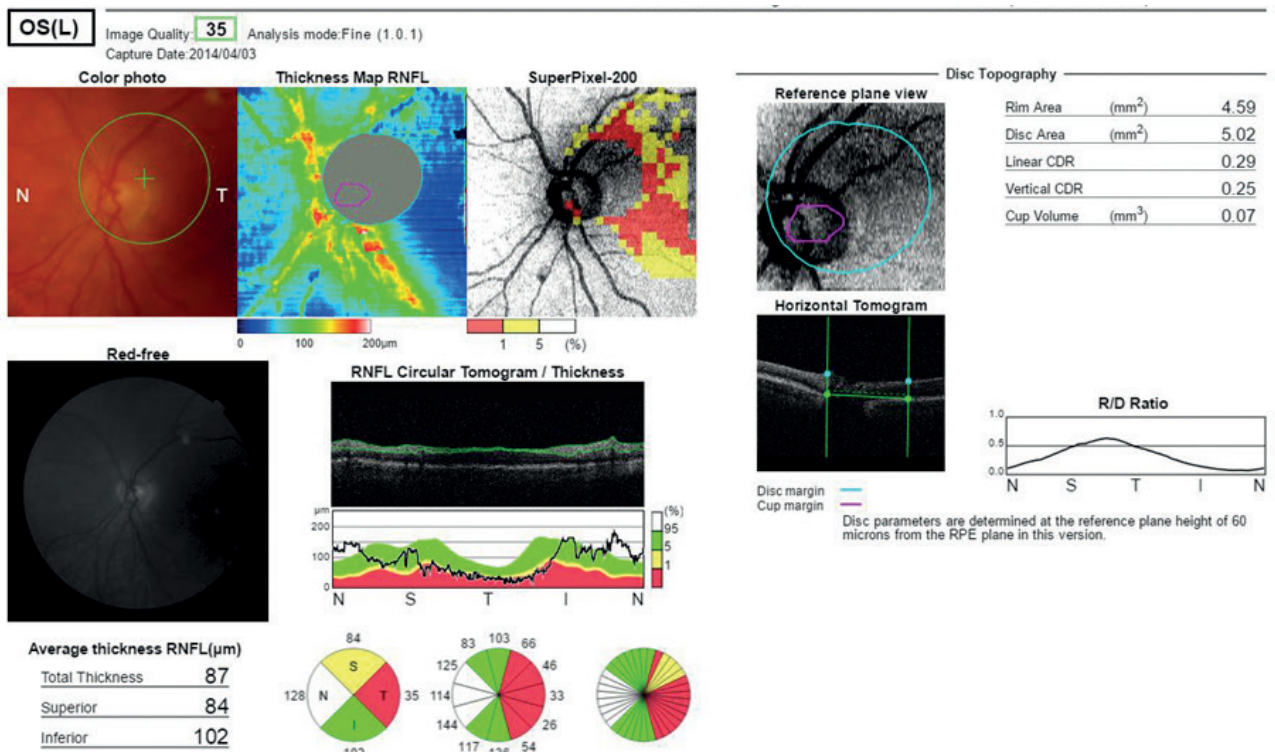
B-scan acquisition poorly centered on the z axis, giving a "truncated cone" appearance.

The absence of segmentation of the truncated image by the software is accompanied by alteration of the RNFL thickness, clearly visible on the thickness map and deviation map, in the nasal sector of the left eye.

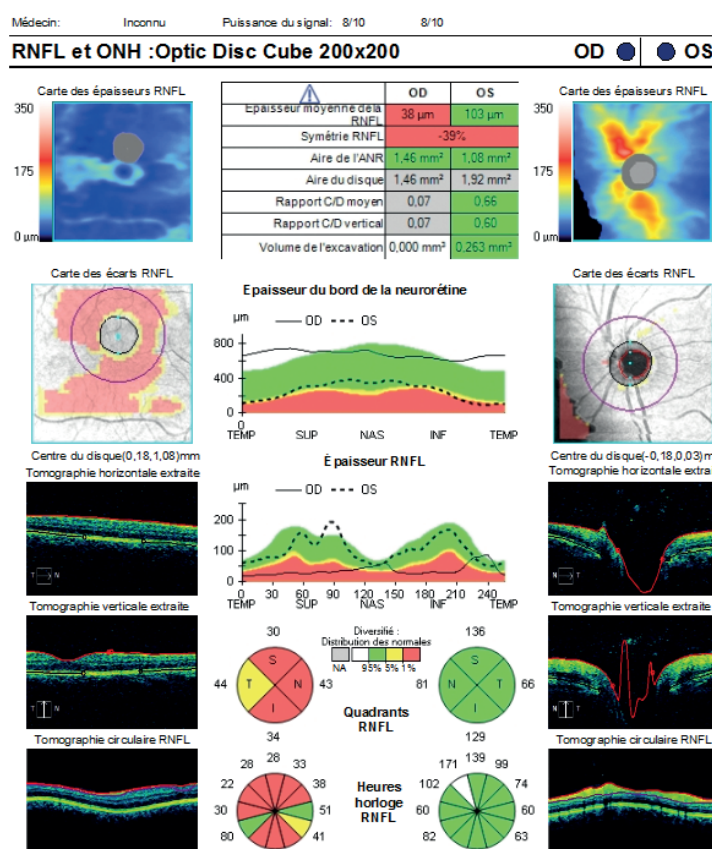
The short depth of focusing of SD-OCT acquisition, about 2 mm, must be kept in mind in order to avoid this type of artifact, which requires another acquisition.



Centering error

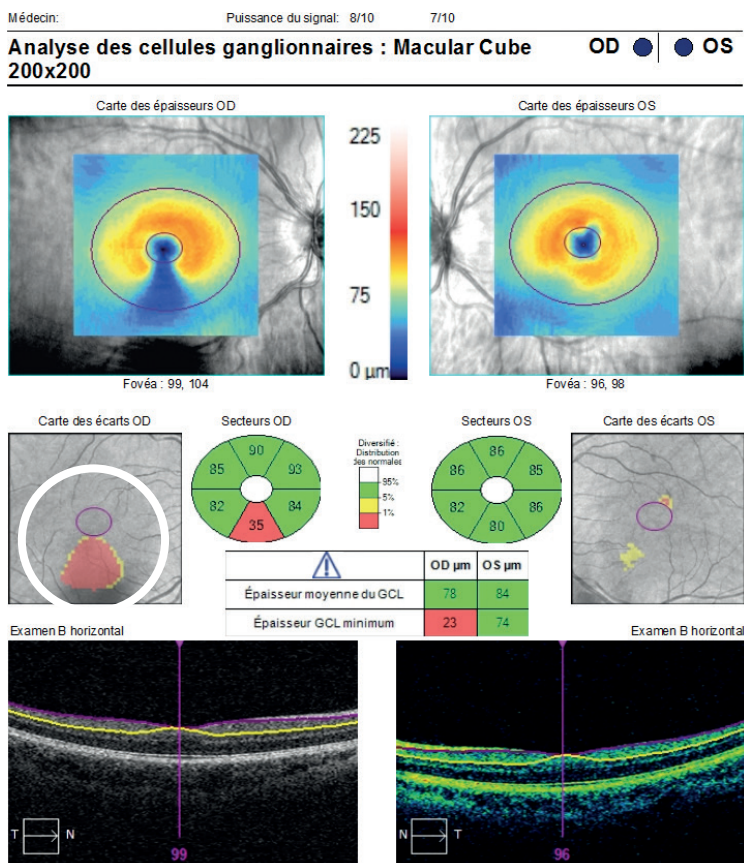


The centering error results in poor segmentation of the retinal layers with abnormal values not corresponding with the normative database. The abnormality is generally very severe and inconsistent with the clinical findings. This type of centering error, often responsible for very severe abnormalities, can be observed with all SD-OCT devices, highlighting the importance of a very attentive approach by the operator during acquisition so that the acquisition can be repeated immediately when necessary.



During acquisition – Device-related factors

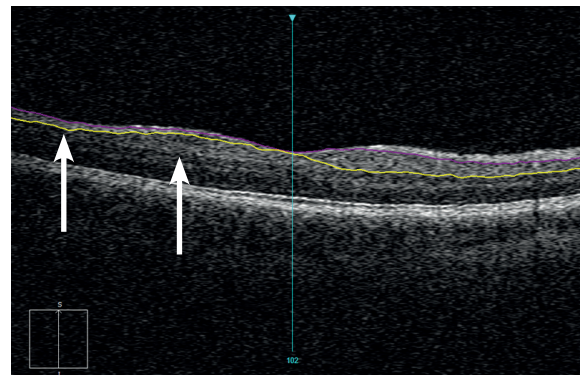
Nonspecific topographic defect Segmentation error



In the presence of a nonspecific GCC defect with apparently normal B-scan segmentation, the analysis must be completed by examining various B-scans in the sector corresponding to the defect.

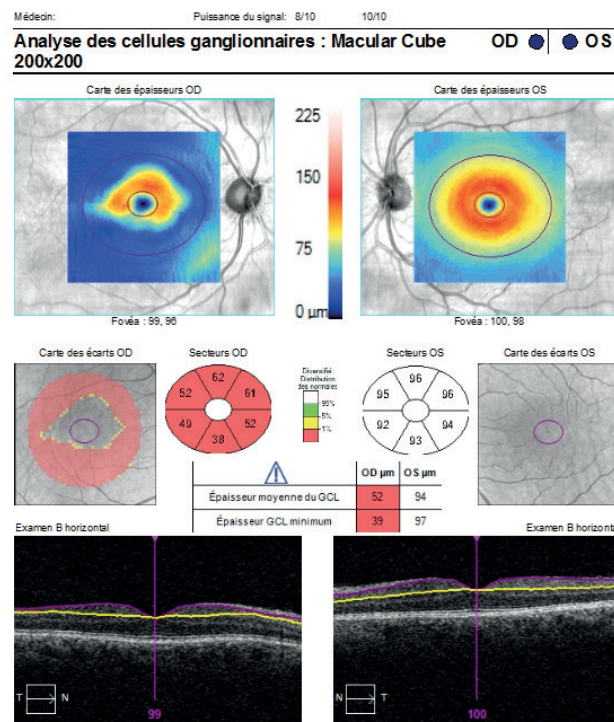
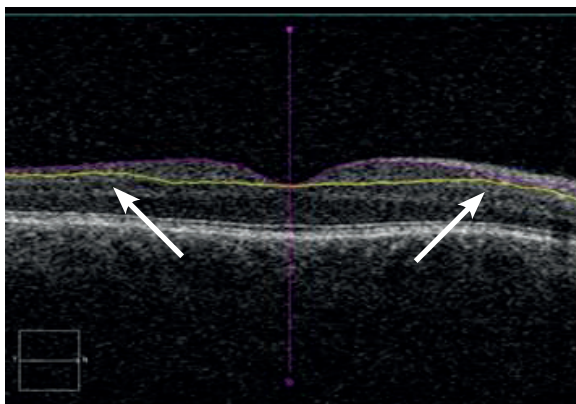
This vertical B-scan through the zone of the defect demonstrates a segmentation error of the macular ganglion cell complex by the SD-OCT analysis software, which failed to correctly segment the various retinal layers. This type of error can be very difficult to detect depending on its site and must be suspected in the case of SD-OCT reports that are inconsistent with the clinical findings.

The SD-OCT analysis software may fail to correctly segment the retinal layers, resulting in a «false-positive» GCC or RNFL defect.

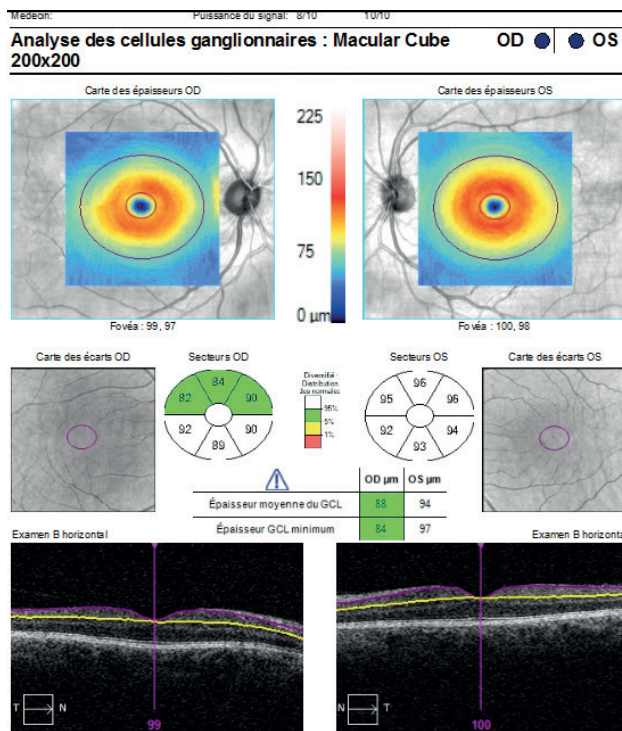
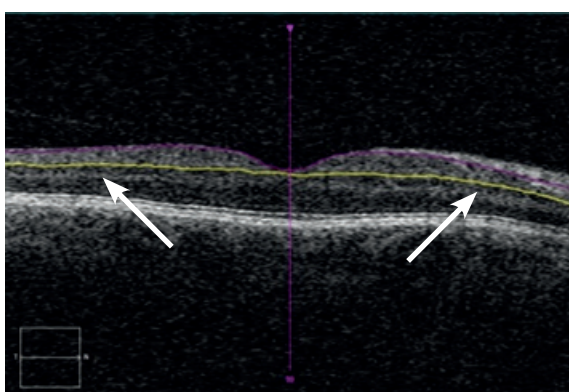


Segmentation error

The SD-OCT analysis software may fail to correctly segment the retinal layers, resulting in a «false-positive» GCC defect, in the right eye in this case.

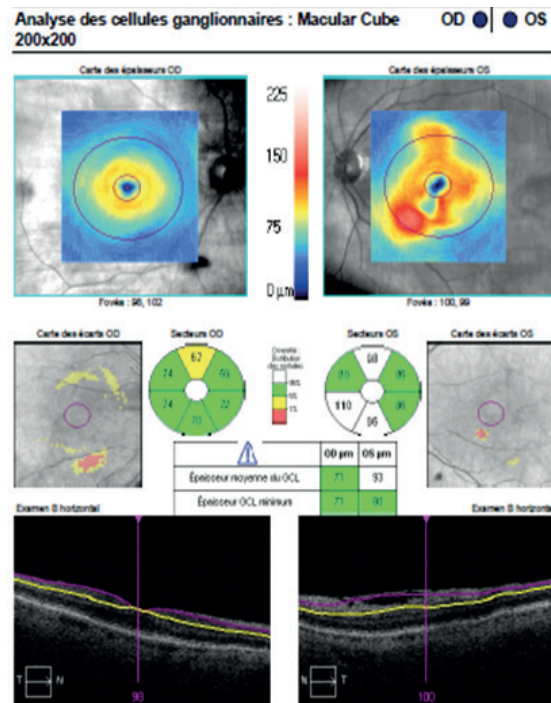


The repeat examination shows good segmentation of the various retinal layers by the analysis software.

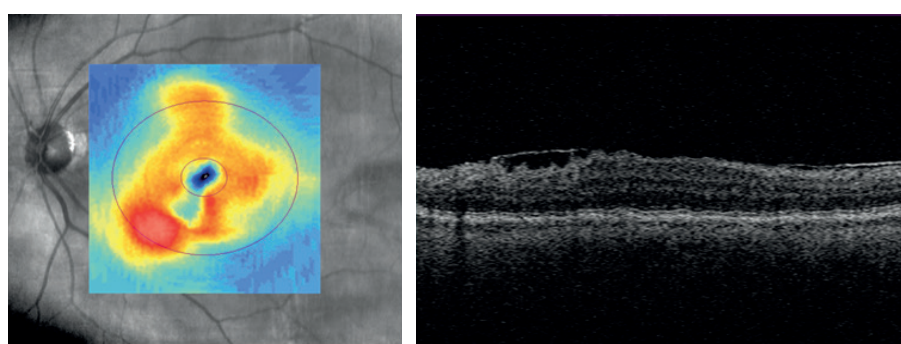


After acquisition

Abnormalities of the vitreoretinal interface Thickened hyaloid, ERM



Careful examination of the B-scan in the lower part of the SD-OCT display shows the presence of an epiretinal membrane (ERM) responsible for increased of thickness of internal retinal layers evaluated by SD-OCT.

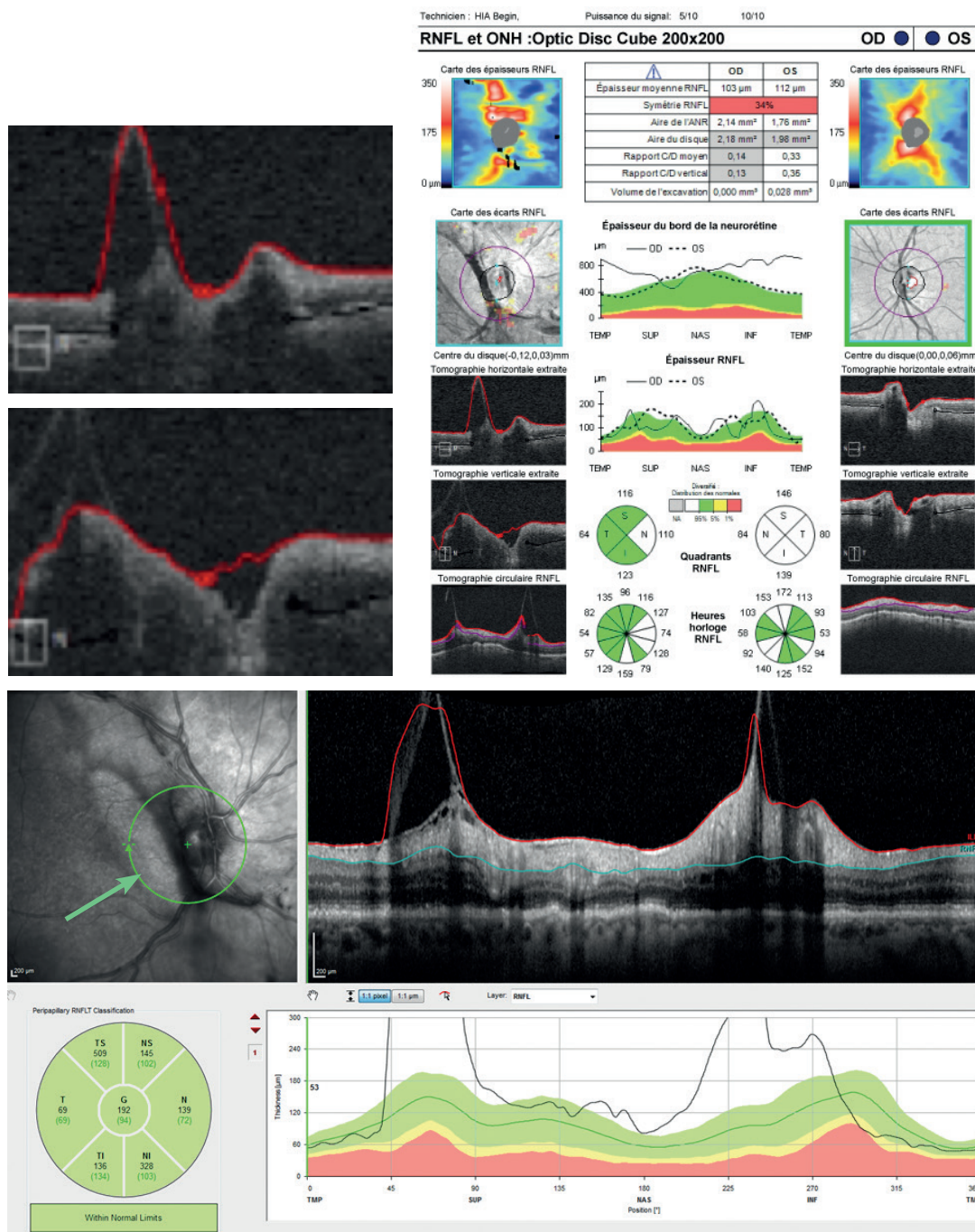


Vitreoretinal traction

In this 91-year-old man, the large right peripapillary vitreoretinal traction accounts for the abnormal RNFL thickness reported on SD-OCT.

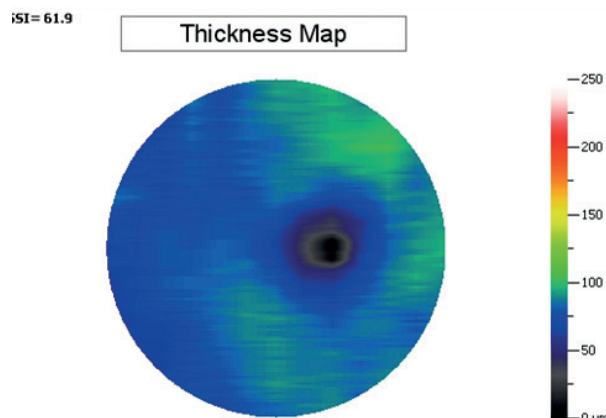
It is clearly visible on the deviation map and on the two magnified B-scans of SD-OCT of the ONH of the Cirrus HD-OCT and on the Spectralis OCT report.

These features highlight the importance of comparing the OCT results with data of the clinical examination and interpreting OCT in the light of the clinical context.

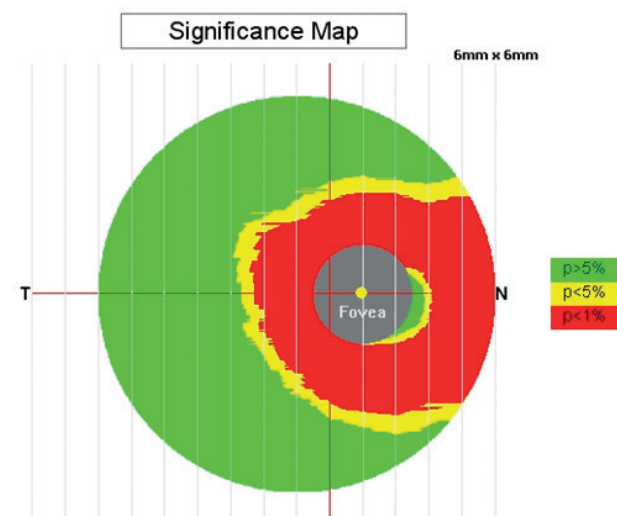


After acquisition

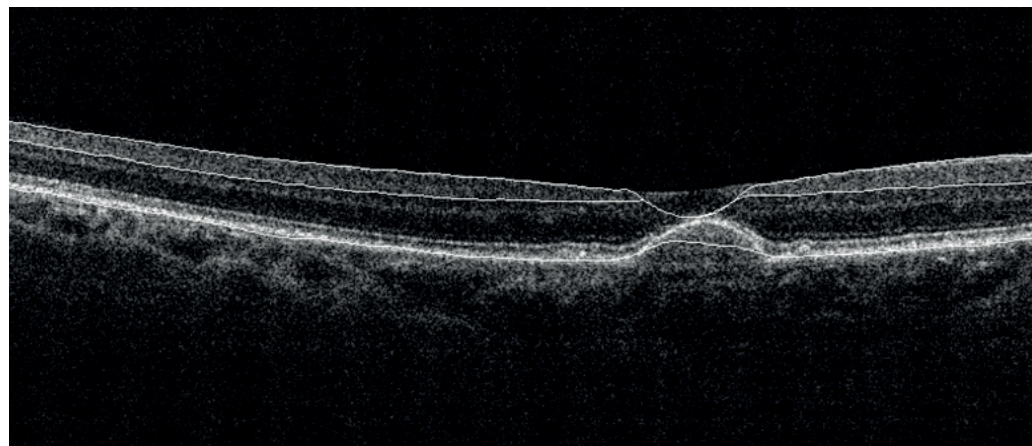
POAG and maculopathy



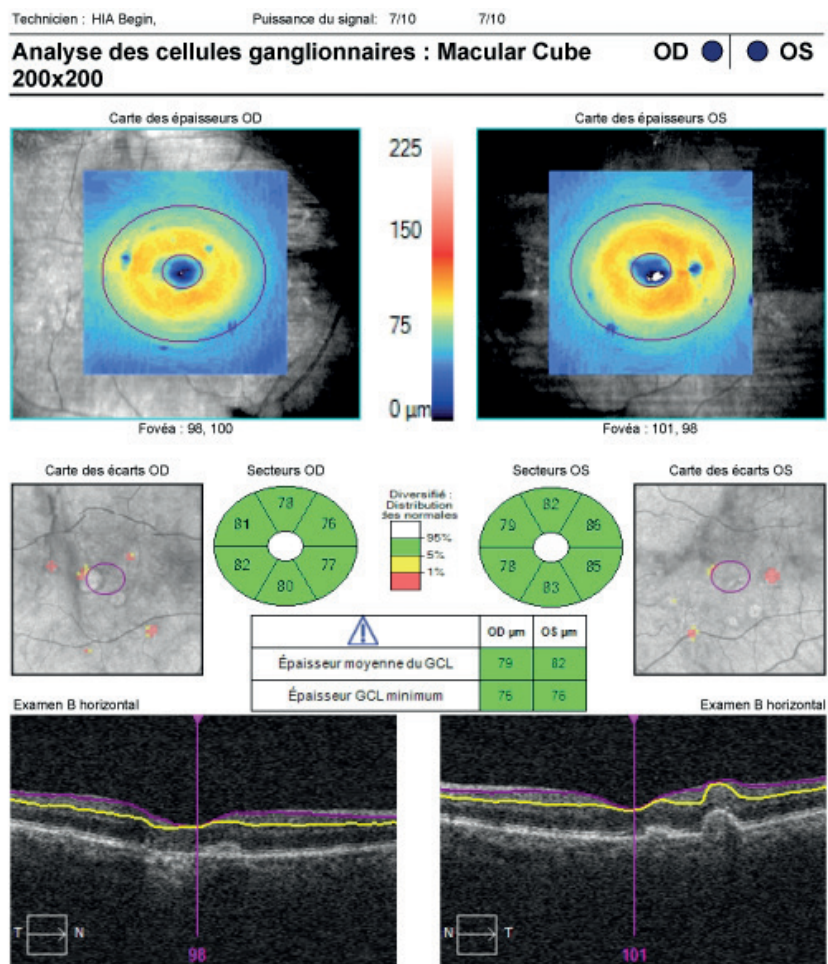
In the presence of a central perifoveal GCC lesion on SD-OCT, a non-glaucomatous central macular lesion should be tried to find on clinical examination and the macular line scan, illustrated in this case by the presence of retrofoveal material.



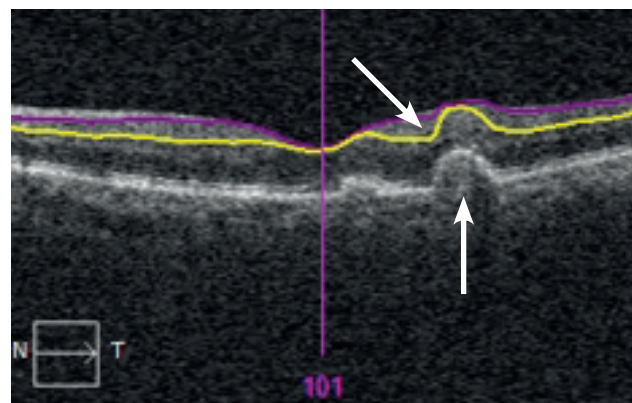
| Average Thi... | Thickness... | Std Dev |
|----------------|--------------|---------|
| Total | 82.13 | |
| Superior | 82.83 | |
| Inferior | 81.43 | |
| Intra Eye ... | 1.40 | 6.47 |
| FLV (%) | 9.229 | |
| GLV (%) | 14.788 | |



POAG and AMD

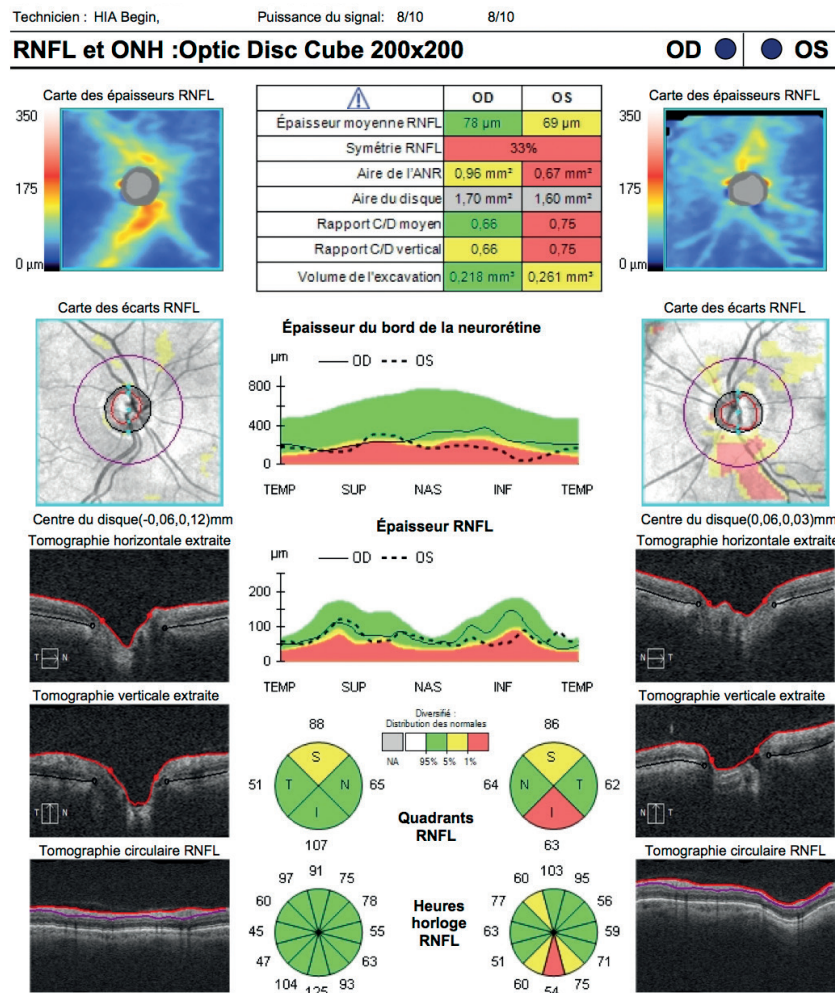


In the case of associated maculopathy, the SD-OCT examination must be compared with clinical examination of the macula and the segmentation B-scan. This retinal layer segmentation must be carefully verified, including projection of drusen and other macular alterations, in order to correctly interpret the results and the GCC defect.



After acquisition

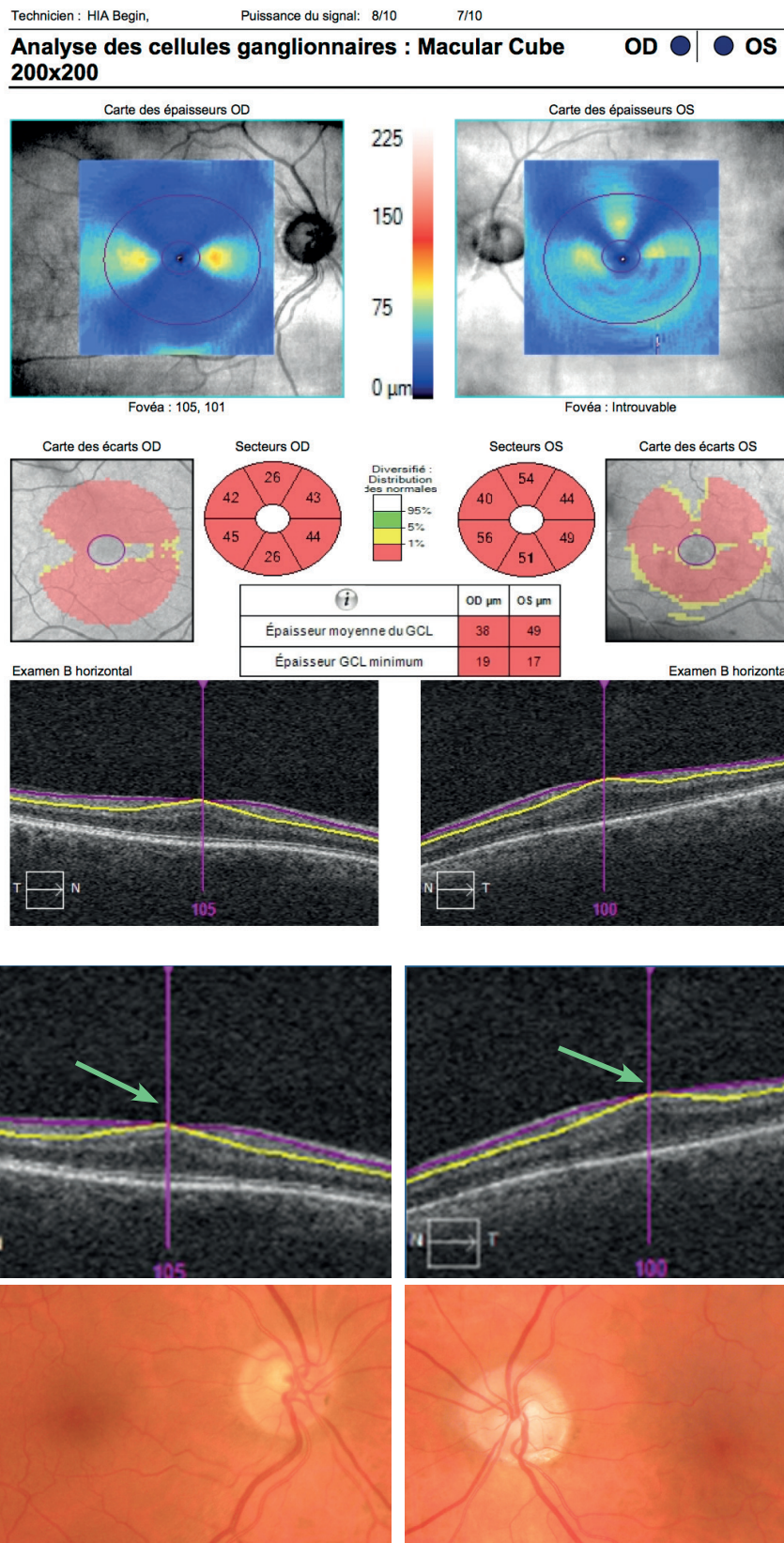
Fovea plana



67-year-old man followed and treated for POAG with isolated paracentral scotoma in the left eye. OCT reveals an inferior RNFL defect in the left eye and a surprising bilateral appearance of the GCC report.. Analysis of B-scans in the lower part of the examination confirms bilateral *fovea plana* without functional repercussions, with visual acuity of 10/10 and no ocular fundus abnormality, allowing this benign dysplasia to be distinguished from macular foveal hypoplasia.

OCT follow-up in these clinical forms is limited to RNFL analysis.

The cover illustration of this book corresponds to 3D SD-OCT analysis of the left optic disc in this patient.



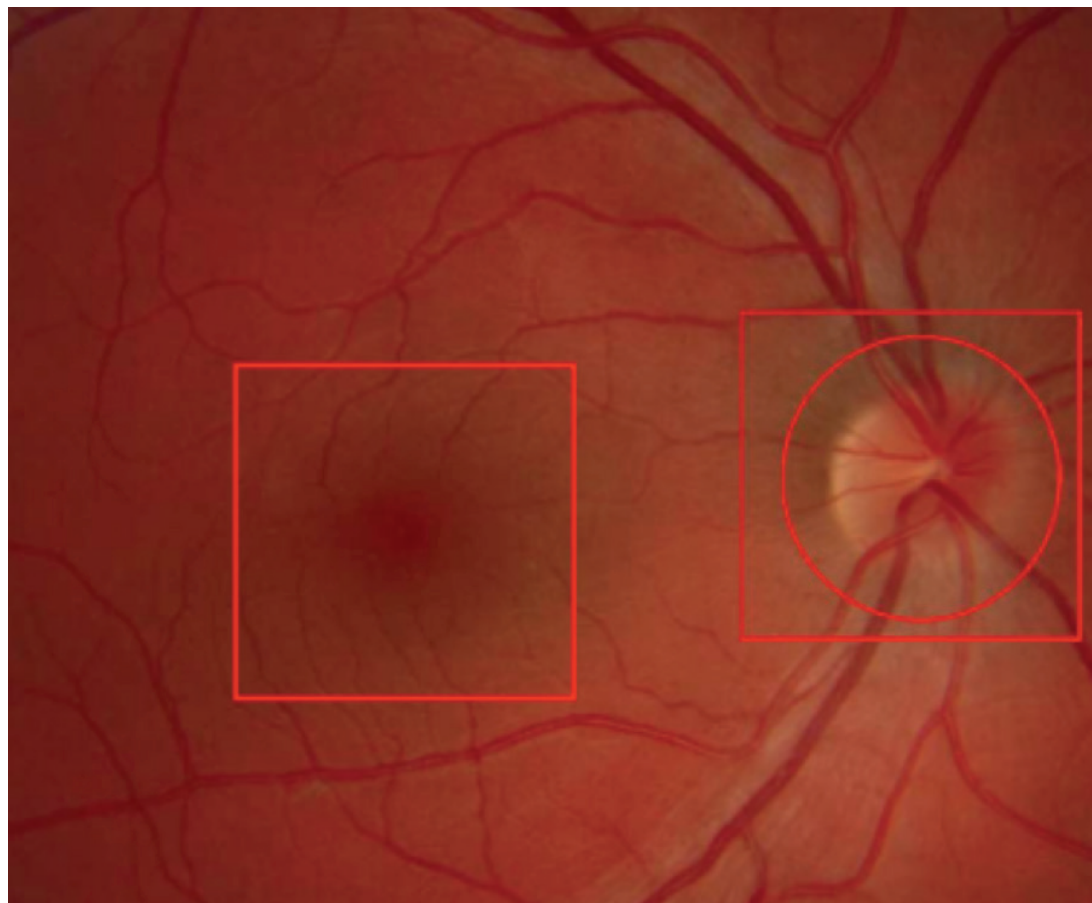


10. SD-OCT markers of progression

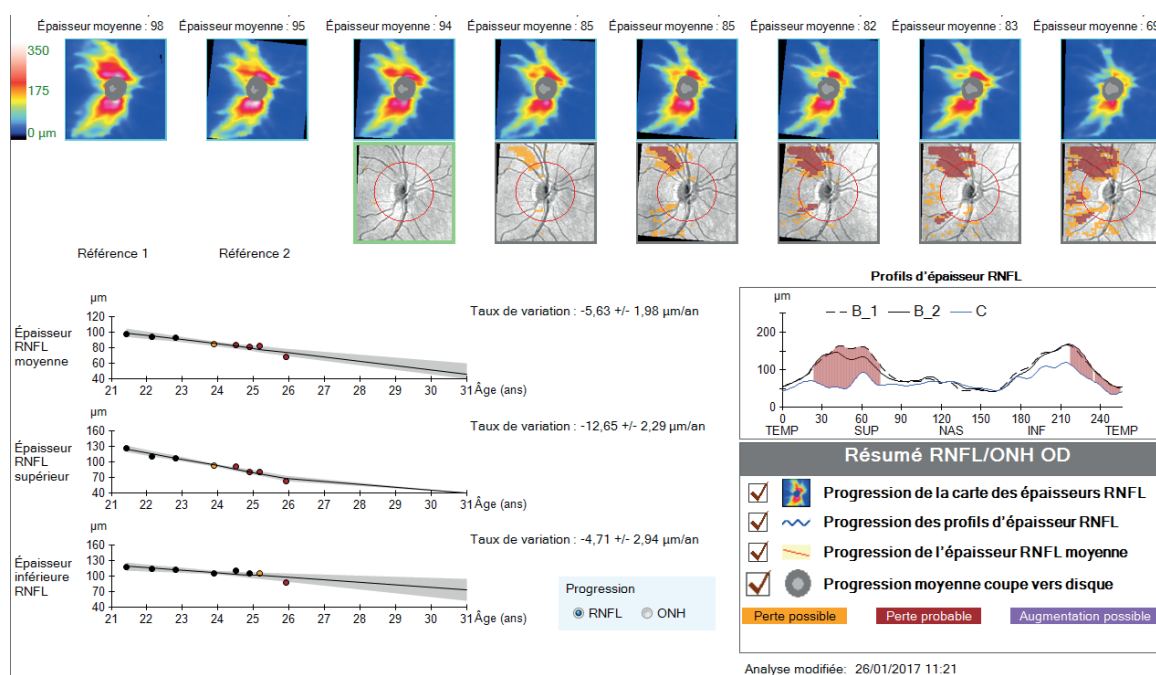
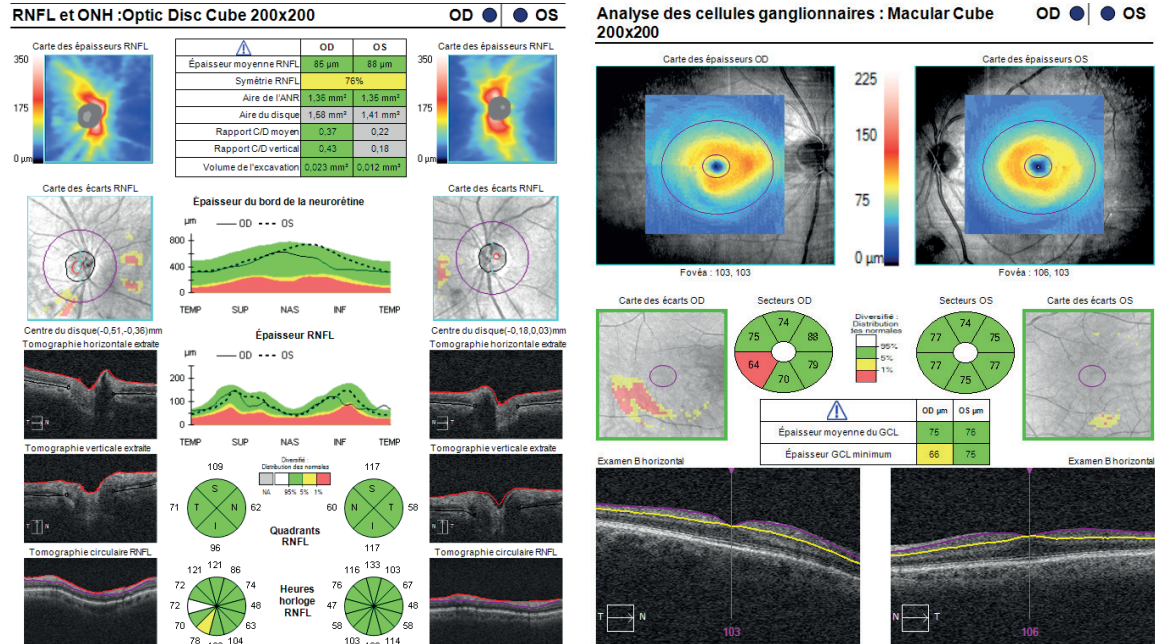
- 10.1. Markers of RNFL progression**
- 10.2. Markers of GCC progression**
- 10.3. New progression analysis**

SD-OCT markers of progression

SD-OCT analysis of glaucoma progression is based on event analysis, which compares single events with reference data to determine the presence of progression, and trend analysis, which quantifies progression by evaluating the rate of deterioration of the various parameters recorded.



In the current state of available technology, these analyses must always be based on reliable examinations performed with the same OCT device in a given patient.



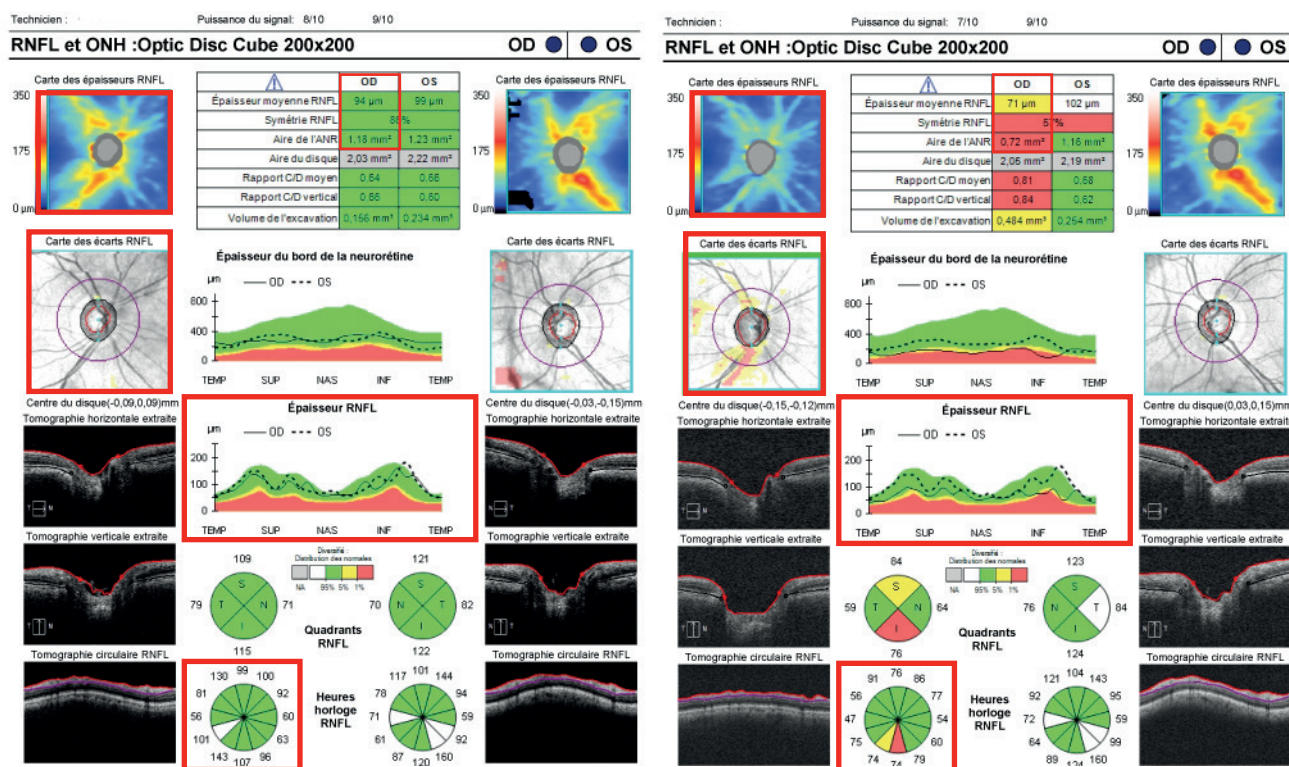
État:

ID du patient

Analysé

Terminer

SD-OCT markers of RNFL progression



4 years

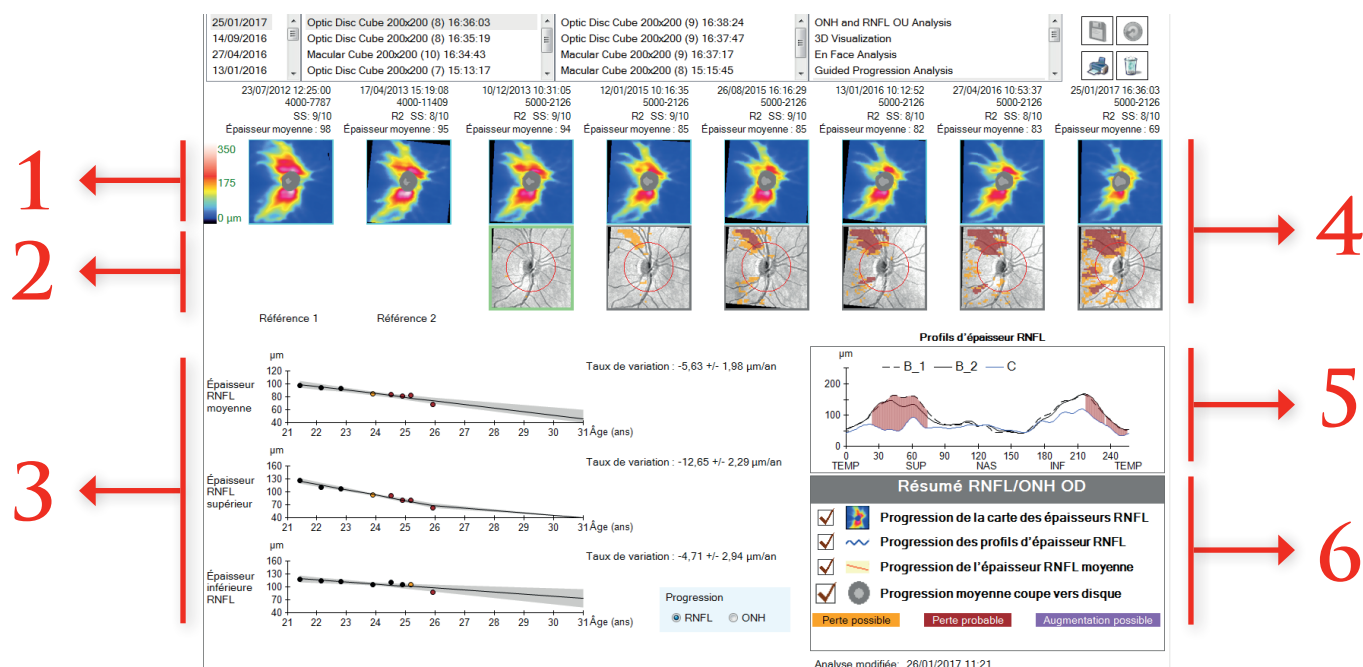
Analysis of glaucoma progression looks for signs of deterioration on colour-coded thickness maps and deviation maps, superimposition of successive RNFL thickness profiles (TSNIT graphs), mean thickness and peripapillary RNFL thickness maps.

Analysis of RNFL progression in this 75-year-old woman reveals progression of each of the parameters evaluated. Clinical judgement may therefore be sufficient to demonstrate progression in these rapidly progressing clinical cases. Colour codes indicate the normal, suspicious or pathological appearance compared to the database of age-matched healthy subjects, but this type of OCT display does not provide any statistical analysis of progression or any trend or event analysis.

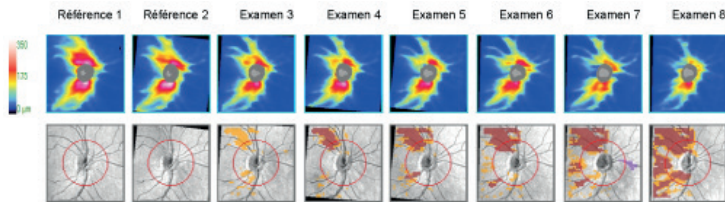
Markers of RNFL progression

All SD-OCT devices propose specific glaucoma progression analysis software comprising trend analysis and, in some cases, automated event analysis.

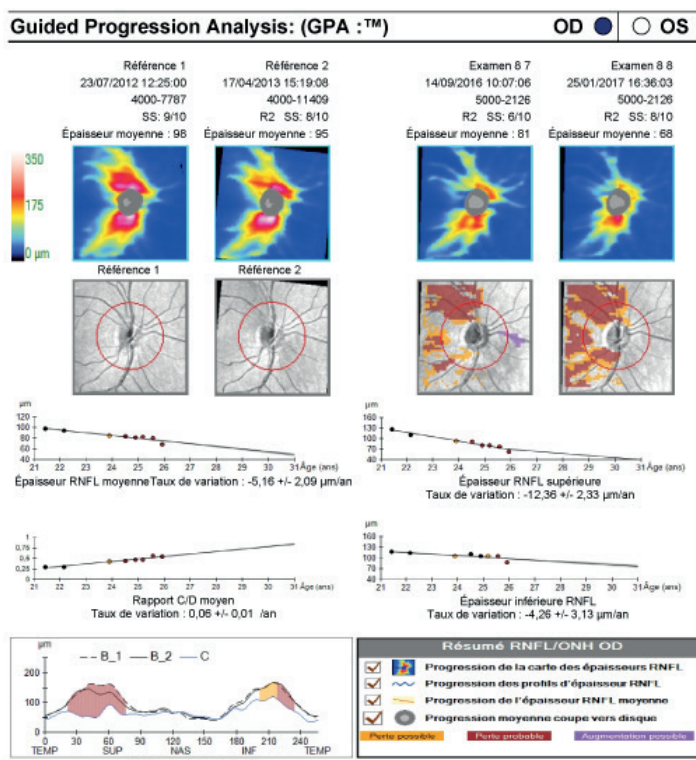
Cirrus HD-OCT Guided Progression Analysis (GPA) comprises automated event analysis and trend analysis. It is with comparison of 2 reliable initial reference examinations. Progression is diagnosed, based on a colour-coded representation (automated event analysis), when the variation exceeds the inter-test variability value of two reference examinations of the patient determined by OCT.



- 1** RNFL thickness maps.
- 2** RNFL thickness deviation maps.
- 3** Mean RNFL thickness trend graphs. *Observation of an isolated weakly negative slope of RNFL progression on trend analysis must not be considered to be a marker of progression.*
- 4** Thickness map and deviation map event analysis compared to 2 reference initial examinations. Significant initial ochre defect (possible progression), confirmed to be brown (likely progression) on subsequent examinations.
- 5** Successive RNFL thickness profiles (TSNIT graphs).
- 6** Summary of RNFL progression analysis.



The initial detection must focus on superior and inferior temporal sectors of the peripapillary RNFL and often at the edges of the maps, where the presence of defects must be carefully investigated.



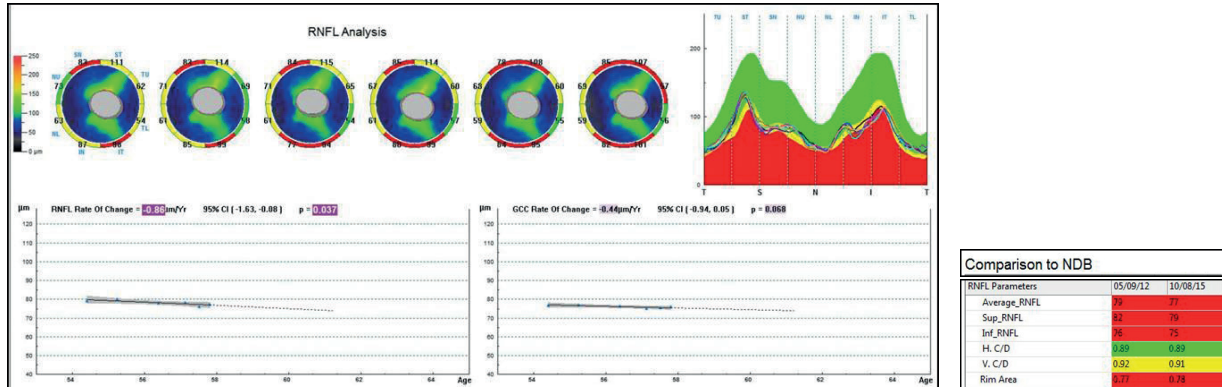
| Paramètres de résumé RNFL et ONH | | | | | | | | | | | |
|----------------------------------|------------------------|---------------------|---------------------------|------|-----------------------------------|------------------------|------------------------|---------------|-------------------|----------------------|------------------------|
| | Date/heure de l'examen | Numéro de série | Méthodes d'enregistrement | PS | Épaisseur moyenne de la RNFL (µm) | RNFL quadrant inf (µm) | RNFL quadrant sup (µm) | Aire de l'ANR | Rapport C/D moyen | Rapport C/D vertical | Volume de l'excavation |
| Référence: | 1 | 23/07/2012 12:25:00 | 4000-7787 | 9/10 | 98 | 118 | 128 | 1,34 | 0,29 | 0,32 | 0,030 |
| Référence: | 2 | 17/04/2013 15:19:08 | 4000-11409 | R2 | 8/10 | 95 | 114 | 112 | 1,32 | 0,31 | 0,35 |
| | 3 | 12/01/2015 10:16:35 | 5000-2126 | R2 | 9/10 | 85 | 106 | 94 | 1,19 | 0,44 | 0,055 |
| | 4 | 26/08/2015 16:16:29 | 5000-2126 | R2 | 9/10 | 85 | 111 | 92 | 1,17 | 0,46 | 0,061 |
| | 5 | 13/01/2016 10:12:52 | 5000-2126 | R2 | 8/10 | 82 | 107 | 82 | 1,11 | 0,48 | 0,071 |
| | 6 | 27/04/2016 10:53:37 | 5000-2126 | R2 | 8/10 | 83 | 106 | 81 | 1,07 | 0,49 | 0,068 |
| | 7 | 14/09/2016 10:07:06 | 5000-2126 | R2 | 6/10 | 81 | 106 | 77 | 1,01 | 0,56 | 0,044 |
| En cours : | 8 | 25/01/2017 16:36:03 | 5000-2126 | R2 | 8/10 | 68 | 89 | 64 | 0,99 | 0,54 | 0,084 |

Automated event analysis - 1

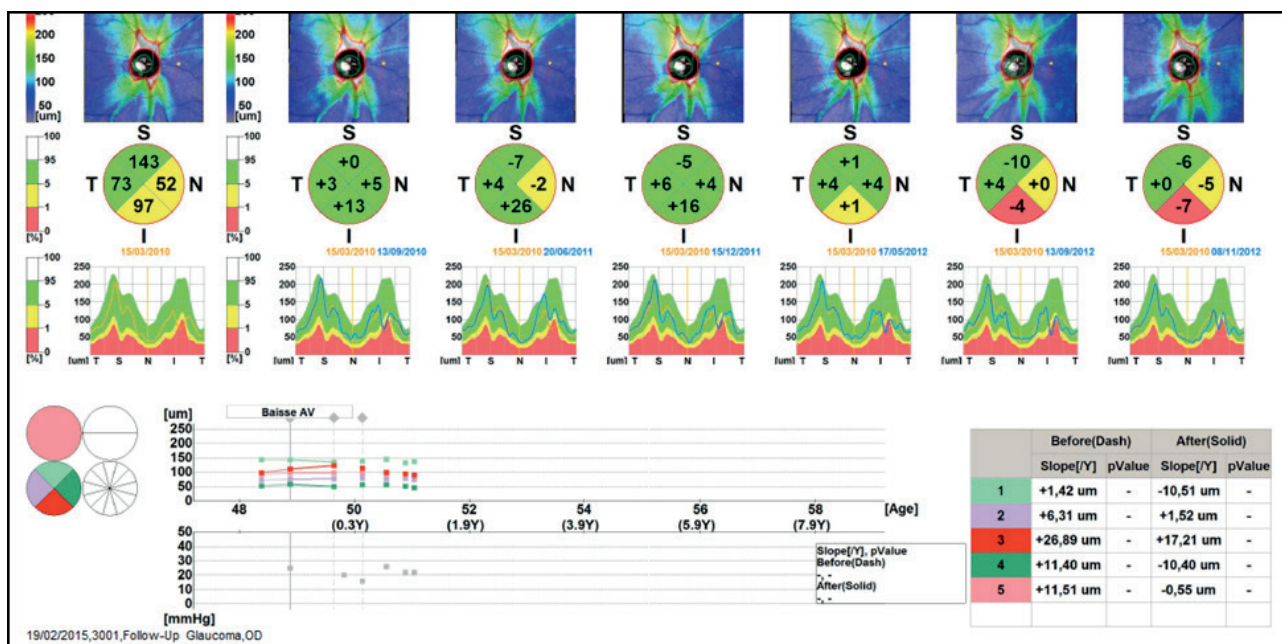
Statistical analysis of the various parameters compared to the initial reference examination indicating possible pathological progression (yellow - ochre), then confirmed likely progression (brown).

It should be stressed that OCT displays are based on statistical analysis of numerical results compared to the results obtained in a limited population of age-matched normal subjects. Any defects detected on OCT must be confirmed by at least 2 follow-up examinations.

Markers of RNFL progression



XR Avanti SD-OCT analysis of RNFL progression (trend analysis).



Nidek RS 3000 SD-OCT analysis of RNFL progression (trend analysis), showing global analysis over 360° and 4 quadrants. It is also possible to individually monitor progression on the twelve 30° sectors of the TSNIT, or the two superior and inferior peripapillary hemi-sectors.

All SD-OCT devices comprise RNFL and GCC progression analysis software.

Evaluation of glaucoma progression must focus on the zones of the superior temporal and inferior temporal meridians, looking for:

- **enlargement of a pre-existing defect (the most frequent case)**
- **appearance of any new defects,**
- **deepening of a pre-existing defect.**

Progressive enlargement of a defect of the RNFL in the superior and inferior temporal meridians is probably a more reliable and more relevant marker of progression, which is easier to visualize than variations on a simple section with a radius of 1.73 mm in these same meridians.

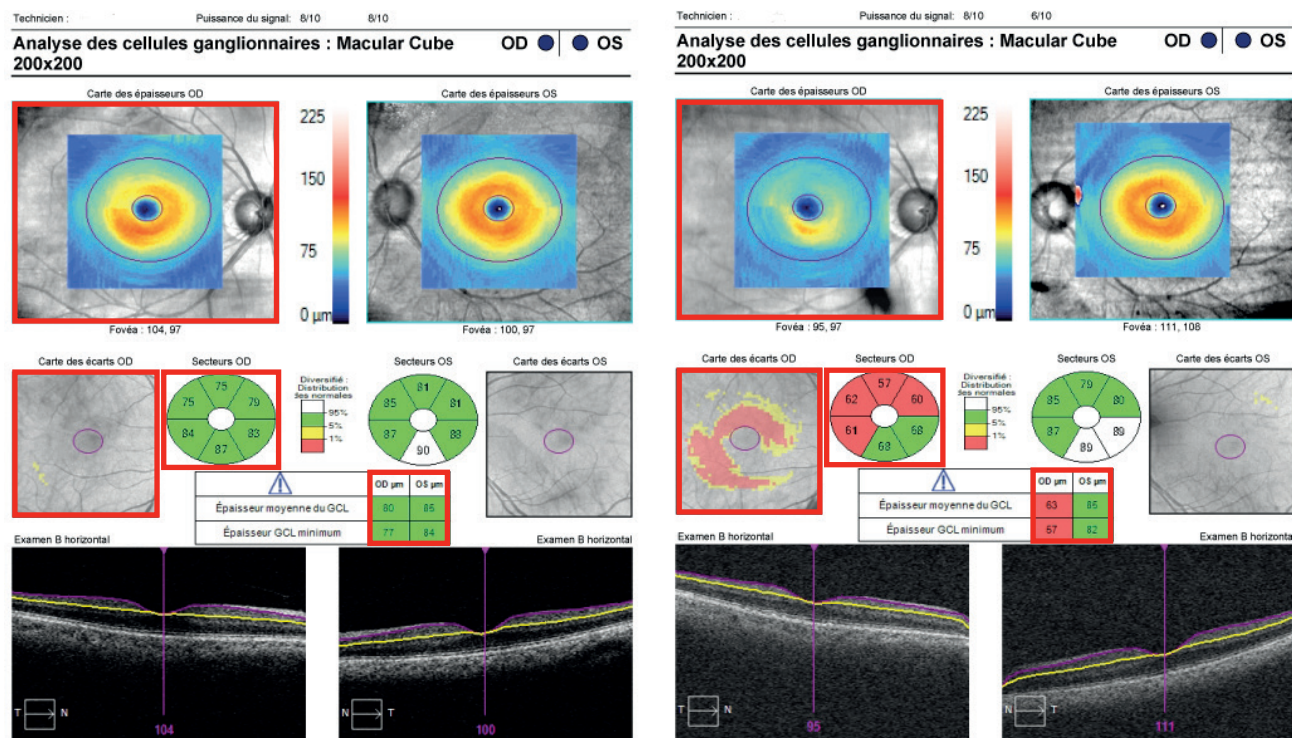
SD-OCT markers of progression remain poorly defined and are essentially limited by the high rate of false-positive results that can be observed in up to 15% of cases.

The reproducibility of repeated measurements of RNFL thickness can vary by 4%, while those of macular GCC can vary by 2%. This non-pathological variability of thickness measurements must be taken into account when interpreting glaucoma progression.

The follow-up of SD-OCT progression analyses remains limited, with a follow-up of up to 5 years for the longest studies, especially as analysis software is continually being improved. Current data indicate a higher risk of developing a functional visual field defect in subjects with a rate of loss of RNFL thickness greater than -1 µm/year.

At this day, a progression cut-off allowing a clear distinction from age-related progression and which takes into account the coefficient of variability of OCT measurements has not yet been defined for either RNFL thickness or GCC.

Markers of GCC progression

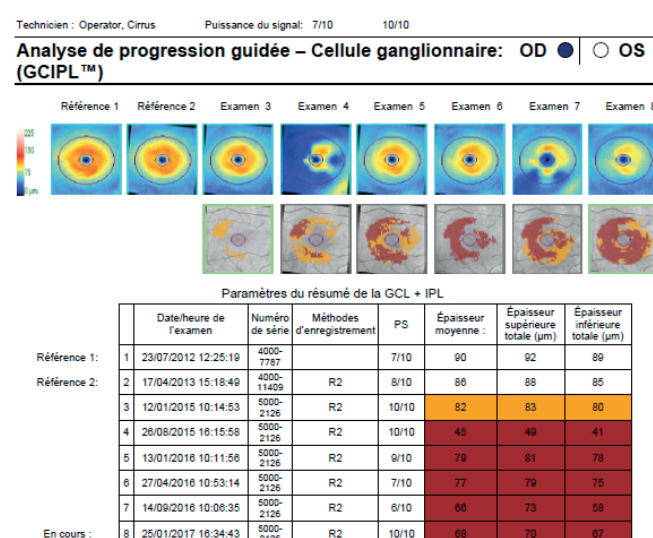
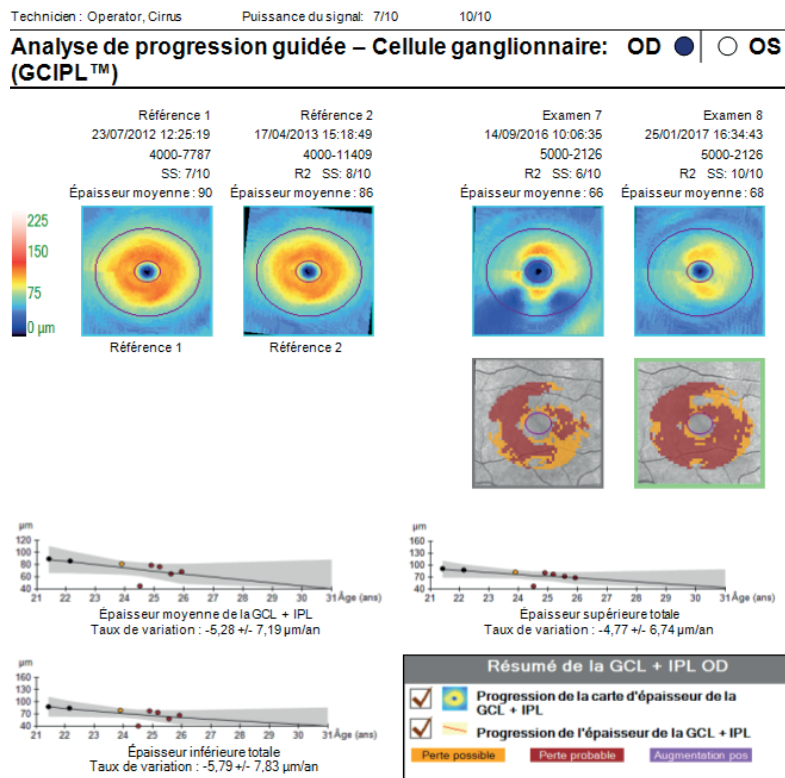


4 years

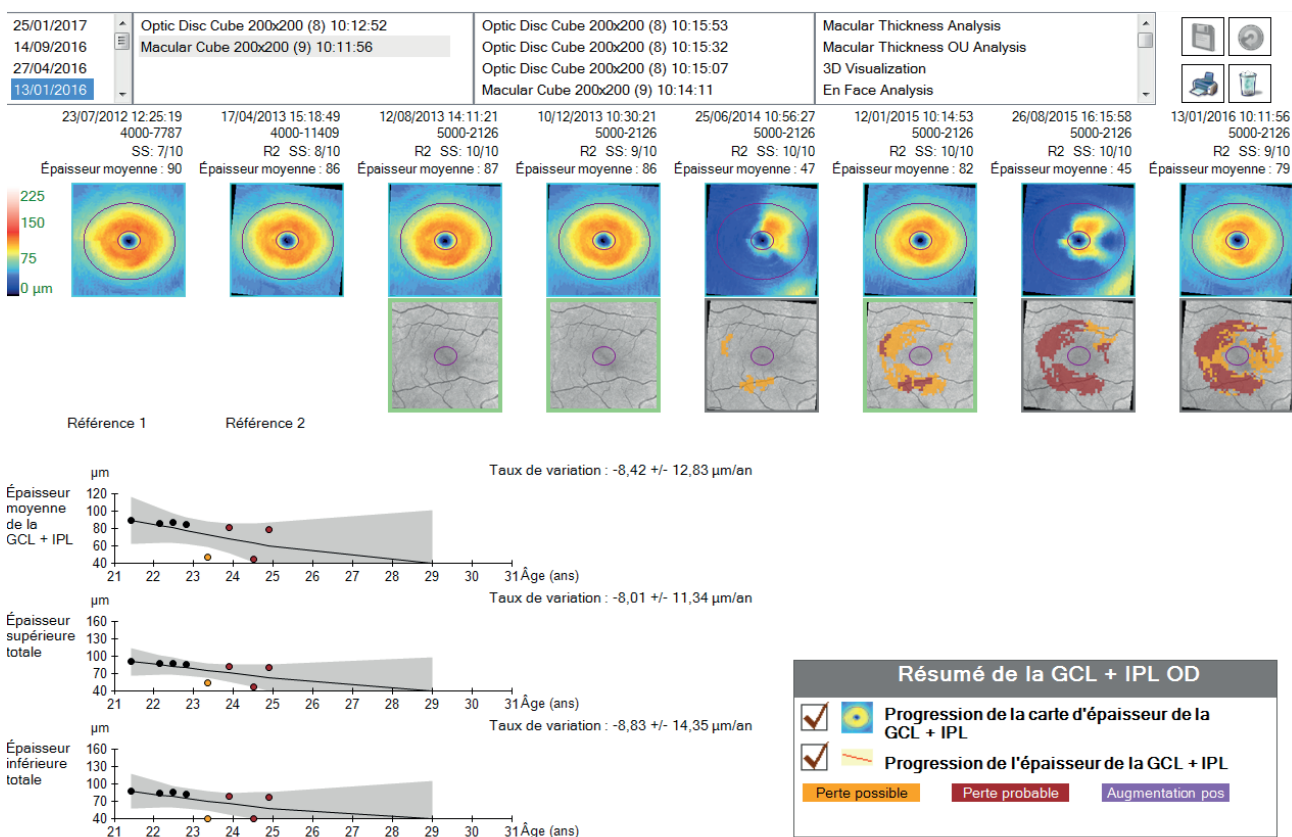
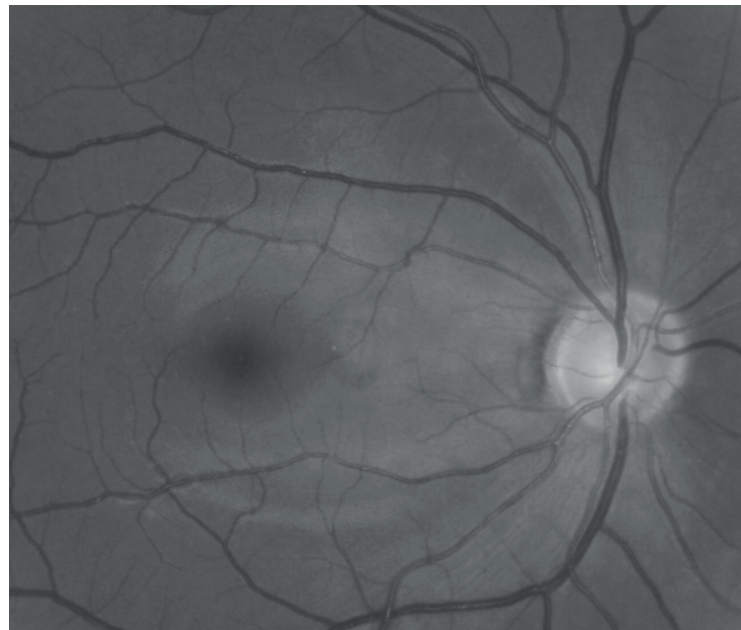
This analysis looks for signs of progression on thickness maps, statistical analysis maps and sectoral thickness maps of the macular ganglion cell complex (GCC).

Ganglion cell complex progression analysis in this 75-year-old patient reveals progression of each of the parameters studied. Clinical judgement can also demonstrate progression in these clinical cases of «quick progressor» patients after ensuring the absence of an associated clinical macular lesion.

Markers of GCC progression



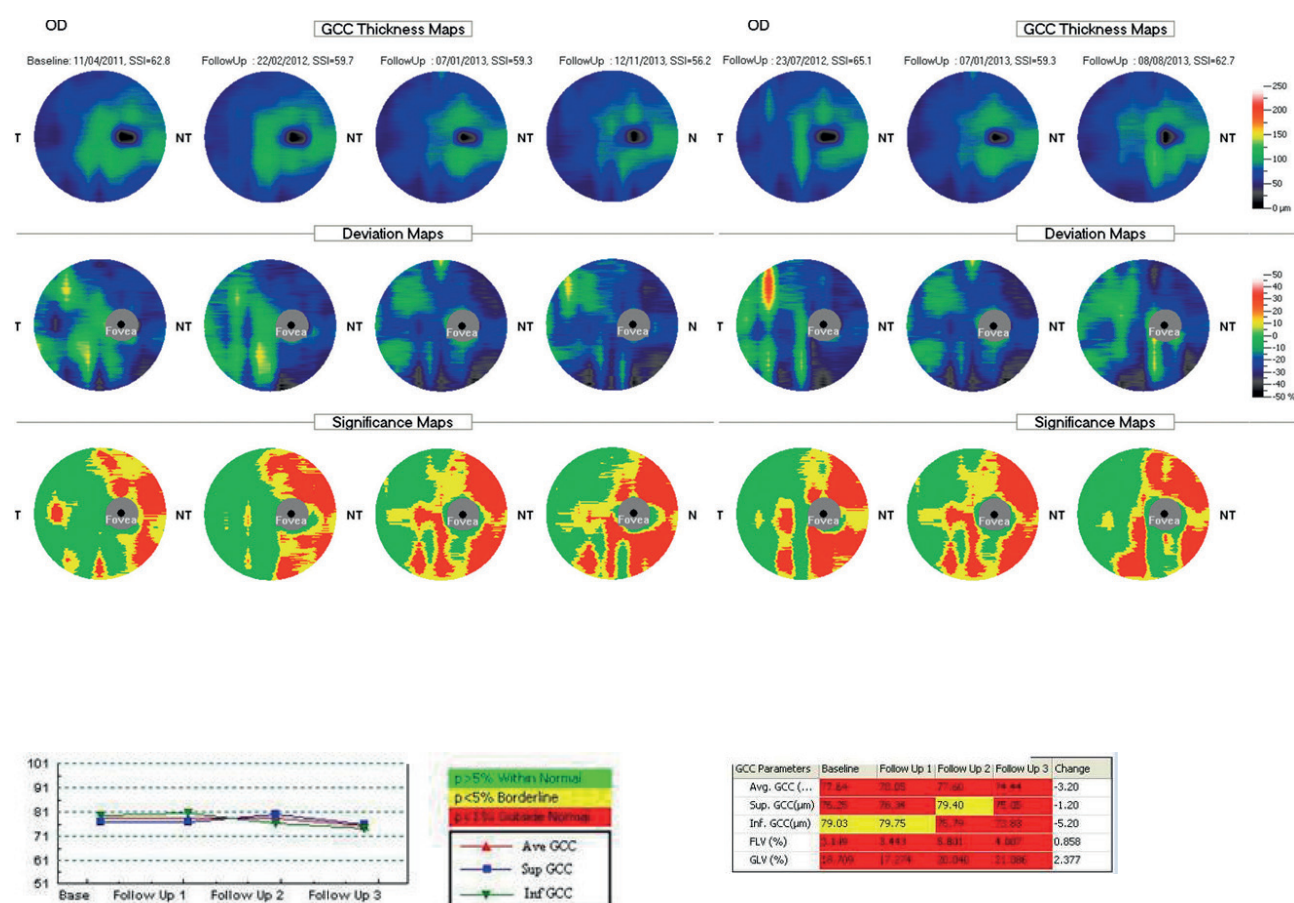
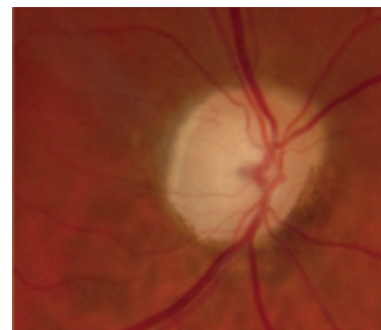
Guided progression analysis (GPA) of the ganglion cell layer also comprises comparison with two reliable initial reference examinations. Progression is confirmed, on colour-codes images, when the variation exceeds the inter-test variability of the patient's two reference OCT examinations. In this 26-year-old patient followed and treated for juvenile glaucoma for 9 years, progression of the ganglion cell complex lesion was confirmed from the third year of the 5 years of follow-up.



Detection of early GCC progression must focus on the temporal zone, especially the inferior temporal zone, of the macular region.

Any GCC progression detected on OCT must be confirmed on at least 2 follow-up examinations.

Markers of GCC progression

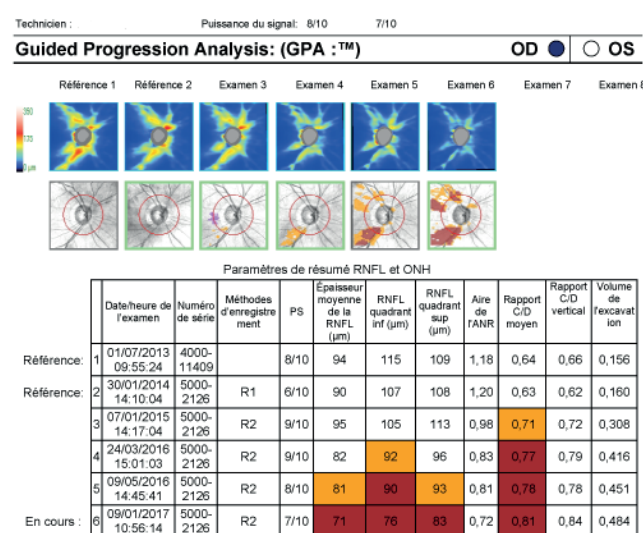
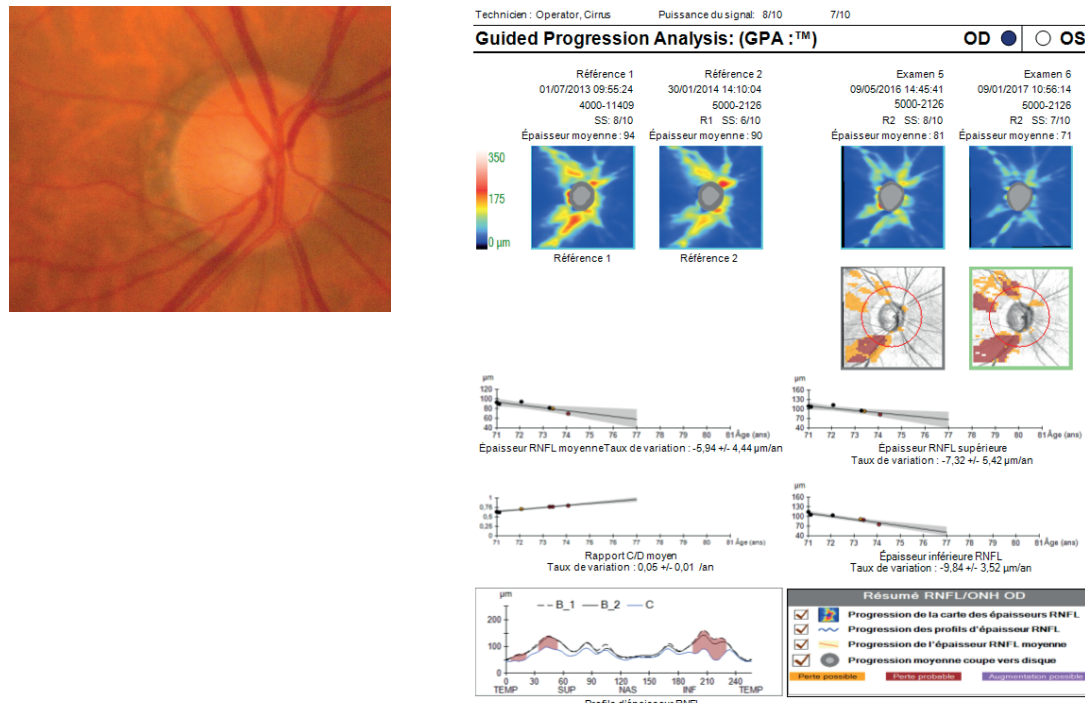


When the slope of trend curves on progression analysis is non-significant or uncertain, progression analysis of complementary indices can provide additional information for evaluation of progression and must be interpreted in the light of clinical findings and visual field examination.

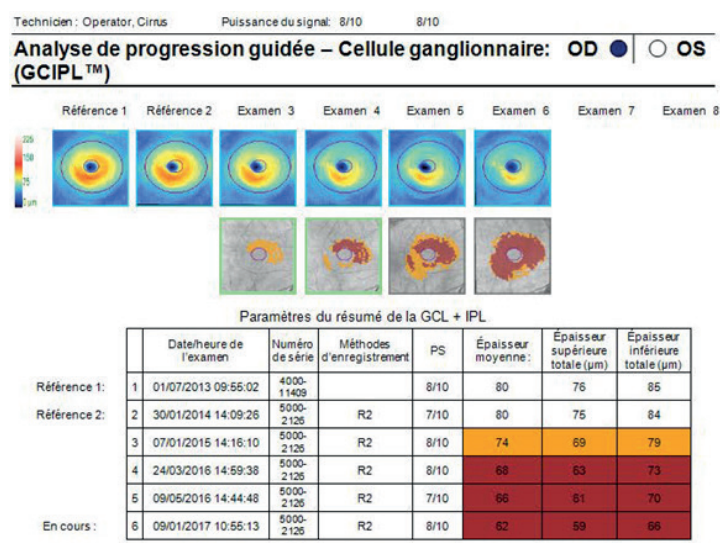
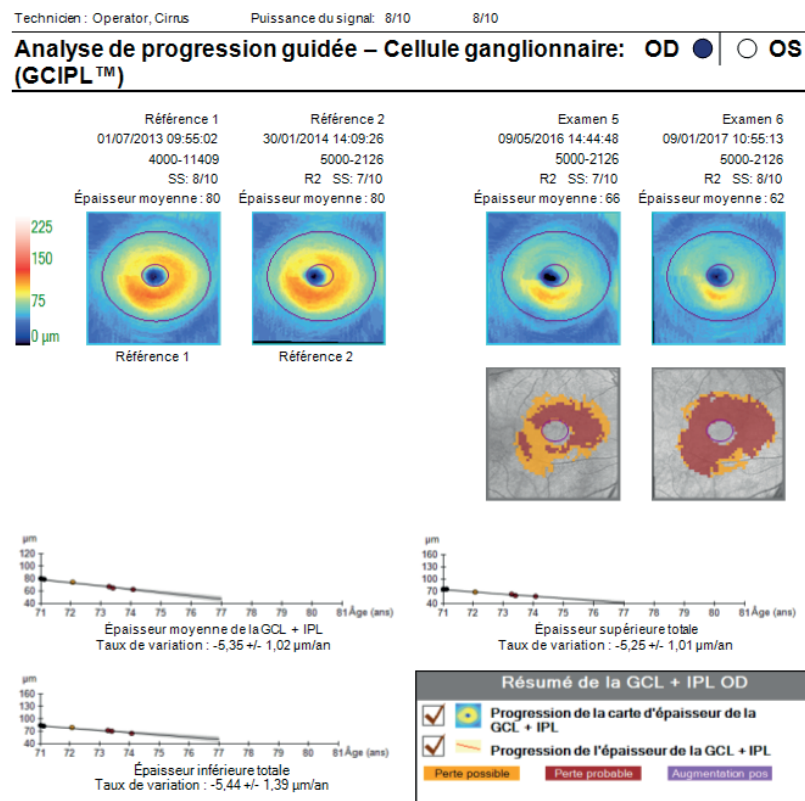
Monitoring of the complementary indices, FLV and GLV provided by XR Avanti SD-OCT and minimum GCL (or GCIPL) provided by Cirrus HD-OCT, appears to provide a major contribution to the monitoring of GCC progression.

Markers of GCC progression

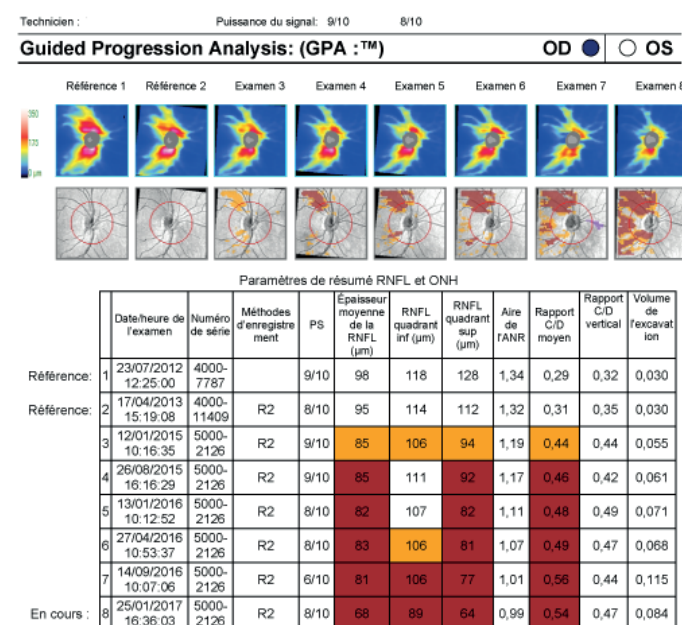
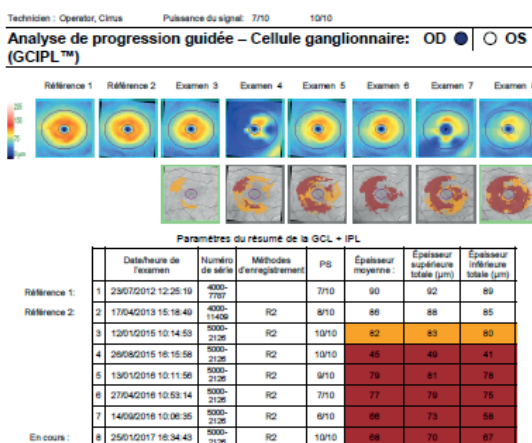
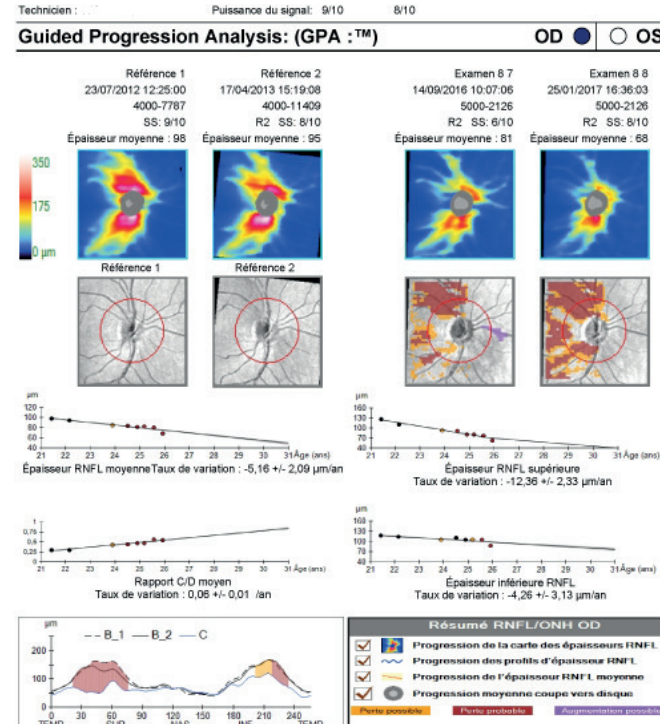
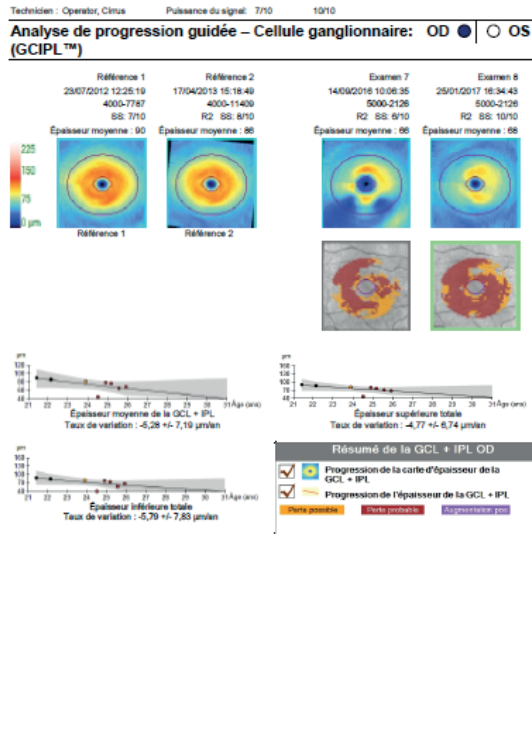
Progression analysis using the recent Cirrus HD-OCT guided progression analysis software in this 75-year-old woman followed and treated for POAG demonstrates a significant RNFL lesion over a period of 1 year between the 3rd and 4th examinations, which was confirmed over the 4 years of follow-up in this patient.

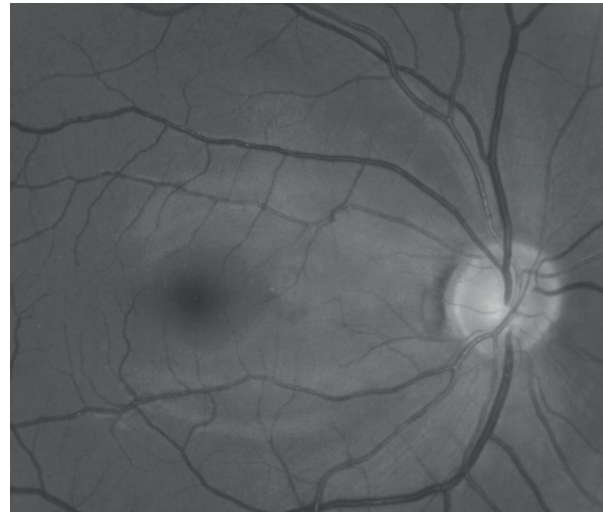


Ganglion cell complex progression analysis reveals significant progression at the same dates, by the second year of follow-up, which was rapidly confirmed in the two superior and inferior macular hemifields.



Markers of GCC progression





In this patient followed for progressive juvenile glaucoma, comparison of RNFL thickness data reveals a concomitant RNFL lesion, which is more extensive than the lesion of the ganglion cell complex of the superior macular hemifield, especially in the superior peripapillary arcuate nerve fibres.

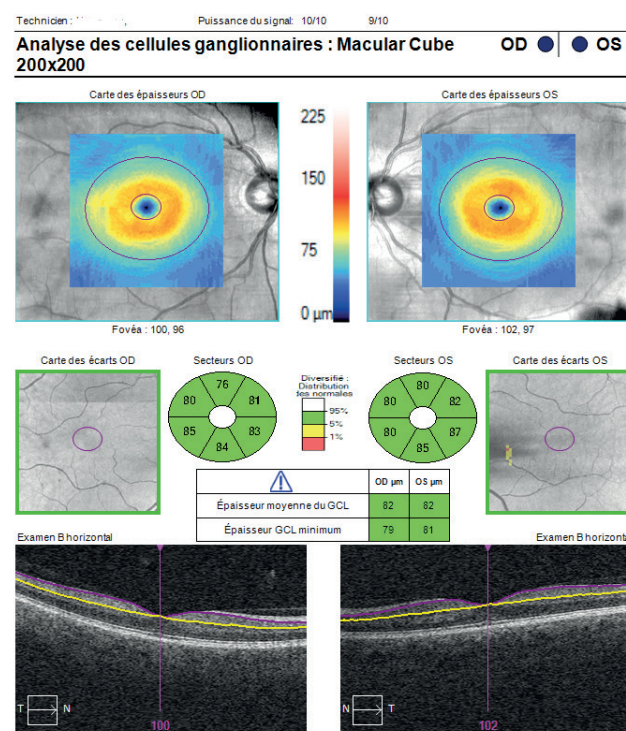
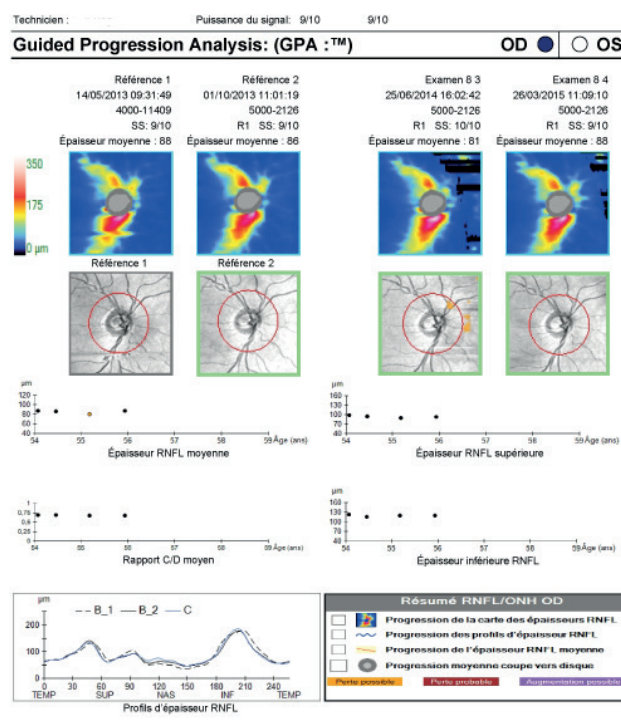
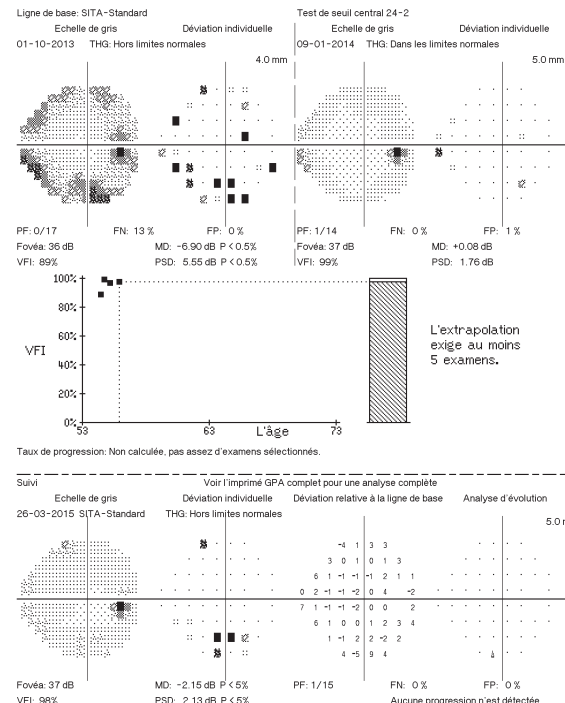
This clinical case clearly illustrates the value of complementary analysis of the peripapillary RNFL and GCC to more precisely determine the extent of the structural lesion.

These data must always be compared with those of clinical and visual field examinations.

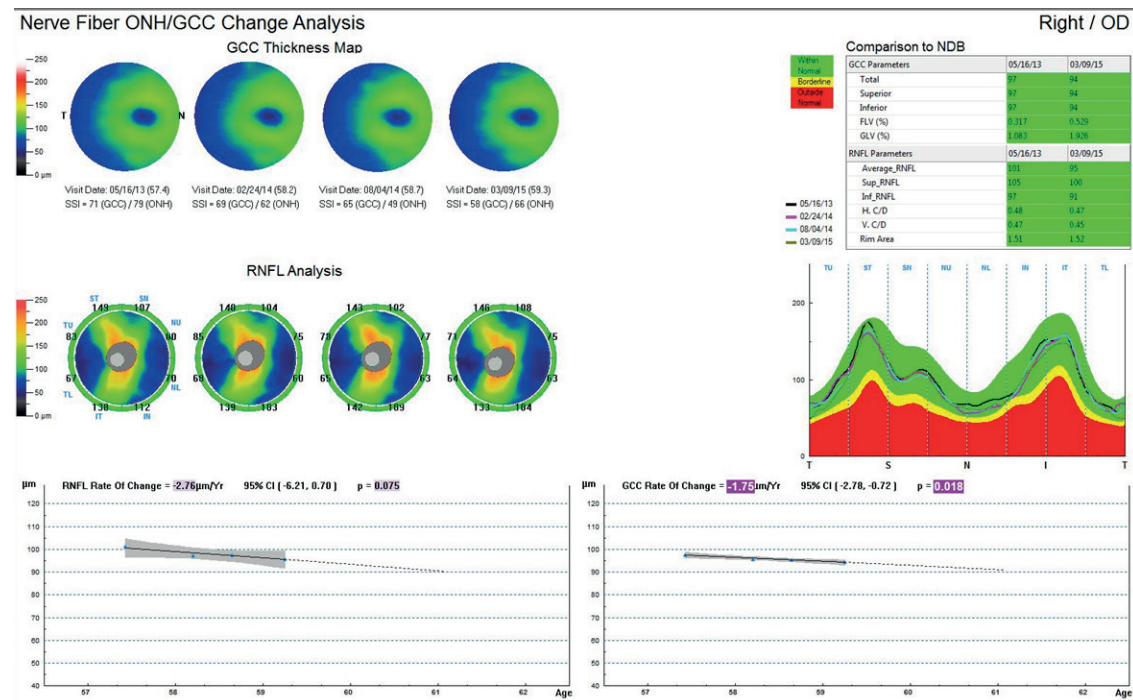
Markers of GCC progression

Glaucoma suspect - 2 years of follow-up

Standard Automated Perimetry (SAP) visual field progression analysis in this glaucoma suspect does not reveal any obvious lesion or any progression with a follow-up of 2 years.



XR Avanti SD-OCT RNFL and GCC progression analysis



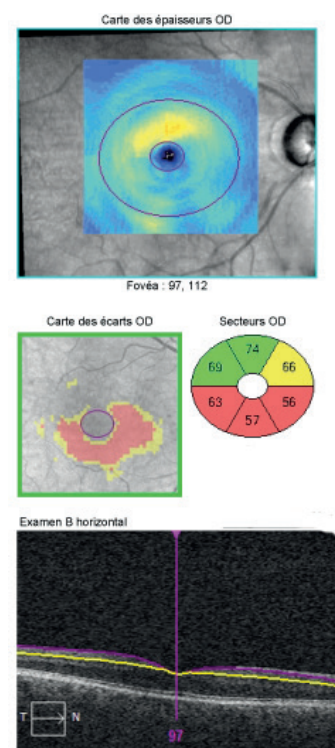
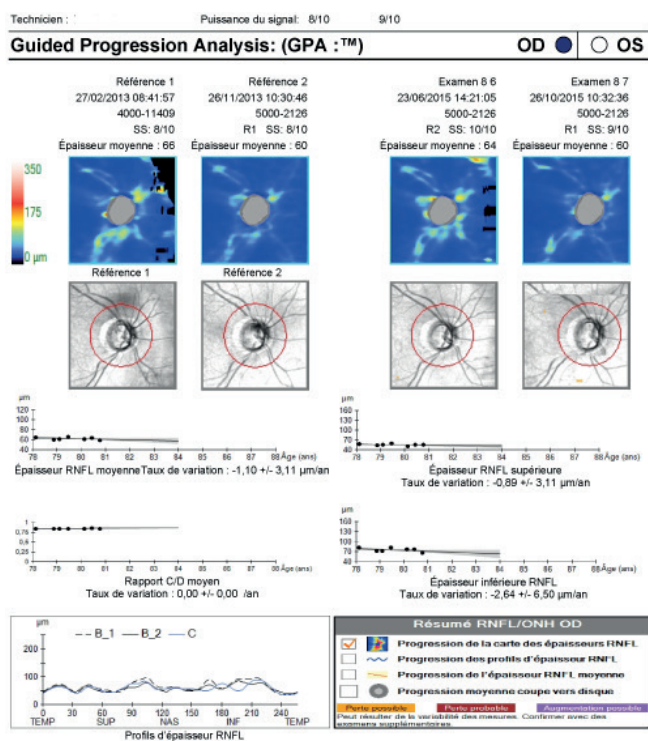
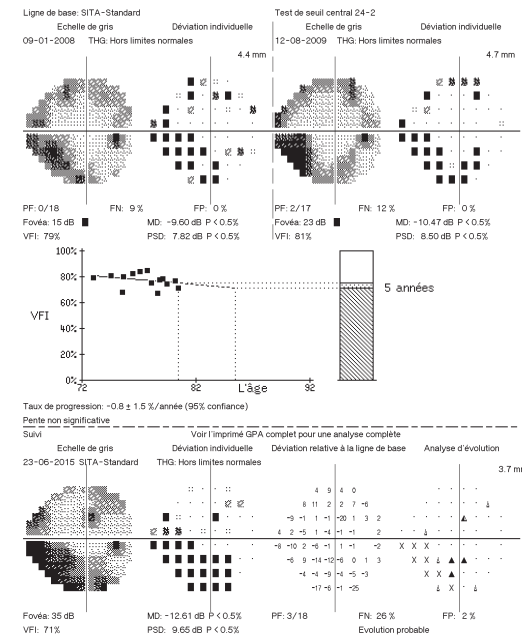
GCC trend analysis suggests significant loss, while evaluation of RNFL and GCC thickness is within normal limits.

This significant GCC trend analysis constitutes a warning sign, justifying closer surveillance of these clinical forms (OHT, preperimetric glaucoma, etc.) after comparison with the findings of clinical examination of the macula.

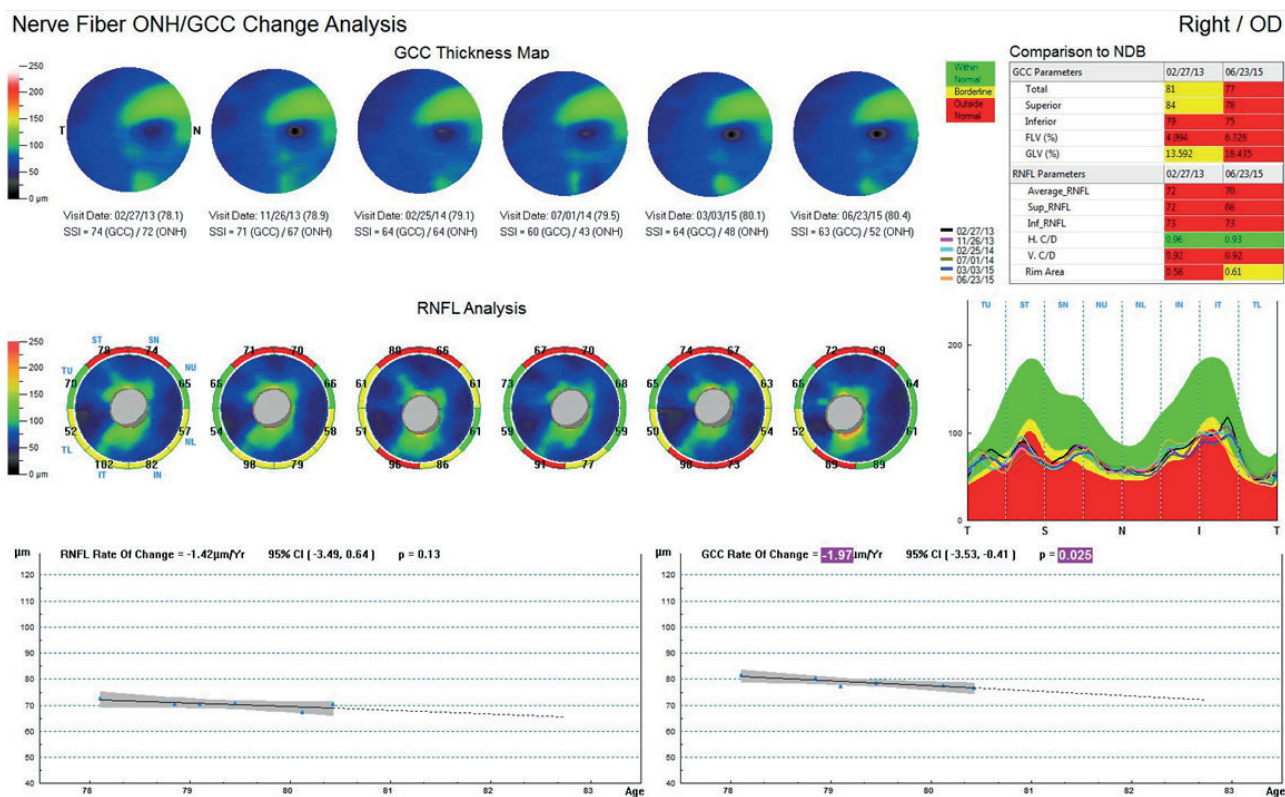
Markers of GCC progression

Follow-up for more than 2 years in a patient treated for advanced POAG

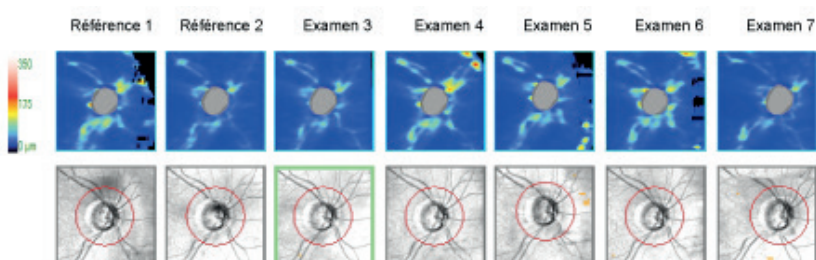
Guided progression analysis in this 68-year-old man followed and treated for POAG reveals likely progression with a significant slope of the visual field index (VFI).



XR Avanti SD-OCT RNFL and GCC progression analysis



Significant loss on GCC trend analysis and a floor effect on RNFL analysis with no significant slope emphasize the value of GCC progression analysis in the follow-up of these advanced clinical forms.

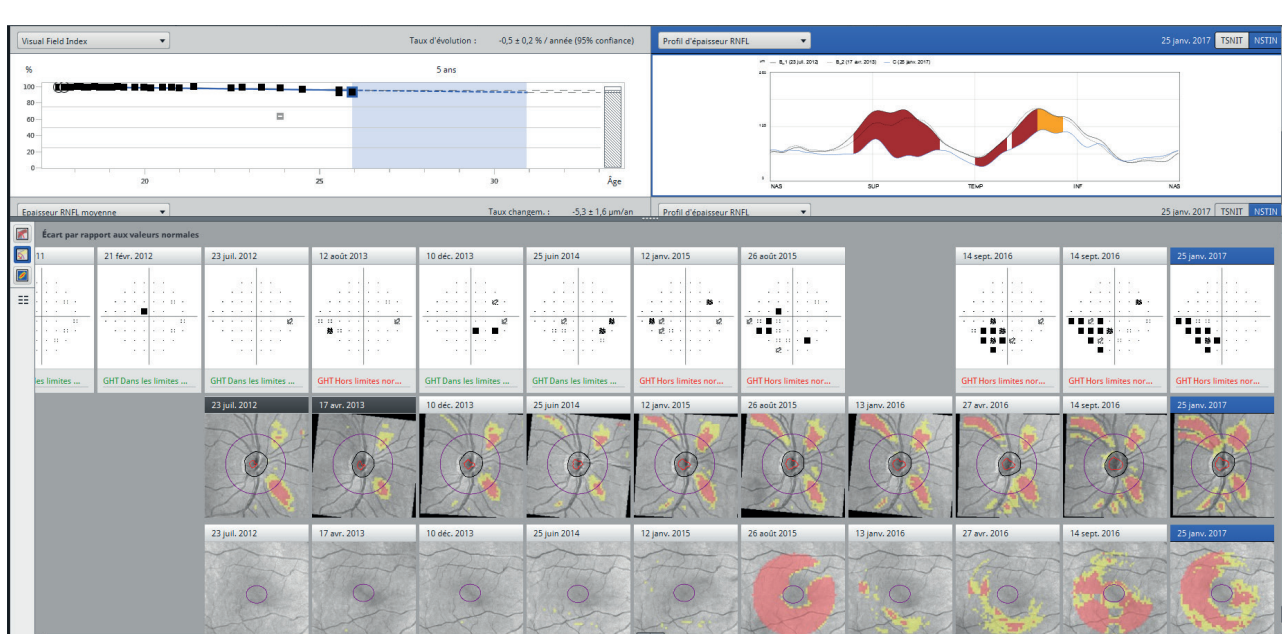
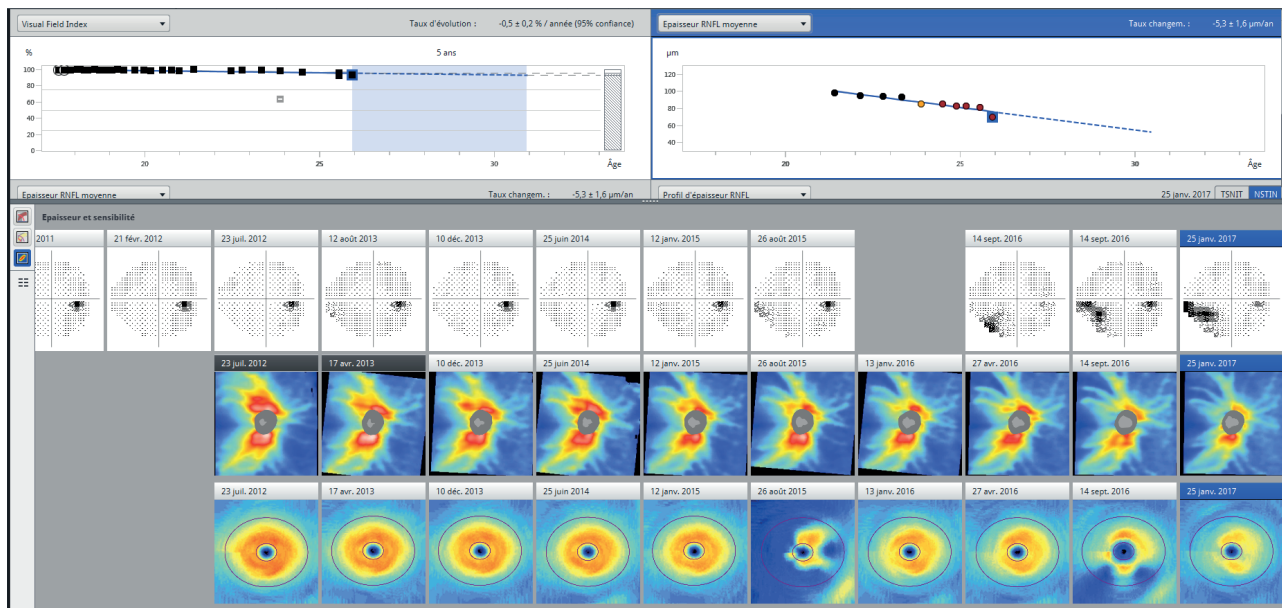


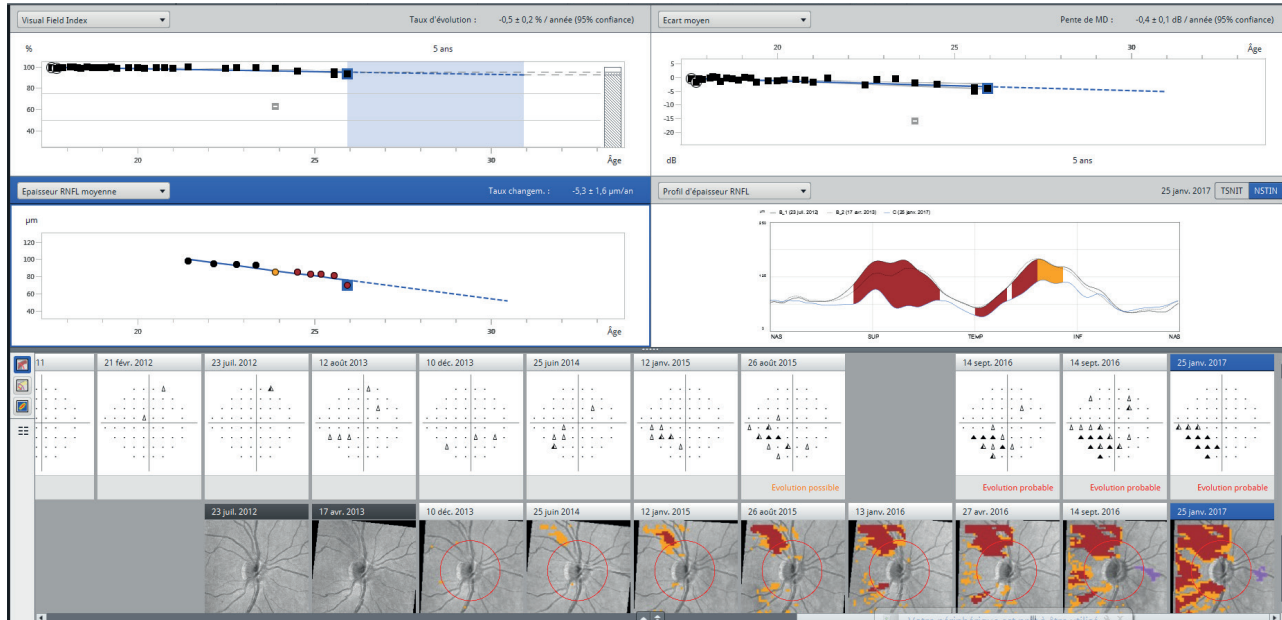
New progression analyses

The new **Glaucoma Workplace 3** software allows comparative analysis of structural and functional lesions.

The course of RNFL thickness and thickness deviations with respect to an age-matched control group can be compared by means of functional impairment slopes (visual field index [VFI], mean deviation [MD]) and defect deviation maps and their time-course.

This analysis can also be compared with RNFL thickness maps, allowing more precise localization and quantitation of RNFL defects.





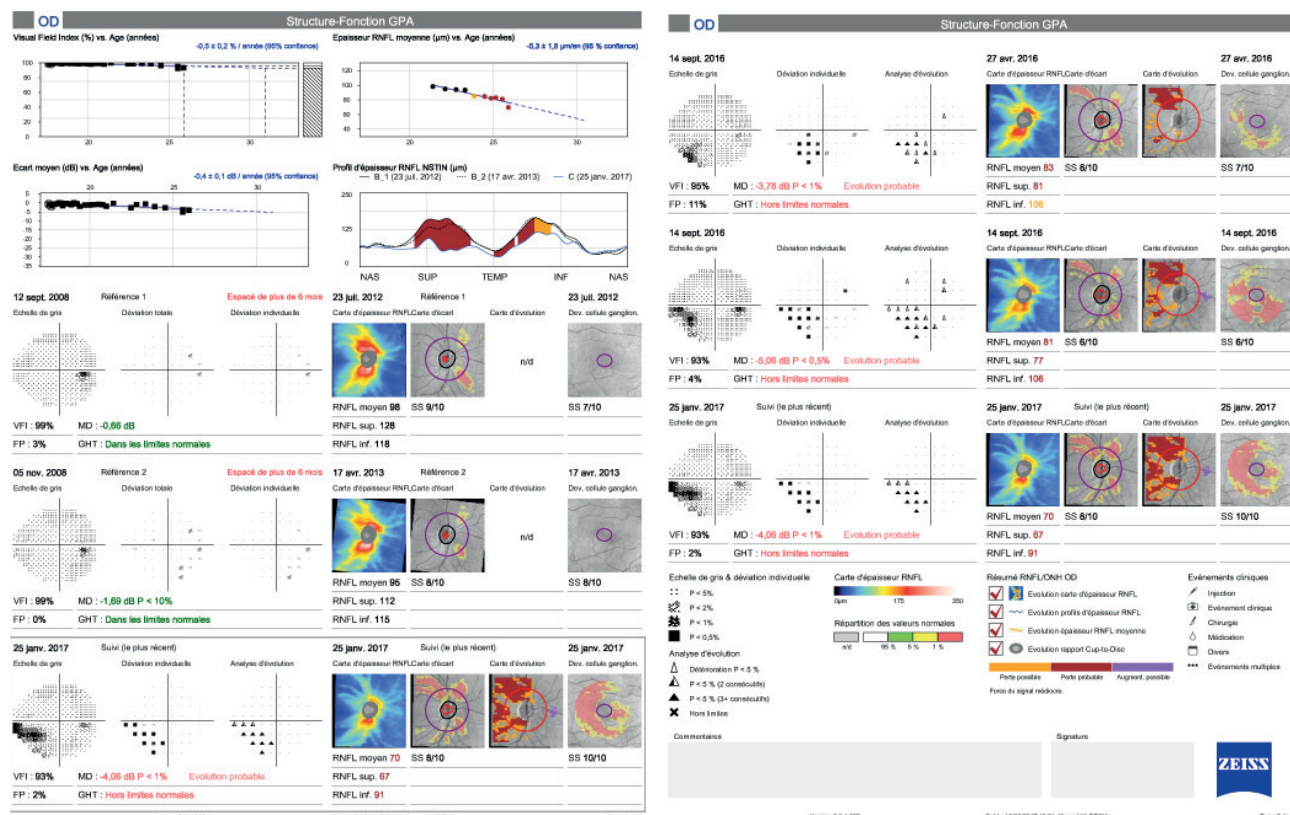
GPA also allows comparison of progression of visual field defects with progression analysis of structural lesions based on comparison of two of the patient's initial follow-up reference examinations with colour-coded representation of progressive defects.

The new software has the advantage of allowing analysis of RNFL thickness maps presented from the nasal horizontal meridian and then the superior, temporal, inferior and nasal meridians, allowing more precise visualization and analysis of early glaucomatous defects situated in the central temporal sectors.

These new methods of analysis, adapted to each clinical situation, allow more precise assessment of other lesions concomitant or subsequent to RNFL lesions and functional impairment of visual fields and their respective rates of progression.

New progression analyses

Glaucoma Workplace 3 Structure Function combination display. Comparative analysis over 9 years of follow-up.



This combined display presents progression analysis of VFI and visual field MD slopes, mean RNFL thickness, superimposed successive RNFL thickness maps in the form of an NSTIN graph, allowing more precise localization and evaluation of central defects. This display provides successive GPA progression analyses of visual fields, RNFL thickness and deviation maps and GCC deviation maps.

New software allows analysis of structural and functional lesions (RNFL, GCC and visual field) and their progression on the same report and at the same dates.

These new reports will certainly provide valuable information on the progression of structural changes and their potential predictability of future clinically relevant functional defects.

The two essential progression analysis techniques combined on the same report will constitute a major advantage to provide more specific and more effective individualized management of patients at the various stages of optic neuropathy.



11. Current place of OCT angiography in glaucoma

OCT angiography and glaucoma

OCT angiography (OCT-A) allows new «en face» mapping of the retinal vascular network and superficial optic nerve.

The value of en face OCT imaging, based on the mean intensity of reflectance of superficial retinal layers just below the vitreous edge of the internal limiting membrane (ILM), over a distance of about 52 µm, has been clearly demonstrated. It provides information about localized, missed or neglected glaucomatous lesions with SD-OCT analysis of RNFL thickness.

The principle of OCT-A consists of performing several very rapid successive sections at the same place and evaluating signal differences between static anatomical structures and moving blood cells. The signal variations emitted by blood cells between two sections allow imaging of blood cells and «en face» visualization of the capillary architecture.

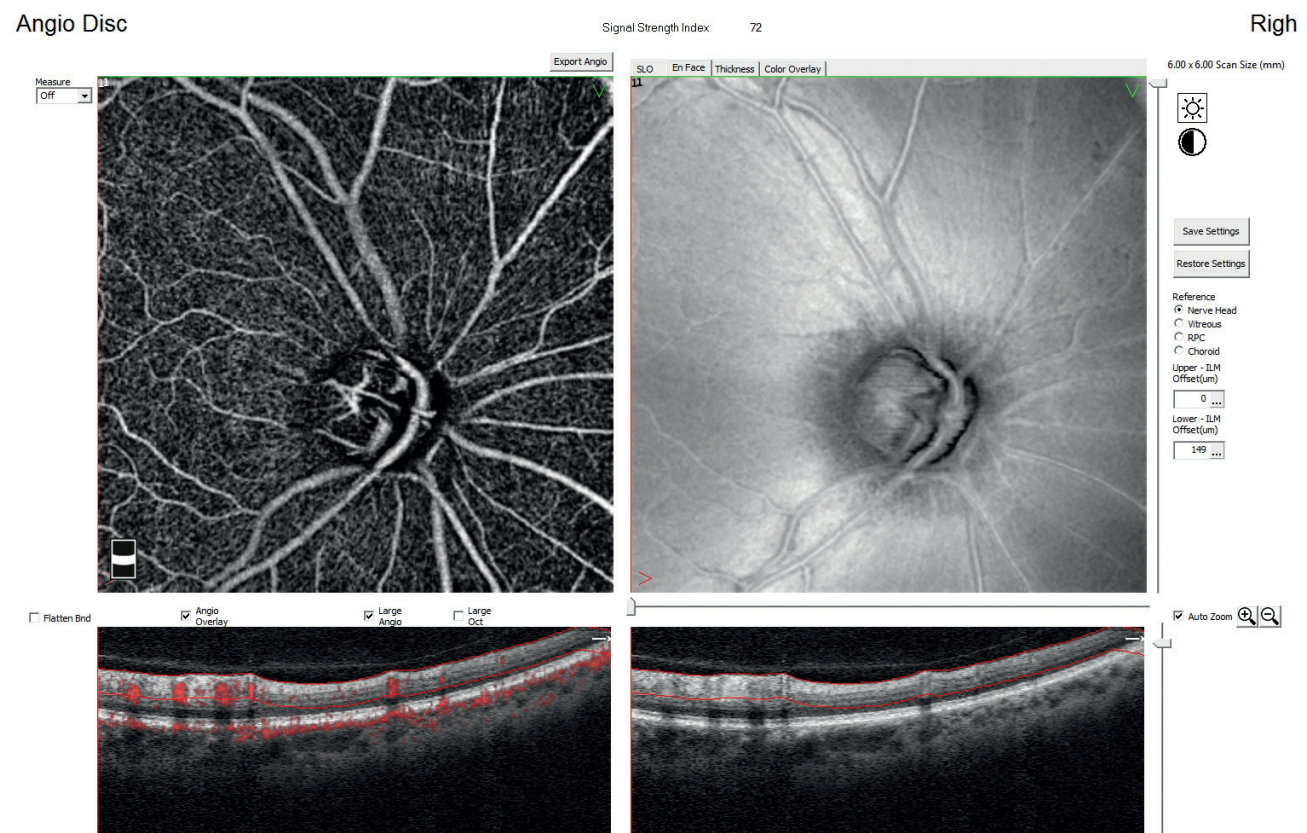
The essential advantage of «en face» imaging, as a result of specific image processing and extraction algorithms (SSADA, OMAG, etc.), is to provide separate visualization of superficial and deep capillary plexuses from the same rapid acquisition.

Various OCT angiography acquisition windows (3x3 mm to 9 x 9 mm) are now available.

Initially developed for macular analysis, the value of OCT angiography for assessment of macular disease has been largely demonstrated.

The first studies conducted in glaucoma are still relatively recent and have essentially focused on the study of the peripapillary capillary network.

Each angiogram obtained is associated with the «en face» OCT image. These 2 images must be analysed together and with the corresponding B-scan to avoid possible artefacts.

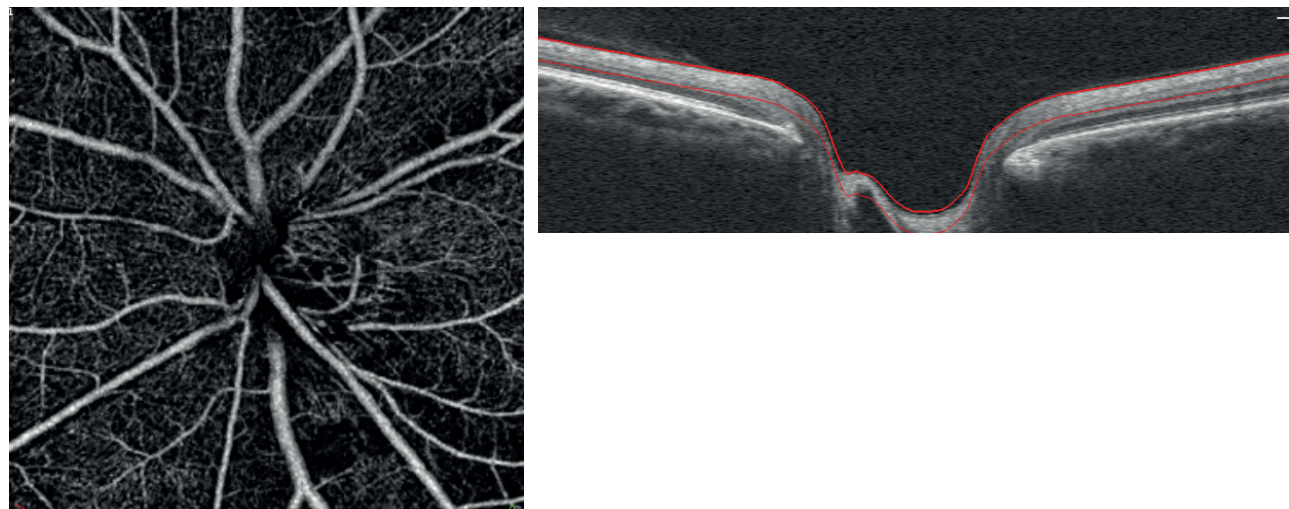
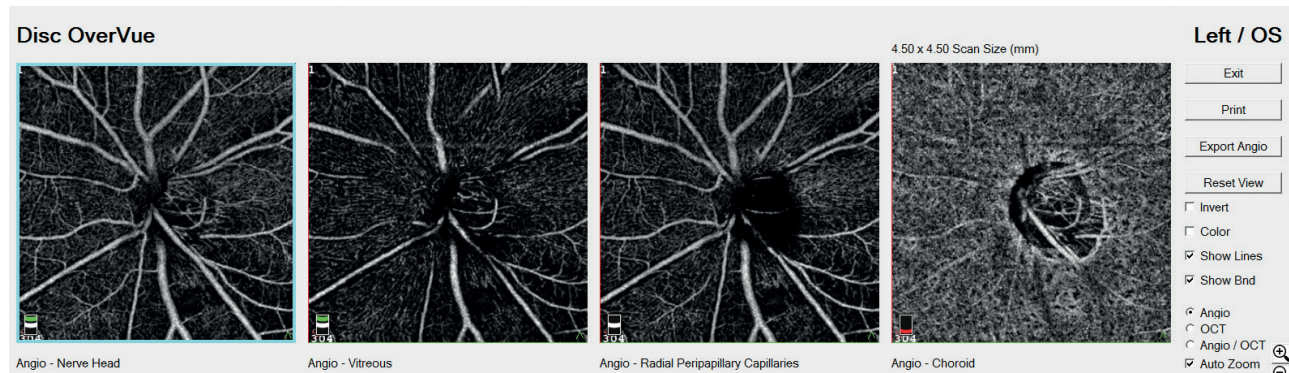


ANGIOVUE OCT ANGIOGRAPHY

OCT angiography and glaucoma

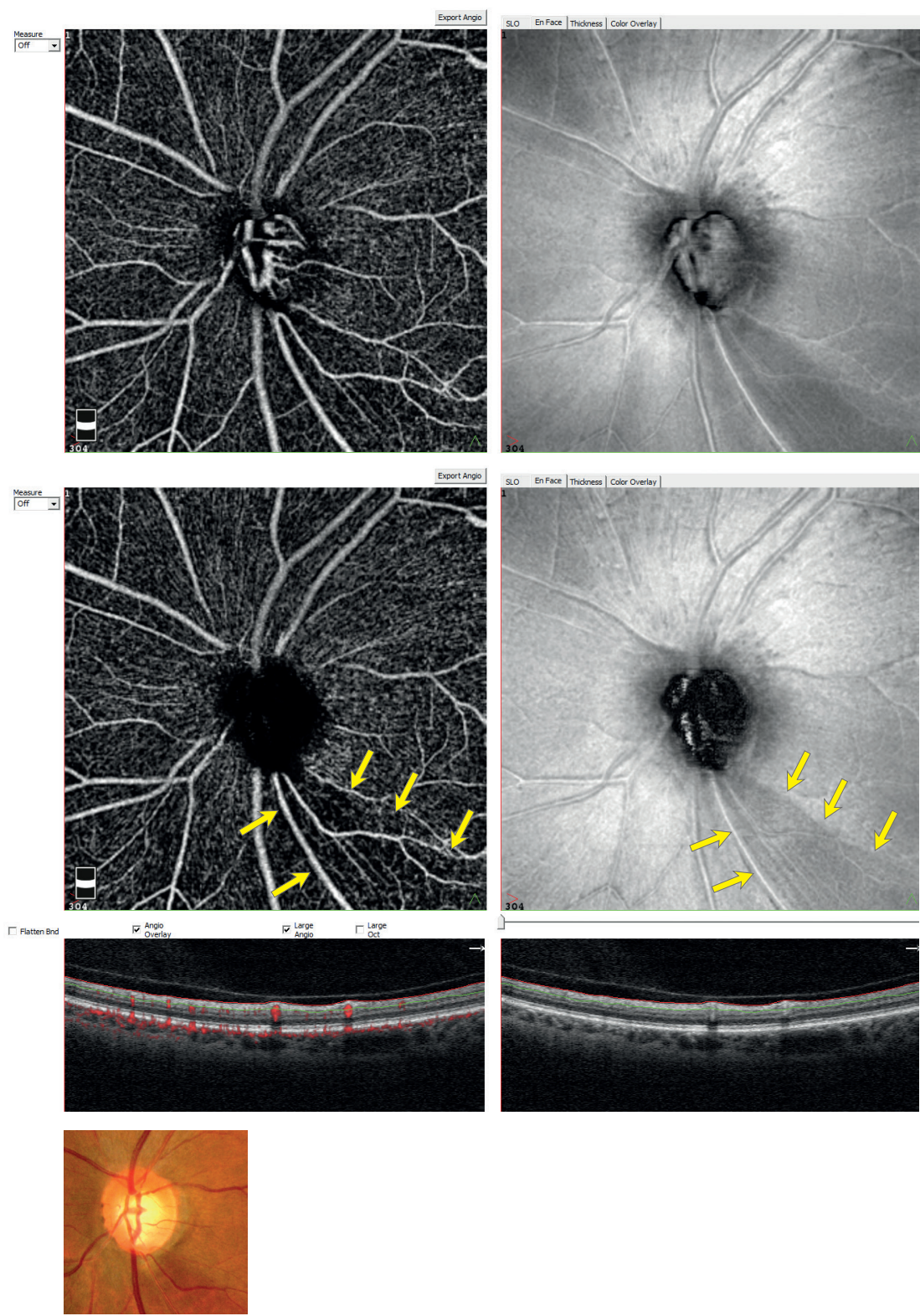
AngioVue OCT angiography software defines 4 preset segmentation thicknesses:

- **Nerve Head**, corresponding to the first 150 µm after the internal limiting membrane (ILM).
- **Vitreous**, corresponding to the zone of the vitreous in the acquisition field with the first 50 µm from the ILM.
- **Radial peripapillary capillaries (RPC)**, corresponding to segmentation of the ILM at the posterior limit of the RNFL.
- **Choroid**, corresponding to the more posterior sector of the retinal pigment epithelium to a depth of 75 µm.



«en face» OCT imaging in this 57-year-old woman followed and treated for POAG, clearly detects the inferior temporal defects and analysis of global RNFL thickness (Nerve Head) on the angiogram detects the localized lesion of the capillary network in the same sector.

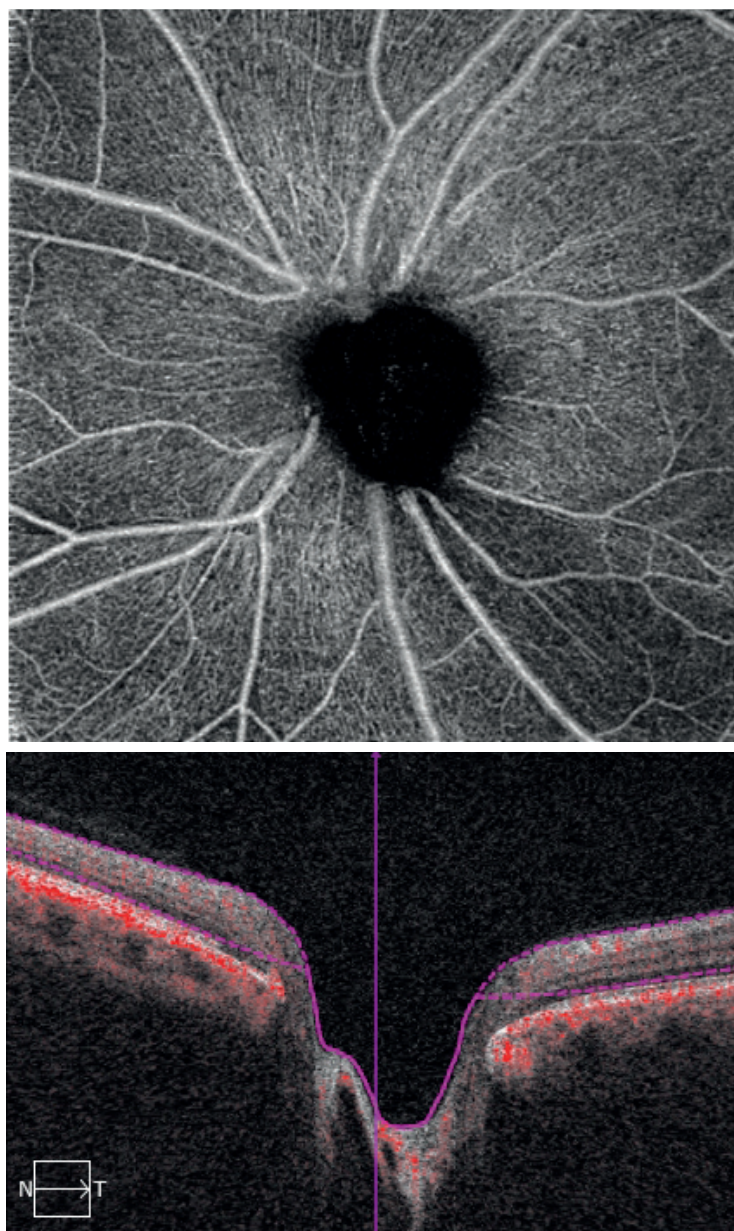
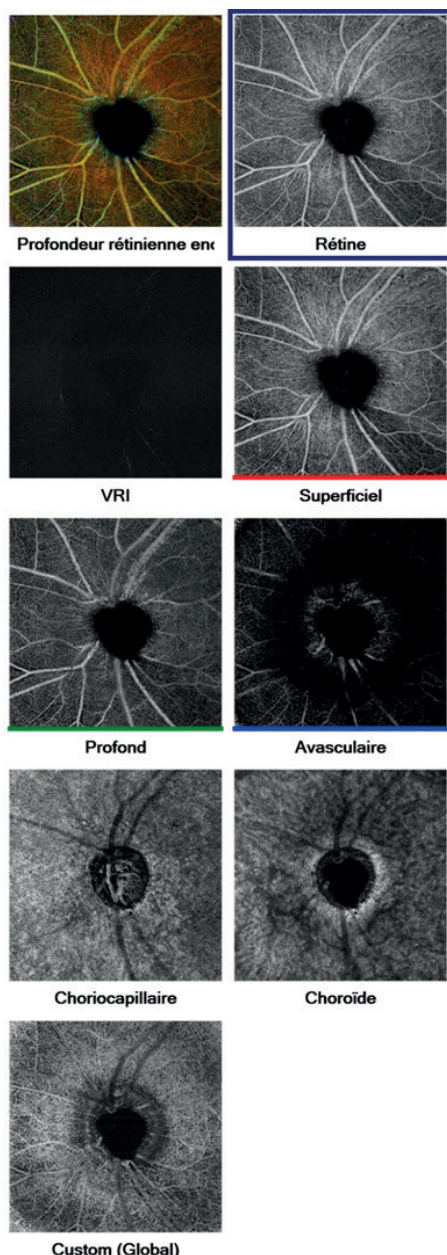
The capillary network lesion is more clearly visualized on analysis of the radial peripapillary capillary (RPC) network on the lower images.



OCT angiography and glaucoma

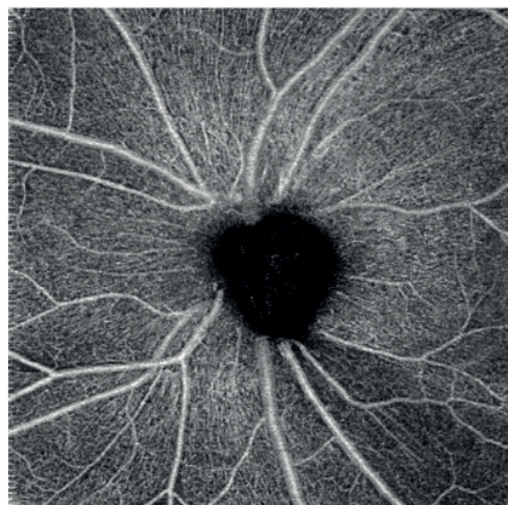
Cirrus HD-OCT Angioplex software also defines several preset segmentation thicknesses:

- **ILM retina** up to 70 µm above the retinal pigment epithelium (RPE) to reduce its hyperreflectivity.
- Superficial **VRI** (vitreoretinal interface) for diseases of the retinal surface.
- **SRL**: superficial retinal layer from the ILM to the inner plexiform layer (IPL) (zone of the superficial vascular network).
- **DRL** : deep retinal layer from the IPL to the outer plexiform layer (OPL).
- **Avascular retina map** of the OPL at the inner segment/outer segment junction (IS/OS).
- **Choriocapillaris and choroid** from 30 µm beyond the RPE to 50 and 115 µm from the RPE.

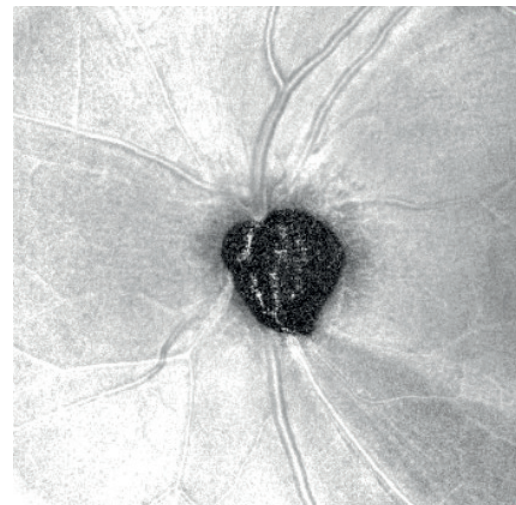


En face image in the same patient, clearly visualizes the inferior temporal defects with Angioplex on Cirrus HD-OCT.

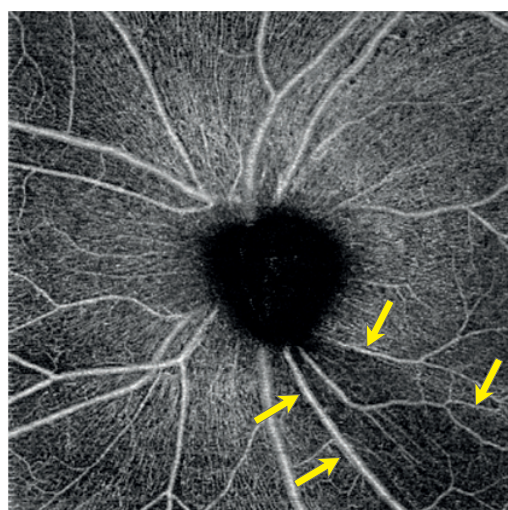
The angiogram demonstrates the localized lesion of the vascular network in the same sector, with more precise segmentation in the superficial retinal network on the lower images.



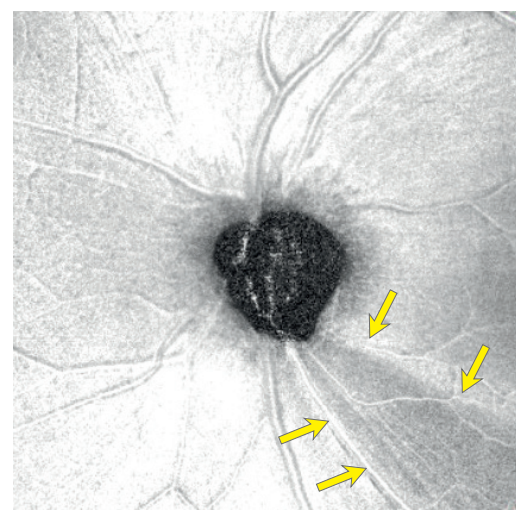
GLOBAL RETINA ANALYSIS



«EN FACE» IMAGE



**SUPERFICIAL RETINAL VASCULAR
NETWORK**



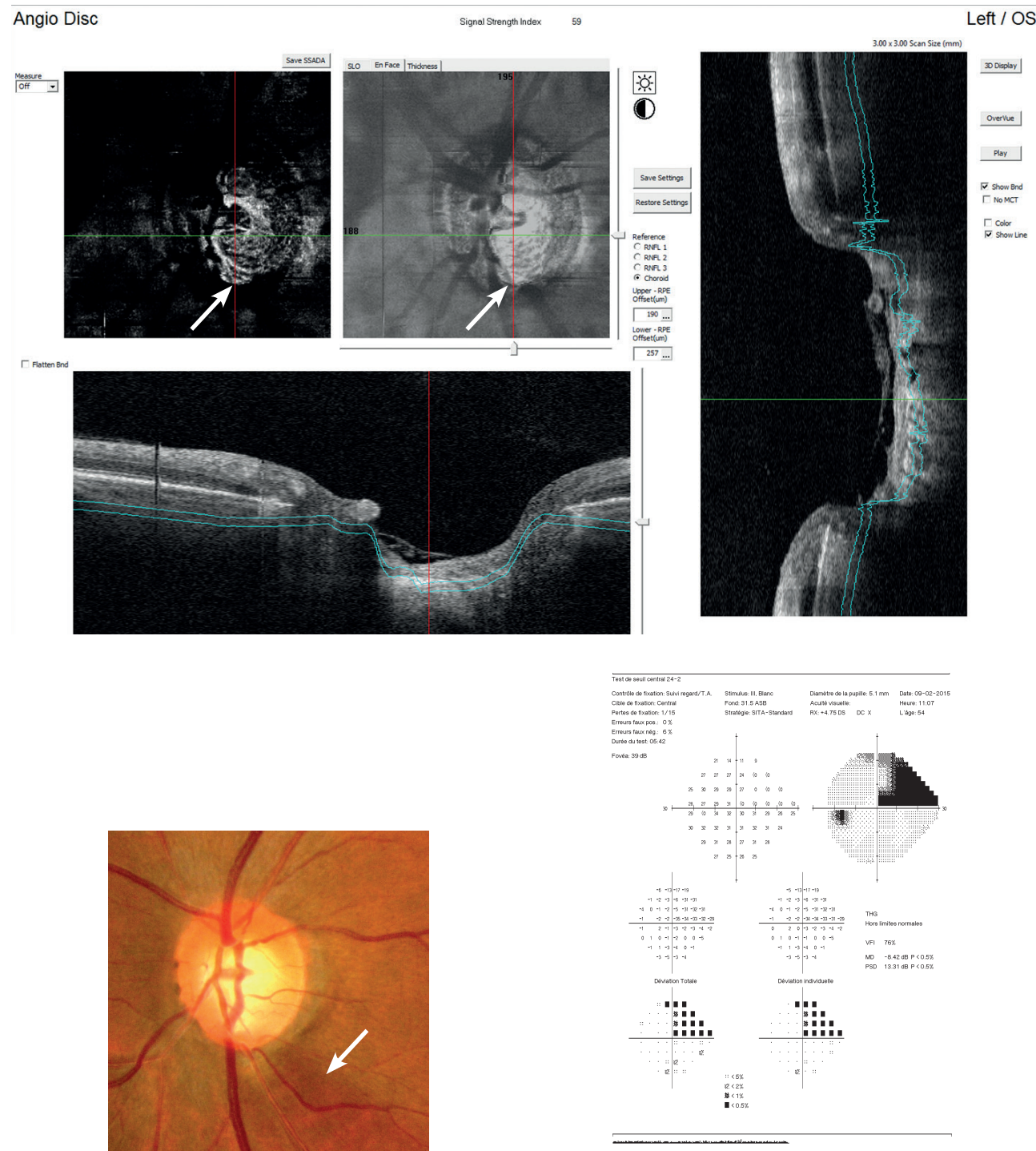
«EN FACE» IMAGE



OCT angiography and glaucoma

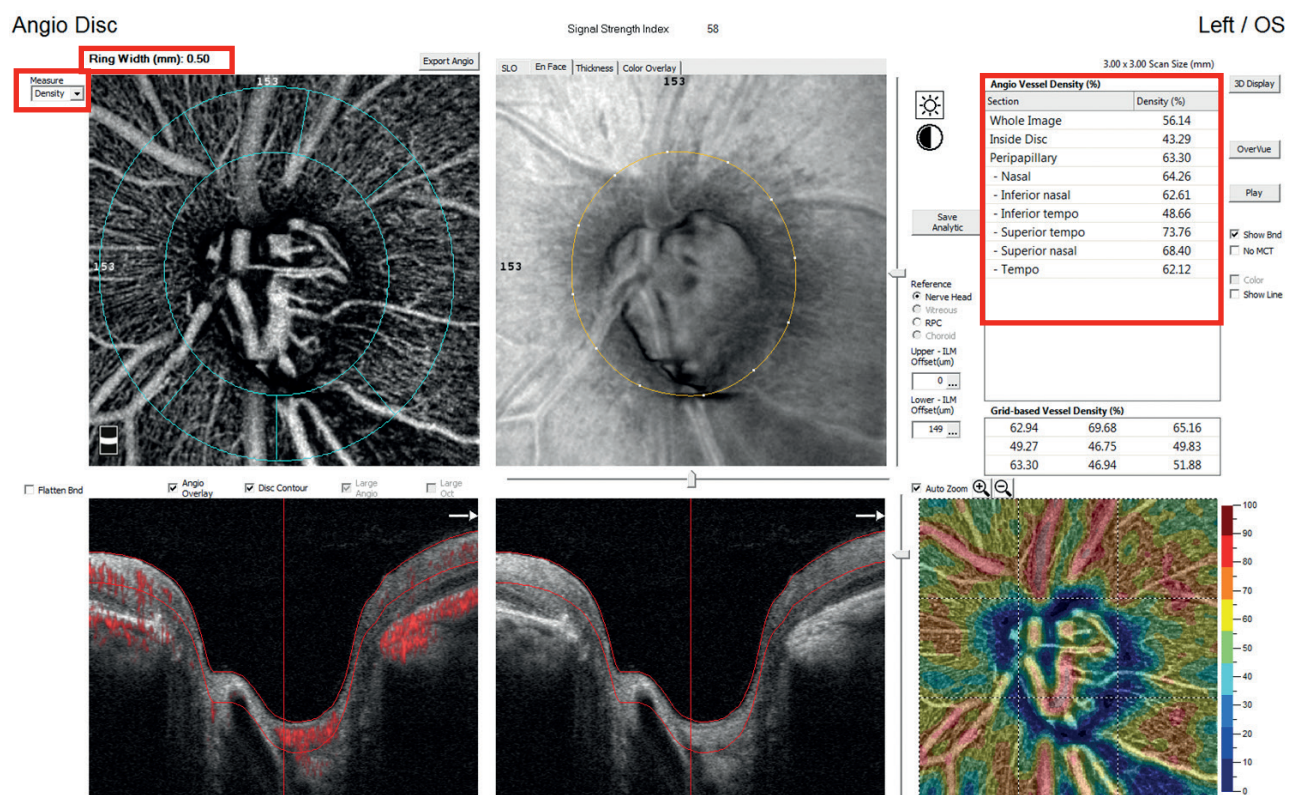
Although the segmentation thicknesses of the retinal layers are defined by the OCT software, they can be modified manually in order to focus on a zone of interest.

Localized segmentation, in this case focusing on the cribriform area, demonstrates enlargement of the pores of the cribriform zone, associated with a reduction of the vascular network, clearly visible on the «en face» image in the inferior temporal sector corresponding to a lesion of the neuroretinal rim and correlated with the functional visual field defect.



OCT angiography provides a new optic disc vessel density index that usefully completes blood flow indices. Only vessel density indices, expressed as a percentage of the area occupied by vessels in the region studied, are currently used in clinical studies at this day.

Recent studies with AngioVue report good reproducibility of peripapillary and ONH vessel density measurements, which are well correlated with the severity of glaucoma.



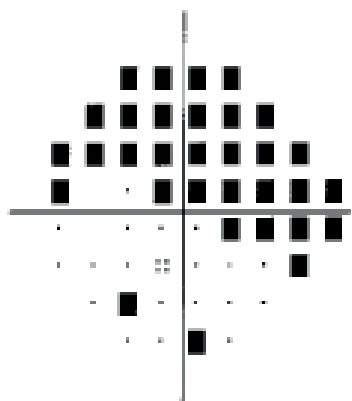
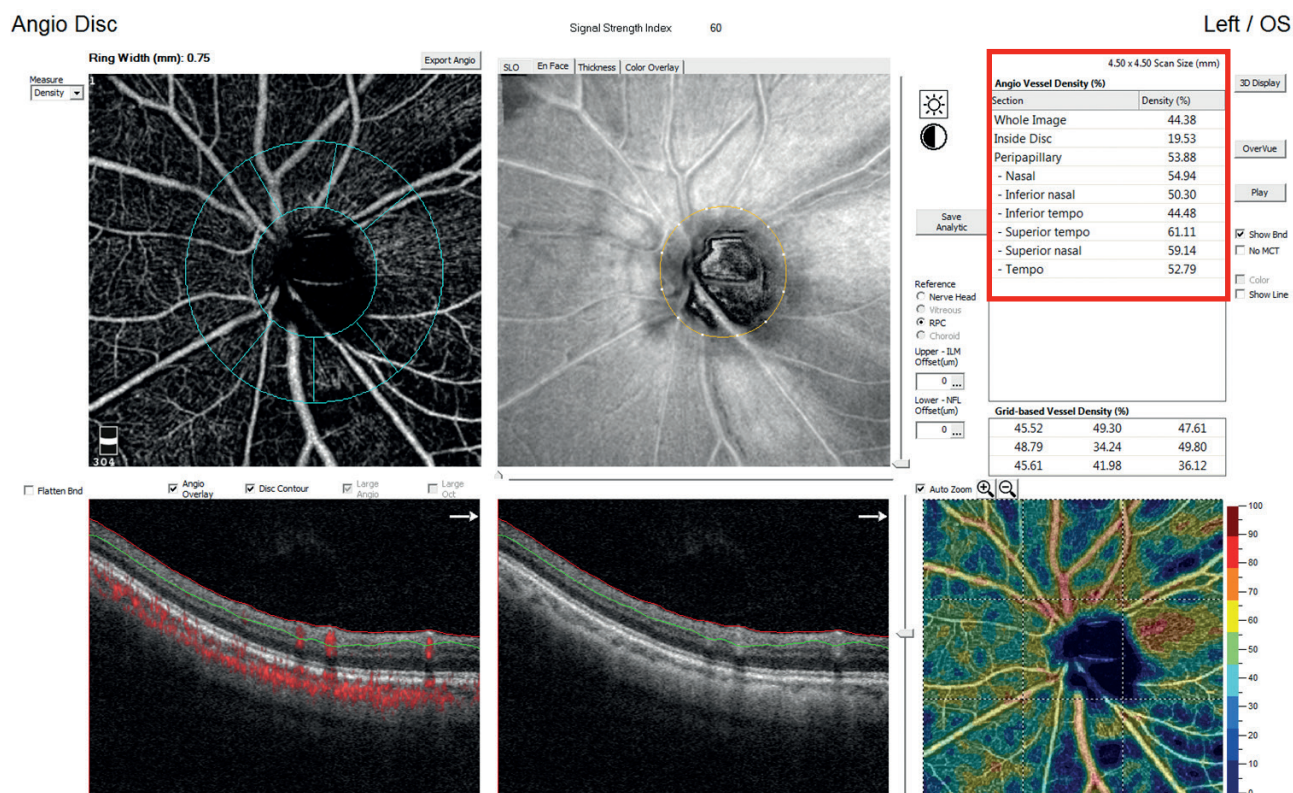
The **vessel density index**, expressed as a percentage, is measured after delineation of the edges of the optic disc (OD), over its entire surface and on 6 sectors of a 0.5 mm large annular peripapillary map. The superior temporal and inferior temporal peripapillary capillary layers are examined in particular detail because of the localized nature of glaucomatous lesions in these territories. This analysis must take into account «en face» images, angiographic images, colour-coded flow density maps, as well as global and sectoral vessel density values expressed as a percentage.

In this patient, AngioVue demonstrates inferior temporal loss of peripapillary vessel density. The RNFL defect is clearly visualized on the «en face» image of the inferior temporal zone with a faint bluish colour in peripapillary zones, corresponding spatially to the colour-coded flow density map.

OCT angiography and glaucoma

In this 65-year-old woman, followed and treated for POAG, OCT angiography demonstrates decreased inferior temporal and superior temporal peripapillary vessel density. The RNFL defect is clearly visualized on the «en face» image of the inferior temporal and superior temporal zones with a faint bluish colour in peripapillary zones, corresponding spatially to the colour-coded flow density map.

OCT angiography can sometimes demonstrate a zone of impaired vessel density in a particular sector, in this case the superior temporal sector, without any functional impairment well detected in the corresponding territory on SAP visual field examination.



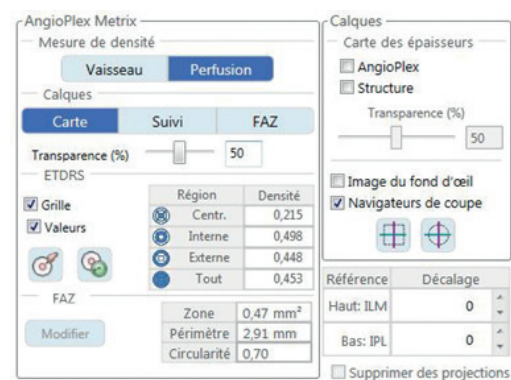
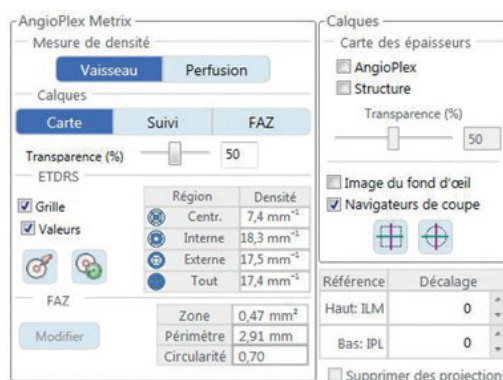
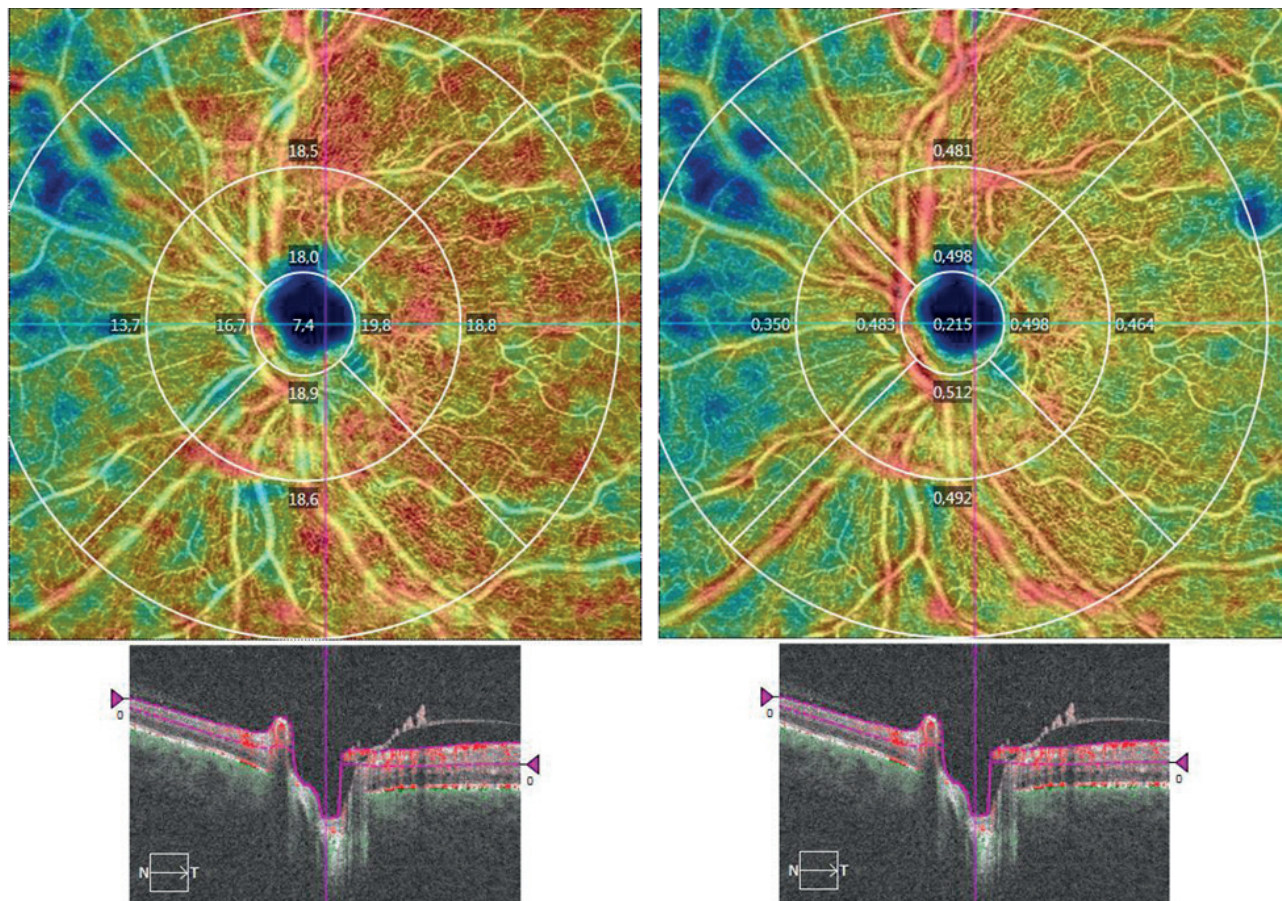
Angioplex OCT angiography on Cirrus HD-OCT evaluates 2 vessel density indices on flow density maps studied according to an ETDRS scale.

VESSEL DENSITY

which is a measure of the total length of blood vessels per unit area (mm/mm²).

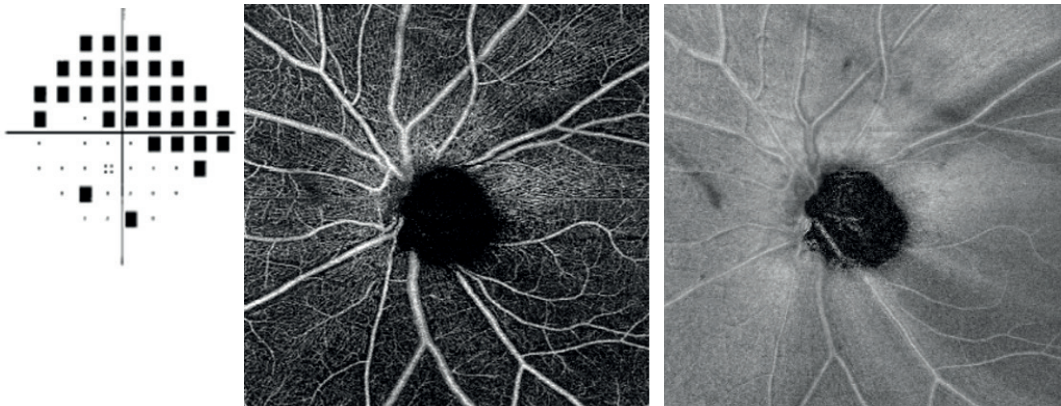
FLOW DENSITY

which is a quotient of the total area of perfused zones/total area of non-perfused zones.

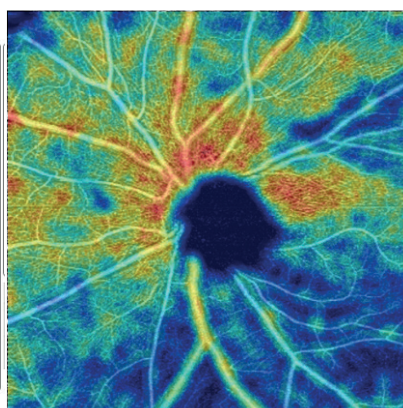
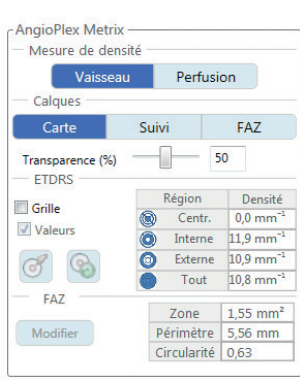


OCT angiography and glaucoma

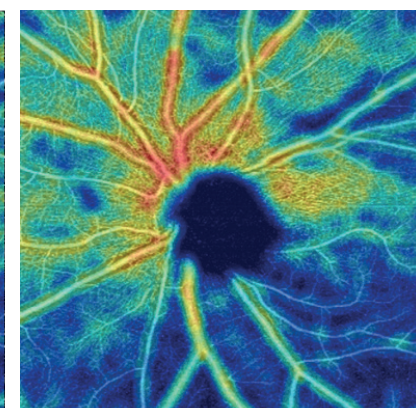
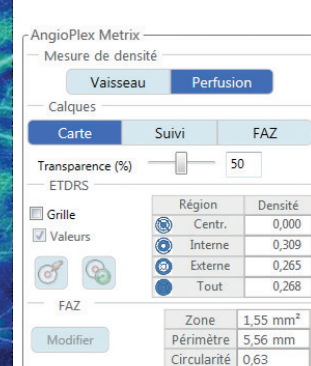
In this 66-year-old woman, followed for advanced POAG, Angioplex Metrix analysis shows alteration of vessel density and flow density parameters in topographic territories closely correlated with the functional visual field defect.



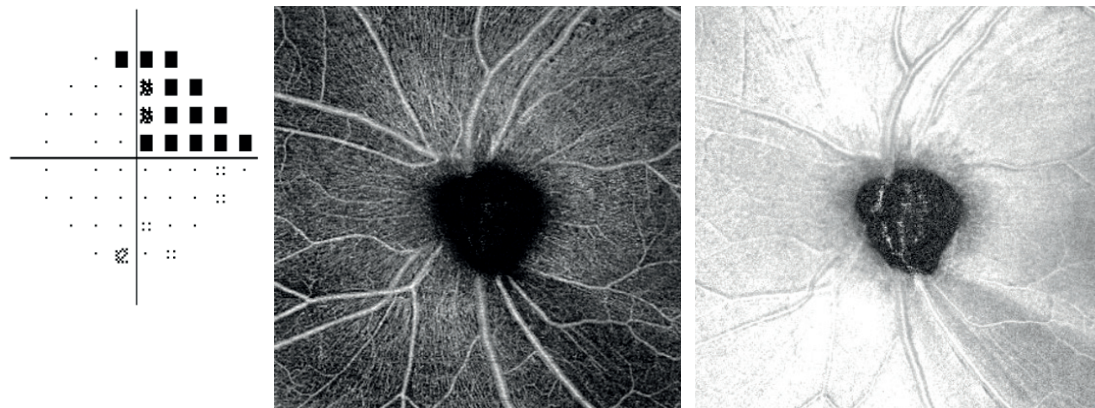
VESSEL DENSITY



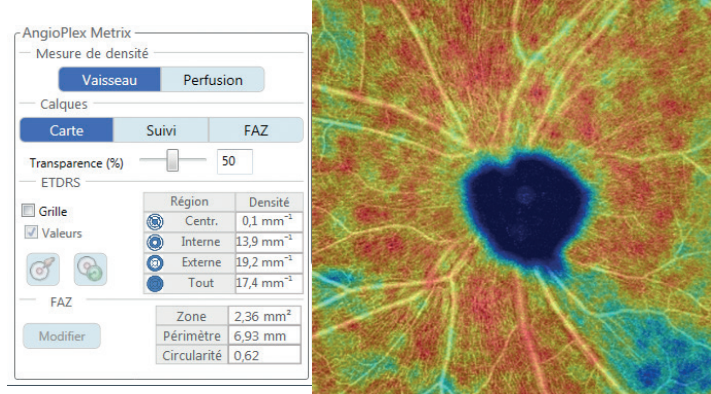
FLOW DENSITY



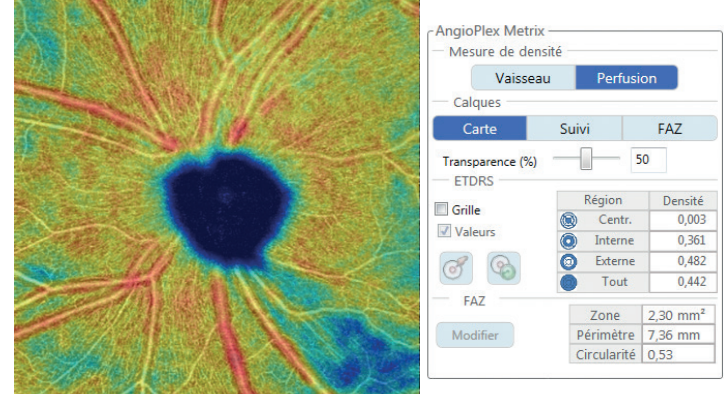
In this 57-year-old woman, followed for early POAG, Angioplex Metrix analysis also reveals alteration of vessel density and flow density parameters in topographic territories closely correlated with the functional visual field defect.



VESSEL DENSITY



FLOW DENSITY



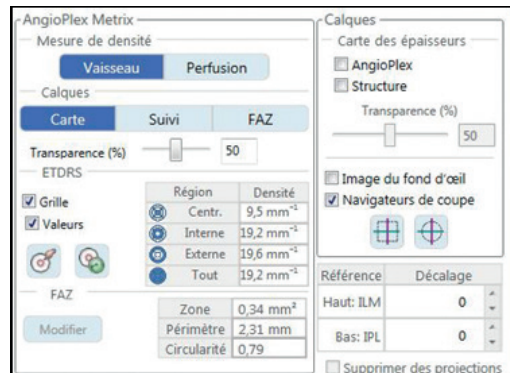
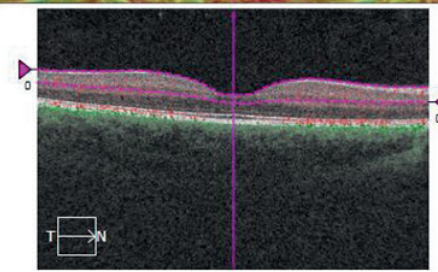
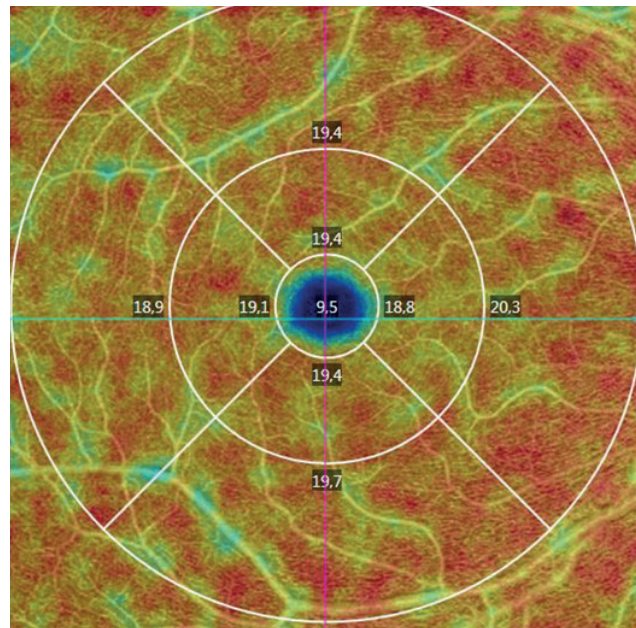
OCT angiography and glaucoma

Angioplex OCT-A on Cirrus HD-OCT evaluates two vessel density indices in the superficial and deep macular vascular networks according to an ETDRS scale.

Analysis of the superficial macular vascular network situated in the macular ganglionic cell layer appears to be particularly useful to evaluate the extent of glaucomatous lesions and their variations in various clinical settings.

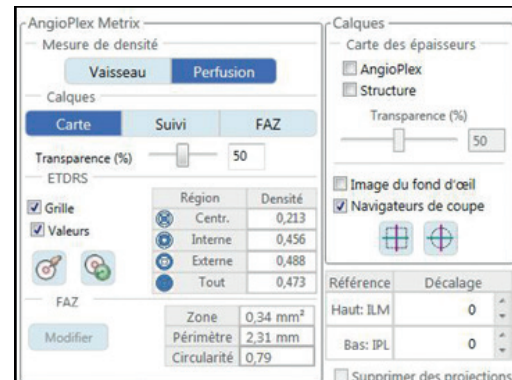
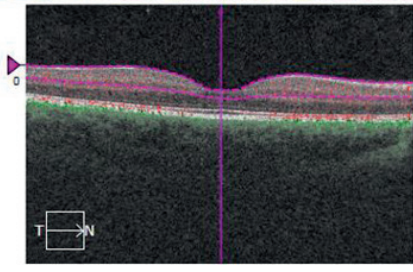
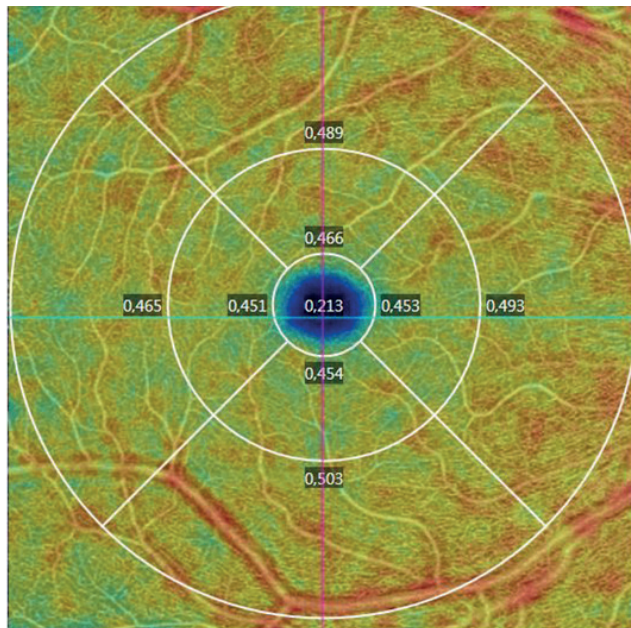
VESSEL DENSITY

measures the total area covered by blood vessels per unit area

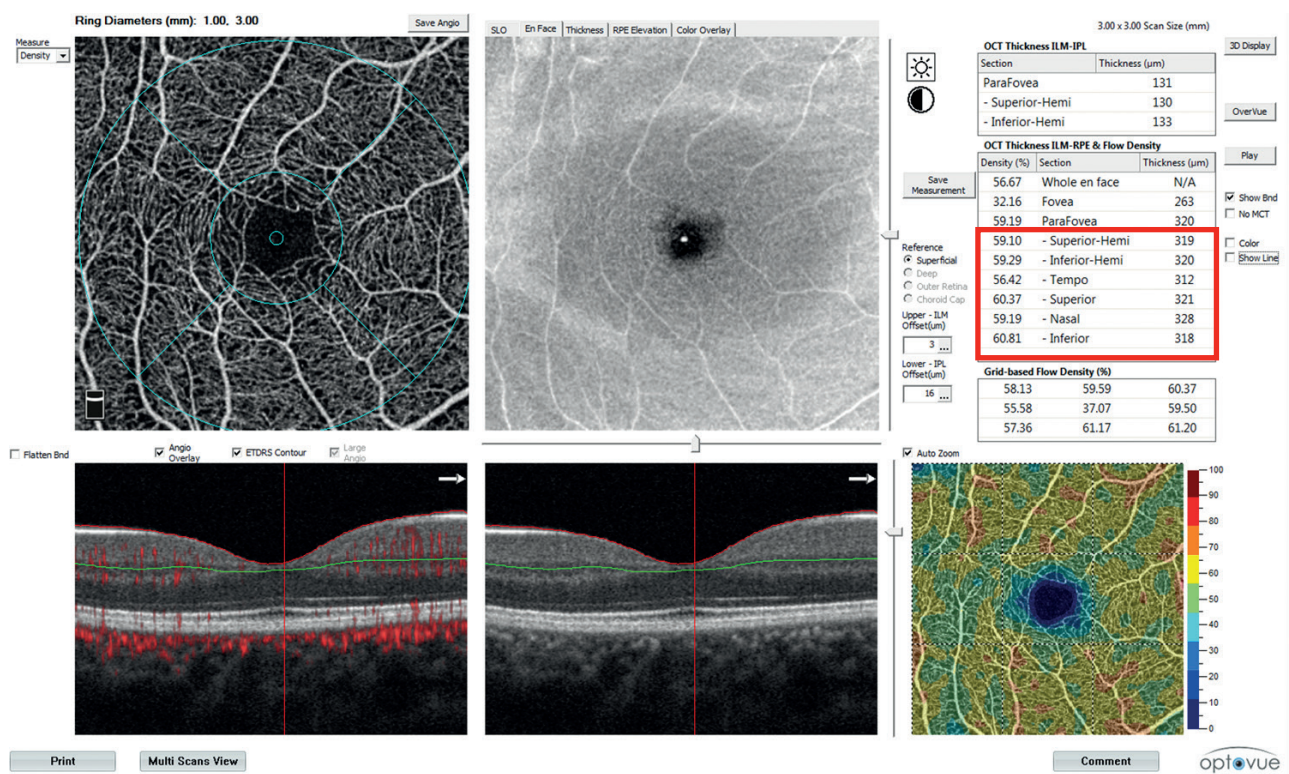


FLOW DENSITY

evaluates the percentage area covered by blood vessels per unit area



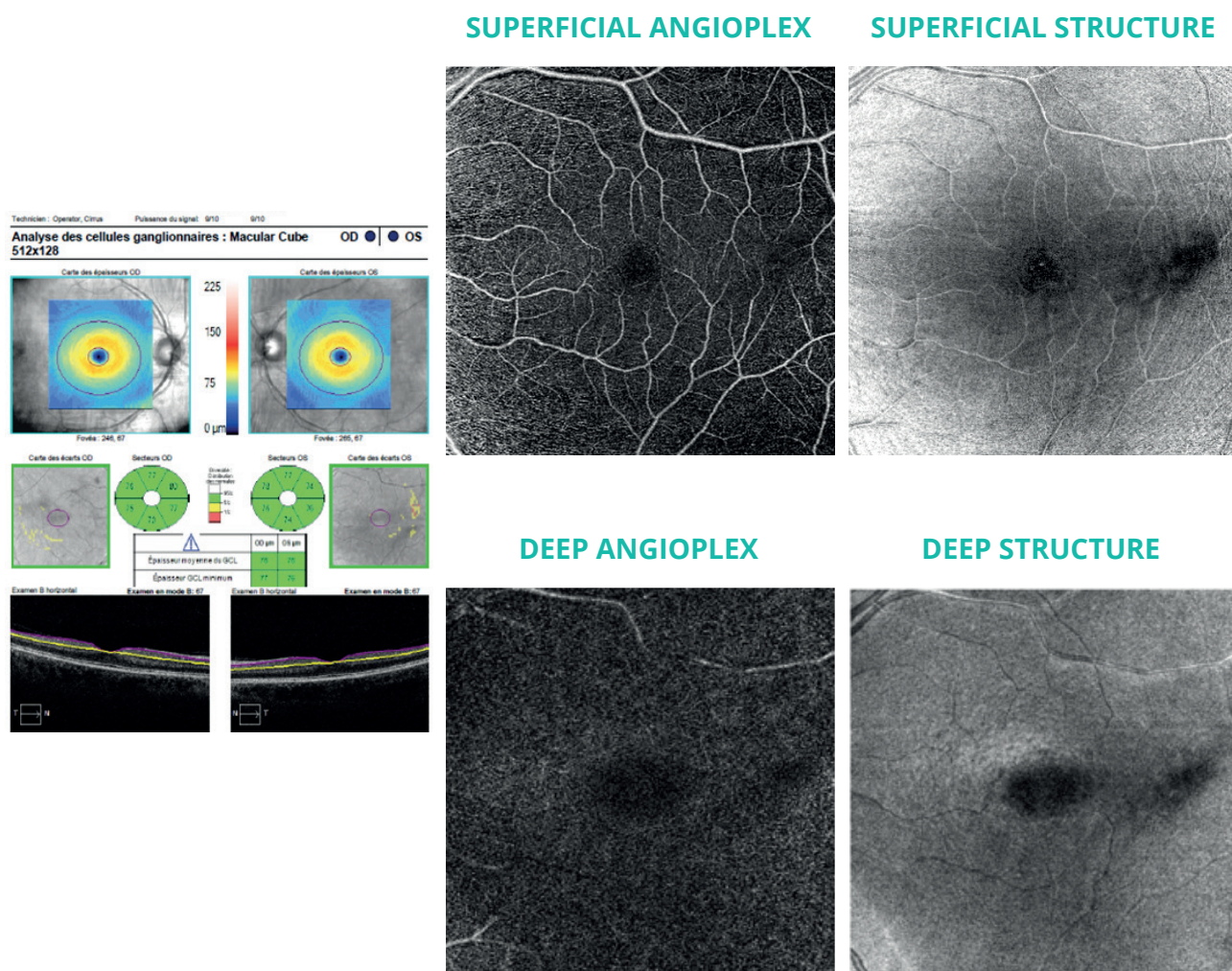
AngioVue macular OCT angiography allows similar analysis of the vessel density, expressed in μm and as a percentage of the area covered by the capillary network, according to an annular macular grid 1 to 3 mm in diameter in 4 different sectors.



OCT angiography and glaucoma

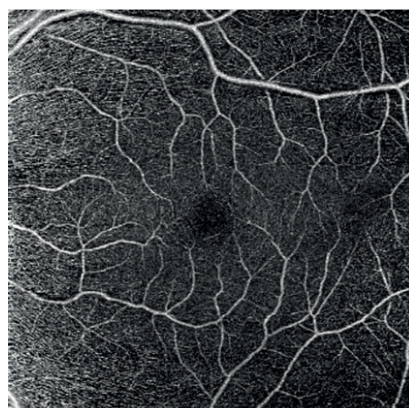
All OCT devices have developed OCT angiography allowing analysis of the superficial and deep capillary network of the macular retina.

For example, Cirrus HD-OCT Angioplex allows analysis of the superficial and deep macular vascular plexuses. Comparative analysis with the thickness ratio of the ganglion cell layer in this case appears to demonstrate a lesion that is spatially well correlated with the two plexuses.

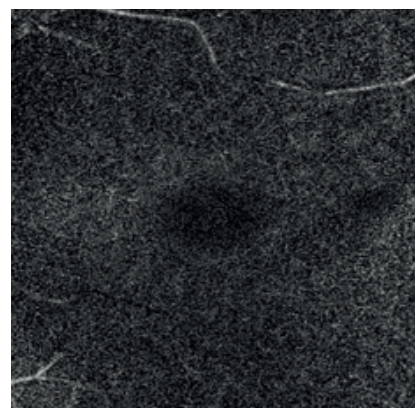


Angioplex Metrix analysis, comprising two evaluation indices, is able to specify the extent of lesion. The vessel density index and the flow density index (expressed as a percentage per unit area) allow monitoring of alterations of the superficial and deep macular vascular networks. The value of these parameters, their reproducibility and their follow-up, particularly those of the superficial capillary network, are currently under evaluation in glaucomatous patients. In the current state of knowledge, the results of these analyses must be interpreted cautiously as a function of the thickness of the various retinal layers demonstrated by SD-OCT and the clinical findings. Monitoring of parameters of the superficial and deep plexuses in this patient will determine progression or stability of the alterations detected.

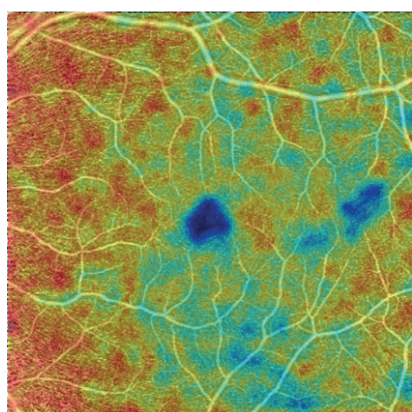
SUPERFICIAL CAPILLARY NETWORK



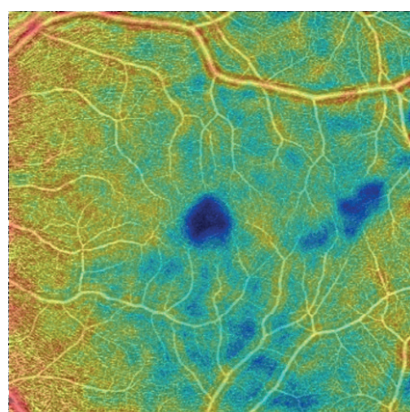
DEEP CAPILLARY NETWORK



VESSEL DENSITY



FLOW DENSITY



Angioplex Metrix cannot currently be used for analysis of vessel density or flow density in the deep retinal vascular network.

AngioPlex Metrix

- Mesure de densité
 - Vaisseau
 - Perfusion
- Calques
- Carte Suivi FAZ
- Transparence (%)
- ETDRS
 - Grille
 - Valeurs
 -
 -
- Région Densité

| | | |
|----------------------------------|---------|-----------------------|
| <input checked="" type="radio"/> | Centr. | 9,2 mm ⁻² |
| <input type="radio"/> | Interne | 15,9 mm ⁻² |
| <input type="radio"/> | Externe | 16,8 mm ⁻² |
| <input type="radio"/> | Tout | 16,4 mm ⁻² |
- FAZ
 - Zone
 - Périmètre
 - Circularité

| | |
|-------------|----------------------|
| Zone | 0,19 mm ² |
| Périmètre | 2,40 mm |
| Circularité | 0,42 |
- Modifier

AngioPlex Metrix

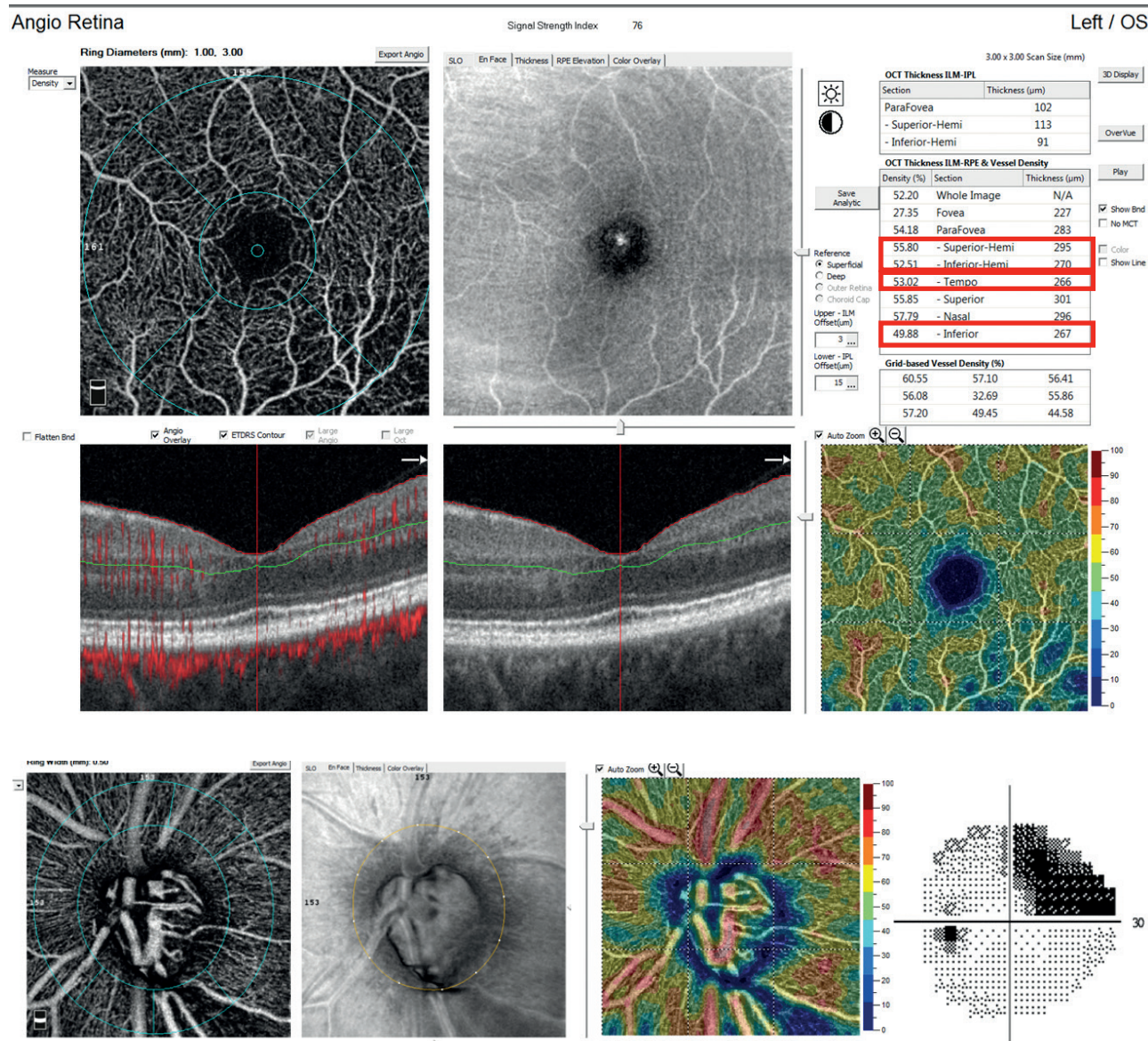
- Mesure de densité
 - Vaisseau
 - Perfusion
- Calques
- Carte Suivi FAZ
- Transparence (%)
- ETDRS
 - Grille
 - Valeurs
 -
 -
- Région Densité

| | | |
|----------------------------------|---------|-------|
| <input checked="" type="radio"/> | Centr. | 0,202 |
| <input type="radio"/> | Interne | 0,371 |
| <input type="radio"/> | Externe | 0,405 |
| <input type="radio"/> | Tout | 0,392 |
- FAZ
 - Zone
 - Périmètre
 - Circularité

| | |
|-------------|----------------------|
| Zone | 0,19 mm ² |
| Périmètre | 2,40 mm |
| Circularité | 0,42 |
- Modifier

OCT angiography and glaucoma

In this patient, OCT angiography demonstrates a decrease in the inferior macular vessel density continuous with a lesion of the peripapillary radial capillary network.



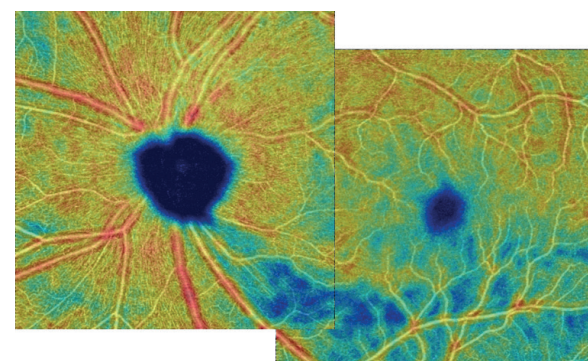
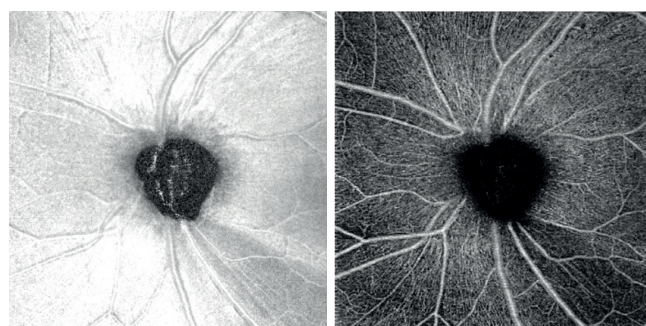
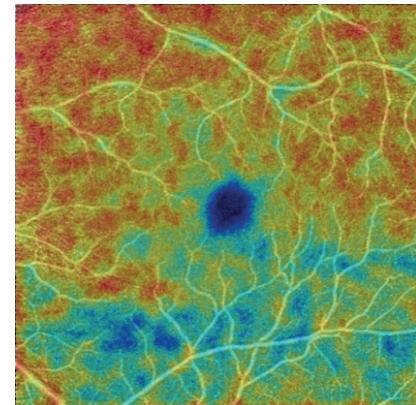
This inferior and inferior temporal lesion of the superficial retinal vascular network is clearly visualized by AngioVue on the image of the capillary network with a faint bluish colour on the colour-coded flow density map.

Cirrus HD-OCT Angioplex analysis demonstrates reduction of the vessel density of the superficial retinal vascular network in the inferior and inferior temporal sectors of the macula, continuous with the lesion of the peripapillary network.

VESSEL DENSITY

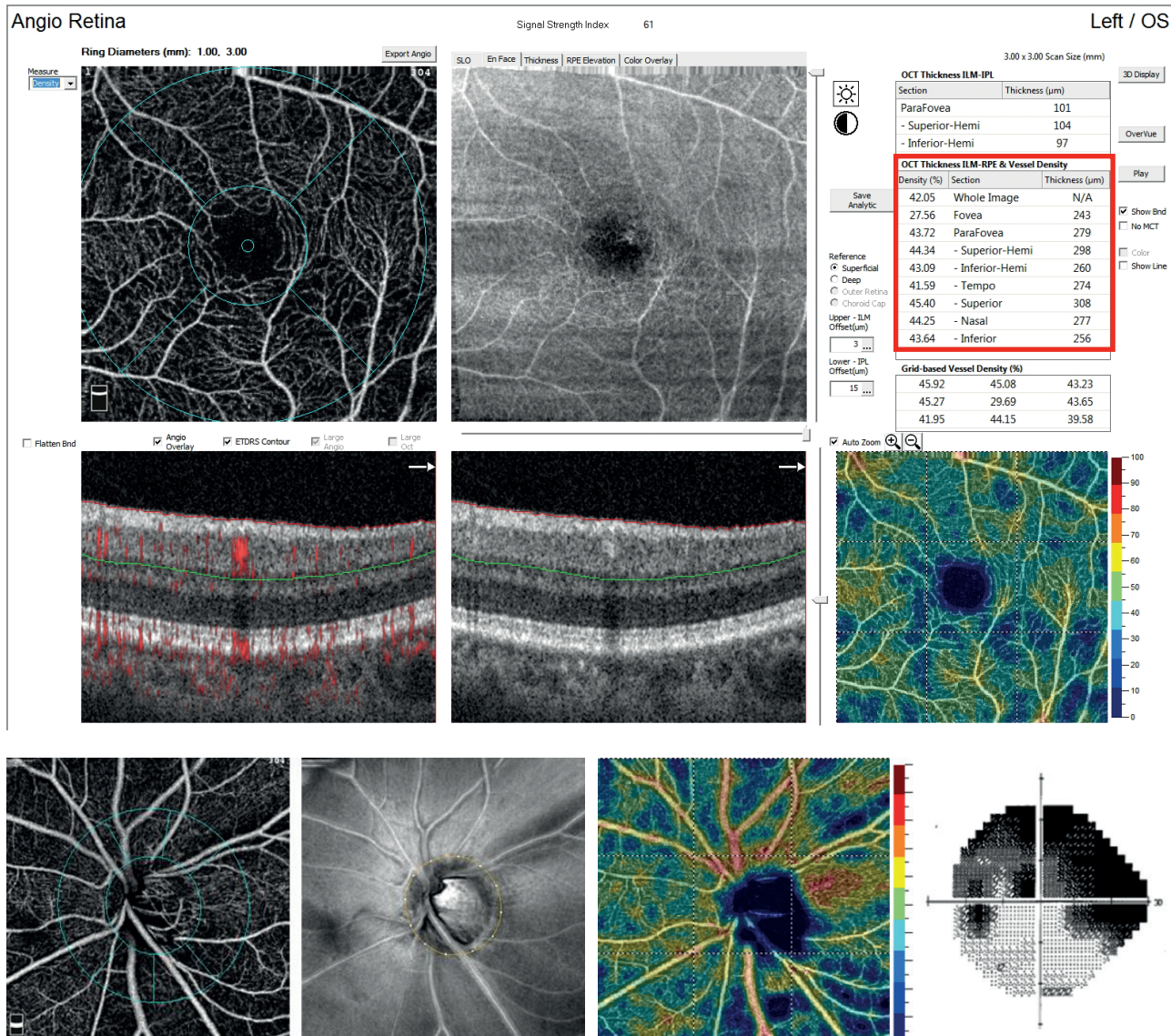


FLOW DENSITY



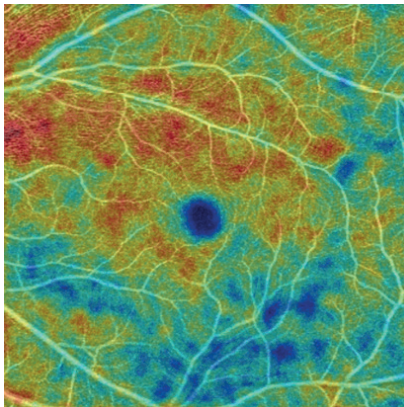
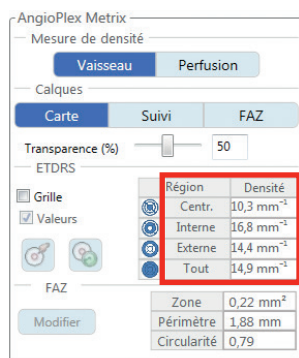
OCT angiography and glaucoma

In this 66-year-old woman, AngioVue demonstrates loss of inferior macular vessel density in the superficial macular vascular network, continuous with the lesion of the peripapillary radial capillary network.

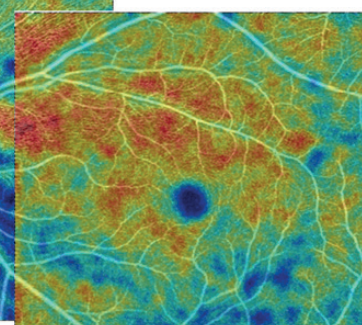
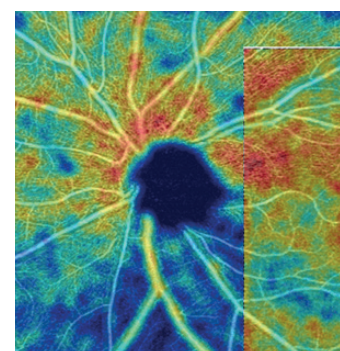
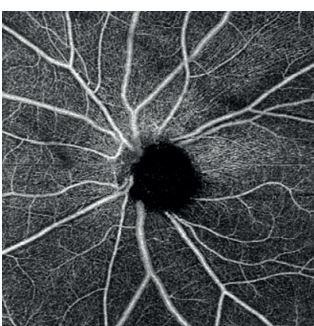
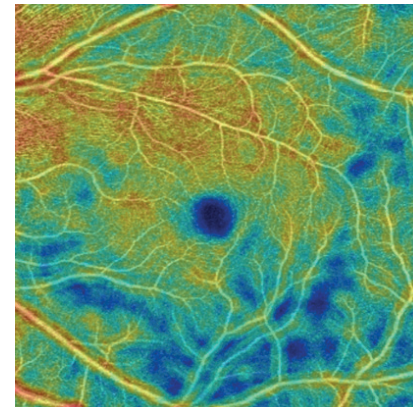


Cirrus HD-OCT Angioplex analysis also shows a reduction of the vessel density of the superficial retinal vascular network in the inferior sector of the macula, continuous with the lesion of the peripapillary network.

VESSEL DENSITY



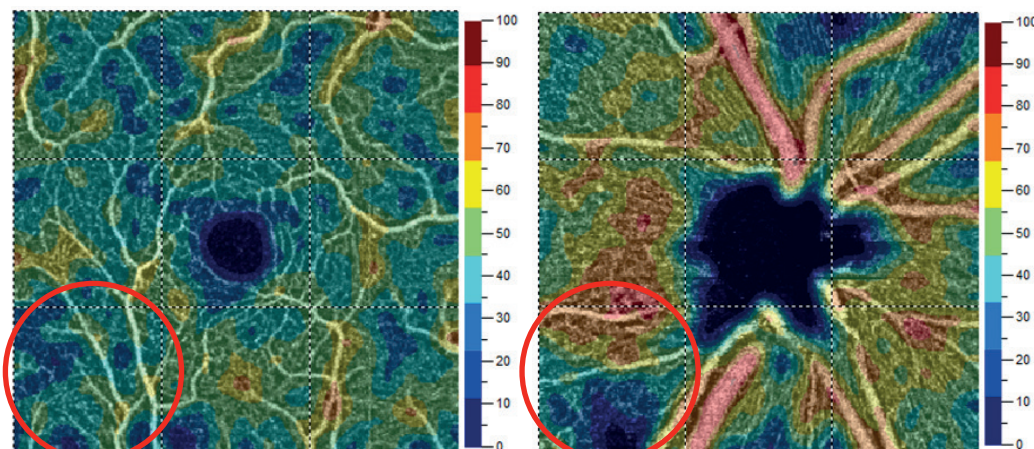
FLOW DENSITY



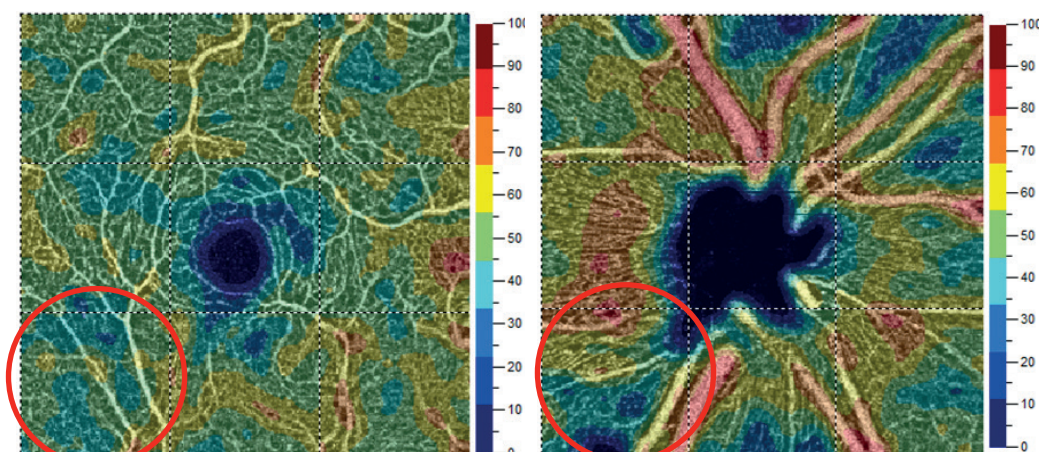
OCT angiography and glaucoma

The preliminary results of density analysis of the superficial retinal vascular network appear to be particularly interesting, as illustrated here, by variations of the vessel density after lowering intraocular pressure by filtering surgery.

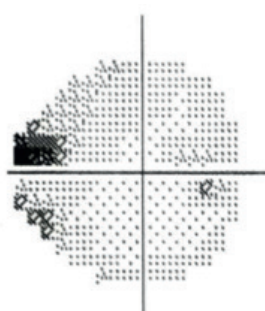
OCT angiography has only recently been used to quantify vessel density, but opens up the prospects of promising studies allowing a new approach to the understanding of vascular factors and their consequences.



PREOPERATIVE OCT ANGIOGRAPHY EVALUATION OF THE SUPERFICIAL RETINAL VASCULAR NETWORK



POSTOPERATIVE EVALUATION AFTER FILTERING SURGERY



Several questions have yet to be resolved

The primary or secondary nature of the vascular changes observed in glaucoma has not yet been fully elucidated.

By demonstrating decreased vessel density in the superficial retinal and peripapillary capillary networks at the various stages of glaucoma, monitoring by OCT angiography could probably improve our knowledge in this field.

Correlation of the preliminary OCT angiography results with data concerning the structural and functional lesion highlights the value of OCT angiography to monitor glaucoma progression.

The dynamic range of OCT angiography, especially evaluation of vessel density and its relationship with glaucoma, remains poorly defined. The correspondence between vascular parameters and RNFL thickness measurements and visual field measurements has yet to be determined.

OCT used for structural evaluation of glaucoma could be useful for functional assessment of the optic nerve by providing vessel density parameters.

If future studies and developments confirm this capacity, OCT angiography could provide a high level of precision due to its rapid analysis of the tissues directly concerned by glaucomatous optic neuropathy.

Development of OCT angiography will also probably allow more precise analysis of the effects of the various available glaucoma treatments on the blood supply of the optic nerve and the development of new treatments acting on the blood supply of the optic nerve.

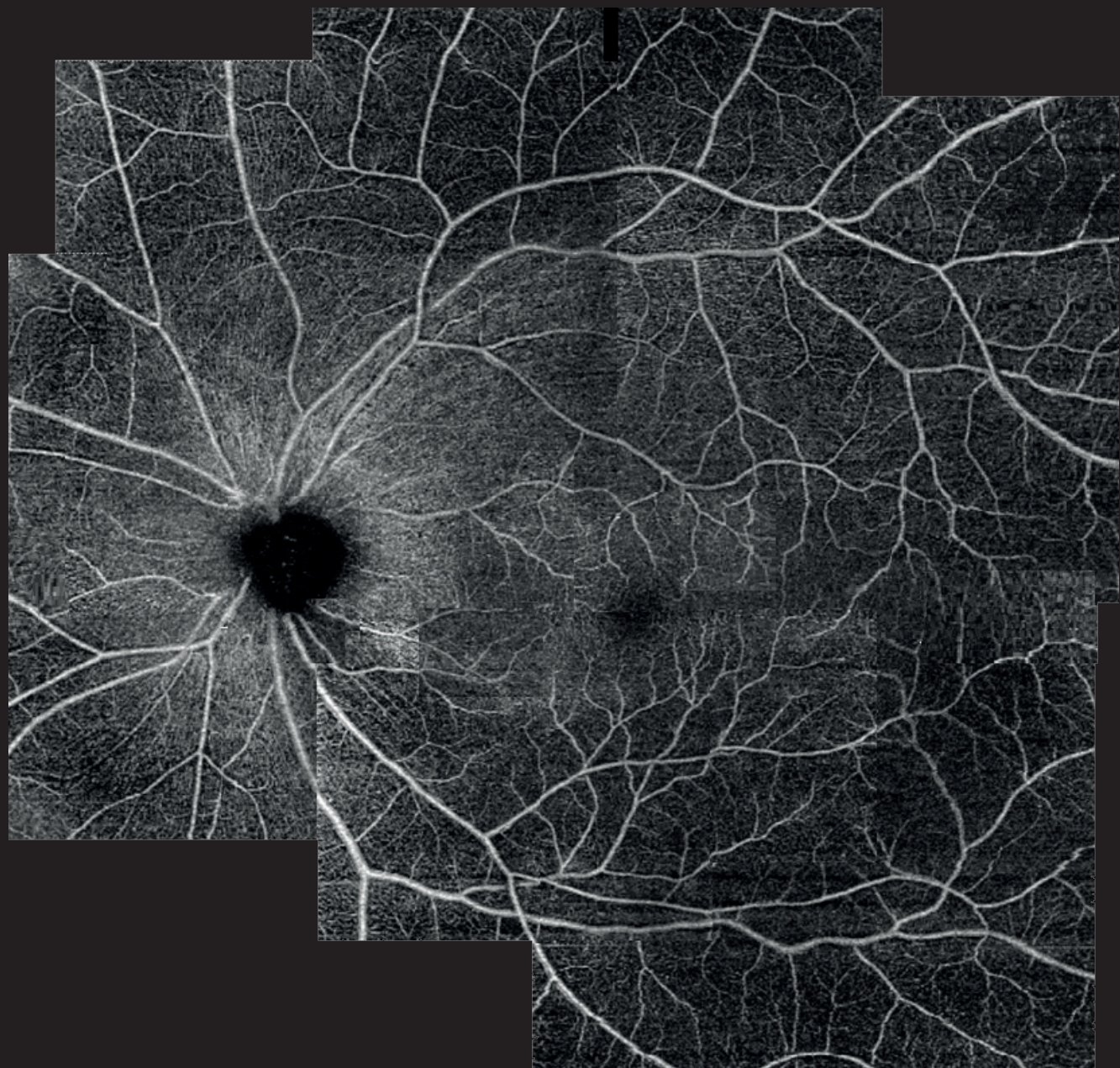
Conclusion

Posterior segment imaging now occupies an important place in the diagnosis and follow-up of glaucoma patients.

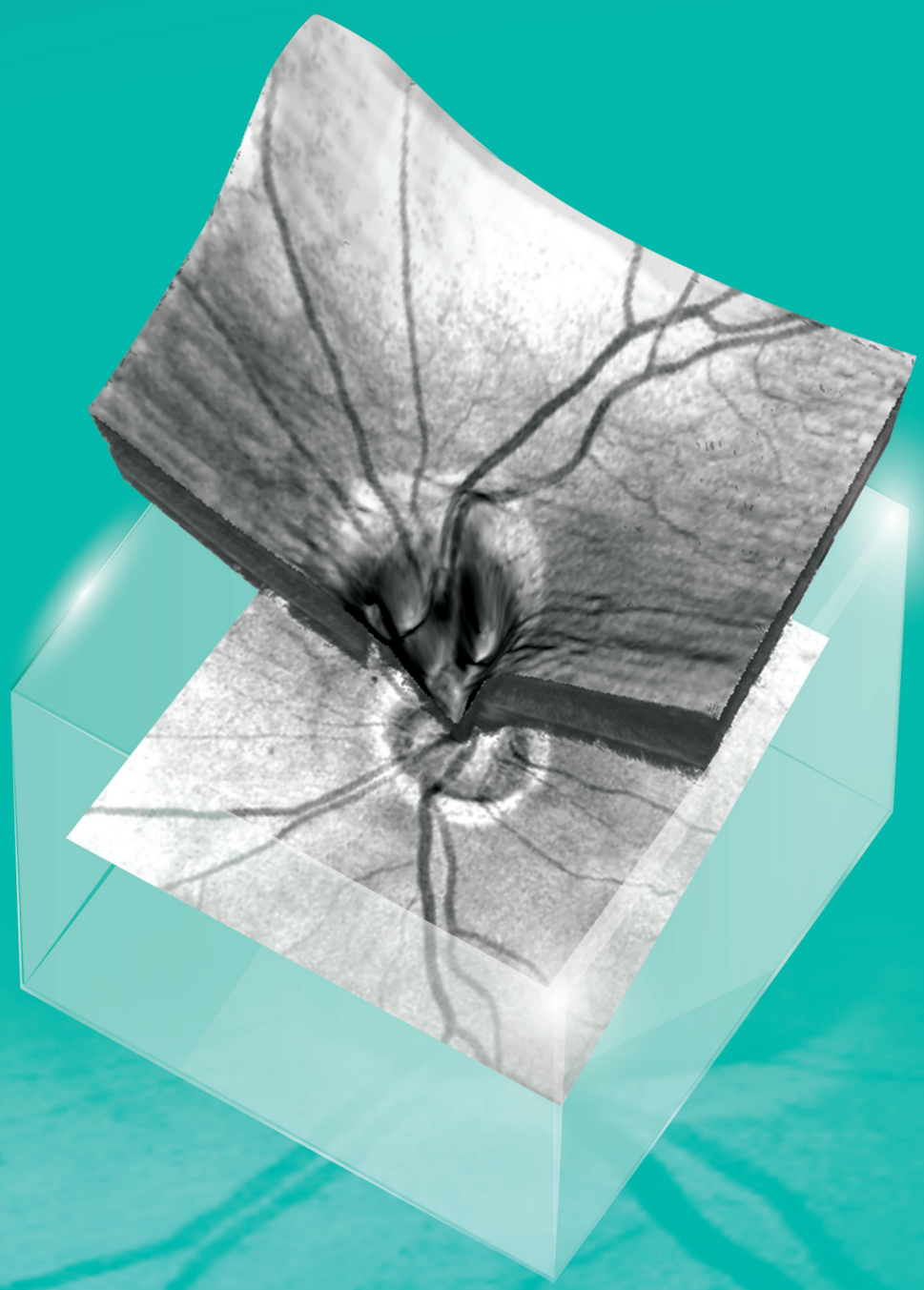
Although the continuous development of SD-OCT image acquisition, extraction and analysis techniques provides a growing body of information, efficient use of these techniques must be based on a good knowledge of the interpretation and limitations of these techniques.

The results of posterior segment imaging must be interpreted cautiously and must never be considered in isolation, but always in comparison with the clinical findings and analysis of the functional impairment.

Optimal use of posterior segment imaging can therefore provide maximum benefit for the management of our patients.



Zeiss - Angioplex posterior pole panoramic view: Superficial retinal vascular network



Anterior segment OCT in glaucoma

Anterior segment OCT

The basic principle of OCT is similar to that of ultrasound, but with the use of light waves instead of ultrasound. OCT has been used for imaging of the posterior segment since 1991, and was rapidly developed for evaluation of the anterior segment, especially in glaucoma.

The spatial resolution of OCT systems specifically designed for anterior segment examination, such as the Visante AS-OCT (Carl Zeiss Meditec, Dublin, U.S.) or SL-OCT (Heidelberg Engineering, Heidelberg, Germany), is 18 µm in the axial plane and 60 µm in the lateral plane. However, many manufacturers now propose additional optics to be placed on posterior segment Spectral-Domain OCT in order to obtain images of the anterior segment with a spatial resolution of about 5 µm. These apparatuses have a better resolution than systems specifically devoted to anterior segment OCT (such as Visante AS-OCT), but not all of them can provide limbus-to-limbus sections of the anterior segment and their wavelength (about 800 nm) limits visualization of angular structures.

Compared to the ultrasound used by UBM, the OCT infrared light beam is very strongly absorbed by the pigmented epithelium of the iris, making it very difficult to analyse structures situated posteriorly to the iris, particularly the ciliary processes.

On the other hand, **AS-OCT examination is easier to perform** than UBM, as it is a non-contact examination performed on a seated patient. Acquisitions can be easily performed in scotopic and photopic conditions in order to vary pupillary dilatation and allow dynamic analysis of angular structures.

Comparison of OCT and UBM



UBM

Precise visualization of the ciliary body and retroiridial structures.



OCT

Easy and rapid
No contact
Better resolution
Dynamic
Seated position



1. Detection of narrow iridocorneal angles and quantitative parameters

Detection of narrow iridocorneal angles and quantitative parameters

Anterior chamber OCT rapidly, simply and noninvasively provides high resolution axial images of the anterior chamber and iridocorneal angle. It is therefore particularly useful for the documentation and detection of narrow or suspicious iridocorneal angles.

Various parameters can be analysed in order to precisely study angle opening: qualitative parameters such as angle configuration, the presence of iridotrabecular appositions, the slope of insertion of the root of the iris on the iridocorneal angle or the presence of peripheral anterior synechiae, but also quantitative parameters similar to those developed for UBM analysis of the iridocorneal angle, such as the angle opening distance at 500 µm (AOD 500), the angle recess area (ARA) and the iridotrabecular angle, and the trabecular-iris space area 500 or 750 in mm² (TISA). These various AS-OCT measurements of the iridocorneal angle are highly reproducible.

These various biometric parameters are limited by anatomical variations of the angle as a function of the state of pupillary dilatation and the meridian analysed, the difficulty of visualizing the landmarks required to obtain these parameters, but especially the lack of evaluation of their exact capacity to evaluate clinical risks. The value of these parameters for the detection of narrow angles in clinical practice has yet to be determined.

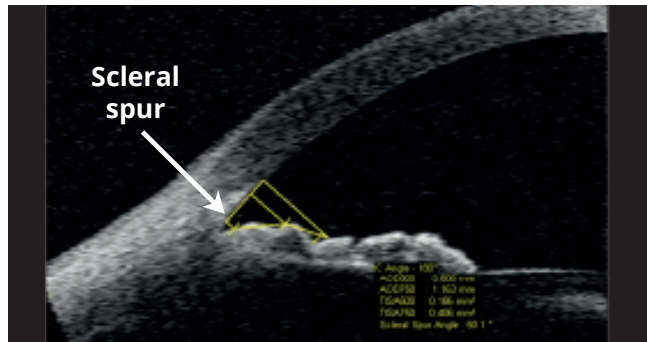


Figure 1:

Semiautomated analysis of quantitative parameters of the iridocorneal angle requires detection of the scleral spur.

AOD 500/750: Angle Opening Distance at 500/750 μ m.

TISA 500/750: Trabecular-Iris Space Area 500/750.

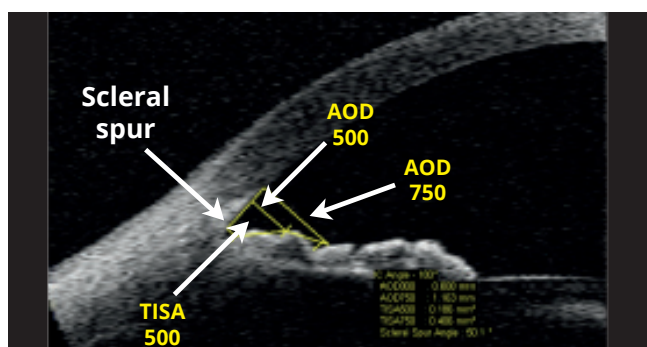


Figure 2:

Example of quantitative parameters used to measure the iridocorneal angle.

AOD 500/750: Angle Opening Distance at 500/750 μ m.

TISA 500/750: Trabecular-Iris Space Area 500/750.

Detection of narrow iridocorneal angles and quantitative parameters

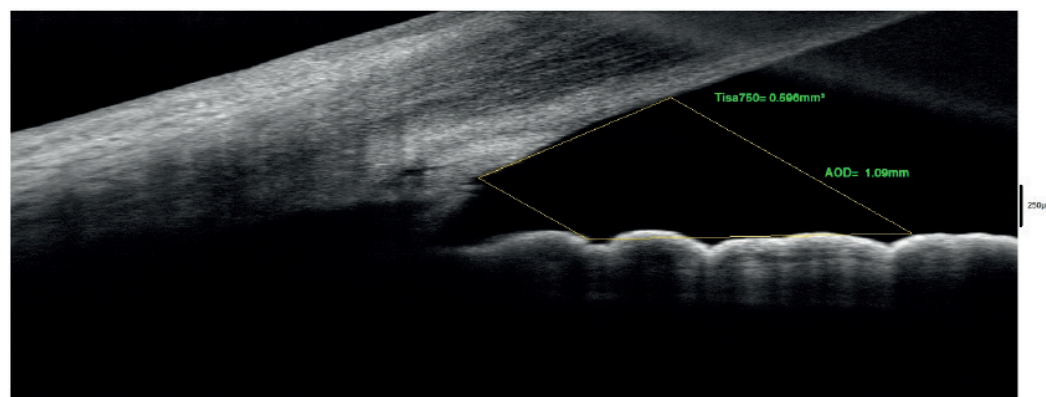


Figure 3:

Example of quantitative parameters used to measure the iridocorneal angle by SD-OCT.
AOD 750: Angle Opening Distance at 750 μm.
TISA 750: Trabecular-Iris Space Area 750.

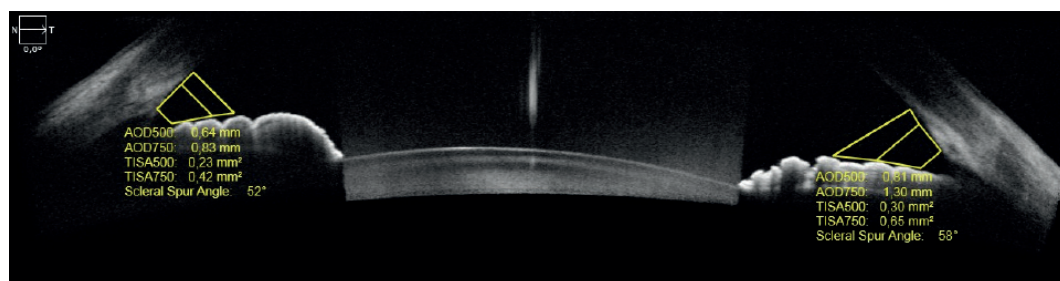


Figure 4:

Example of quantitative parameters used to measure the iridocorneal angle by SD-OCT.
AOD 500/750: Angle Opening Distance at 500/750 μ m.
TISA 500/750: Trabecular-Iris Space Area 500/750.

Detection of narrow iridocorneal angles and quantitative parameters

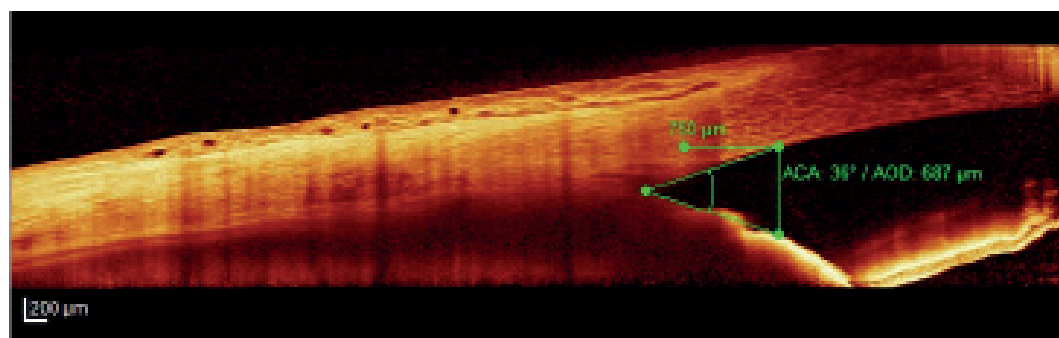


Figure 5:

Example of quantitative parameters used to measure the iridocorneal angle by Spectral-Domain OCT and anterior segment OCT.

AOD: Angle Opening Distance at 750 μm .

ACA: Anterior Chamber Angle.



Figure 6:

Semiautomated analysis of quantitative parameters of the iridocorneal angle in a patient with an open angle.



Figure 7:

Semiautomated analysis of quantitative parameters of the iridocorneal angle in a patient with a narrow angle.

Detection of narrow iridocorneal angles and quantitative parameters

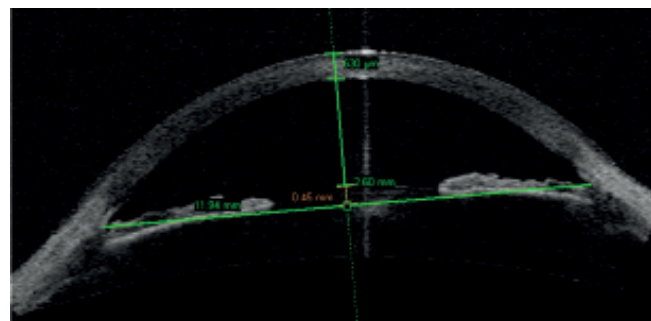


Figure 8:

Measurement of the lens vault corresponds to the distance between the anterior surface of the lens and a line through the two scleral spurs in the centre of the cornea. It is a useful marker of the participation of the lens in mechanisms leading to iridocorneal angle closure. Example of measurement of a 450-micron lens vault.

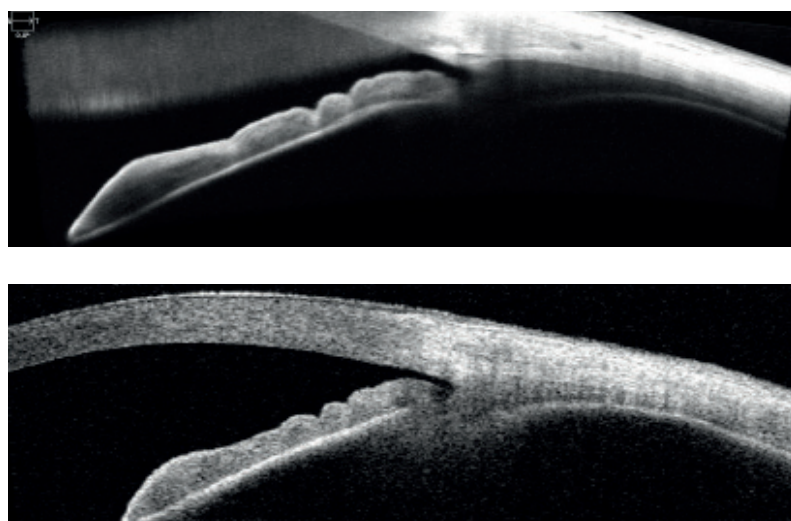


Figure 9:

Comparison of spectral-domain (top) and time-domain (bottom) OCT images of the iridocorneal angle. Spectral-domain OCT provides better resolution, but the details are clearly visible with both techniques.

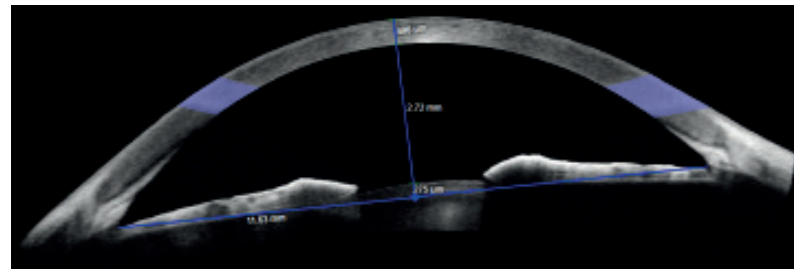


Figure 10:

Anterior chamber spectral-domain OCT.

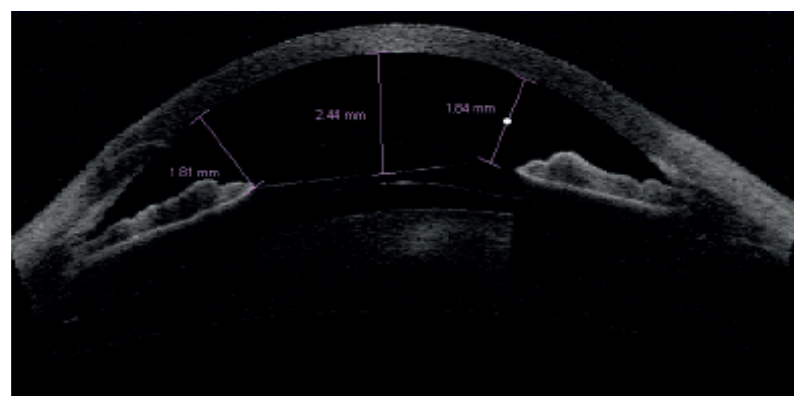


Figure 11:

Measurement of the distances between a posterior chamber implant (lens implant) placed anteriorly to the lens and the corneal endothelium.

Detection of narrow iridocorneal angles and quantitative parameters

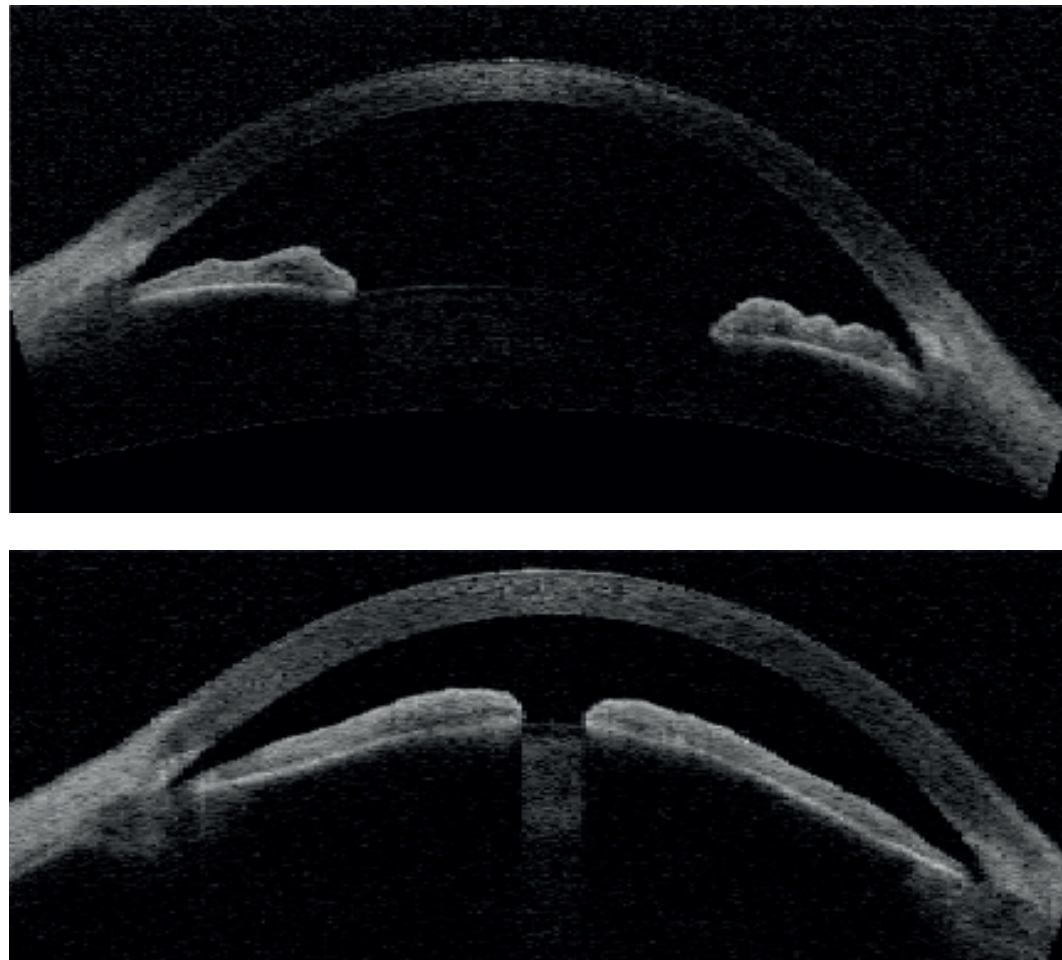


Figure 12:

Value of OCT for documentation of the anterior segment and iridocorneal angle. Top: open angle and deep anterior chamber. Bottom: open angle, but shallow anterior chamber. This documentation can be used to show the possible anatomical risks to the patient and explain the proposed treatment, and constitutes a valuable follow-up tool.

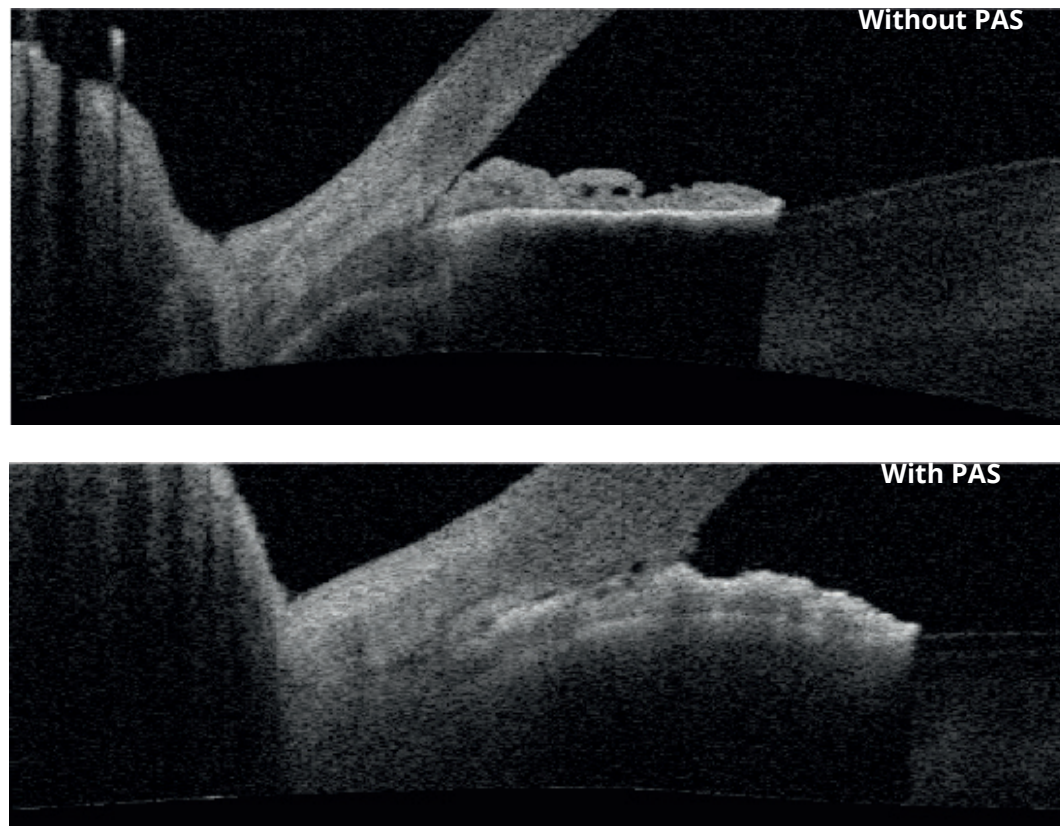


Figure 13:

OCT image of the iridocorneal angle showing a closed angle associated with iridotrabecular apposition (top) and a closed angle associated with the presence of peripheral anterior synechiae (PAS) (bottom).



2. Analysis of the mechanisms of angle closure

- 2.1. Pupillary block**
- 2.2. Plateau iris mechanism**
- 2.3. Lens mechanisms**
- 2.4. Malignant glaucoma**
- 2.5. Choroidal effusion**
- 2.6. Other forms of secondary iridocorneal angle closure**

Anterior segment imaging has provided a better understanding of the various mechanisms responsible for iridocorneal angle closure, such as pupillary block, direct angle closure by a plateau iris mechanism, lens mechanisms, cilio-lenticular block and ciliochoroidal effusion. Finally, some secondary causes, such as iridocorneal endothelial (ICE) syndromes, intraocular inflammation or neovascular glaucoma can also induce angle closure due to the presence of peripheral anterior synechiae (PAS).

Pupillary block

Pupillary block is the mechanism most commonly involved in primary iridocorneal angle closure. It corresponds to apposition between the iris and the anterior surface of the lens at the pupil. This contact generates a pressure gradient between the posterior and anterior chambers of the eye, resulting in anterior displacement of the peripheral iris, which can induce intermittent or permanent angle closure with contact between the peripheral iris and the trabecular meshwork.



Figure 14:

UBM image of a closed iridocorneal angle due to pupillary block, with convexity and anterior displacement of the iris, inducing iridocorneal angle closure. UBM is able to eliminate a plateau iris mechanism.

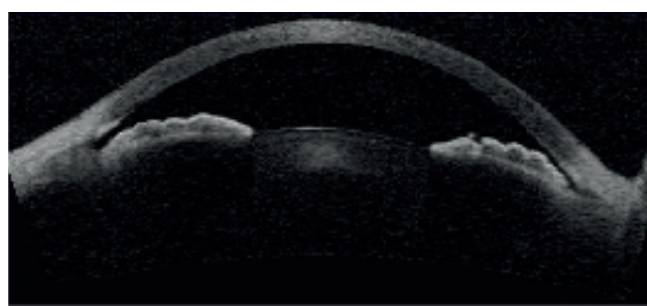


Figure 15:

OCT image of a narrow iridocorneal angle without iridotrabecular apposition related to pupillary block associated with a lens mechanism.

Pupillary block

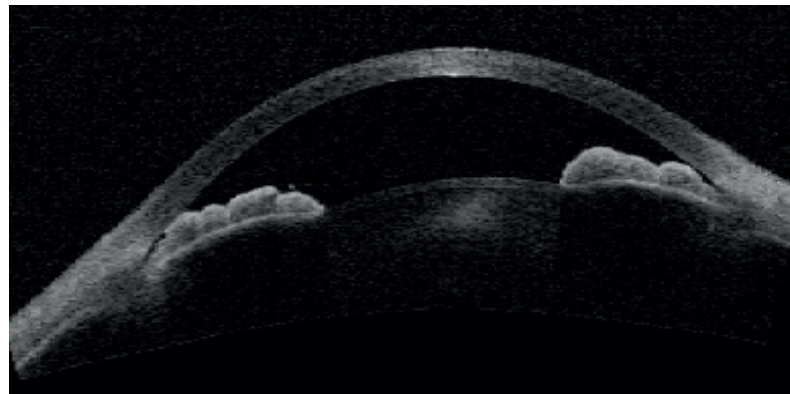


Figure 16:

OCT image of a closed iridocorneal angle with iridotrabecular apposition related to pupillary block associated with a lens mechanism.

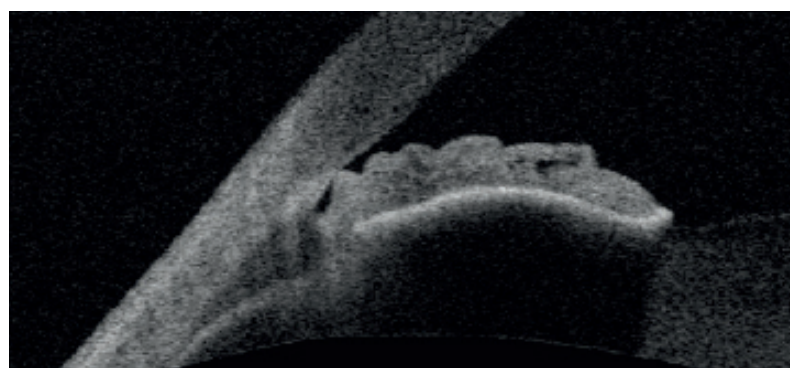


Figure 17:

OCT image of a narrow iridocorneal angle related to pupillary block, with convexity and anterior displacement of the iris, inducing iridocorneal angle closure with iridotrabecular apposition.

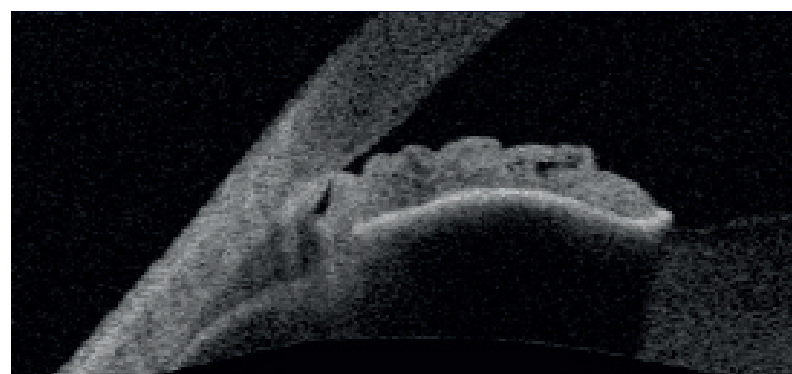
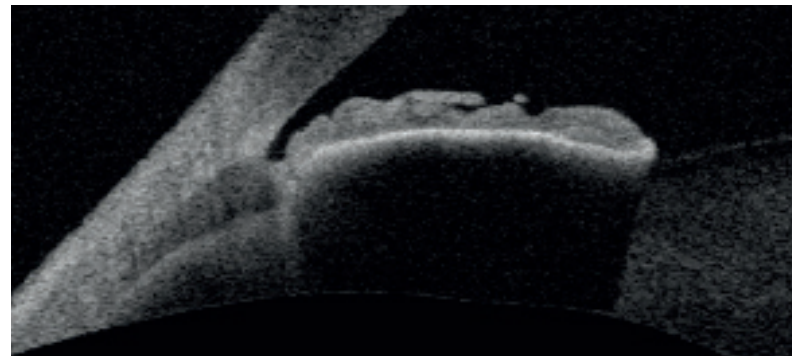


Figure 18:

OCT image of a closed iridocorneal angle related to a pupillary block mechanism. Dynamic analysis shows iridotrabecular apposition under low luminosity conditions. Top: image under photopic conditions. Bottom: image under scotopic conditions.

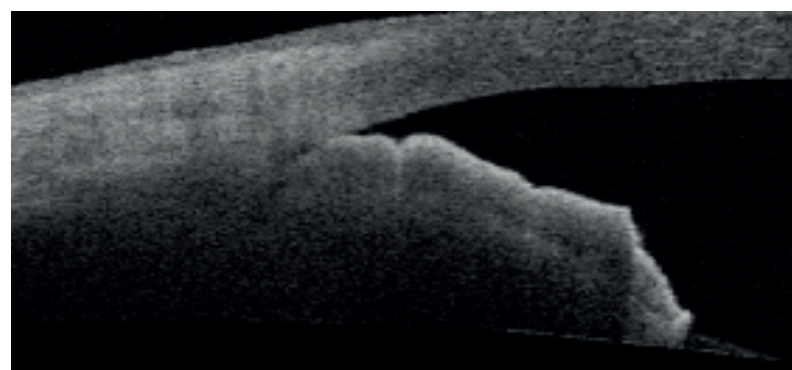


Figure 19:

OCT image of a narrow iridocorneal angle related to pupillary block.

Plateau iris mechanism

Plateau iris mechanism is diagnosed in the presence of anteriorly positioned ciliary processes that close the anterior chamber recess, inducing anterior displacement of the root of the iris and thereby blocking the iridocorneal angle. Plateau iris is defined as persistence of this mechanism in the presence of patent iridotony, which relieves the frequently associated pupillary block.

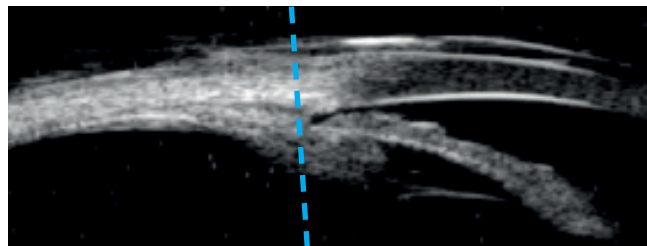


Figure 20:

UBM image of a closed iridocorneal angle related to a plateau iris mechanism. Anterior rotation of the ciliary processes displaces the root of the iris anteriorly, causing iridocorneal angle closure. Ciliary processes are situated anteriorly to a line perpendicular to the sclera passing through the scleral spur.

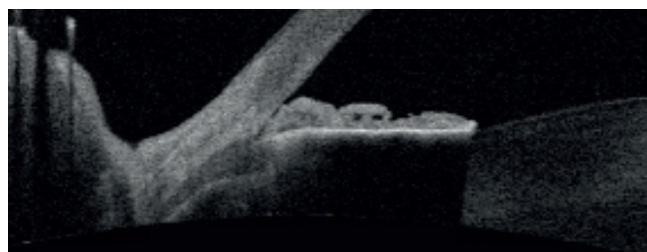


Figure 21:

OCT image of a closed iridocorneal angle related to a plateau iris mechanism. The iris forms an angle in the periphery then becomes flattened in the centre. The root of the iris is in contact with the trabecular meshwork. The ciliary processes are not clearly visible, but this image suggests their anterior displacement.

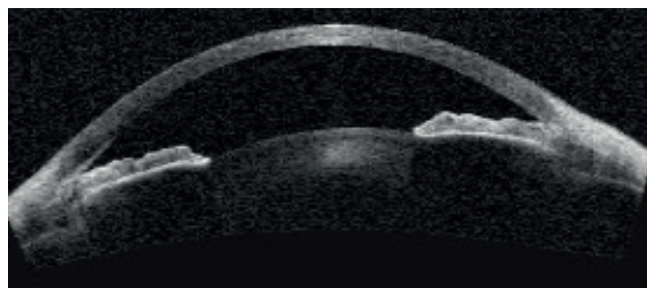


Figure 22:

OCT image of a deep anterior chamber associated with a closed iridocorneal angle related to a plateau iris mechanism, showing bilateral iridotrabecular apposition with the root of the iris in contact with the trabecular meshwork. The iris forms an angle in the periphery, then becomes flatter in the centre.

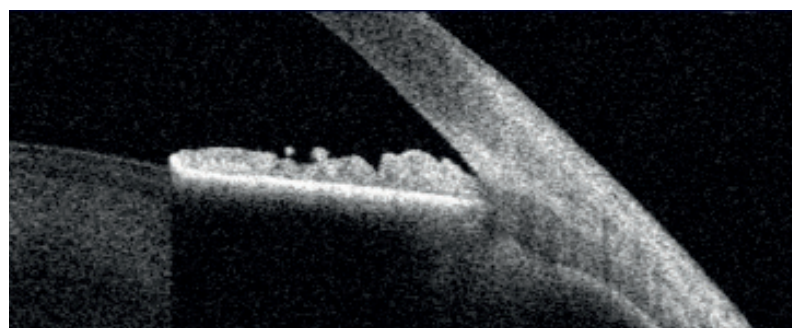


Figure 23:

OCT image of a closed iridocorneal angle related to a plateau iris mechanism with no associated pupillary block. The iris forms an angle in the periphery, then becomes flatter in the centre. The root of the iris is in contact with the trabecular meshwork. Ciliary processes are not clearly visible, but this image suggests their anterior displacement. An iridotomy may be ineffective.

Plateau iris mechanism

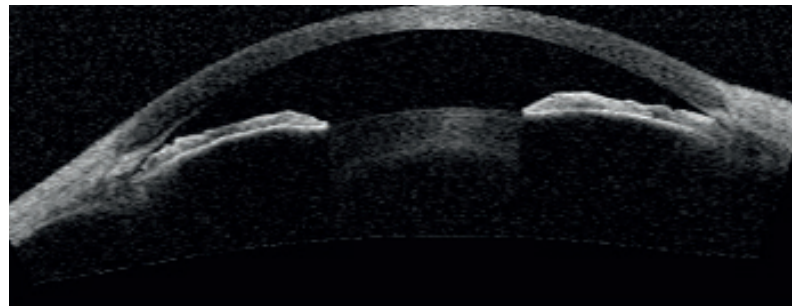


Figure 24:

OCT image of a closed iridocorneal angle related to a plateau iris mechanism associated with a pupillary block mechanism on a large lens.

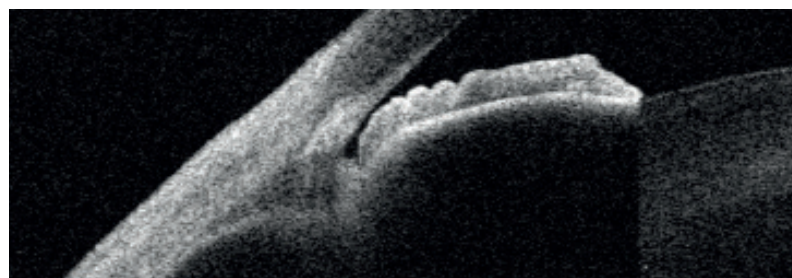


Figure 25:

OCT image of a closed iridocorneal angle related to a plateau iris mechanism probably associated with pupillary block.

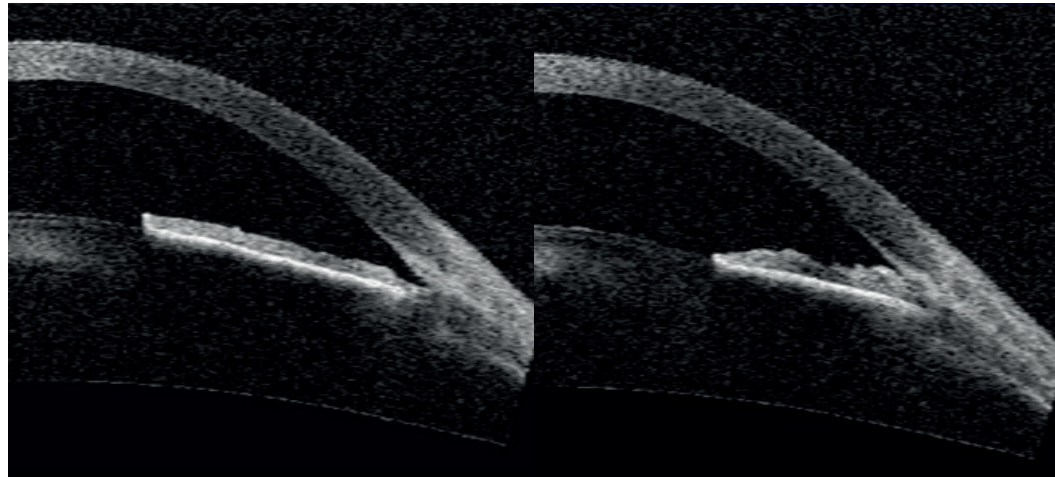


Figure 26:

OCT image of a closed iridocorneal angle related to a plateau iris mechanism. Dynamic analysis shows complete angle closure with iridotrabecular apposition during dilatation. Left: image under photopic conditions. Right: image under scotopic conditions.

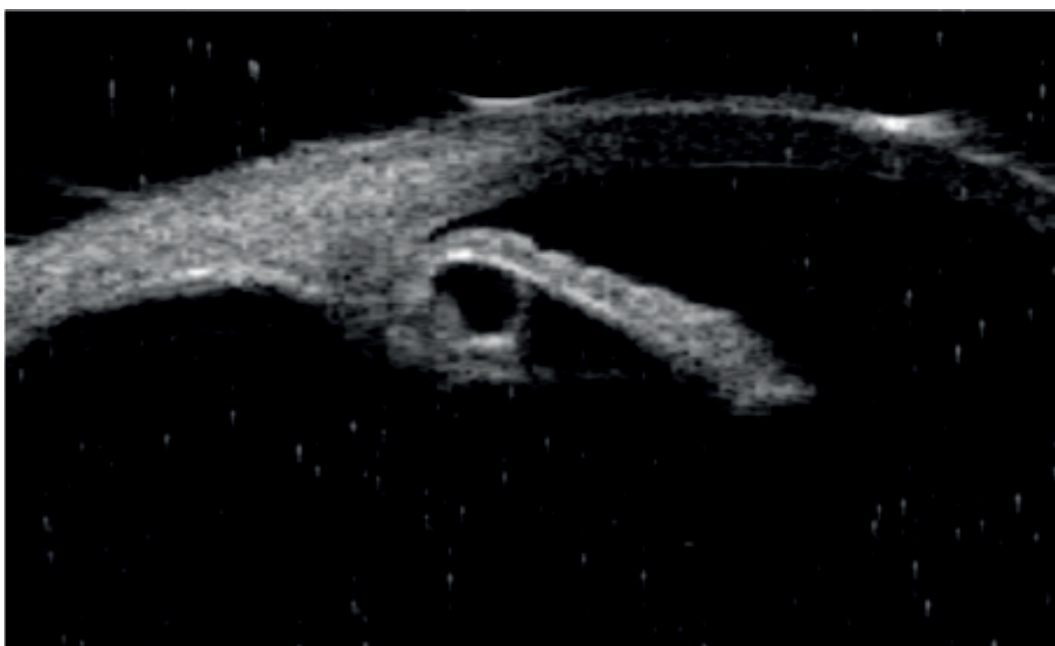


Figure 27:

UBM image of a closed iridocorneal angle related to iridociliary cysts giving a pseudo-plateau iris appearance.

Lens mechanisms

Age-related enlargement of the lens or more anterior positioning of the lens can increase pupillary block or even induce complete closure of the iridocorneal angle. Cataract surgery could be considered in this case. Peripheral iridotomy could constitute an interim solution when the lens is perfectly clear or when the patient prefers to avoid cataract surgery. In these cases of narrow angle, in which cataract surgery is considered, it is important to identify plateau iris syndrome, which constitutes a risk factor for malignant glaucoma.

Other lens abnormalities can also induce secondary iridocorneal angle closure, such as microspherophakia or spontaneous subluxation due to zonular laxity or traumatic subluxation.

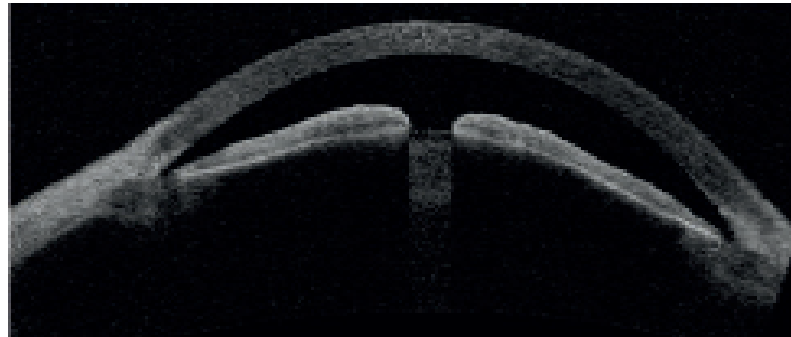


Figure 28:

OCT image of an open iridocorneal angle, but with a very shallow anterior chamber related to a lens mechanism. There is a risk of angle closure in the case of mydriasis.



Figure 29:

OCT image of a narrow iridocorneal angle with iridotrabecular apposition related to a lens mechanism. There is a very high risk of angle closure in the case of mydriasis.

Lens mechanisms

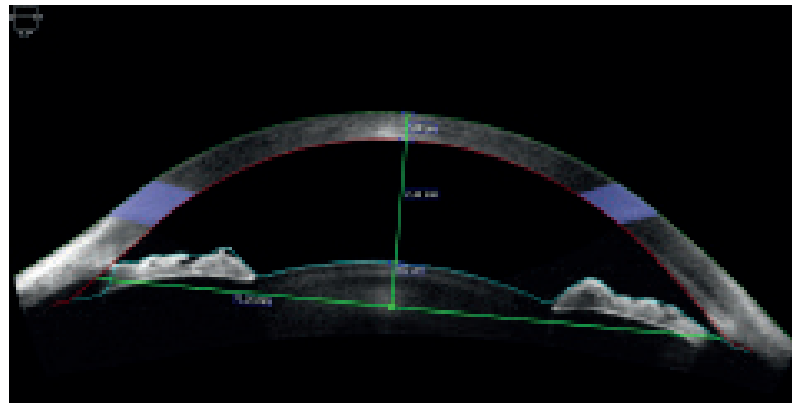


Figure 30:

OCT image of a partially closed iridocorneal angle with iridotrabecular apposition related to a lens mechanism.

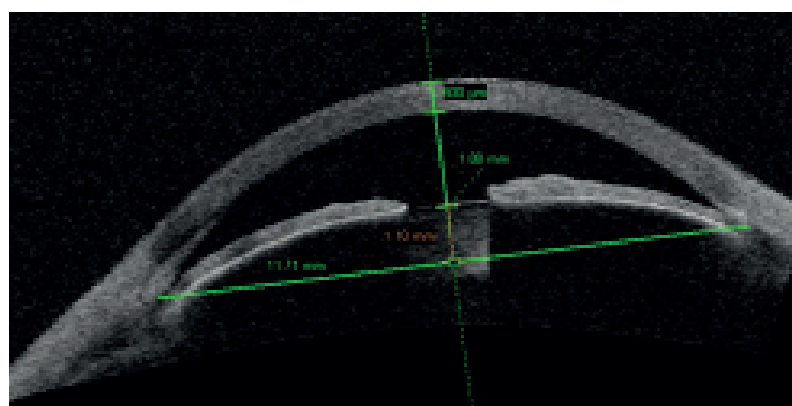


Figure 31:

OCT image of a closed iridocorneal angle with iridotrabecular apposition related to a lens mechanism. Measurement of the lens vault provides quantitative evaluation of the role played by the lens in angle closure (1100 microns). The lens is considered to be associated with a high risk of iridocorneal angle closure for values higher than 600 to 900 microns.

Malignant glaucoma

Malignant glaucoma is defined as closure of the anterior chamber accompanied by an elevated IOP in the presence of a visible iridotomy and in the absence of clinically detectable choroidal detachment. Malignant glaucoma is rarely a primary disease and is commonly observed after filtering surgery, especially in the presence of a narrow iridocorneal angle. Ciliary block associated with misdirection of aqueous humor towards the vitreous constitutes the main mechanism involved in the pathogenesis of malignant glaucoma. The lens or intraocular implant is then pushed anteriorly, reducing the depth of the anterior chamber and closing the iridocorneal angle.

The risk of malignant glaucoma must be considered before any surgery on plateau iris syndrome and malignant glaucoma should be suspected after cataract surgery in the case of unexplained postoperative myopia, as the iris-capsular bag-implant is pushed anteriorly in the case of malignant glaucoma, inducing myopia.

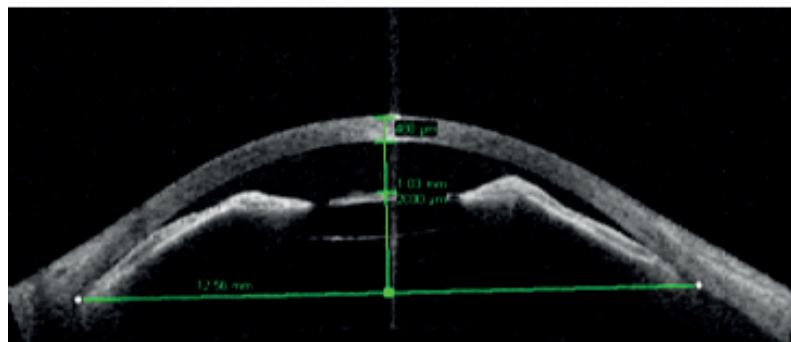


Figure 32:

OCT image of a closed iridocorneal angle with a shallow anterior chamber and anterior displacement of the iris and ciliary body in the case of malignant glaucoma. An implant is also visible in the posterior chamber.

Ciliochoroidal effusion

Ciliochoroidal effusion can occur in the context of various diseases, such as nanophthalmos, inflammatory diseases, retinal detachment surgery, central retinal vein occlusion, glaucoma surgery or with certain medications. It consists of oedema of the ciliary body inducing anterior rotation of the ciliary processes, causing iridocorneal angle closure. A suprachoroidal effusion or peripheral choroidal or retinal detachment can also induce anterior displacement of the iris and ciliary body and iridocorneal angle closure.

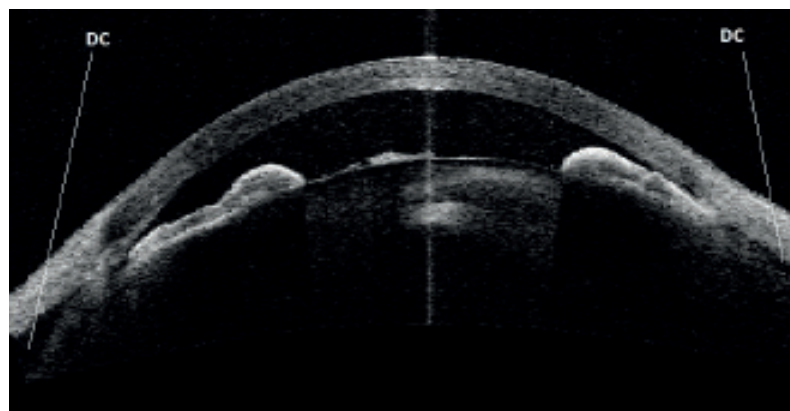


Figure 33:

OCT image of a closed iridocorneal angle with a shallow anterior chamber and anterior displacement of the iris and ciliary body associated with a peripheral choroidal detachment (DC) and ciliary body oedema.

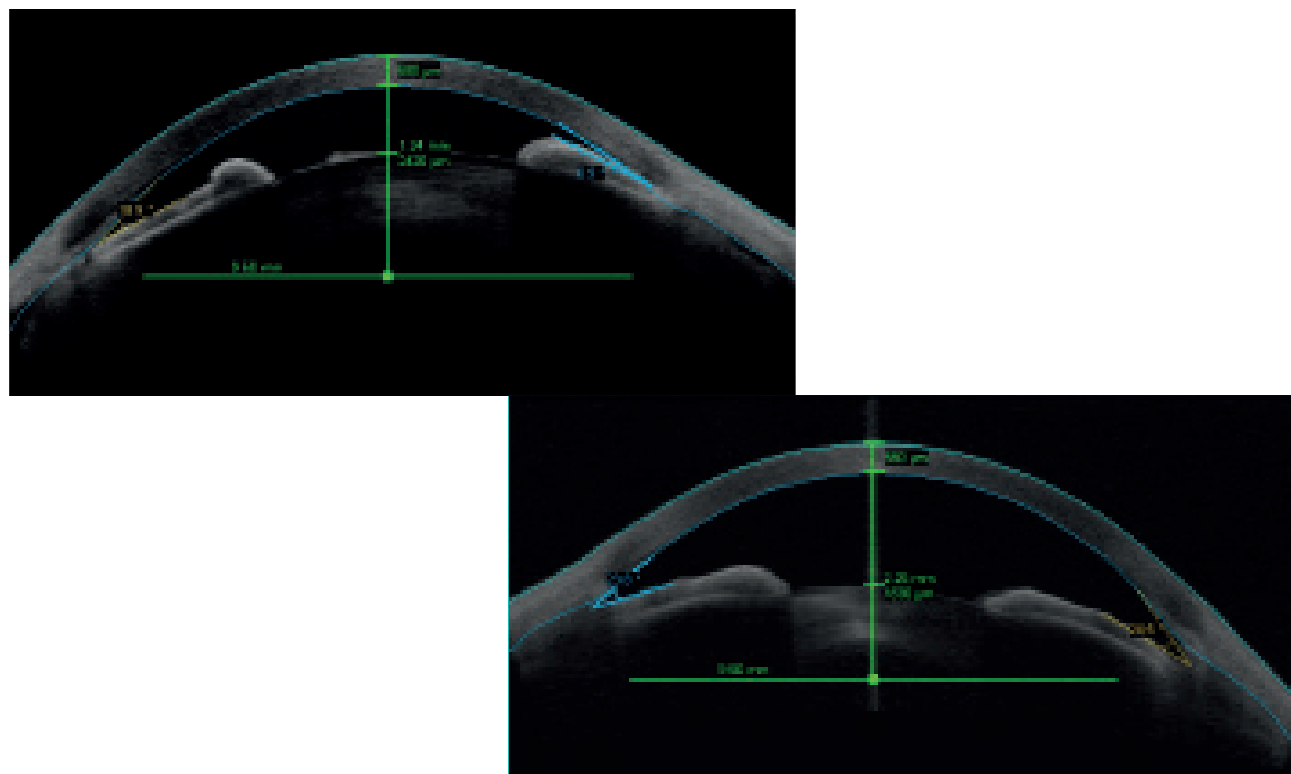


Figure 34:

Uveal effusion syndrome with anterior displacement of the iris and ciliary body and angle closure induced by an antiepileptic, topiramate. Top: during treatment. Bottom: spontaneous resolution after stopping treatment.

Other forms of secondary iridocorneal angle closure

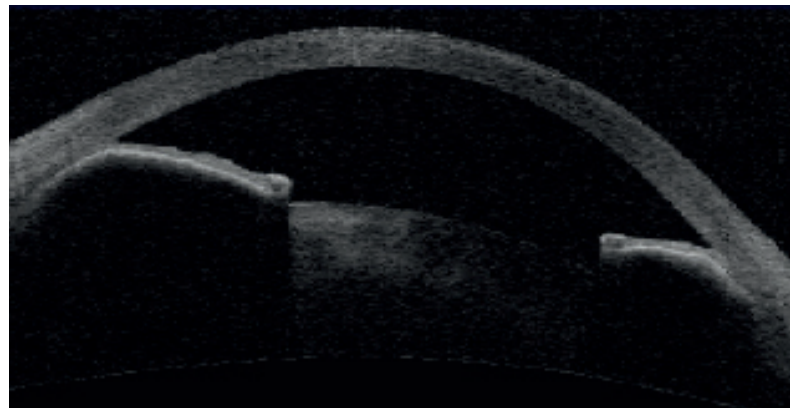


Figure 35:

Bilateral peripheral anterior synechiae inducing anterior attraction of the iris in the context of stage IV neovascular glaucoma.



Figure 36:

Neovascular glaucoma: smooth appearance of the iris and inflammatory membrane over the lens. The iridocorneal angle is not closed, but the intraocular pressure is elevated due to obstruction of the trabecular meshwork by the fibrovascular membrane.





Figure 37:

Examples of neovascular glaucoma with angle closure.



Figure 38:

Examples of neovascular glaucoma with angle closure and total iris retraction.

Other forms of secondary iridocorneal angle closure

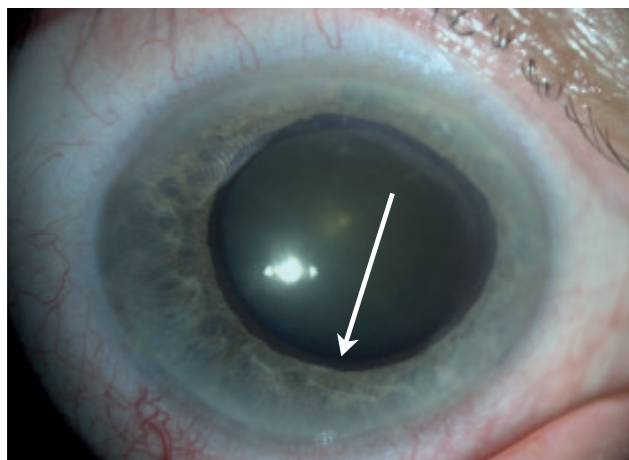
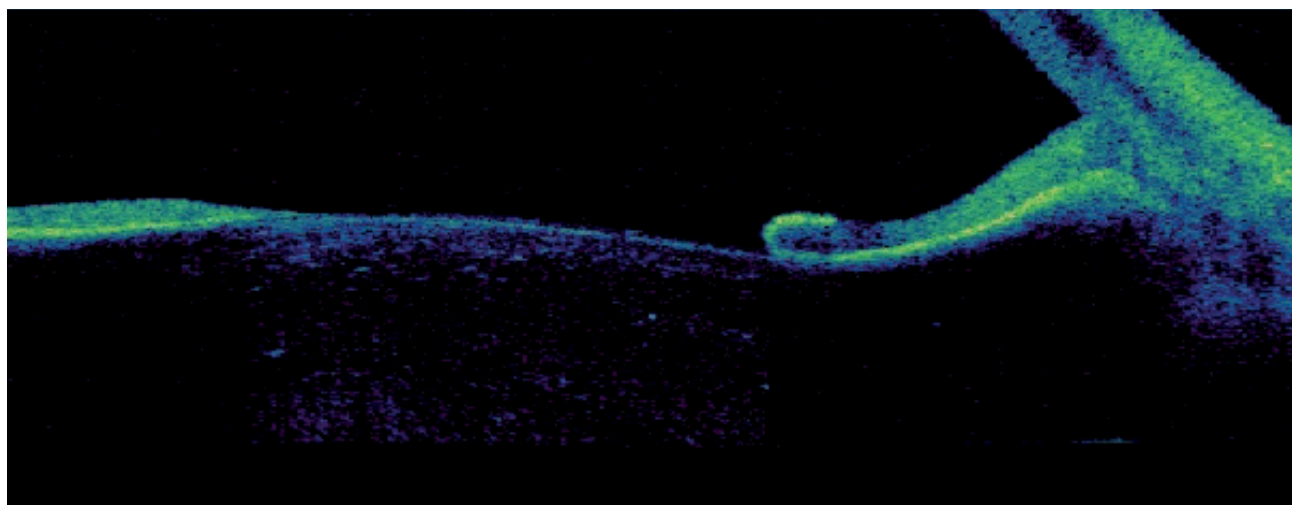


Figure 39:

Neovascular glaucoma with angle closure and uveal ectropion.





3. Analysis of the mechanisms of other forms of secondary glaucoma

Analysis of the mechanisms of other forms of secondary glaucoma

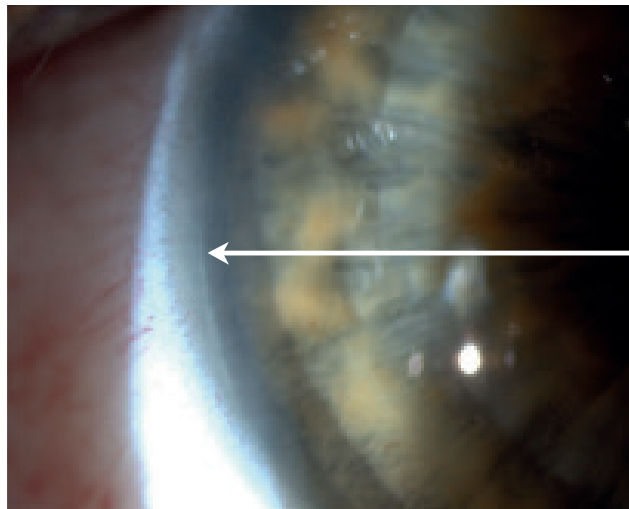


Figure 40:
OCT image of the iridocorneal angle with a posterior embryotoxon.

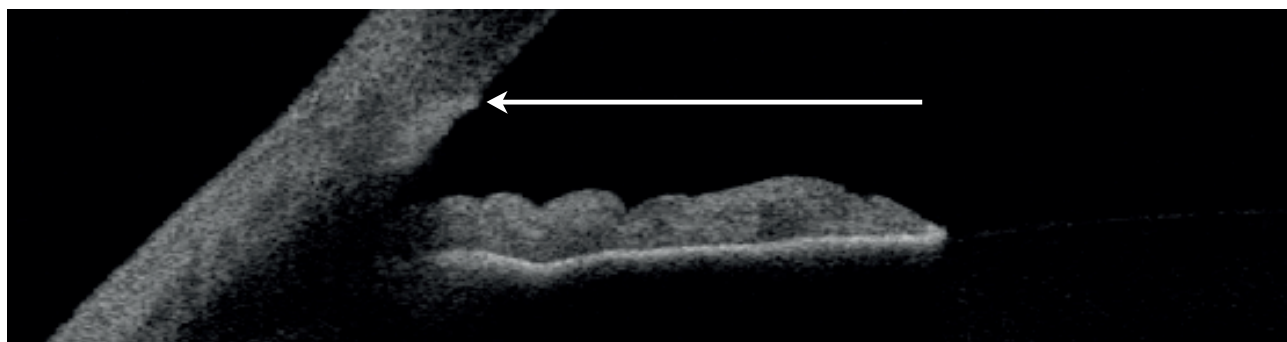
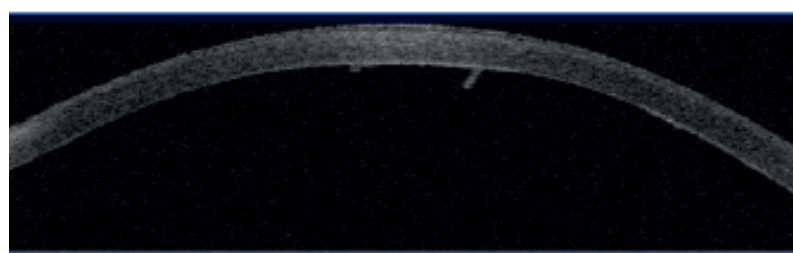
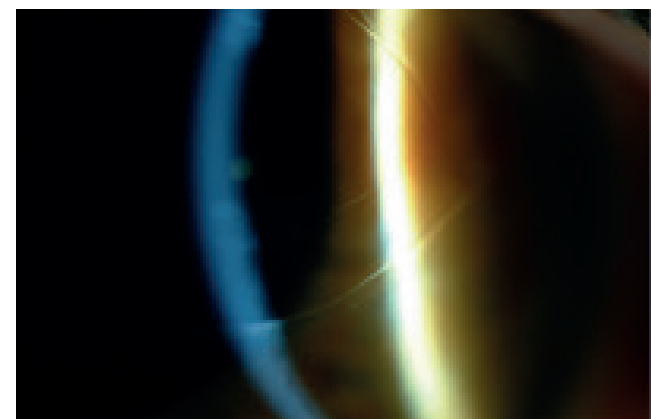
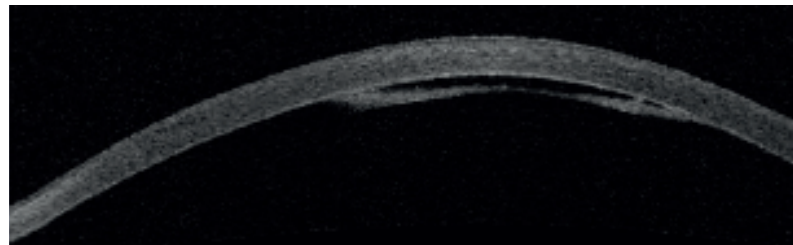


Figure 41:

Haab's striae in a case of congenital glaucoma.



Analysis of the mechanisms of other forms of secondary glaucoma



Figure 42:

UBM image of a very deep anterior chamber associated with posterior concavity of the iris and iridozonular contact in a case of pigment dispersion syndrome.

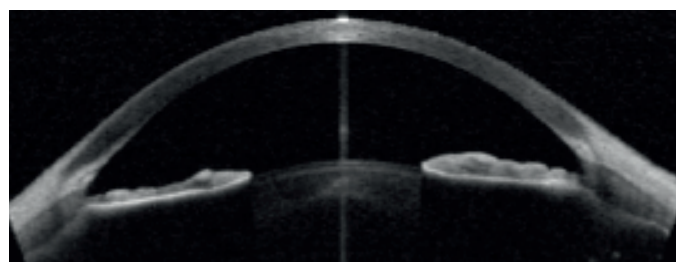
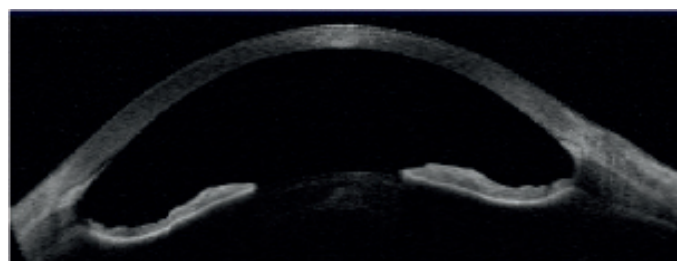


Figure 43:

OCT image of a very deep anterior chamber associated with posterior concavity of the iris and iridolens and probably iridozonular contact in a case of pigment dispersion syndrome. Top: before iridotomy. Bottom: after iridotomy, disappearance of the reverse pupillary block. Note the high reflectivity of the trabecular meshwork, which may correspond to its hyperpigmentation.

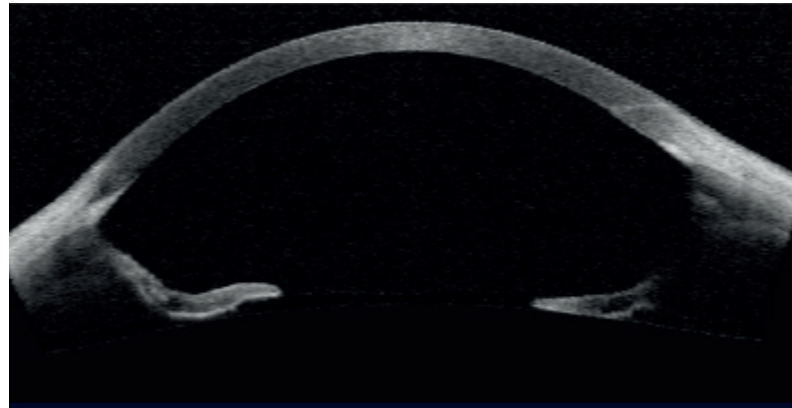


Figure 44:

Image of reverse pupillary block after cataract surgery with an increased pressure gradient between the anterior and posterior chambers of the eye, inducing a posterior concavity of the iris associated with contact between the posterior surface of the iris and the posterior chamber implant. The anterior chamber is particularly deep in this case.

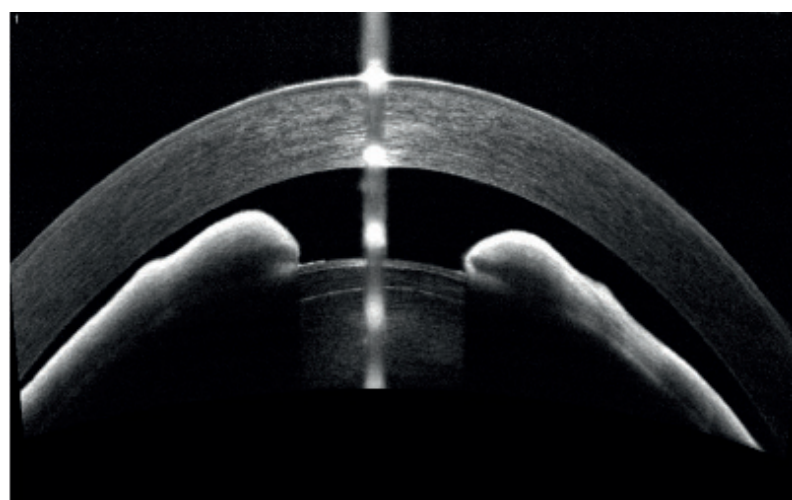


Figure 45:

Image of microphthalmia.



4. Follow-up of surgery and laser surgery

4.1. Follow-up of surgery and laser surgery

4.2. Follow-up of trabeculectomy

Follow-up of surgery and laser surgery

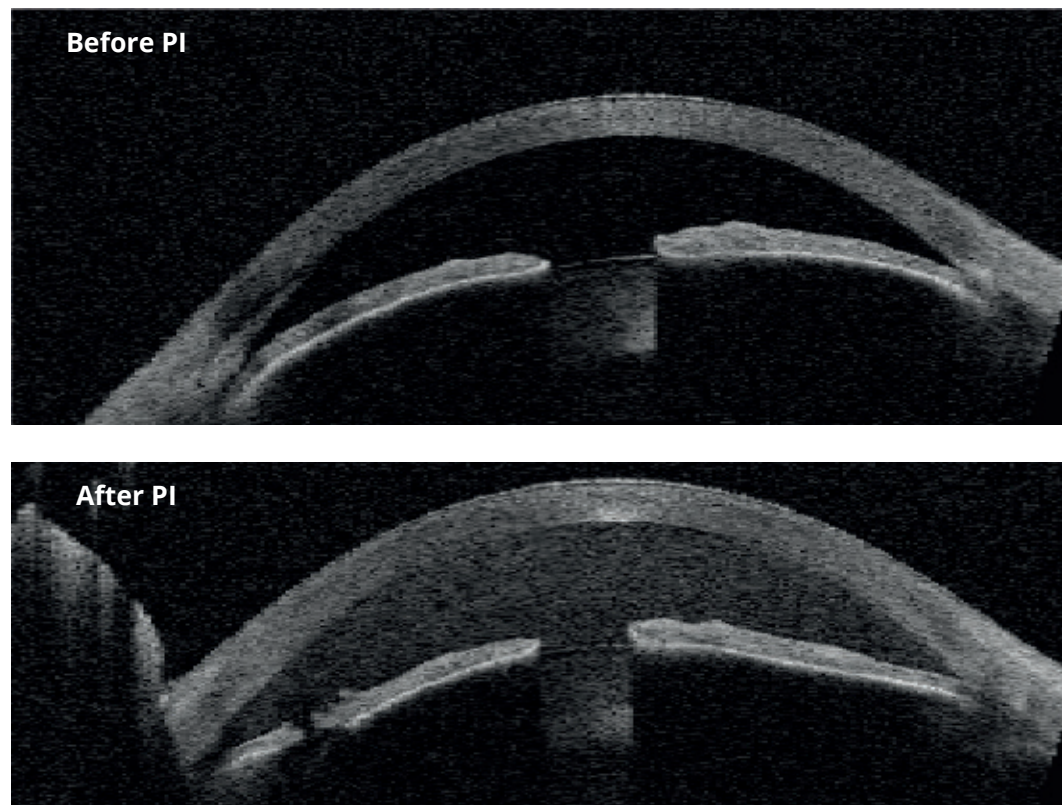


Figure 46:

OCT image showing the anatomical changes induced immediately after peripheral iridotomy.

The deeper anterior chamber is associated with reopening of the iridocorneal angle. Iridotomy is transfixing. The anterior chamber still contains pigment.

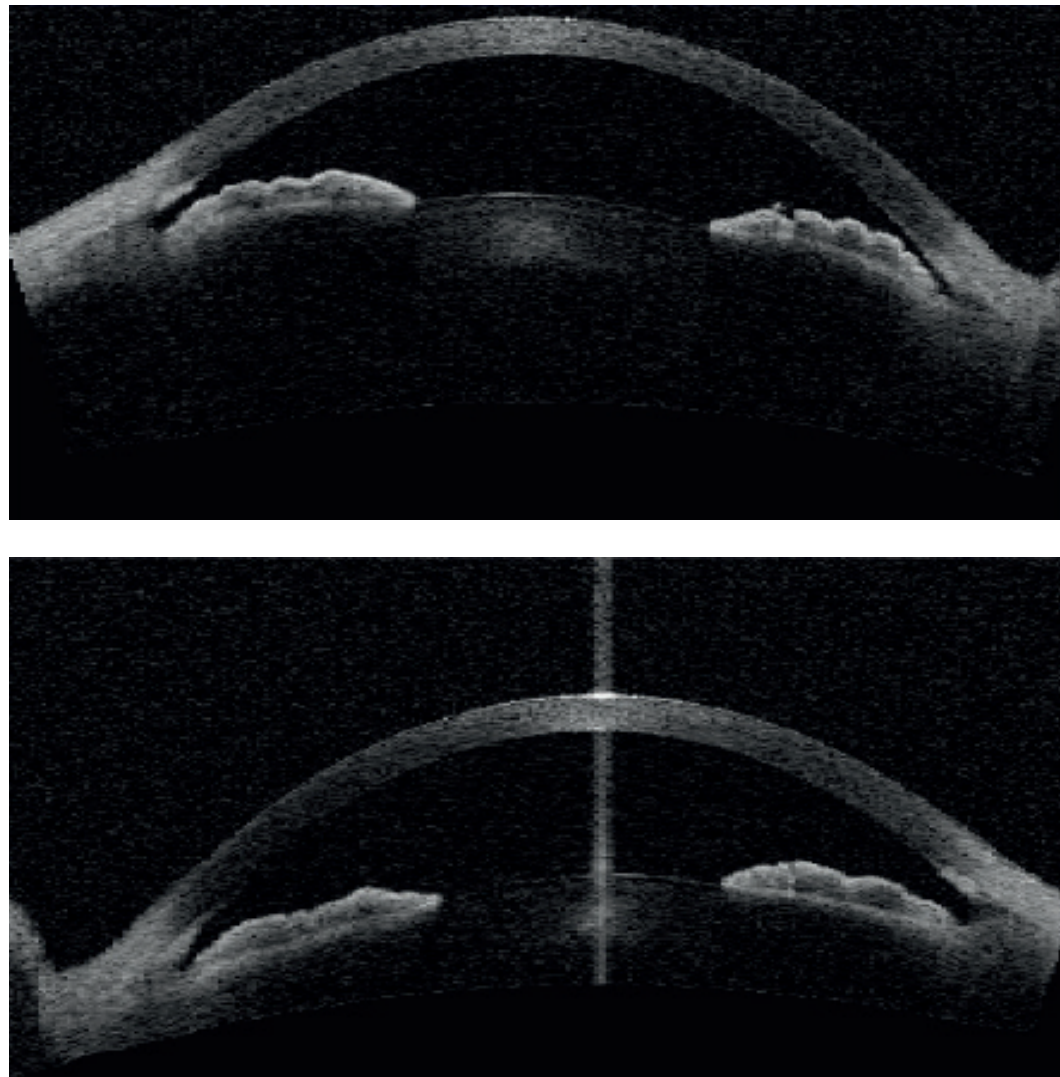


Figure 47:

OCT image showing the long-term anatomical changes induced by laser peripheral iridotomy. The deeper anterior chamber is associated with reopening of the iridocorneal angle.

Follow-up of surgery and laser surgery

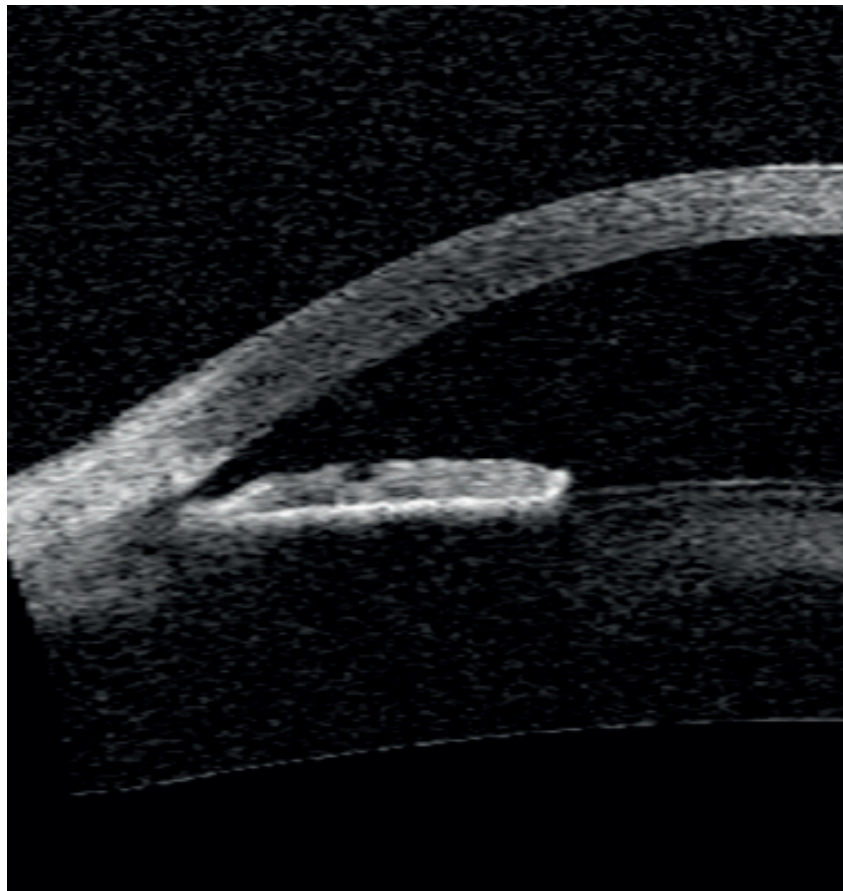
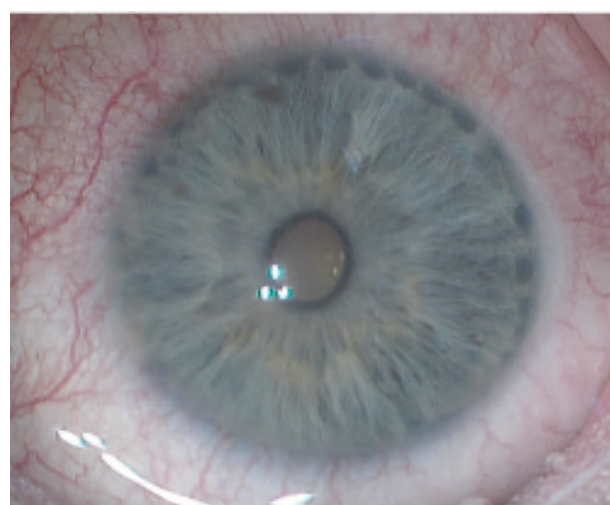


Figure 48:

OCT image showing the anatomical changes induced by iridoplasty in a case of plateau iris syndrome. Thinning of the root of the iris is associated with iris hyperreflectivity related to the laser scar. The iridocorneal angle is open.



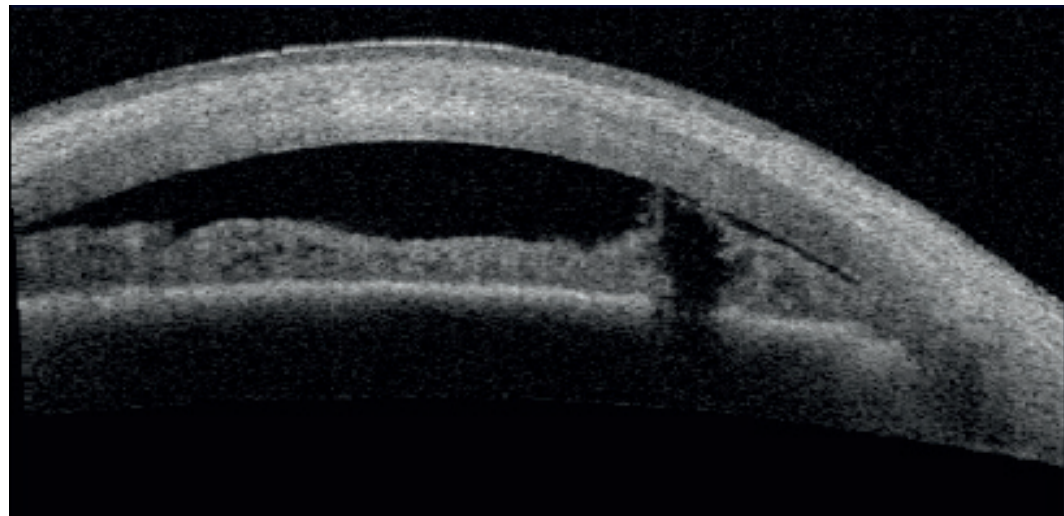


Figure 49:

OCT image of the peripheral iris showing a partially transfixing iridotomy.

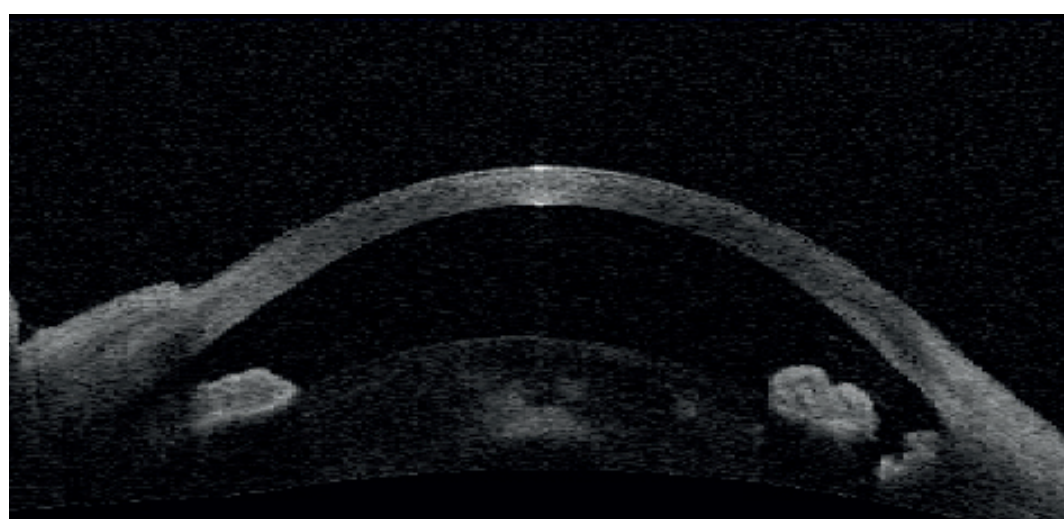


Figure 50:

OCT image showing a completely transfixing iridotomy.

Follow-up of filtering surgery

Trabeculectomy and non-penetrating deep sclerectomy (NPDS) are associated with the formation of a filtering bleb related to the postoperative tissue healing process. UBM and anterior segment OCT allow evaluation of the internal morphology of the filtering bleb. Anterior segment imaging improves our understanding of the mechanisms of filtration and their failure, and is useful for postoperative follow-up, which remains a major element in the prognosis of this surgery.

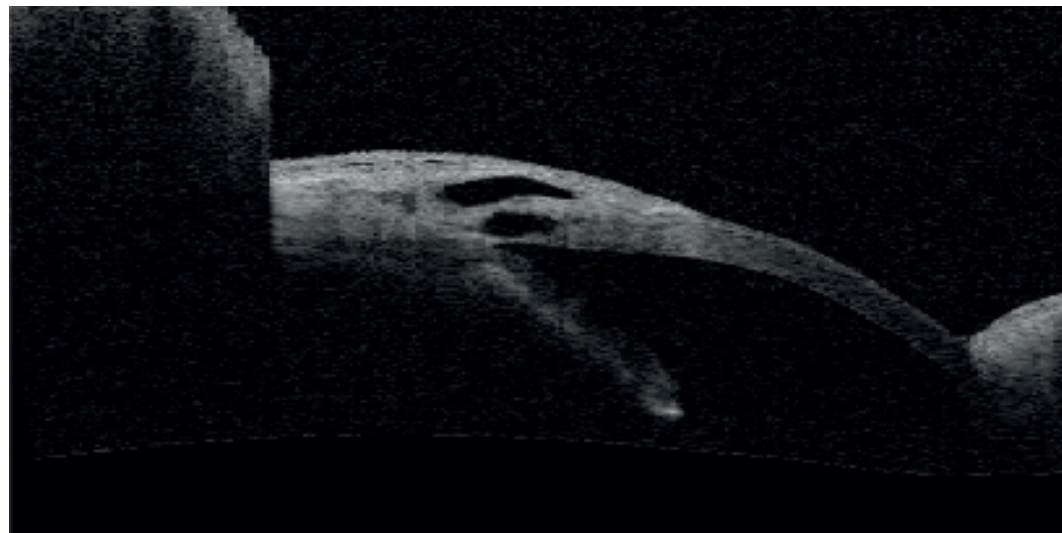


Figure 51:

OCT image of the non-penetrating deep sclerectomy operative site showing the various anatomical planes: residual trabeculo-Descemet's membrane, which separates the anterior chamber and the decompression chamber, the scleral flap and the conjunctival bleb.

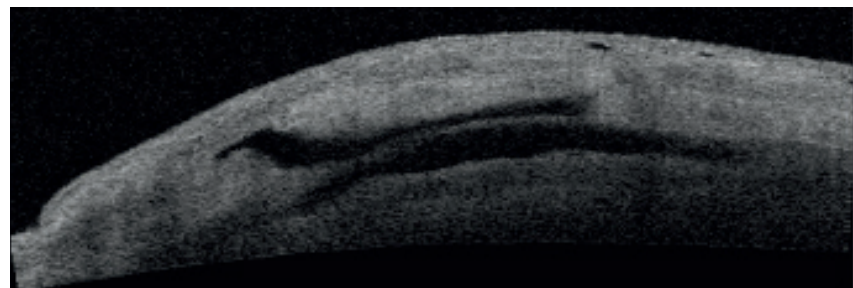
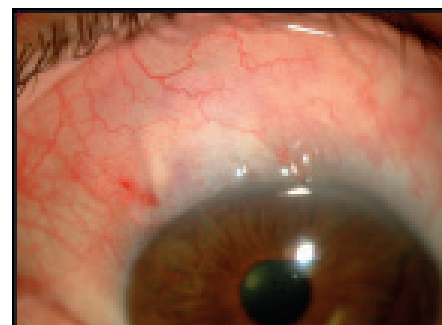
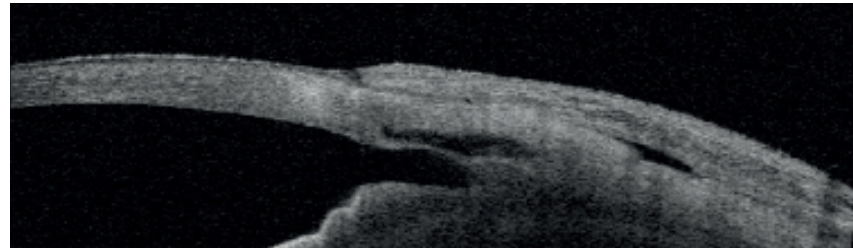


Figure 52:

OCT image of a functioning filtering bleb after non-penetrating deep sclerectomy. Note the presence of a hyporeflective space underneath the scleral flap corresponding to a decompression space. The conjunctiva is heterogeneous, comprising visible microcysts and reflecting effective filtration. Top: perpendicular to the limbus. Bottom: parallel to the limbus.

Follow-up of filtering surgery

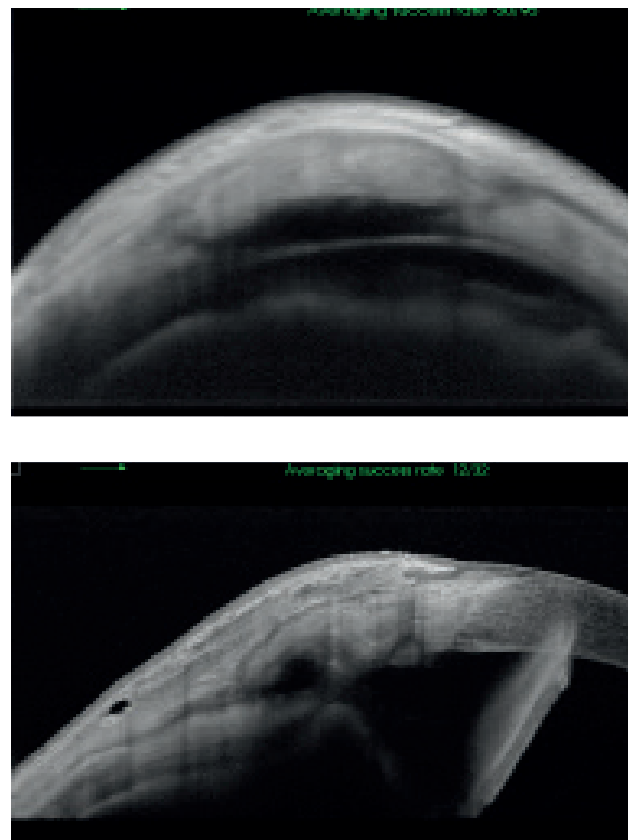


Figure 53:
Similar images on Swept-Source OCT.

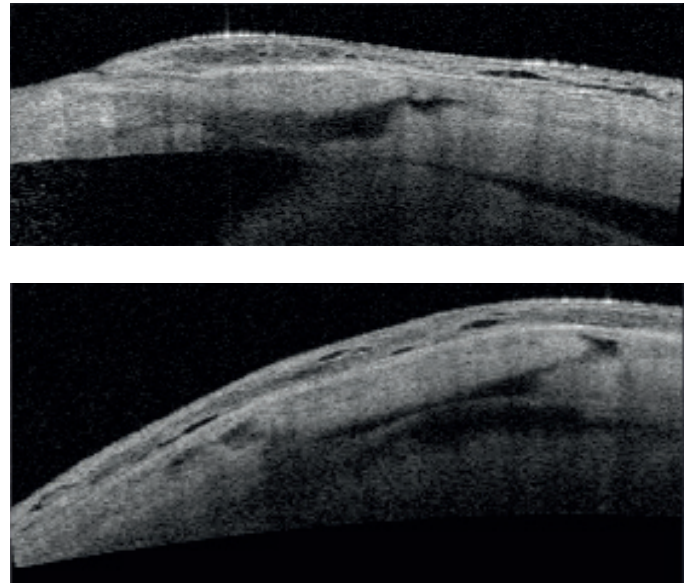


Figure 54:

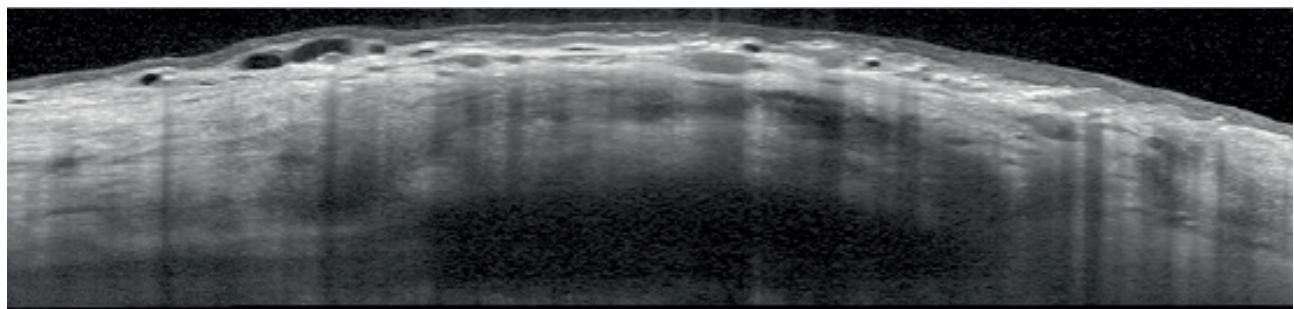
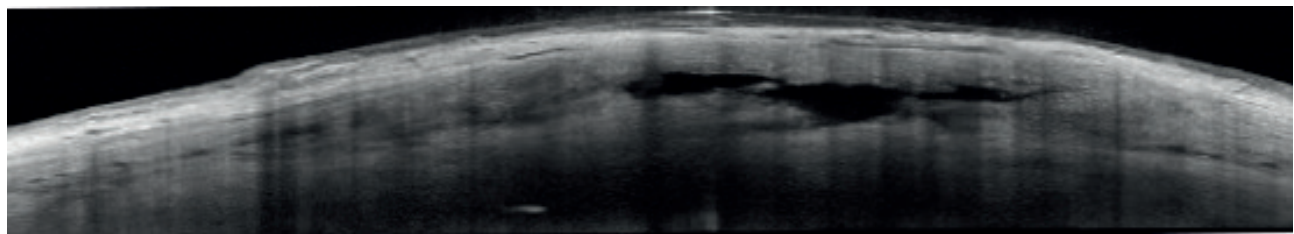
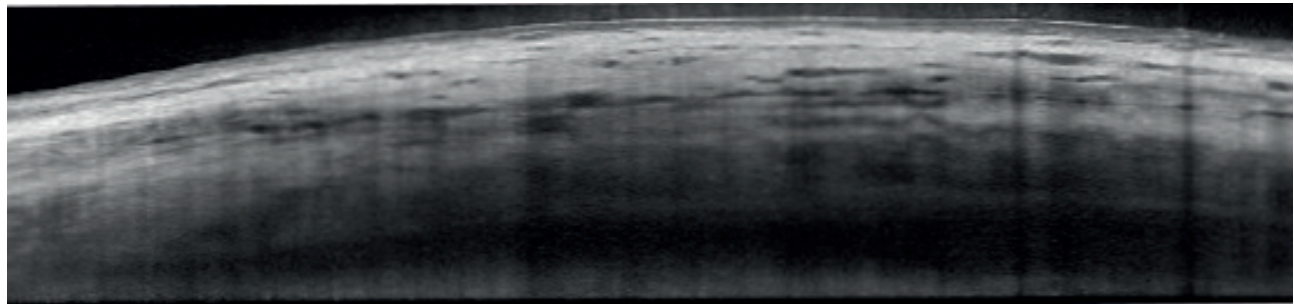
OCT image of a functioning filtering bleb after non-penetrating deep sclerectomy. Note the presence of a hyporeflective space underneath the scleral flap corresponding to a decompression space. The conjunctiva is heterogeneous with visible microcysts reflecting good filtration. Top: perpendicular to the limbus. Bottom: parallel to the limbus.

Follow-up of filtering surgery



Figure 55:

Spectral-Domain OCT image of a functioning filtering bleb after non-penetrating deep sclerectomy. Note the presence of numerous hyporeflective spaces in the conjunctiva reflecting the passage of aqueous humor.



Follow-up of filtering surgery

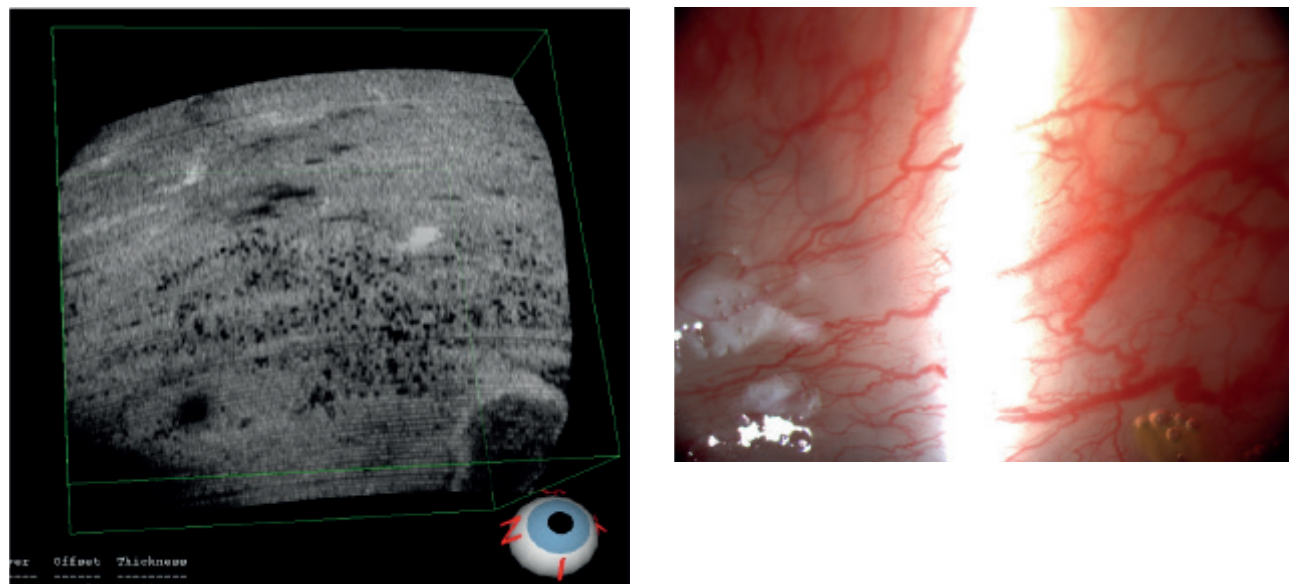


Figure 56:

Clinical images and *en face* Spectral-Domain OCT images showing microcysts on the surface of a functioning filtering bleb. The presence of microcysts is a sign of transconjunctival passage of aqueous humor.

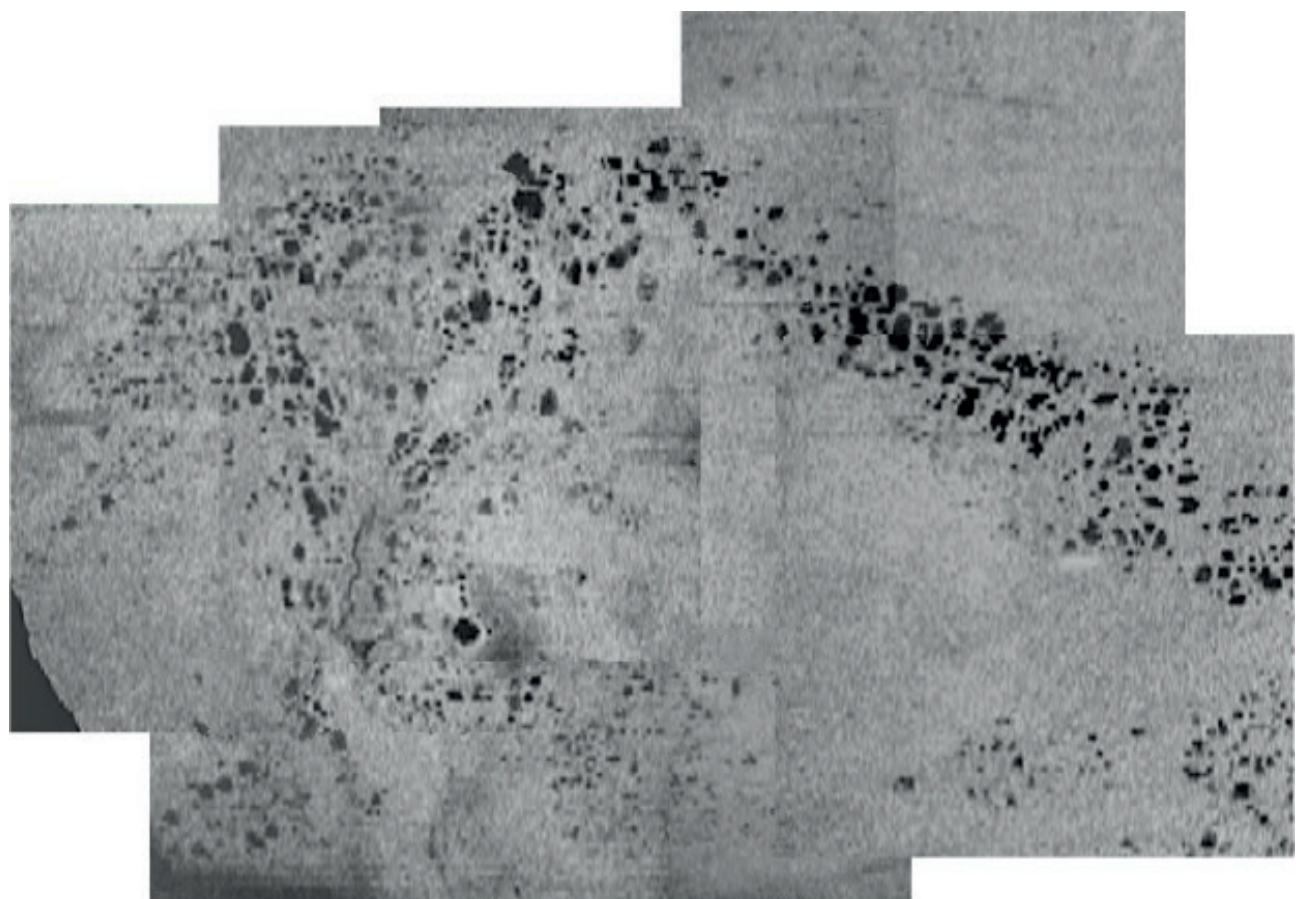


Figure 57:

Assembly of *en face* OCT images showing microcysts on a functioning filtering bleb.

Follow-up of filtering surgery

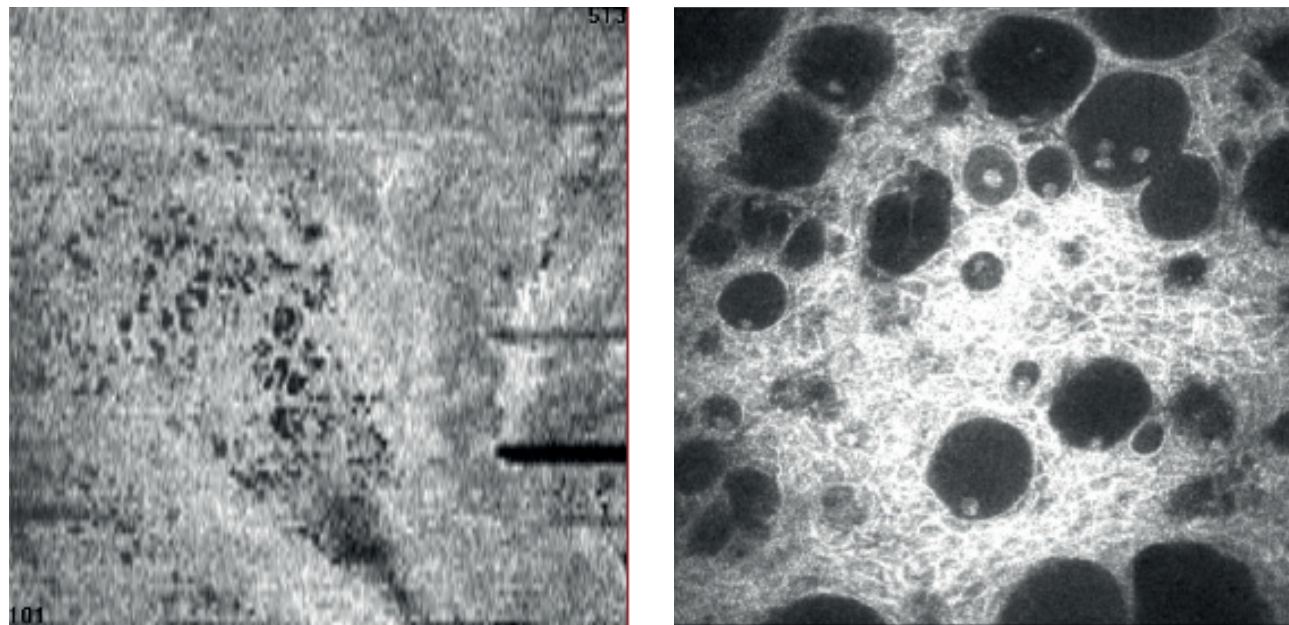


Figure 58:

En face OCT and confocal microscopy images of microcysts. The scales are different, as confocal microscopy provides images measuring 400×400 microns and visualizes highly magnified microcysts, while OCT demonstrates the distribution of these microcysts over a larger area.

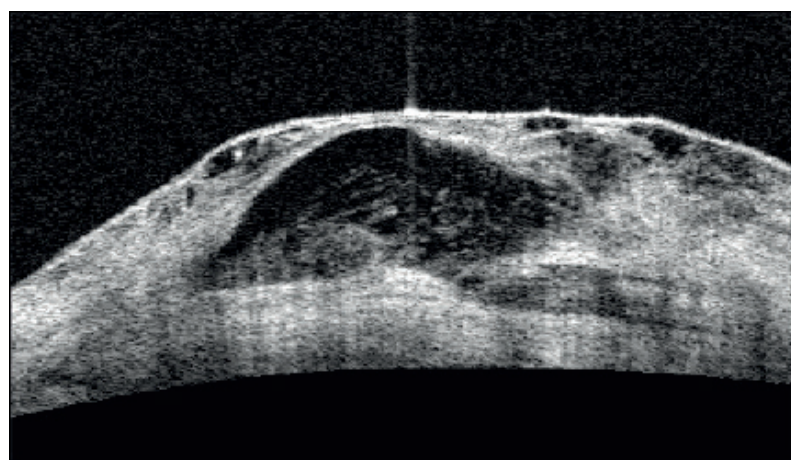
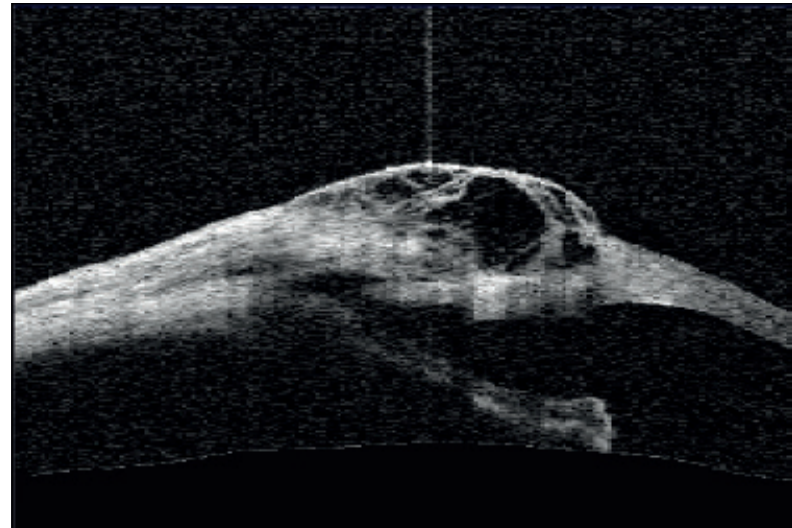


Figure 59:

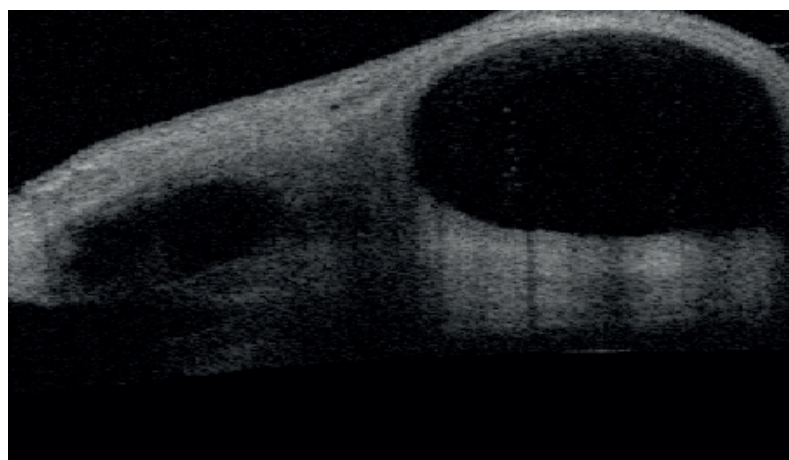
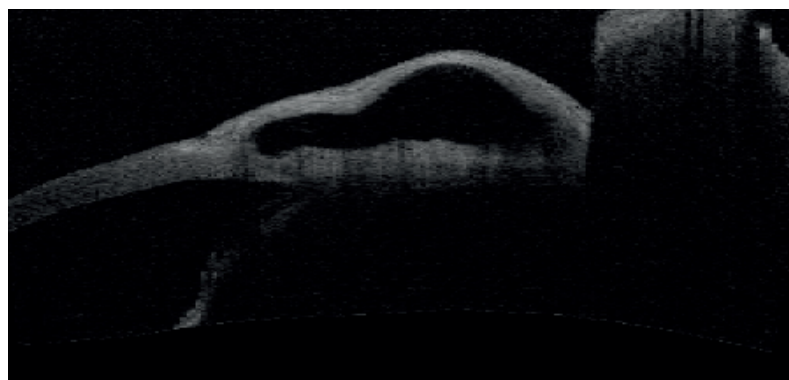
OCT images of a functioning but cystic thin-walled filtering bleb after trabeculectomy associated with the use of mitomycin. Note the thin wall and the multilobular appearance.

Follow-up of filtering surgery



Figure 60:

OCT image of a poorly functioning encapsulated filtering bleb. Note the dense, hyperreflective conjunctival thickening, corresponding to fibrosis that blocks filtration.



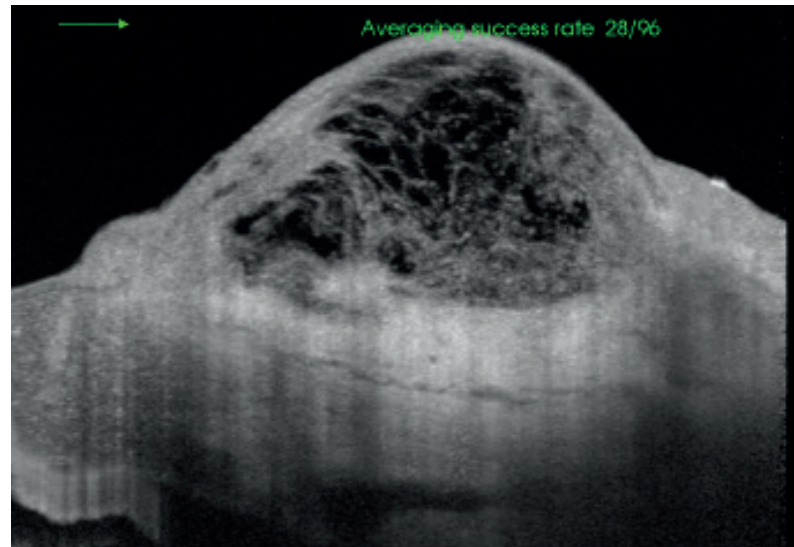


Figure 61:

Swept-Source OCT image of an overfiltering bleb (after mitomycin).

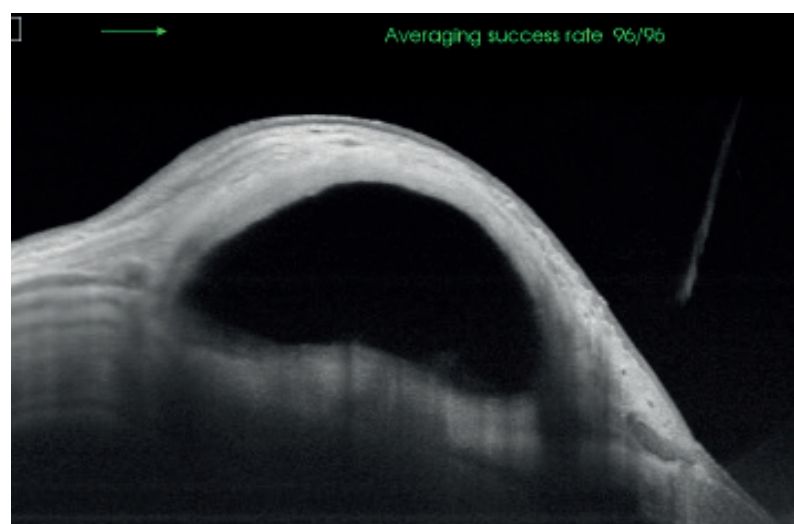


Figure 62:

Swept-Source OCT image of an encapsulated bleb.

Follow-up of filtering surgery

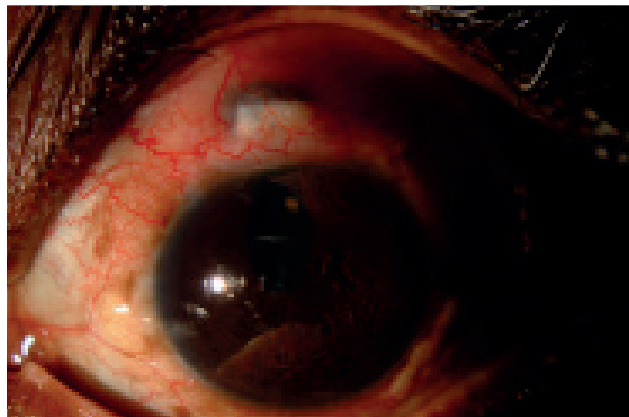


Figure 63:

Spectral-Domain OCT image of severe iris incarceration in the non-penetrating deep sclerectomy operative site. The iris corresponds to the most posterior hyperreflective tissue. The conjunctival tissue is homogeneous with no visible microcysts, reflecting the absence of aqueous humor filtration.

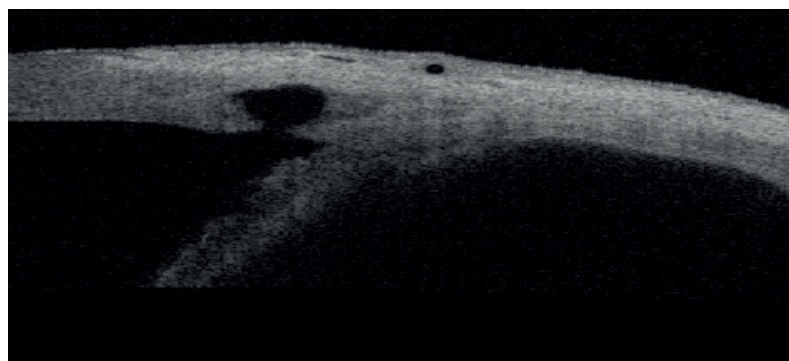
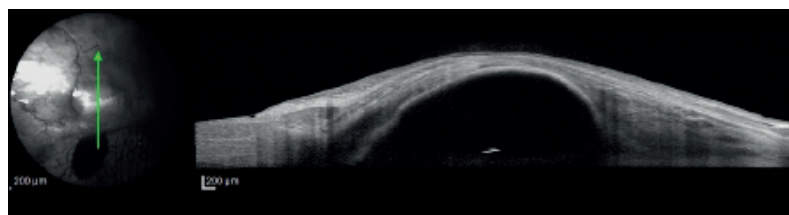


Figure 64:

OCT image of a flat fibrotic bleb despite goniopuncture after non-penetrating deep sclerectomy.

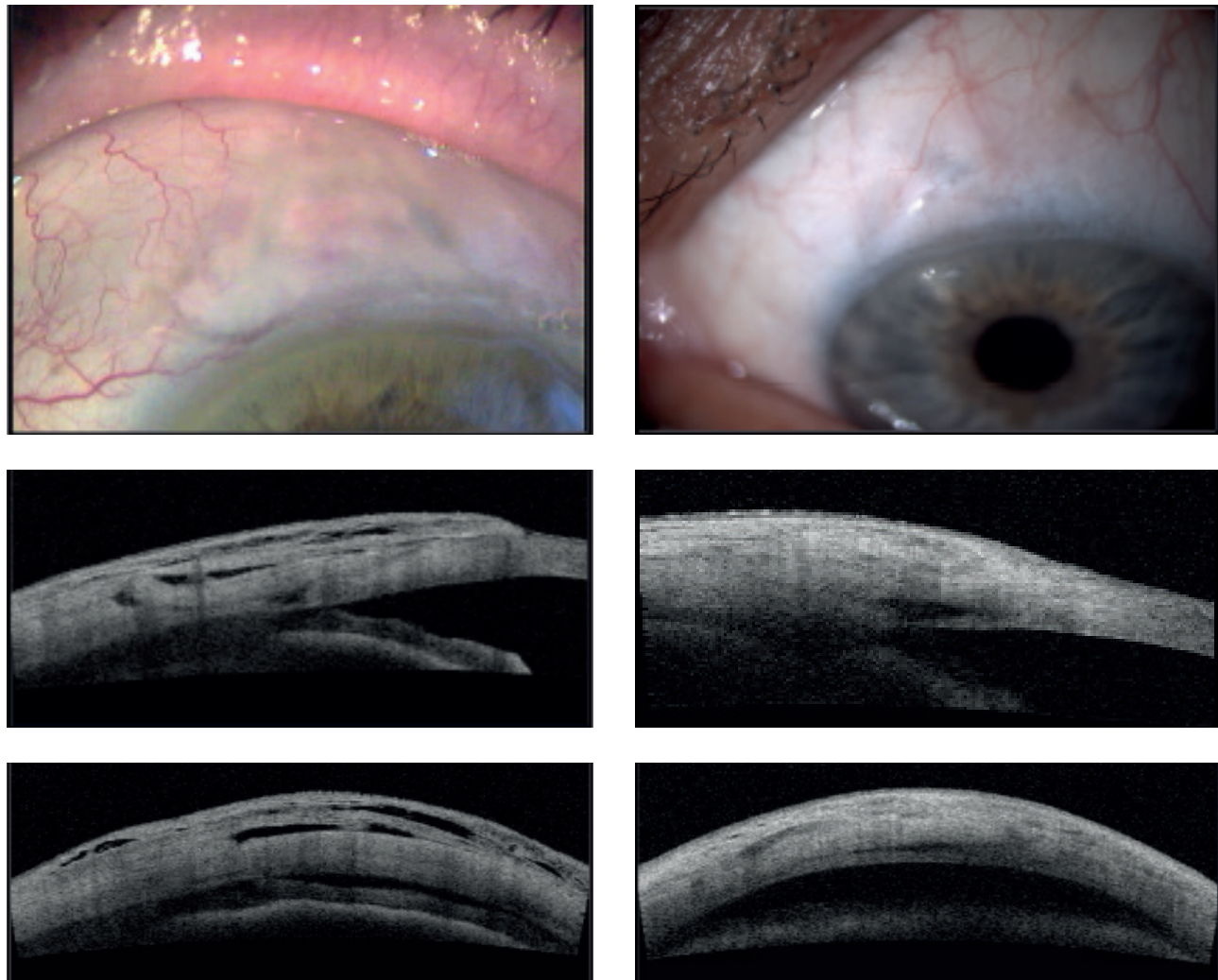


Figure 65:

OCT image of two flat filtering blebs. Left: the filtering bleb nevertheless presents signs of functioning with heterogeneous conjunctival tissue and passage of aqueous humor. Right: there are no signs of transconjunctival passage of aqueous humor.

Follow-up of filtering surgery

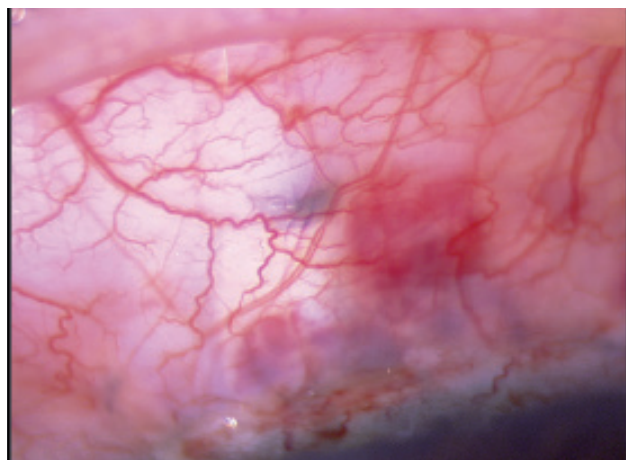
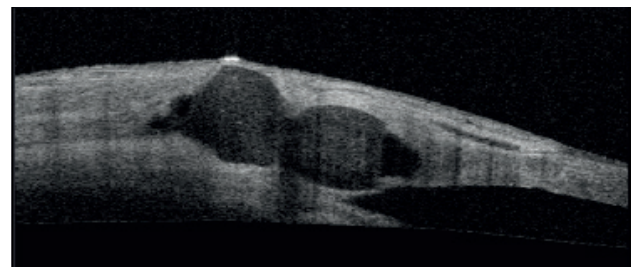
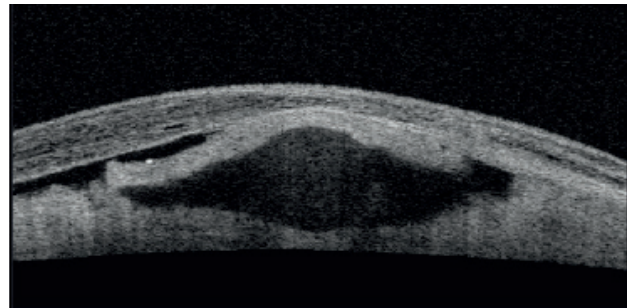


Figure 66:

OCT image of the non-penetrating deep sclerectomy (NPDS) decompression chamber after insertion of an Aquaflow® drain. This drain maintains the patency of the decompression chamber and is designed to promote filtration after NPDS.



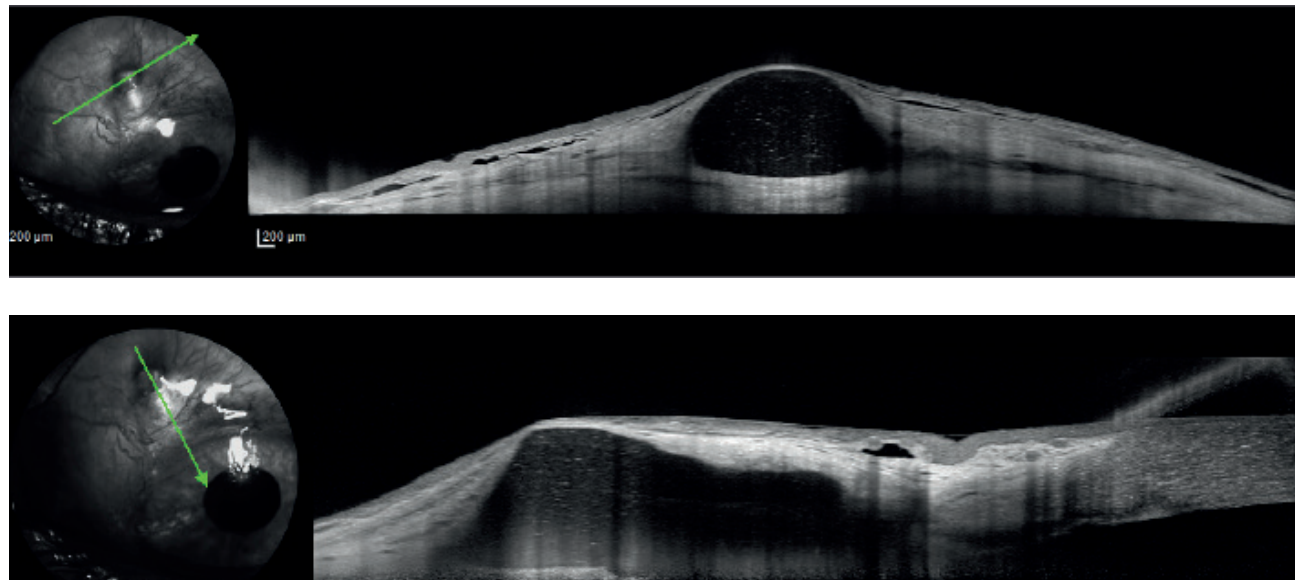


Figure 67:

Spectral-Domain OCT of the non-penetrating deep sclerectomy (NPDS) decompression chamber after insertion of an Aquaflow® drain.

Follow-up of filtering surgery

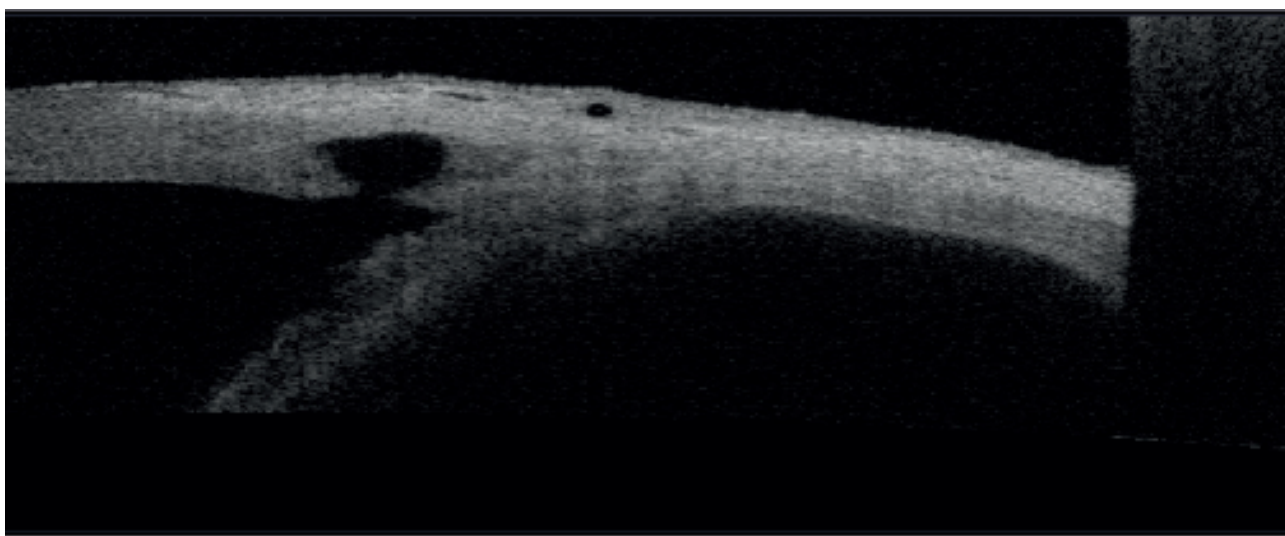
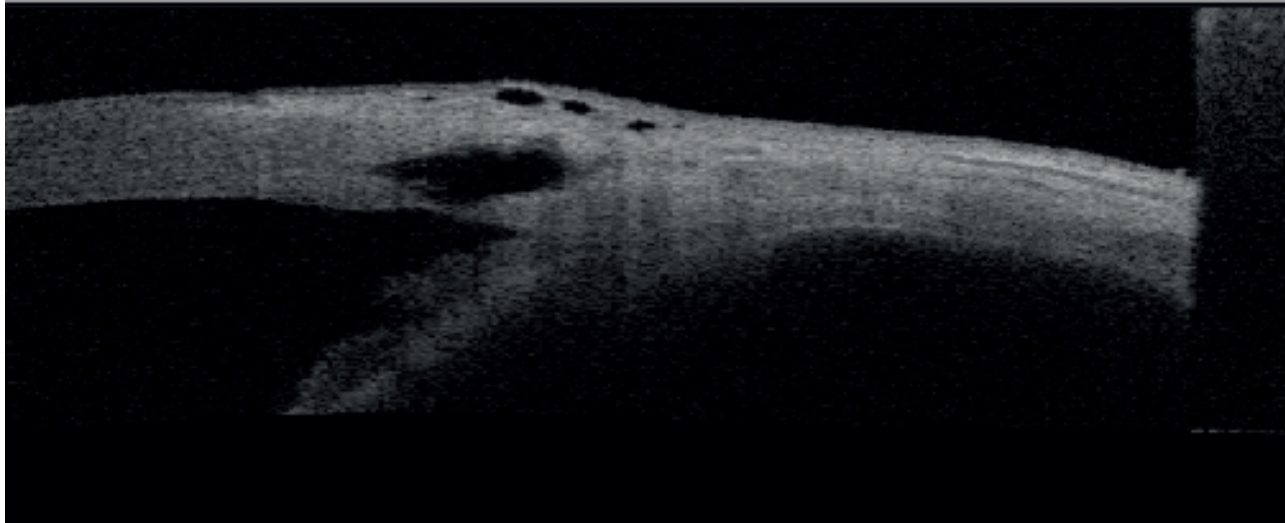


Figure 68:

OCT image of the filtering bleb of non-penetrating deep sclerectomy before (top) and after (bottom) goniopuncture.

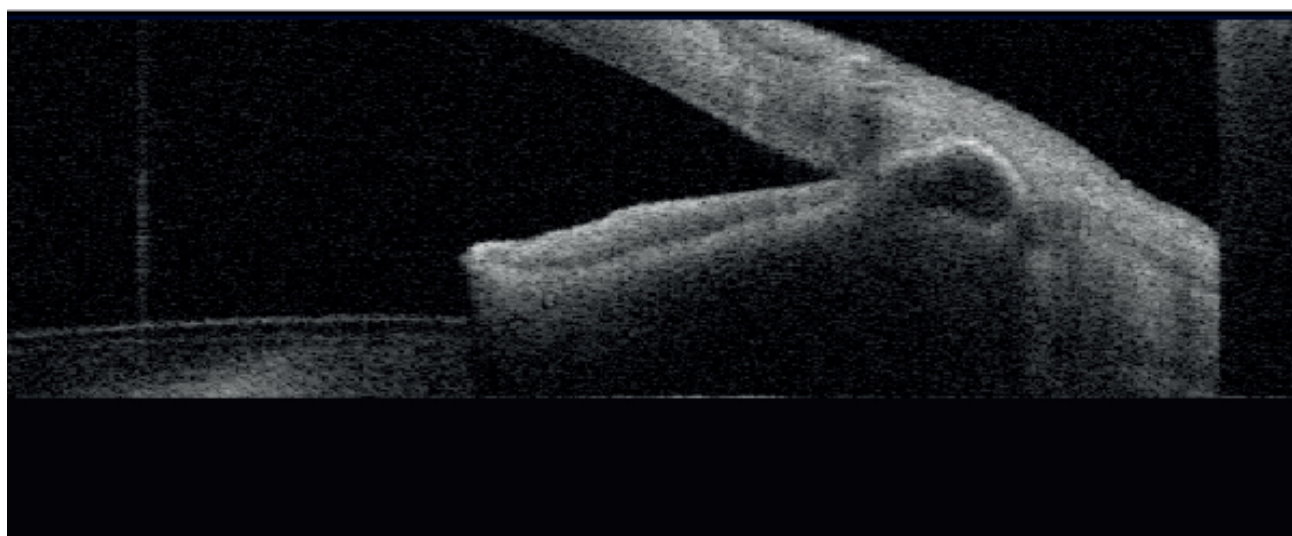
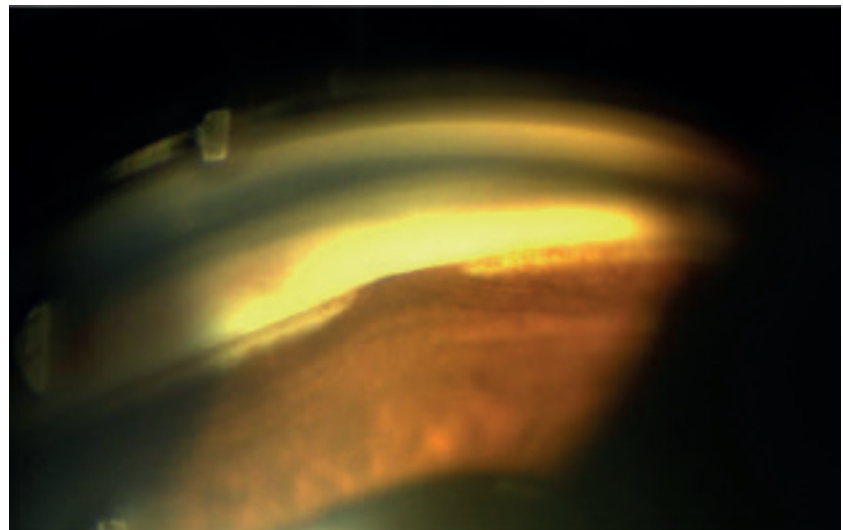


Figure 69:

OCT image of the filtering bleb of a non-penetrating deep sclerectomy with iris incarceration.

Follow-up of filtering surgery

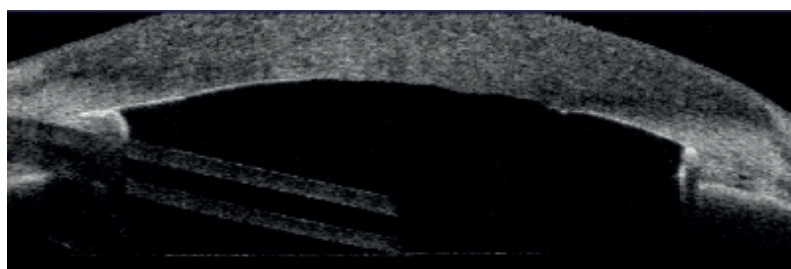


Figure 70:

OCT images of the positioning of the tube of a drainage valve and its anatomical relations with the cornea.

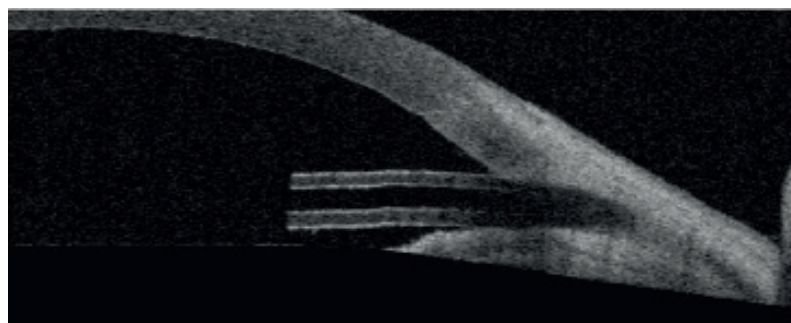
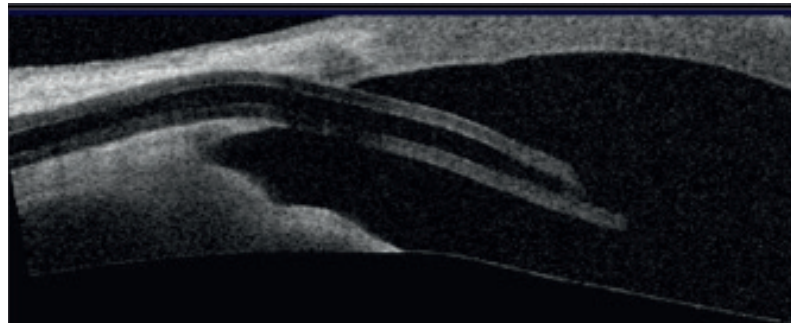


Figure 71:

OCT images of the positioning of the tube of a drainage valve and its anatomical relations with the cornea.

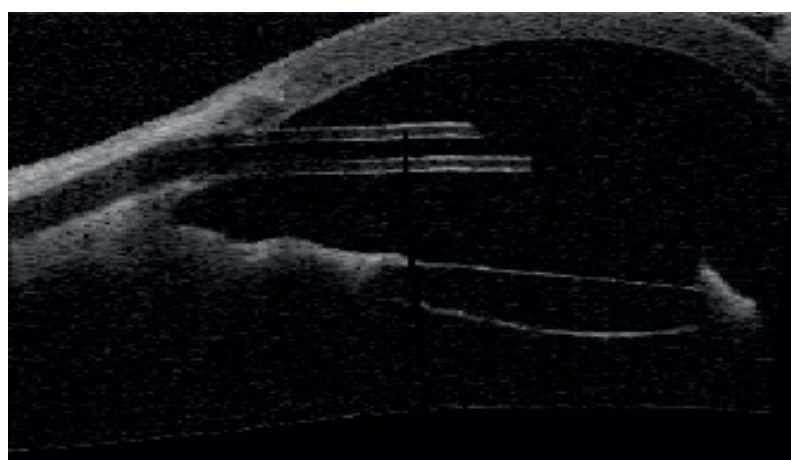


Figure 72:

OCT images of the positioning of a drainage tube in the anterior chamber. Also note the synechiae between the iris and the posterior chamber implant.

Follow-up of filtering surgery

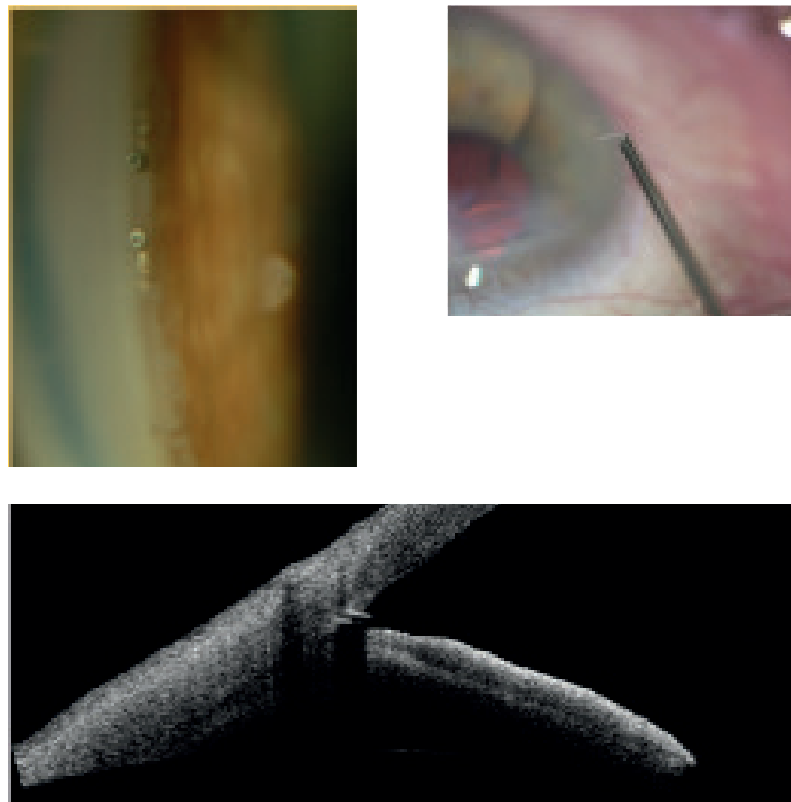


Figure 73:

IStent® drain implanted through the trabecular meshwork. Gonioscopic and OCT images of the device and the stents.

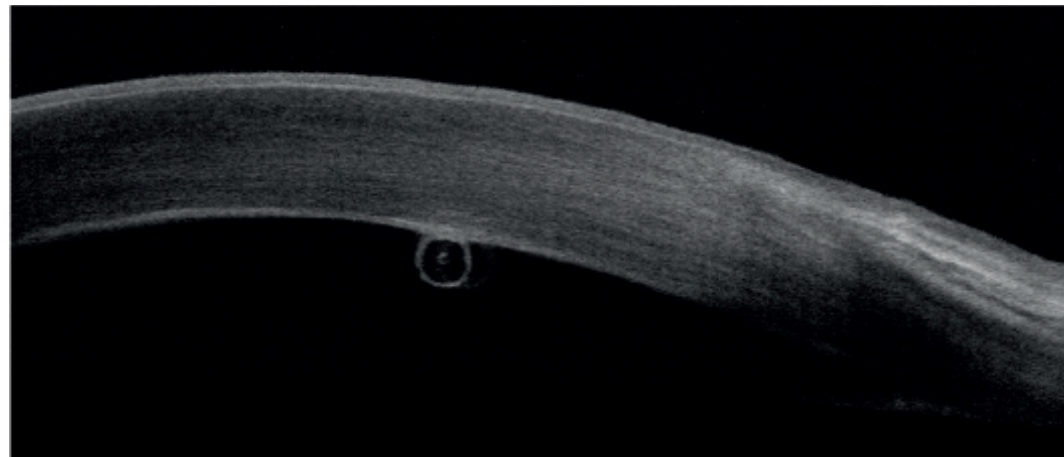


Figure 74:

XEN microtube: intracameral appearance.

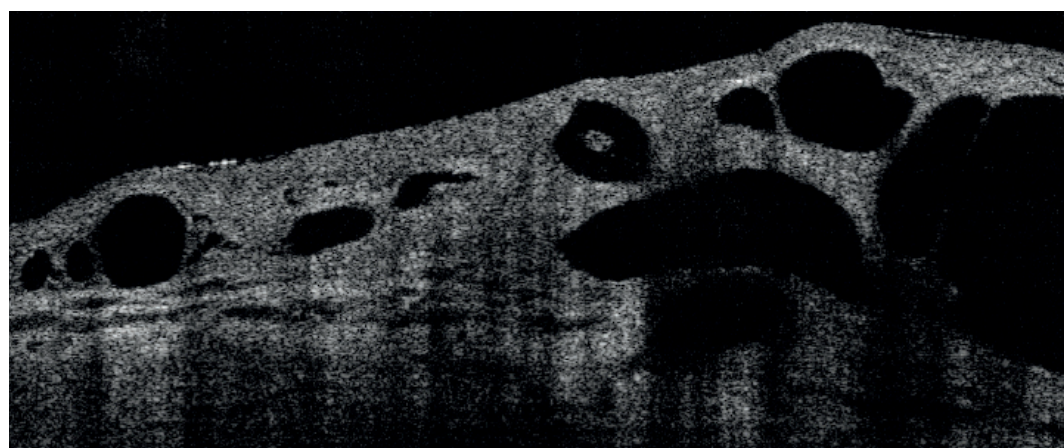


Figure 75:

XEN microtube: appearance of the subconjunctival tube and the surrounding filtering bleb.

Follow-up of trabeculectomy

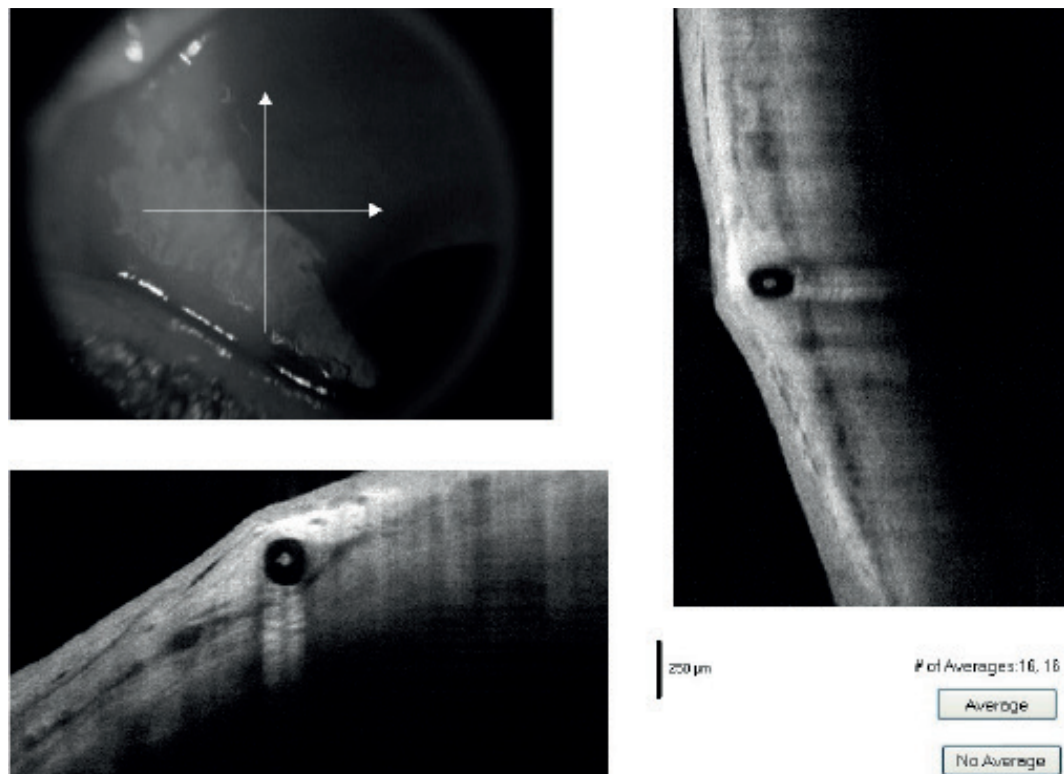


Figure 76:
XEN microtube: transscleral course.



5. New imaging developments: direct visualization of vessels of the trabecular meshwork and Schlemm's canal

New imaging developments:

direct visualization of vessels of the trabecular meshwork
and Schlemm's canal

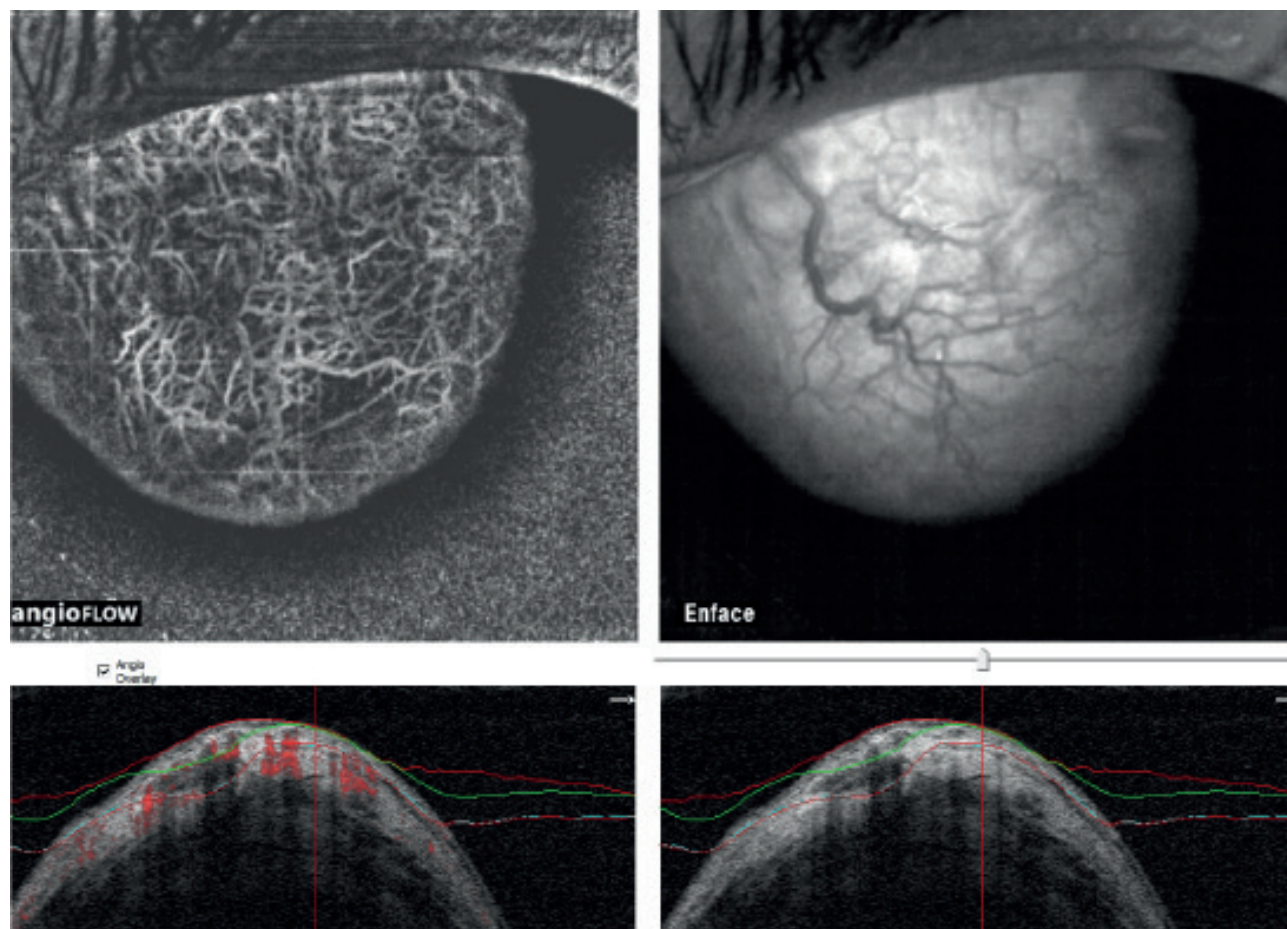


Figure 77:
OCT angiography of a functioning bleb.

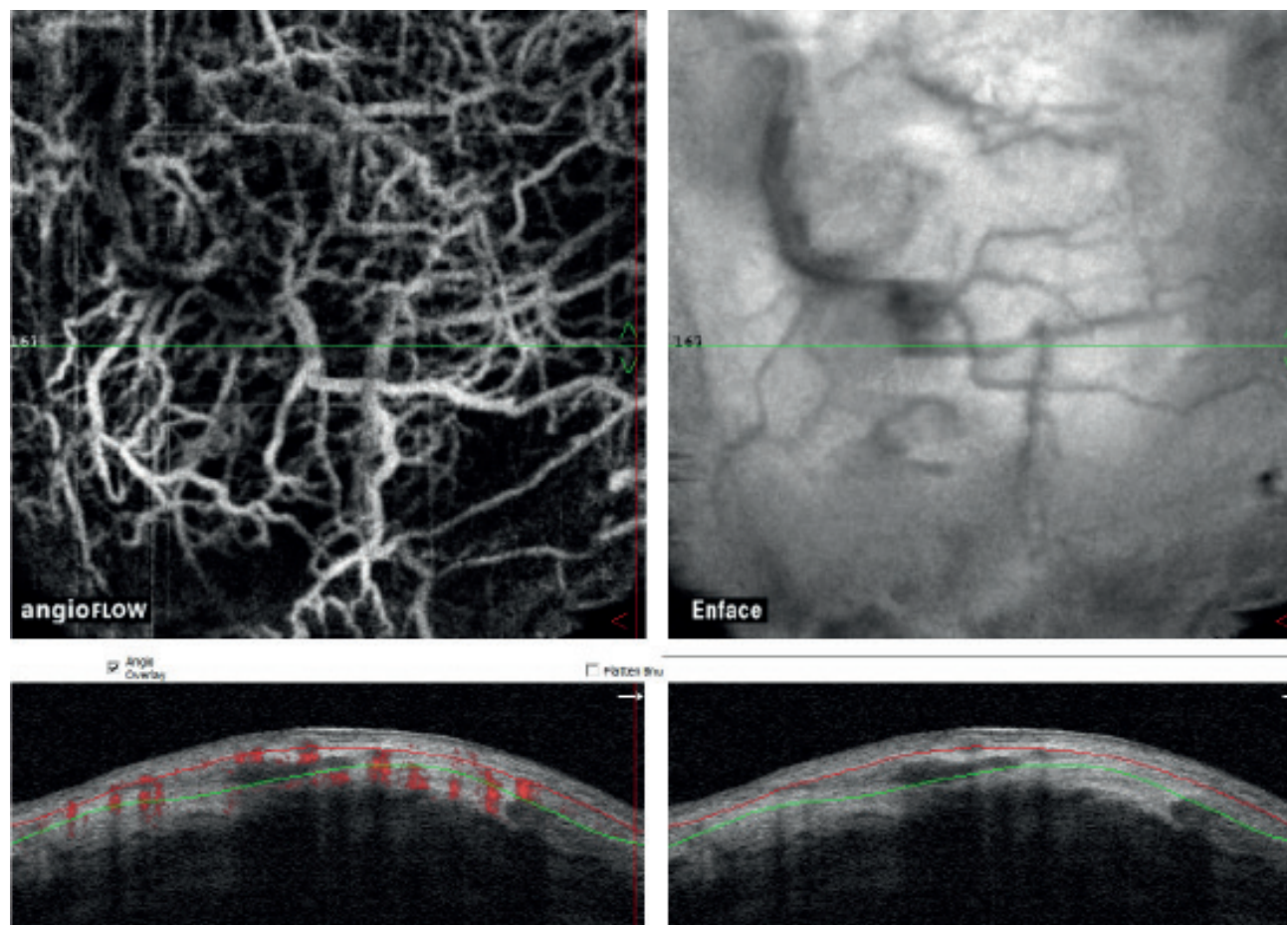


Figure 78:

OCT angiography of a bleb undergoing fibrosis marked by a high blood supply.

New imaging developments:

direct visualization of vessels of the trabecular meshwork and Schlemm's canal

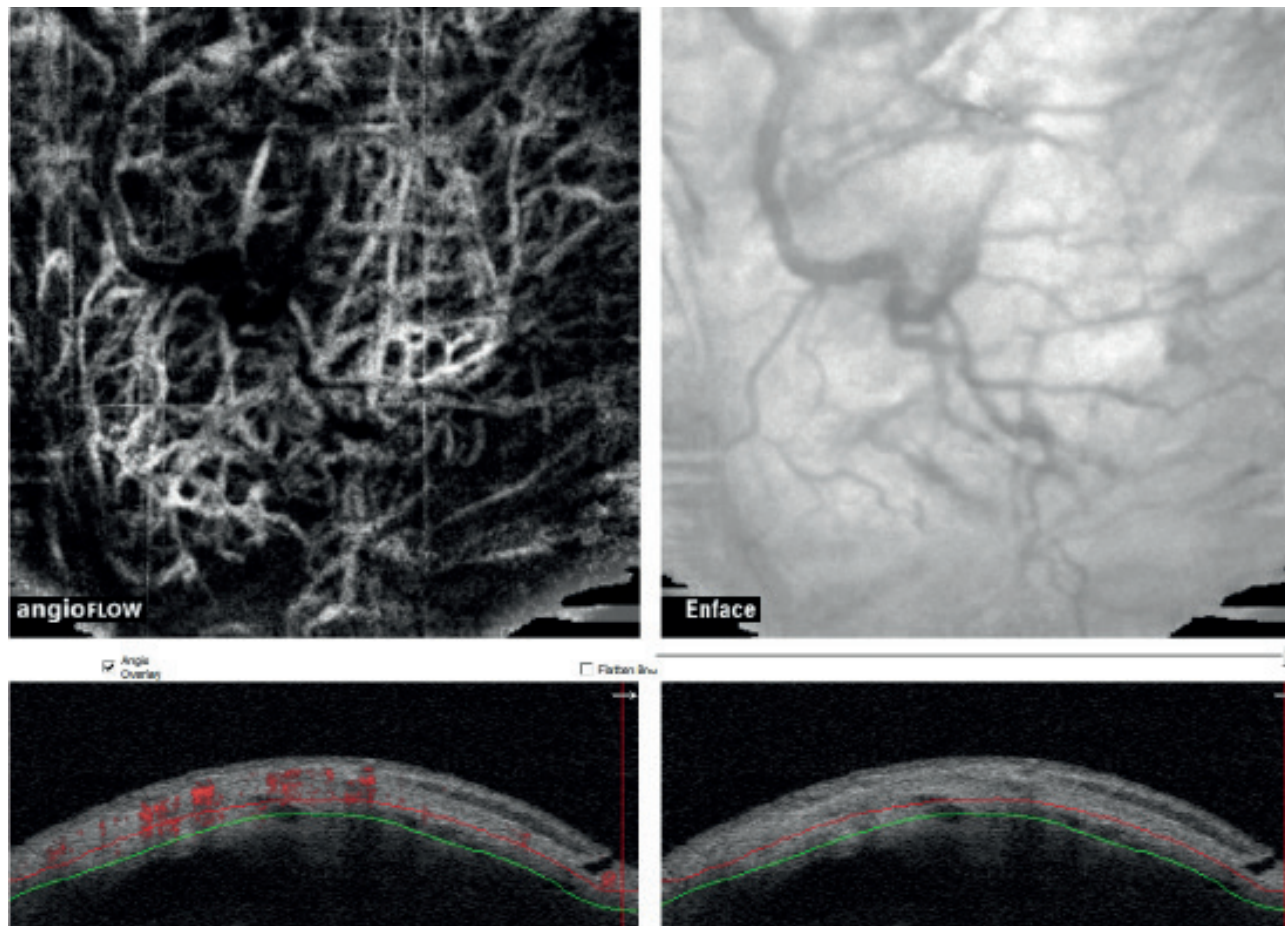


Figure 79:

OCT angiography of the same bleb in a deeper plane. The vascular pooling is suggestive of ongoing fibrosis.

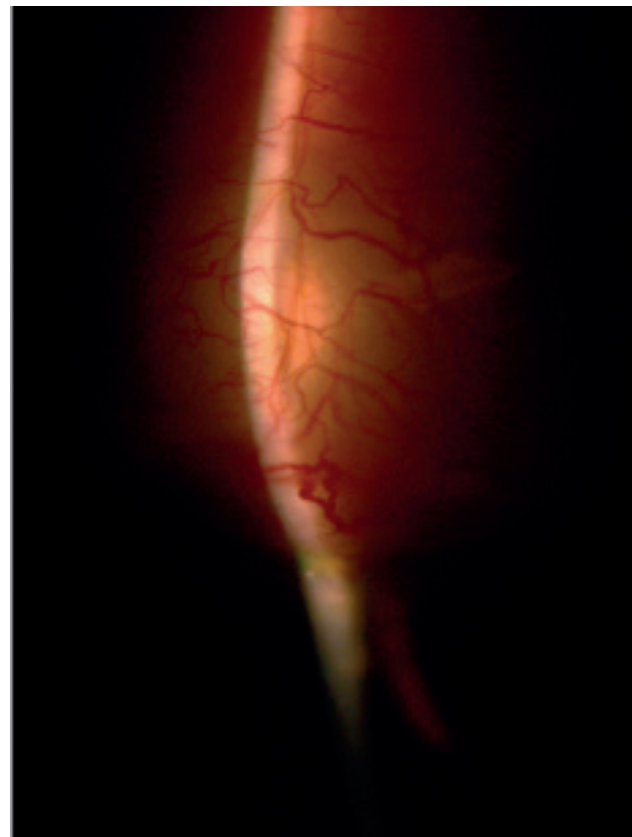
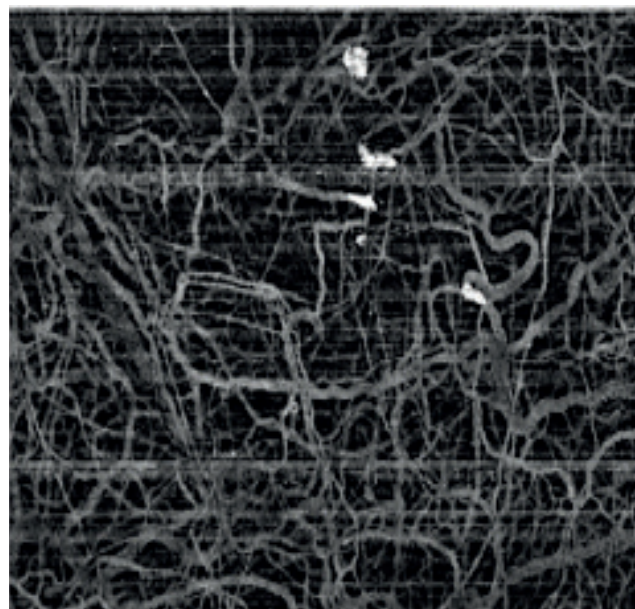
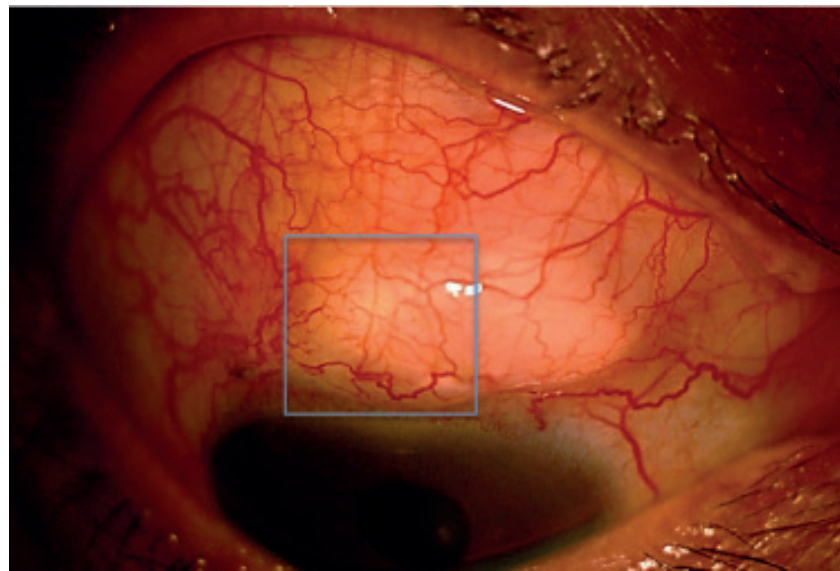


Figure 80:
OCT angiography of a fibrotic bleb 3 months postoperatively.

New imaging developments:

direct visualization of vessels of the trabecular meshwork and Schlemm's canal

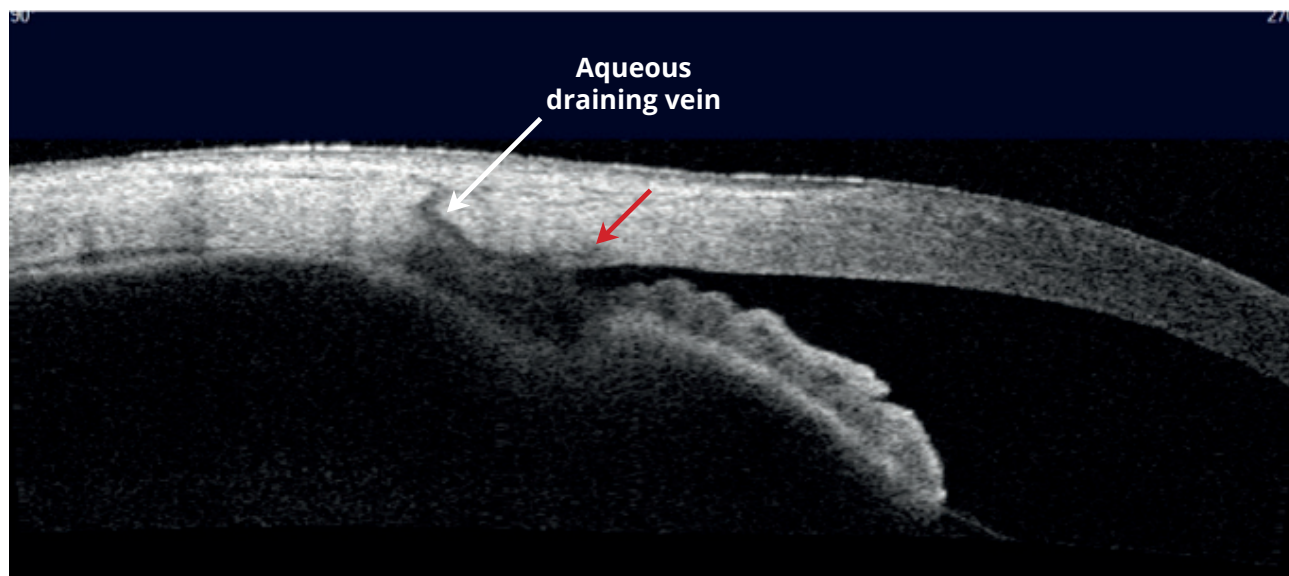


Figure 81:

Swept-Source OCT imaging of the iridocorneal angle visualizing a draining venule (white arrow) and Schlemm's canal (red arrow).

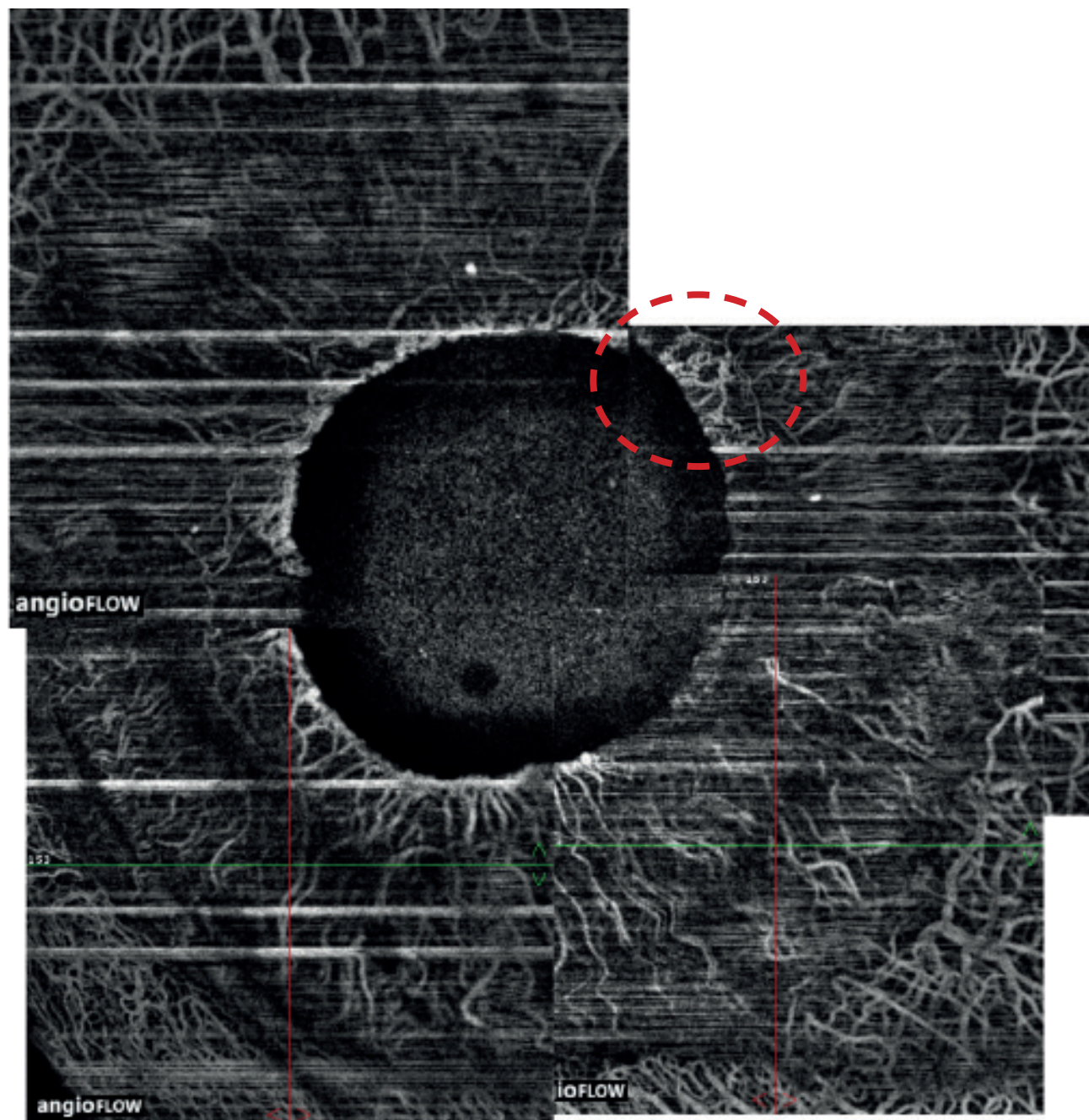


Figure 82:

OCT angiography of the iris in a case of rubeosis iridis.

New imaging developments:

direct visualization of vessels of the trabecular meshwork
and Schlemm's canal

